

Mikaela Solberg
Henrik Helgeland
Luis Alvarez

Design, Implementation and Optimization of an Autonomous Miniature Rig for Directional Drilling

Contribution to the Drillbotics 2022 Competition

Master's thesis in Petroleum Geoscience and Engineering
Supervisor: Alexey Pavlov, Tor Berge Gjersvik, Sigbjørn Sangesland
June 2022

Mikaela Solberg
Henrik Helgeland
Luis Alvarez

Design, Implementation and Optimization of an Autonomous Miniature Rig for Directional Drilling

Contribution to the Drillbotics 2022 Competition

Master's thesis in Petroleum Geoscience and Engineering
Supervisor: Alexey Pavlov, Tor Berge Gjersvik, Sigbjørn Sangesland
June 2022

Norwegian University of Science and Technology
Faculty of Engineering
Department of Geoscience and Petroleum

Abstract

Digital solutions and automated processes are revolutionizing many sectors, including the oil and gas industry. Since 2016, Drilling System Automation Technical Section (DSATS) and Society of Petroleum Engineers (SPE) have arranged the Drillbotics[®] competition to engage students to solve challenges within drilling automation. In a multidisciplinary team, students are encouraged to find solutions to problems that are not described in textbooks. The main task is to design, build and optimize a fully autonomous miniature drilling rig that can drill a directional well in a 30 x 60 x 60 cm rock sample and hit specified targets. The well path is constrained by a maximum inclination of 30° and an azimuth change of 15°.

The competition consists of two phases, where phase I was conducted in the fall of 2021 through submission of the report “Design Report NTNU – Drillbotics 2022 Phase I” [24]. Furthermore, phase II is an extension of phase I, where the objective is to implement and test the miniature drilling rig. This master’s thesis covers phase II of the competition and presents the work carried out by Henrik Helgeland, Mikaela Solberg and Luis Alvarez during the spring semester of 2022.

Health, Safety and Environment (HSE) has been prioritized throughout the project. Human factors has also been a major focal point towards this year’s Drillbotics competition. A thorough study on these topics has therefore been conducted. Potential safety hazards have been assessed and protective measures for mitigation have been taken to ensure a safe and healthy work environment. The team’s situational awareness has been improved through training and role assignment. Similarly, bow tie diagrams have been studied and applied to identify major hazardous events and implement prevention and recovery barriers for the project.

The miniature drilling rig consists of several interconnected systems. The hoisting system uses a hoisting motor to provide vertical displacement of the guide frame. As a result, weight on bit is transmitted through an aluminium drill pipe. The drilling system transfers torque from the top drive motor, along a titanium rod and to the drill bit. Four enhanced drill bits have been designed and manufactured to optimize the drilling performance. Additionally, a new drill chuck has been acquired to improve the grip of the rod.

The azimuth system orients the Bottom Hole Assembly (BHA) by applying torque to the drill pipe. This enables the miniature rig to generate an azimuth change. The required inclination is, on the other hand, built using a fixed bent sub that is integrated into the BHA. The circulation system is a semi-closed system that ensures sufficient hole cleaning and cooling of the drill bit. Recently, a diverter has been designed and implemented to prevent rock cuttings from accumulating on the laboratory floor. This has eliminated potential hazards related to slippery surfaces and handling of toxic chemicals.

A previously developed control system in Matlab and Simulink has been further advanced and improved to increase overall rig performance. The Graphical User Interface (GUI)

enables the operator to control the rig in either manual or fully autonomous mode. An integrated sensor card in the BHA provides real time measurements to predict the position and orientation downhole. The Nonlinear Model Predictive Control (NMPC) is used to steer the bit towards a pre-generated well trajectory reference that is based on a new novel trajectory planning method called Dubins Curves. Based on target inputs, a 3D Dubins Curve ensures the shortest well path with a curvature constraint determined by the bent sub.

A total of 62 wells have been completed throughout the project. These have been drilled with the objective to test the materials used, analyse the drill bits, optimize the drilling parameters and verify the actual drilled well trajectory. The results indicate that the system is mechanically robust, has excellent drilling efficiency and sufficient directional control to reach the different targets. A virtual demonstration of the rig was held at a BRU21 conference in Trondheim. This allowed the team to perform a test run under competition circumstances. The run was successful and the rig appears to be well tuned for the Drillbotics competition on the 16th of June 2022. Note that the results from the competition itself are not included in this thesis, as the submission deadline has expired before the competition date.

Sammendrag

Digitale løsninger og automatiserte prosesser revolusjonerer mange sektorer, inkludert olje- og gassindustrien. Siden 2016 har DSATS og SPE arrangert Drillbotics[®] konkurransen for å engasjere studenter til å løse utfordringer innen boreautomatisering. I et tverrfaglig team oppfordres studentene til å finne løsninger på problemer som ikke er beskrevet i lærebøker. Hovedoppgaven er å designe, bygge og optimalisere en fullt autonom miniatyrborerigg som kan bore en avviksbrønn i en 30 x 60 x 60 cm steinprøve og treffe forhåndsbestemte punkter. Brønnbanen er begrenset av en maksimal inklinasjon på 30° og en asimut-endring på 15°.

Konkurransen består av to faser, hvor fase 1 ble gjennomført høsten 2021 ved innlevering av rapporten “Design Report NTNU – Drillbotics 2022 Phase I” [24]. Videre er fase 2 en forlengelse av fase 1, hvor målet er å implementere og teste miniatyrboreriggen. Denne masteroppgaven dekker fase 2 av konkurransen og presenterer arbeidet utført av Henrik Helgeland, Mikaela Solberg og Luis Alvarez i løpet av vårsemesteret 2022.

Helse, miljø og sikkerhet har vært høyst prioritert gjennom hele prosjektet. Menneskelige faktorer har også vært et stort fokus for årets Drillbotics-konkurranse. Det er derfor gjennomført en grundig undersøkelse av disse temaene. Potensielle sikkerhetsfarer har blitt vurdert og det er iverksatt beskyttelsestiltak for å redusere risikoen for å sikre et trygt og sunt arbeidsmiljø. Lagets situasjonsforståelse er forbedret gjennom opplæring og rolletildeling. Tilsvarende har bow tie diagrammer blitt studert og brukt for å identifisere farlige hendelser og implementere forebyggings- og gjenopprettingsbarrierer for prosjektet.

Miniatyrboreriggen består av flere sammenkoblede systemer. Heisesystemet bruker en heisemotor for å gi vertikal forskyvning av boresystemet. Som et resultat blir vekten på borekronen overført gjennom et aluminiumsborerør. Boresystemet overfører dreiemoment fra top drive motoren, langs en titanium stang og videre til borekronen. Fire forbedrede borekroner er designet og produsert for å optimalisere boreytelsen. I tillegg er det anskaffet en ny drill chuck for å forbedre grepet på titanium stangen.

Asimutsystemet orienterer nedihullskonfigurasjonen (BHA) ved å påføre dreiemoment på borerøret. Dette gjør at miniatyrriggen kan generere en asimut-endring. Den nødvendige inklinasjonen er derimot bygget ved hjelp av en bøyd sub som er integrert i BHA. Sirkulasjonssystemet er et semi-lukket system som sikrer tilstrekkelig hullrensing og kjøling av borekronen. Det har blitt designet og implementert en diverter for å hindre at borekaks samler seg på laboratoriegulvet. Dette har eliminert potensielle farer knyttet til glatte overflater og håndtering av giftige kjemikalier.

Et tidligere utviklet kontrollsystem i Matlab og Simulink har blitt ytterligere utviklet og forbedret for å øke den generelle ytelsen til boreriggen. Et grafisk brukergrensesnitt gjør det mulig for operatøren å kontrollere riggen i enten manuell eller autonom modus. Et integrert sensor kort i BHA gir sanntidsmålinger for å forutsi posisjon og orientering nede i brønnen. NMPC kontroll brukes til å styre borekronen mot en forhåndsgenerert

brønnbanereferanse som er basert på en ny brønnplanleggingsmetode kalt Dubins kurver. Basert på forhåndsbestemte koordinater sikrer en 3D Dubins-kurve den korteste brønnbanen med en krumningsbegrensning bestemt av den bøyde suben.

Totalt er 62 brønner ferdigstilt gjennom prosjektet. Disse er boret med formål å teste materialene som brukes, analysere borekronene, optimalisere boreparametrene og verifisere den faktisk boret brønnbanen. Resultatene indikerer at systemet er mekanisk robust, har utmerket boreeffektivitet og tilstrekkelig retningskontroll for å nå de ulike punktene i steinprøven. En virtuell demonstrasjon av riggen ble holdt på en BRU21-konferanse i Trondheim. Dette tillot laget å utføre en testboring under konkurranseforhold. Boringen var vellykket og riggen ser ut til å være godt optimalisert for Drillbotics konkurransen den 16. juni 2022. Merk at resultatene fra selve konkurransen ikke er inkludert i denne avhandlingen fordi innleveringsfristen er før selve konkurransedatoen.

Acknowledgements

This multidisciplinary project has been a result of the joint work of countless people from Norwegian University of Science and Technology (NTNU) and external companies. The team is grateful for their contribution throughout this project.

To start with, the team wants to show their appreciation to the main supervisors Alexey Pavlov, Tor Berge Gjersvik and Sigbjørn Sangesland. They have been actively involved throughout the entirety of the project from August 2021 to June 2022. Their continuous support and advice has been of great value. John-Morten Godhavn from Equinor also deserves a special thank you for his inputs and ideas in the supervisor meetings.

The team also wants to recognize the lab support team consisting of Noralf Vedvik, Torkjell Breivik, Terje Bjerkan and Håkon Myhren. Their practical experience has greatly benefited the team in terms of intervention and modification of the rig. Thank you for always providing suggestions and solutions to difficult challenges.

Moreover, the team wants to acknowledge the Department of Geoscience and Petroleum (IGP) at NTNU for facilitating such a comprehensive project. The lab infrastructure and technical resources have been crucial for the success of the project. The department has provided financial support through the BRU21 program.

A special appreciation is given to our long standing external partners. Equinor has contributed to the funding of the project, while Lyng Drilling has provided knowledge of the drill bit modeling process and manufactured several drill bits. Thank you for your support and for providing the team with insights to the industry.

Furthermore, the team would like to express their gratitude to Society of Petroleum Engineers (SPE) and Drilling System Automation Technical Section (DSATS) for organizing the Drillbotics competition. Thank you for providing the team with the opportunity to expand our knowledge within drilling automation. It has prepared us for our upcoming career paths within the drilling industry.

Finally, we want to thank our families and friends who have supported us along this journey. They have inspired and motivated the team to work hard and focus towards the completion of the project.

Table of Contents

Abstract	i
Sammendrag	iii
Acknowledgements	v
Abbreviations	xviii
List of Figures	xix
List of Tables	xxviii
1 Introduction	1
2 Competition Objectives and Requirements	3
3 Organization	5
3.1 Team	5
3.2 Roles and Responsibilities	7
3.3 Project Management	8
3.4 Tracking of Drilling Activities	9
4 HSE	11
4.1 Covid-19	12

4.2	Potential Safety Hazards	13
4.2.1	Ergonomic hazards	13
4.2.2	Mechanical hazards	13
4.2.3	Electrical hazards	14
4.2.4	Chemical hazards	14
4.3	Protective Measures to Mitigate Safety Hazards	15
4.3.1	General Protective Measures	15
4.3.2	Ergonomic Protective Measures	16
4.3.3	Mechanical Protective Measures	17
4.3.4	Electrical Protective Measures	18
4.3.5	Chemical Protective Measures	18
4.4	HSE Learnings	19
5	Human Factors	20
5.1	Human Factors Theory	20
5.2	Automation and Human Factors in the Drilling Industry	23
5.2.1	Advantages of Automation in the Drilling Industry	24
5.2.2	Implementation of Automated Systems with Respect to Human Factors	24
5.3	Human Factors in the Drillbotics Competition	26
5.3.1	Improve Situational Awareness	26
5.3.1.1	Situational Awareness Training	26
5.3.1.2	Computer screen positioning arm	27
5.3.1.3	Distance to Next Target Point	28
5.3.2	Bow Tie Risk Assessment	29
5.3.2.1	Bow Tie Sections	29
5.3.2.2	Bow Tie Analysis for Drillbotics	30
6	Theoretical Background	31

6.1	Directional Drilling	31
6.1.1	Types of Directional Wells	32
6.1.2	Well Path Geometry	32
6.1.3	Well Profile Terminology	32
6.1.4	Survey Calculation Methods	35
6.2	Bottom Hole Assembly (BHA)	38
6.2.1	Directional Steering	38
6.2.2	Positive Displacement Motor (PDM)	39
6.2.2.1	Power Section	39
6.2.2.2	Bent Housing	40
6.2.2.3	Transmission Section	41
6.2.2.4	Bearing Section	42
6.2.3	Rotary Steerable System (RSS)	42
6.2.4	Dog Leg Severity (DLS) based on BHA Specifications	43
6.3	Drill String Mechanics	44
6.3.1	Pipe Twist Off	44
6.3.2	Pipe Bending	46
6.3.3	Rod Stresses	46
6.3.4	Buckling	46
6.3.5	Burst	49
6.3.6	Fatigue	49
6.3.7	Natural Frequency	50
6.4	Drill Bit	51
6.4.1	Types of Drill Bits	52
6.4.2	Bit Profile and Cone Angle	53
6.4.3	Cutter Layout	55
6.4.4	Cutter Orientation	56
6.4.5	Force Balance	57

6.5	Drilling Hydraulics	58
6.5.1	Hole Cleaning	58
6.5.2	Pressure Losses	60
6.5.2.1	Pipe Pressure Losses	61
6.5.2.2	Bit Pressure Losses	61
6.6	Mechanical Specific Energy (MSE)	62
7	Mechanical Rig Design	65
7.1	Drillbotics Rigs 2017-2021	65
7.2	Rig Framework	66
7.2.1	Chargeable Weight Calculations	67
7.3	Drillbotics 2022 Rig	68
7.4	Hoisting System	69
7.4.1	Hoisting Motor	70
7.4.2	Carriage Mount	71
7.4.3	Load Cell	71
7.4.4	Safety Limit Switches	72
7.5	Drilling System	72
7.5.1	Top Drive Motor	73
7.5.2	Top Drive Connection and Drill Chuck	74
7.5.3	Rod	74
7.5.4	Drill Pipe	75
7.5.5	Stabilizers	75
7.6	Azimuth Control System	76
7.6.1	Hollow Shaft Gearbox with Rotary Table	77
7.6.2	Azimuth Servo Motor and Right Angled Gearboxes	77
7.6.3	T-shaft	79
7.6.4	Torque Sensor	79

7.7	Circulation System	80
7.7.1	Hydraulic Swivel	80
7.7.1.1	Swivel House	80
7.7.1.2	Hollow Swivel Shaft	81
7.7.1.3	Roller Bearings	82
7.7.1.4	Sealing Section	82
7.7.1.5	Drill Pipe Connection	83
7.7.2	Diverter	83
7.8	Electrical System	84
7.8.1	DAQ	84
7.8.2	Downhole Sensor	85
7.8.3	Overview Electrical System	85
7.9	Wireless Communication Options	86
7.9.1	Bluetooth Communication Option	86
7.9.2	Wireless Communication Alternatives	86
7.10	Bottom Hole Assembly Design	87
7.10.1	Original BHA Design	87
7.10.1.1	Stabilizers	88
7.10.1.2	Sensor Housing	89
7.10.1.3	Bent Sub	89
7.10.1.4	Wear Plate	90
7.10.1.5	Bit Sub	90
7.10.2	Wireless BHA Design	90
7.10.2.1	Combined Sensor Housing and Lower Stabilizer	91
7.10.2.2	New Wear Plate	92
7.11	Drill Bit	92
7.11.1	Old NTNU Drill Bits	93
7.11.2	New NTNU Drill Bits	94

7.11.3	Drill Bit Specifications	98
7.11.4	Drill Bit Modelling Process	98
8	Design Limits and Constraints	101
8.1	Mechanical Limitations	101
8.1.1	Well Path	102
8.1.2	Pipe Bending	104
8.1.3	Rod Stresses	106
8.1.4	Pipe Buckling	108
8.1.5	Pipe Burst	111
8.1.6	Twist Off	111
8.1.7	Drill Pipe and Rod Fatigue	112
8.1.8	Natural Frequency	113
8.1.9	Drilling Rate	114
8.1.10	Bit Tilt	115
8.1.11	Hydraulics	115
8.1.11.1	Hole Cleaning	115
8.1.11.2	Pressure Losses	116
8.1.12	Overview of Mechanical Limitations	117
8.2	Rig Power Consumption	118
8.2.1	Top Drive Motor	118
8.2.2	Hoisting Motor	119
8.2.3	Azimuth System	119
8.2.4	Torque Sensor	120
8.2.5	Computer	120
8.2.6	Total Power Consumption	120
9	Risk Analysis for Rig Components	121
9.1	Top Drive Motor and Hoisting Motor	123

9.2	Drill Chuck and Top Drive Connection	123
9.3	Rod	123
9.4	Hollow Shaft Gearbox, Azimuth Motor and Right Angled Gearboxes	123
9.5	Azimuth Torque Sensor	124
9.6	Load Cell	124
9.7	T-shaft	124
9.8	Hydraulic Swivel	125
9.9	Drill Pipe	125
9.10	Drill Pipe Connection	125
9.11	Drill Floor Stabilizer	125
9.12	Riser and Diverter	126
9.13	USB Cable and Connections	126
9.14	BHA Components	126
9.15	Sensor Card	126
9.16	Universal Joint	127
9.17	Drill Bit	127
9.18	Computers	127
10	Control System Design	128
10.1	Matlab and Simulink	128
10.2	Autonomous States	129
10.3	GUI	131
10.4	PID Controller	132
10.4.1	PID Tuning	135
10.4.2	PID Implementation in the Control System	136
10.4.2.1	PID Tuning Example for WOB	137
10.4.2.2	WOB PID Controller	137
10.4.2.3	Azimuth Torque PID Controller	138

10.5	Kalman Filter	138
10.5.1	Kalman Filter Theory	139
10.5.2	Extended Kalman Filter	140
10.5.3	Kalman Filter Implementation	141
10.5.3.1	Hoisting velocity estimation	141
10.5.3.2	Azimuth Rotation Velocity Estimation	142
10.6	Position Estimate	142
10.6.1	Model Methodology	142
10.6.2	Orientation Estimate	144
10.6.2.1	Gravity Field Model	144
10.6.2.2	Azimuth and Inclination Calculation	144
10.7	Model Predictive Control	145
10.7.1	Model Predictive Control Implementation	145
10.8	Well Trajectory Reference	146
11	Downhole Sensor Orientation	147
11.1	Sensor Card	147
11.2	Accelerometer	148
11.3	Magnetometer	149
11.3.1	Earth's Magnetic Field	149
11.3.2	Magnetometer Sensor	151
11.4	Gyroscope	152
11.5	Orientation estimation	153
11.5.1	Roll, Pitch and Yaw Calculation	154
11.6	Calibration	155
11.6.1	Accelerometer Calibration	155
11.6.2	Magnetometer Calibration	158
11.7	Azimuth or Yaw Calculation	161

12 Well Trajectory Planning	162
12.1 Dubins Curve	162
12.2 3D Dubins Curve	163
12.3 Competition Well Trajectory	166
12.4 Well Trajectory Properties	168
13 Testing and Qualification	172
13.1 Functional Test	172
13.1.1 Top Drive Motor and Hoisting motor	173
13.1.2 Load Cell	173
13.1.3 Azimuth System	174
13.2 Drill Pipe and Rod Tests	175
13.2.1 Combined Bending Test	175
13.2.2 Drill Pipe Twist Off	177
13.2.3 Rod Twist Off	179
13.2.4 Buckling	180
13.3 Rock Sample Testing	181
13.3.1 Full Scale Rock Sample Calculations	181
13.3.2 Test Sample Calculations and Procedure	182
13.3.3 Results	184
13.4 Diverter Test	185
13.5 Drill Bit Analysis	186
13.5.1 Testing Description	186
13.5.2 Drill Bit Wear	186
13.5.3 Vibrations	189
13.5.4 Borehole Quality	190
13.5.5 Rate of Penetration	191
13.5.6 Overall Performance and Ranking	192

13.6	Drill Bit Vibration Observation	193
13.7	Drilling Optimization Tests	194
13.7.1	Testing Description	195
13.7.2	Optimal Parameters for Vertical Drilling	196
13.7.3	Optimal Parameters for Deviated Drilling	197
13.8	Sensor Card Test and Well Path Verification	198
13.9	Bru21 Conference Demo	200
13.9.1	Well Trajectory	200
13.9.2	Autonomous States	201
14	Project Accounting	208
14.1	Funding Distribution	208
14.2	Unlisted Expenses	208
14.3	Incurred Costs	209
15	Challenges and Lessons Learned	211
15.1	Project Management	211
15.1.1	Covid-19 Impacts	211
15.1.2	Lab and Workshop Schedule	212
15.1.3	Allocation of Fixed Roles While Drilling	212
15.2	Rig Alignment	212
15.3	Connection Between Drill Pipe and BHA	214
15.4	Universal Joint	214
15.5	Wear Plate Improvement	216
15.6	Leakage in Swivel and Drill Pipe Connection	217
15.7	Leakage in T-shaft	218
15.8	Drill Chuck	218
15.9	Rod Twist Off	219
15.10	Intervention of Drill Bits	220

15.11	Integration of the Sensor Card in the BHA	221
15.11.1	Integration Process	222
15.11.2	Challenges and Modifications	225
15.11.3	Potential Improvement	228
15.12	Computer and Control System Related Challenges	229
15.12.1	Load cell and Hoisting Motor	229
15.12.2	Implementation of New Computer	229
15.12.3	Simulink Data Acquisition Problem	230
16	Conclusion	232
17	Future Work	234
17.1	Rock Sample Positioning	234
17.2	Protective Glass	235
17.3	BHA Back Up	235
17.4	Length of BHA	236
17.5	Stabilizer Gauge	236
17.6	Sensor Card Size	236
17.7	Pilot Hole Bit	236
17.8	Wireless Communication with Downhole Sensor	237
17.9	Magnetometer Development	237
17.9.1	Fluxgate Magnetometer	237
17.9.2	Artificial Magnetic Pulses	237
17.9.3	Material Selection	238
	Bibliography	239
	Appendices	247
A	Drillbotics 2022 Guidelines	247

B Bowtie Diagrams	287
C Cuttings Transportation Derivation	289
D Rig Derrick	291
E Hoisting Motor	292
F Top Drive Motor	293
G Drill Chuck	295
H Riser	297
I Hollow Shaft Gearbox	298
J Azimuth Servo Motor	300
K Azimuth Right Angle Gearbox	301
L T-Shaft	302
M Torque Sensor	303
N Hydraulic Swivel	304
O Diverter Design	306
P BHA Components	307
Q Drill Bit	314

Abbreviations

API American Petroleum Institute.

BHA Bottom Hole Assembly.

CRS Critical Rotary Speed.

DAQ Data Acquisition.

DLS Dogleg Severity.

DOC Depth of Cut.

DSATS Drilling System Automation
Technical Section.

DTM Downhole Turbine Motor.

GUI Graphical User Interface.

HMI Human Machine Interface.

HSE Health, Safety and Environment.

IGP Department of Geoscience and Petro-
leum.

ITK Department of Engineering Cybernet-
ics.

MPC Model Predictive Control.

MSE Mechanical Specific Energy.

NCS Norwegian Continental Shelf.

NIPH Norwegian Institute of Public
Health.

NMPC Nonlinear Model Predictive Con-
trol.

NPT Non Productive Time.

NTNU Norwegian University of Science
and Technology.

PDC Polycrystalline Diamond Compact.

PDM Positive Displacement Motor.

PPE Personal Protective Equipment.

RC Radius Of Curvature.

ROP Rate Of Penetration.

RPM Revolutions Per Minute.

RSS Rotary Steerable System.

SPE Society of Petroleum Engineers.

TSP Thermally Stable Polycrystalline.

TVD True Vertical Depth.

UCS Uniaxial Compressive Strength.

UDP User Datagram Protocol.

WOB Weight On Bit.

List of Figures

- 3.1 NTNU Drillbotics team members. 6
- 3.2 NTNU Drillbotics Organizational Structure. 6
- 3.3 Drillbotics team roles. 7
- 3.4 Gant diagram used for project management. 8
- 3.5 Example of form used for tracking of drilling activities. 10

- 4.1 Motion of powered components on the drilling rig. 14
- 4.2 Safety decision hierarchy used to determine protective measures [39]. 15
- 4.3 Correct PPE during cementing and rig maintenance. 16
- 4.4 Safety Board. 16
- 4.5 Protective cabinet encasing the drilling rig. 17
- 4.6 Emergency stop switch. 18
- 4.7 Safety card example from a real incident. 19

- 5.1 Original Fitts list [11]. 22
- 5.2 Present day survey results of Fitts list [11]. 22
- 5.3 Computer screen setup NTNU Drillbotics 2021. 27
- 5.4 Adjustable arm for second monitor 28
- 5.5 GUI with the distance to next target point marked with a red square. 28
- 5.6 Bow tie analysis diagram [99]. 29
- 5.7 Bow tie analysis for a projectile event. 30

6.1	Types of well paths [23].	32
6.2	Deviated well terminology [23].	33
6.3	Inclination (I) and azimuth (A) [23].	34
6.4	Dogleg Angle (ϕ) [23].	35
6.5	Tangential method [23].	35
6.6	Average angle method [23].	36
6.7	Radius of curvature [23].	36
6.8	Balanced tangential method [23].	37
6.9	Minimum curvature method [23].	37
6.10	Standard PDM showing main components [23].	39
6.11	Rotor and stator combination [23].	40
6.12	Lobe arrangement [23].	40
6.13	Bent housing [10]	40
6.14	Adjustable bent sub connection procedure [38].	41
6.15	U-joint and flexible rod [23].	42
6.16	Different flow paths [25].	42
6.17	RSS variants [23].	43
6.18	Parameters for Equation 6.9 [23].	44
6.19	Stress components acting on the drill pipe [55].	45
6.20	Helical and sinusoidal buckling [19].	47
6.21	Cyclic stress in deviated wells [3]	49
6.22	S-N curve [94]	50
6.23	Components of a roller cone bit [23].	52
6.24	Components of a PDC bit [23].	52
6.25	Drilling shale using shear and compressive stress [23].	53
6.26	Bit profile shape and characteristics [43].	54
6.27	Deep and shallow cone angle [43].	54
6.28	Cutter layout with cutter density increased towards the gauge [42].	55

6.29	Two types of cutter layout [18].	56
6.30	Cutter back rake angle [23].	56
6.31	Cutter side rake angle [43].	57
6.32	Traditional cutter layout leading to inefficient drilling [18].	57
6.33	Rearranging the cutter layout angularly leading to efficient drilling [18]. . .	58
6.34	Interaction between friction factor f and Reynolds Number Re for the interaction between a particle in the Newtonian fluids [22].	59
6.35	Plot presenting relationship between MSE and WOB [104].	63
6.36	Effect of the WOB on the depth of the cut.	64
7.1	Rig framework without components.	66
7.2	Acrylic glass cover.	67
7.3	Rig in folded position.	68
7.4	NTNU Drillbotics 2022 rig.	68
7.5	Principle that the hoisting system builds on [25].	70
7.6	Hoisting motor.	70
7.7	Load cell.	71
7.8	Upper safety limit switch.	72
7.9	Drilling system.	73
7.10	Top drive connection and drill chuck.	74
7.11	Titanium rod.	75
7.12	Aluminium drill pipe.	75
7.13	Upper and lower stabilizer with manual hoisting mechanism.	76
7.14	Azimuth control system.	77
7.15	Hollow shaft gearbox with a rotary table [51].	77
7.16	Azimuth servo motor components.	78
7.17	Gearbox.	78
7.18	Brass T-shaft [9].	79
7.19	Torque sensor installed.	79

7.20	Hydraulic swivel fixed on the carriage mount [9].	80
7.21	Swivel house.	81
7.22	Swivel shaft cross section [9].	81
7.23	Connection between the swivel shaft and brass T-shaft [9].	81
7.24	Roller bearings in the swivel housing [9].	82
7.25	Housing cross section with O-rings marked in red [9].	82
7.26	Drill pipe arrangement from top: nipple, drill pipe, O-ring, spring collet and collet nut.	83
7.27	Diverter.	84
7.28	USB-6212 DAQ [63].	84
7.29	Arduino Nano 33 BLE [28].	85
7.30	Overview electrical system.	85
7.31	Wireless data transfer options.	87
7.32	Original BHA design showing all components [9].	88
7.33	Upper stabilizer design.	88
7.34	Sensor housing.	89
7.35	Bent Sub.	89
7.36	Wear plate.	90
7.37	Bit sub design.	90
7.38	BHA design wireless solution.	91
7.39	Lower stabilizer design.	91
7.40	Redesigned wear plate.	92
7.41	NTNU Bit 1 and NTNU Bit 2.	93
7.42	Qualitative evaluation of NTNU Bit 1.	94
7.43	NTNU Bit 1 cutter distribution.	95
7.44	Sharp and bevel cutters.	95
7.45	NTNU Bit 3 and NTNU Bit 4.	96
7.46	Cutting distribution of NTNU Bit 1 and NTNU Bit 5 and 6.	96

7.47	Bit body of NTNU Bit 1 and NTNU Bit 5 and 6.	97
7.48	NTNU Bit 5 and NTNU Bit 6.	97
7.49	NTNU drill bits.	98
7.50	2D sketch and basic 3D model of the drill bit body.	99
7.51	Top and side view of 3D cutter structure.	99
7.52	Final bit body.	100
7.53	3D printed drill bit mould and final product.	100
8.1	Well path restricted by a 30° inclination while assuming a constant build rate.	103
8.2	Well path with a 15° azimuth change.	104
8.3	Various axial stresses plotted in function of RC , P , and WOB	105
8.4	Axial bending stress plotted against RC	105
8.5	Aluminum pipe 7075-T6.	106
8.6	Comparative stresses as function of RC compared with the yield strength.	107
8.7	Comparative stresses plotted against RC and compared with material strength for titanium grade 5 pipe.	107
8.8	Maximum WOB versus the unsupported drill pipe length for different end conditions.	108
8.9	Top and bottom section of drill pipe for top and bottom hole drilling.	109
8.10	Drill pipe twist off torque versus WOB	111
8.11	Cylinder lateral surface area [93].	116
9.1	Colors for risk classification.	121
10.1	Simulink GUI Example.	129
10.2	Overview autonomous states [12].	129
10.3	GUI for manual mode.	131
10.4	GUI for autonomous mode.	132
10.5	PID Controller block diagram [109].	133
10.6	Illustration of the proportional error [57].	134

10.7	Illustration of the integral error [57].	134
10.8	Illustration of the derivative error [57].	134
10.9	Types of responses for a PID controller [109].	135
10.10	PID block in Simulink [9].	136
10.11	WOB PID controller in Simulink [9].	138
10.12	Azimuth torque PID controller in Simulink [9].	138
10.13	Extended Kalman Filter block in Simulink [72].	141
10.14	ROP estimation using a Kalman state observer in Simulink [9]	141
10.15	Azimuth velocity estimation using a Kalman filter in Simulink [9]	142
11.1	Arduino Nano 33 BLE [28].	148
11.2	Accelerometer principle [81].	148
11.3	Earth's magnetic field [23].	149
11.4	Magnetic field inclination according to the US/UK World Magnetic Model (WMM) [49].	150
11.5	Earth's magnetic field (vector B or F) and its components [23].	150
11.6	LSM9DS1 Magnetometer [29].	151
11.7	Undisturbed electrons flowing straight [81].	151
11.8	Voltage measurement in the plate in function of the magnetic field strength and direction [81].	152
11.9	Coriolis Effect used for gyroscope [81].	152
11.10	Gyroscope principle [81].	153
11.11	NED and BODY frames [49].	154
11.12	Accelerometer set in different static positions for calibration measurements.	156
11.13	Magneto Software used for accelerometer calibration.	157
11.14	Calibrated vs uncalibrated accelerometer data.	157
11.15	Soft and Hard iron effects on magnetometer readings.	158
11.16	Calibration matrix A and vector B generation with Magneto.	159
11.17	Magneto results for calibrated magnetometer data.	159

11.18	Calibrated vs uncalibrated magnetometer data.	160
11.19	Sensor with and without housing.	161
12.1	CCC and CSC families [68]	163
12.2	Dubins curve properties.	164
12.3	Well trajectory with arbitrary targets.	168
12.4	Characteristics of the curved sections.	169
12.5	Characteristics of the straight section.	169
12.6	Inclination for the curved and straight section, respectively.	170
12.7	Azimuth calculated from a point's tangent vector in the xy plane.	171
13.1	Set up top drive and hoisting motor functional test.	173
13.2	Experimental set up azimuth control system functional test.	174
13.3	Experimental set up. 15 cm of displacement is marked on the floor.	176
13.4	Roll test conducted after combined bending test.	176
13.5	Twist off experimental set up.	177
13.6	Drill pipe twist off.	178
13.7	Rod twist off test set up.	179
13.8	Buckled drill pipe.	180
13.9	Test cylinder.	182
13.10	Mixing of cement.	183
13.11	RTR-4000 UCS Experimental set up.	184
13.12	Test samples after UCS experiment.	184
13.13	Installed diverter.	185
13.14	State of drill bits before testing.	187
13.15	State of drill bits after testing.	187
13.16	Wear and damage of drill bit 5 and 6, respectively.	188
13.17	Gauge ring.	189
13.18	Smooth and tortuous borehole quality.	191

13.19	Alibaba pilot hole bit.	193
13.20	Accelerometer noise with Alibaba pilot hole bit.	194
13.21	Accelerometer noise with Lyng bit.	194
13.22	Results of sensor card test along positive y-axis.	199
13.23	Measured horizontal displacement of 12.5 cm when rock sample is tilted on the side.	200
13.24	Planned and drilled well trajectory.	201
13.25	Autonomous states differentiated by trends in WOB and ROP.	202
13.26	Rotational velocity for drill vertical state.	203
13.27	WOB for drill vertical state.	203
13.28	ROP for drill vertical state.	203
13.29	Torque for drill vertical state.	204
13.30	Orientation of BHA for target intersection state.	205
13.31	Rotational velocity for target intersection state.	205
13.32	WOB for target intersection state.	205
13.33	ROP for target intersection state.	206
13.34	Torque for target intersection state.	206
15.1	Rig alignment.	213
15.2	Alignment plates	213
15.3	One of two flat sides marked in red.	215
15.4	Copper paste and set screw.	215
15.5	New welded threads in the universal joint.	216
15.6	Wear on different components.	216
15.7	Improved wear plate design.	217
15.8	Drill pipe connected to hydraulic swivel.	217
15.9	Water flowing through safety outlet.	218
15.10	Worn drill chuck tool.	219
15.11	Old drill chuck disassembled for cleaning.	219

15.12	Rod twist off during drilling.	220
15.13	Drill bit intervention.	221
15.14	Position of the sensor card and cable in the BHA.	221
15.15	Original and guillotine cut sensor card.	222
15.16	Original and carpet knife trimmed cable.	222
15.17	Sensor card and cable covered in thin layer of epoxy.	223
15.18	Epoxy dispensing gun.	224
15.19	Epoxy sealing the sensor card and USB cable.	224
15.20	Soldered cable with protective shrinking tubes.	224
15.21	Water test.	225
15.22	Plasti Dip and URC200D coating on sensor card.	226
15.23	Micro USB connection secured with electrical tape.	226
15.24	Sensor card coated with Tec7 using the dispensing gun.	227
15.25	Improperly sealed sensor card with Epoxy.	227
15.26	Potting Compounds.	228
15.27	Back up solution.	228
15.28	Wrong load cell reading when no WOB is applied at static conditions.	229
15.29	How to enable that Matlab can receive data from other devices.	230
15.30	No data received by Simulink.	230
15.31	Simulink receives data.	231
17.1	Furniture board for rock positioning [50].	235
B.1	Bow Tie Analysis for an electrical shock event.	287
B.2	Bow Tie Analysis for a cement related event.	287
B.3	Bow Tie Analysis for a rock handling event.	288
C.1	Relationship between Re and f for settling particles in Newtonian fluids [22].	290

List of Tables

- 5.1 Five levels of automation [15]. 21
- 6.1 Different values for K based on end condition [36]. 47
- 7.1 Drill bit specifications. 98
- 8.1 Design parameters. 102
- 8.2 Maximum allowable WOB for the drill pipe excluding the BHA. 110
- 8.3 Maximum allowable WOB for the drill string including the BHA. 110
- 8.4 Drill pipe twist off limit for several horizontal displacements. 112
- 8.5 Rod twist off limit. 112
- 8.6 Results of Hole Cleaning Calculations. 115
- 8.7 Pressure losses in different sections of the system. 117
- 8.8 Overview of Mechanical Limitations 118
- 8.9 Estimates of the hoisting motors power consumption at different RPM values. 119
- 8.10 Rig Power Consumption. 120
- 9.1 Risk matrix before risk mitigation 122
- 9.2 Risk matrix after risk mitigation 122
- 12.1 Input parameters for Dubins curve. 167
- 12.2 Unknown direction vectors of Dubins curve. 167

13.1 Top drive and hoisting motor functional testing results	173
13.2 Load cell functional test	174
13.3 Azimuth system functional test	175
13.4 Drill pipe twist off test results	178
13.5 Rod twist off test results	179
13.6 Results from UCS test	185
13.7 Five tests for drill bit analysis.	186
13.8 Qualitative results of drill bit wear.	187
13.9 Quantitative results of drill bit wear.	189
13.10 Sound levels of various drill bits.	190
13.11 Borehole qualities of various drill bits.	191
13.12 Rate of penetration of various drill bits.	192
13.13 Drilling optimization tests for the vertical section.	195
13.14 Drilling optimization tests for the deviated section.	196
13.15 Results of the drilling optimization tests for the vertical section.	196
13.16 Results of the drilling optimization tests for the deviated section.	198
14.1 Wage Estimate for students and employees.	209
14.2 Summary of all expenses related to the Drillbotics project. Exchange rate where 1 USD = 9.71 NOK.	210

Introduction

An increasing focus on the green shift in the oil and gas industry is forcing companies to become more efficient by reducing both their costs and carbon footprint. To ensure a stable supply of oil and gas, new innovative solutions are required that can reduce costs and carbon footprint per barrel produced. Automation of manual processes is an important contributor in achieving more efficient operations. With increased demand for energy, less profitable fields can also become profitable if the economic margins can be increased with automation in the industry.

OG21, a national technology strategy in Norway presents that 28% of the total costs of a well on the Norwegian Continental Shelf (NCS) are linked to drilling and well operations [87]. Out of these costs, around 35% are directly related to drilling rig rental. In addition, the drilling industry is known for being the major contributor of the total Non Productive Time (NPT) of the whole project. The NPT is often related to human error or technical issues [14]. Therefore, by automating human controlled processes, rig time and NPT can be significantly reduced, creating a big potential to reduce costs and improve efficiency.

The drilling industry already uses technology that enables autonomous processes such as directional drilling and tripping. In addition, systems already exist to perform real time data analysis from sensors while drilling. This allows drilling dysfunctions to be detected more quickly by leaving computers to monitor the drilling parameters instead of humans. Nevertheless, the biggest challenge seems to be the integration of various automated systems to function as a comprehensive system. Usually, drilling rigs are composed of components and systems from different suppliers, and getting multiple autonomous systems to cooperate will be an important focus in the near future [97].

Automation of offshore drilling operations also allows personnel to be relocated onshore. This is already in use in the industry today with several existing operation centers on land. As a result, a specialist can work on multiple field simultaneously [97]. The benefits from this implies increased efficiency and reduction of costs.

The safety for people and environment is also one of the driving factors in automat-

ing drilling operations. Manual operations and maintenance that have previously been performed by humans can be replaced by automated systems and robots. An example of protecting the personnel from heavy equipment is the use of iron roughnecks that can make tubular connections on the drill floor [86]. This implies that personnel can be moved out of the red zone on the drill floor, helping to increase both safety and efficiency.

In 2008, the organization Drilling System Automation Technical Section (DSATS) was formed by a number of Society of Petroleum Engineers (SPE) representatives with the aim of accelerating automation in the drilling industry [90]. Since then, the organization has researched various tools and systems that can automate different aspects of drilling operations. In 2014, DSATS first organized the Drillbotics[®] competition for university students to motivate and engage young people to come with innovative solutions in drilling automation and technology [90].

Norwegian University of Science and Technology (NTNU) has been an important contributor to Drillbotics. The university participated in the competition for the first time in 2016 and ended up in second place. It is worth noting that NTNU is the only university that has won the competition twice, both in 2017 and 2021. Unfortunately, in 2019 and 2020, it was not possible for NTNU to participate due to unforeseen circumstances.

The competition objectives for Drillbotics 2022 involves drilling a deviated well in a homogeneous sandstone with an autonomous system. With various given constraints, the miniature rig must be capable of drilling a maximum inclination of 30° and an azimuth change of 15° . According to the guidelines, a closed loop control of the rig in combination with downhole sensors is a requirement. The well needs to have a vertical section and a deviated section to hit multiple targets points that are given on the competition day. All teams are expected to stay within a US\$ 10 000 budget to cover expenses related to hardware, software and labor [90].

This master's thesis demonstrates the work and preparations prior to the Drillbotics competition to be held on the 16th of June 2022. The team already started the working on the project in the autumn of 2021 by submitting an initial design report for the first phase of the competition. During the spring semester of 2022, the team implemented new solutions to the rig and optimized the drilling performance through research, testing and analysis. Due to the scope of the project and the number of people involved, project management has been crucial to the success of the project. In addition, safety for people and environment has been the highest priority during all phases of the project.

Competition Objectives and Requirements

As the competition objectives have not been altered between phase I and II of the competition, this chapter is taken directly from the project report that was submitted as the specialization project fall 2021 [24].

The Drillbotics competition has been arranged by DSATS since 2014. Every year, each participating team has been challenged to drill through a rock sample given by DSATS on the competition day. In 2014, the main objective was to drill vertically through the rock sample as fast as possible. This challenge was first achieved in 2018 by the NTNU team. As soon as a team reached the goal, the guidelines for the competition were updated with new challenges. In 2019, directional drilling was introduced, which required only a change in inclination from the vertical. In 2020 and 2021 the challenge required a change in both inclination and azimuth while drilling, and this is also the main challenge for the competition this year.

In short version, the main objectives according to the guidelines in the 2022 Group B competition are as follows [90]:

- *Hit one or more targets at one or more vertical depth(s) and X/Y coordinates.*
- *No wellbore inclinations in excess of 30° from vertical, 15° change in azimuth, or 10" displacement.*

As previous years, the competition has different requirements related to automation of the drilling system [90]:

- *Drilling mode/survey mode switching must be automated.*
- *Steering requirements must be calculated autonomously.*
- *Directional surveying process must be entirely autonomous.*

- *Dogleg severity required to hit target(s), distance/direction to plan must be autonomously calculated at each survey station on the rig floor display.*

There are also several other mechanical requirements given by the guidelines. For the drill bit, a 1.5" bit will be provided by DSATS, but the team can also decide to design their own bit. The drill pipe that should be used in the competition is an aluminum or stainless steel pipe with an OD of 0.375" and length of 36". The rock sample provided by DSATS is a homogeneous sandstone with dimensions of 12" W x 24" L x 24" H, and the uniaxial compressive strength of the sample will be provided. Lastly, Drillbotics requires the teams to stay within a budget of US\$ 10 000 [90].

Organization

NTNU Drillbotics is a comprehensive project involving multiple people. A good organization structure is therefore required to ensure good teamwork, communication and efficient project development. The organization consists of a student core team assisted by supervisors and lab engineers.

In the following chapter, the team and supporting organization will be introduced. In addition, the delegation of roles and responsibilities are presented. Furthermore, the project management strategy used to maintain efficiency and progression is described.

3.1 Team

The team representing NTNU at the group B physical rig competition consist of four students. Three are from the Department of Geoscience and Petroleum (IGP) and study petroleum engineering with a specialization within drilling. The fourth member is studying cybernetics and belongs to the ITK. The multidisciplinary aspect allowed the members from different technical backgrounds to collaborate and share knowledge in a diverse working environment. The team members are presented in Figure 3.1.

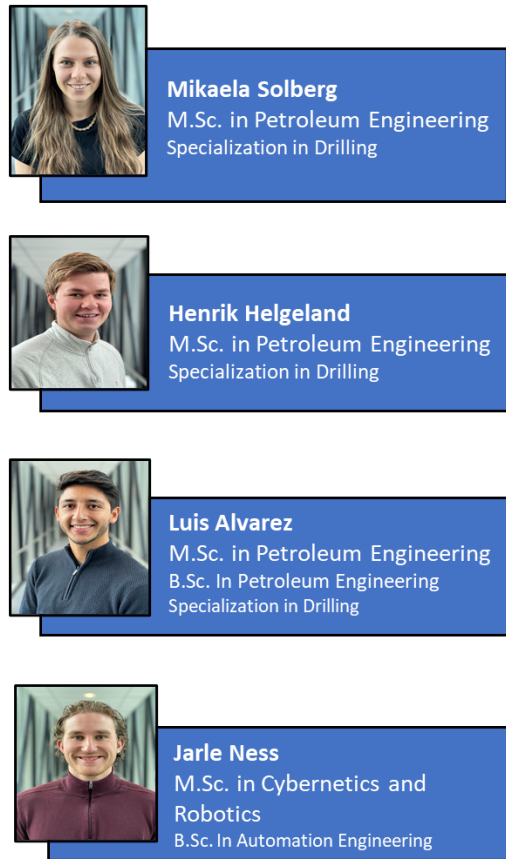


Figure 3.1: NTNU Drillbotics team members.

A support team consisting of both supervisors and lab engineers was formed to assist the core team. The organization structure is presented in Figure 3.2.

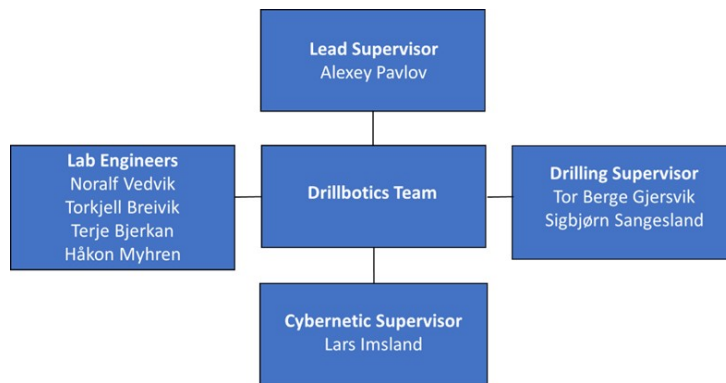


Figure 3.2: NTNU Drillbotics Organizational Structure.

There are four supervisors that are actively involved in the technical design and theoretical implementation of the system. They come from the IGP department and ITK department and are given the positions as lead supervisor, cybernetics supervisor and drilling supervisors.

The team also receives support from four lab engineers. Two senior engineers are respons-

ible for technical recommendations and suggestions for the rig design and maintenance. In addition, two lab engineers in the workshop are in charge of the practical work on the rig. These two are also in charge of the actual machining of pieces and equipment for the rig.

Both the supervisors and lab engineers have been part of the NTNU Drillbotics organization for many years, and provide the team with valuable feedback and lessons learned from previous experiences.

3.2 Roles and Responsibilities

Once the team was established, the team gathered to determine the most effective approach to proceed with the development of the project. Taking into account that this project is based on many years of previous experience, the team first decided to review earlier reports. After a better understanding of the scope of the project, the team identified the task that needed to be fulfilled to meet the competition objectives. With these in mind, roles and responsibilities could be assigned to the individual team members.

The roles and responsibilities shown in Figure 3.3 were allocated based on the individual's technical background, set of skills and personal preference. It was also possible for members to take on tasks that were somewhat outside their area of competence, which made it possible to gain a deeper understanding and expand their knowledge.

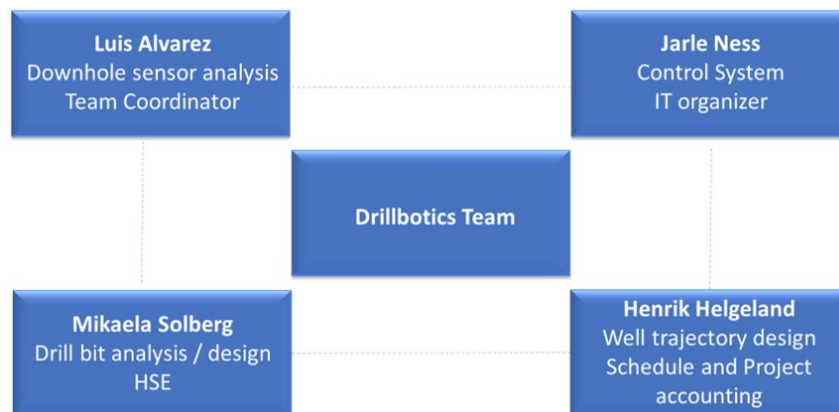


Figure 3.3: Drillbotics team roles.

The idea behind the designation of roles and responsibilities was to have a clear path and specific tasks that each member will work on. Following this approach, it was possible to work on different goals in parallel to ensure project efficiency and progress. In addition, there was a low threshold to ask for help, and the members were always available to help each other. This work ethic was not limited to the work within the core team, but it was also applied to the work carried out with the lab engineers and with the supervisors. As a result, an open working environment was obtained, where the exchange of new ideas

and collaboration between different parties was possible.

3.3 Project Management

The team used a project management scheme to organize the essential tasks to be performed throughout the project. A Gant diagram as shown in Figure 3.4, was best suited for this application as the tool allowed for a clear overview of the project.

			Number#	1	2	3	4	5	6	7	8
			Week	w9	w10	w11	w12	w13	w14	w15	w16
			Mon	28-Feb	7-Mar	14-Mar	21-Mar	28-Mar	4-Apr	11-Apr	18-Apr
			Fri	4-Mar	11-Mar	18-Mar	25-Mar	1-Apr	8-Apr	15-Apr	22-Apr
#	Activity	Progression	Responsible							Easter	
2	Testing	96%									
2.1	Rig alignment	90%	Luis								
2.2	Functioning test	98%									
	Hoisting RPM	100%	All								
	Top drive RPM	100%	Henrik								
	Azimuth RPM	100%	Mikaela & Henrik								
	Load cell WOB	90%	Henrik								
2.3	DP / rod	92%									
	Bending	100%	Mikaela & Henrik								
	Buckling	100%	Mikaela								
	Twist off	90%	Mikaela								
	Natural frequency	90%	Luis								

Figure 3.4: Gant diagram used for project management.

The Gant diagram allowed the tasks to be clearly defined and visualized. It also allowed task to have fixed deadlines and be allocated to a specific individual. A column was used to display the progression of each task with a percentage which gave the team members an indication of project development.

Under this methodology, the main objectives for the competition were divided into sub objectives or specific tasks, which facilitated the team to solve small problems separately. In addition, in case that one task proved to be more challenging than expected and it required more time, the Gant diagram provided a good overview of the current state of the project. Rearrangement of resources or changes in deadlines were therefore done without a problem.

In addition to the diagram, the team aimed to be in close contact while permitting other members to work efficiently. For this reason, a main office near the lab was used as the center of operation. Here, the meetings within the team were held, proposals for the project were discussed and the general plan for the competition with a review of the deadlines were checked every week.

Throughout the semester, some tasks were performed in small groups of two or three people. For this reason, an additional office was acquired to allow for collaboration without disturbing the remaining team members from performing individual tasks.

Microsoft Teams was used as a communication and sharing platform throughout the semester. This allowed remote collaboration and easy access to the group members at all times. Important documents could be organized and stored in a safe manner.

Finally, the tool used for writing the thesis was Overleaf. This open source online application was used because it allowed multiple users to work on the same document simultaneously. In addition, working with a tool online that is constantly updating itself with the latest changes made, will eliminate the problem of the obsolete copies.

3.4 Tracking of Drilling Activities

A lot of time will be spent in the lab to test the rig before the competition. Many students and technicians will be involved, and there will be up to four different operators of the rig at most. To organize drilling activities and make the analysis easier in retrospect, a form always had to be filled out prior to a drilling operation. Here, various drilling parameters and observations had to be filled in during and after the drilling operation. Using this method ensures that all drilling related activities are tracked and put into a system. In addition, every use of the rig has a cost, and this form ensures every test performed has a purpose. An example that illustrates the use of this procedure is shown in Figure 3.5, where the specific case was to test a new drill bit design in the testing and qualification phase of the project.

Test number: 07			
Team members present: Henrik and Mikaela			
Purpose of test	Drill bit analysis - ROP		
Output file	Run 07 - Bit 1 - Curved Section		Bit in gauge Y
Formation	Concrete B20, 3L/25kg		Bit wear Y
Rod / DP number	1 / 1		Bit damage N
Bit number	1		Twist-off N
Bit mass (before/after)	213.895/ 213.814	g	Buckling N
WOB	11/14	kg	Vibrations Y
RPM	850	rpm	Other issues N
Max top drive torque		Nm	General comments: Set screw came loose and stopped drilling at 17 cm below KOP. The lower stabilizer unscrewed.
Max azimuth torque	-	Nm	
Distance drilled	10 + 17	cm	
Time drilled	3 m 46 s 20 m 16 s	Min	
Average ROP	2.65 0.84	cm/min	
Hole quality	Smooth		

Figure 3.5: Example of form used for tracking of drilling activities.

HSE

The safety of personnel and environment is of highest importance in all operations and projects that involves engineering activities. The oil and gas industry is a world leader in Health, Safety and Environment (HSE). All operations, whether on land or offshore, take HSE very seriously and have it as a basis in everything that is carried out. The industry is considered very risky because of the use of powerful heavy equipment, high pressures, and highly flammable chemicals. If something should go wrong in the handling of these, it can have catastrophic consequences. For that reason, the industry has developed several regulations that all companies have to follow. The regulations cover both risk and function-based requirements [91].

Despite strong regulations, there are still frequent injuries in the industry. Almost 200 personal injuries on the Norwegian Continental Shelf (NCS) were reported to Petroleum Safety Authority Norway in 2020. Out of these, 25 were classified as serious injuries that will result in permanent damage. In addition, 11 injuries on constructions and maritime systems were reported in the same year [92]. This illustrates that the industry has a clear potential for improvement within HSE. A key in this work is to learn from already happened injuries and analyze how it can be avoided in the future.

Having good safety and HSE procedures is also very important for everyone involved in the Drillbotics project. The most basic measure is to facilitate and ensure that correct Personal Protective Equipment (PPE) is always used when required. In the beginning of the semester, all team members had to take a walk-through in the lab. The most important with this tour was to learn how to act in the lab and where to find fire extinguishers and emergency exits. Afterwards, an online course and mandatory questionnaire needed to be handed in and approved to get access to the lab.

It is also important to think safety in every single activity related to the Drillbotics project, even though it is not directly related. An example of this can be that the operator should not be in the lab and operate the drilling rig if he is tired or unfocused. It is important that everyone involved has a low threshold to report such incidents, so that accidents are avoided before they happen.

In the following chapter general theory about HSE will be presented. Furthermore, the different hazards present during construction, operation and maintenance of the Drillbotics rig will be identified and analyzed in detail.

4.1 Covid-19

The Covid-19 pandemic has been a continuous hazard that the team members always had to keep in mind throughout the year. The biggest consequence is if someone on the team or support staff should become ill, because it can then have impact on the progress of the project. At the beginning of the semester, guidelines and procedures were established that everyone involved had to follow. The most important is of course to avoid the spread of the virus, but action plans were also created in case anyone became infected with the virus. The Norwegian Institute of Public Health (NIPH) has published general advice that has always been followed to reduce the risk of infection within the team. The most important measures are as follows [48]:

- Keep the social distance of 1 meter.
- Avoid coughing or sneezing near each other.
- Everyone who feels sick must stay at home and take a quick test.
- Anyone who has the opportunity to be vaccinated should do so.
- Persons that are confirmed infected by Covid-19 must stay at home for 4 days.

If any of the people involved in the Drillbotics project deviated from the above advice, there was always a low threshold to report. In addition, several other actions were implemented by the team to be precautionary. To be able to always maintain the one meter distance, the team members have several offices at their disposal. As a measure to reduce droplet infection, personal PPE was distributed.

If someone should be unlucky enough to be infected with the virus, it is important that they stay home in isolation so that the rest of the team will hopefully stay healthy. The infected person can collaborate with the rest of the team via Microsoft Teams, if the person feels well enough. In this way, efficiency and progress in the project are ensured even if everyone is not present at the university.

Norwegian authorities have predicted that most residents will be infected by the virus this spring. For that reason, this has also already affected some of the members of Drillbotics. Due to thorough preparation with procedures and regulations, this has gone smoothly and has had little impact on the progress of the project. The most important has clearly been to limit the infection within the team when it first occurs. The reason for this is because the team depends on there always being someone present in the lab to avoid halting the project.

4.2 Potential Safety Hazards

The Drillbotics project poses a number of safety hazards. To ensure a high HSE standard, the team is required to identify and evaluate all the potential hazards that may be present before starting any kind of work. Such an approach will allow the team to make a plan and take the preventative measures needed to secure the workplace before, during and after an operation. The safety hazards associated with this project are ergonomic, mechanical, electrical and chemical hazards.

4.2.1 Ergonomic hazards

Ergonomic hazards refer to activities that cause physical stress or strain on the musculo-skeletal system. Among these are repetitive work, poor posture and manual handling such as heavy lifting and forceful movement of equipment. Individuals who do not perform these tasks with care may suffer injuries such as fatigue, muscle strains and lower back pains [30].

4.2.2 Mechanical hazards

Mechanical hazards are related to powered or manually operated equipment that can cause harm. The powered components on the miniature drilling rig consist of the top assembly, drill string, rod and drill bit. The direction of motion of these components is shown in Figure 4.1. Mechanical injuries related to entanglement, friction and impact from ejected components may arise if this equipment is operated unsafely. Wounds due to pinching and crushing, on the other hand, may occur if manual handling of the framework alignment bolts, protective glass and jack trolley is performed incorrectly [45].

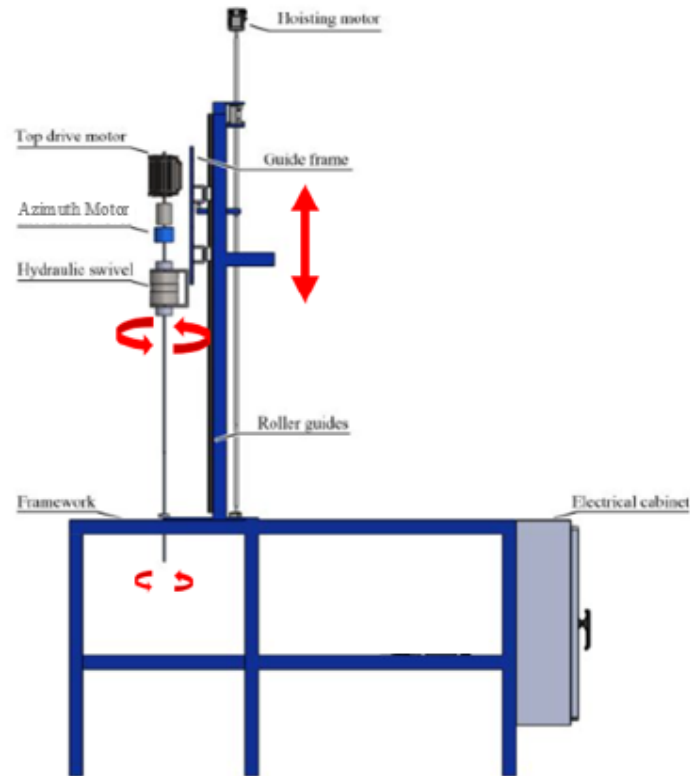


Figure 4.1: Motion of powered components on the drilling rig.

4.2.3 Electrical hazards

Electrical hazards are created by exposure to electricity and arise during operations and work-overs of electrical systems. The most critical threat occurs when electrical equipment is improperly installed and maintained. Such a fault can lead to equipment damage from short circuits and fires, as well as personal injuries from electrical shocks and burns [107].

4.2.4 Chemical hazards

Chemical hazards refer to substances that pose potential health risks. The drilling fluid is a common hazard in the oil and gas industry due to its composition. However, it will not inflict any dangers on the team, equipment or environment since tap water is used. Instead, the chemical hazards in this project are associated with cement during rock sample production and rock cuttings management. The cement dust can cause allergic reactions, skin irritation, respiratory complications and chemical burns to the eyes [56].

4.3 Protective Measures to Mitigate Safety Hazards

The team implemented various protective measures to mitigate the safety hazards associated with the Drillbotics project and to maintain a safe and healthy work environment. The controls were determined with respect to the safety decision hierarchy shown in Figure 4.2. Protective measures in the higher hierarchy levels were prioritized and exhausted before considering lower levels as they are more effective in mitigating the safety hazard. Finally, the effects of the controls were examined to ensure they complied with the HSE regulations [39].

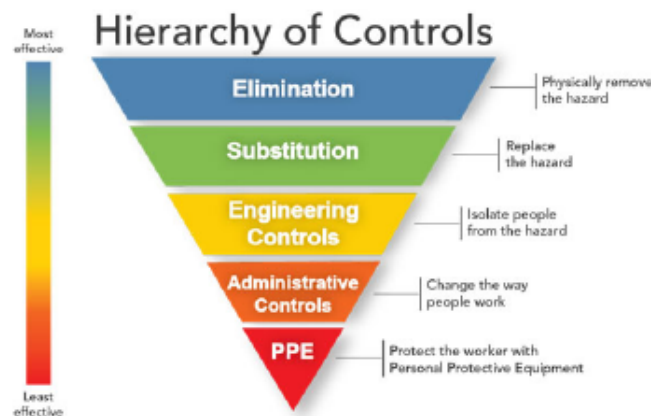


Figure 4.2: Safety decision hierarchy used to determine protective measures [39].

The protective measures implemented for the general project and more specifically against the ergonomic, mechanical, electrical and chemical hazards are presented in the following subsections.

4.3.1 General Protective Measures

Everyone involved in the project has a stop work authority. This requires all work to be ceased immediately if an individual feels a condition or behaviour is unsafe and poses a danger to the personnel, equipment or environment. The hazard must be investigated and corrected before any work is to continue. Using the stop work authority to prevent safety hazards is both responsible and effective [2].

The essential PPE is worn by personnel to protect and minimize the exposure to the projects potential safety hazards. Safety glasses is mandatory in the workshop at all times. Additional PPE is dependent on the ongoing work. Safety shoes and protective impact gloves are for example used when manoeuvring the large rock sample, while dust masks, disposable gloves and overalls must be worn when handling cement and rock cuttings. The correct PPE worn by the team during cementing and rig maintenance is shown in Figure 4.3.

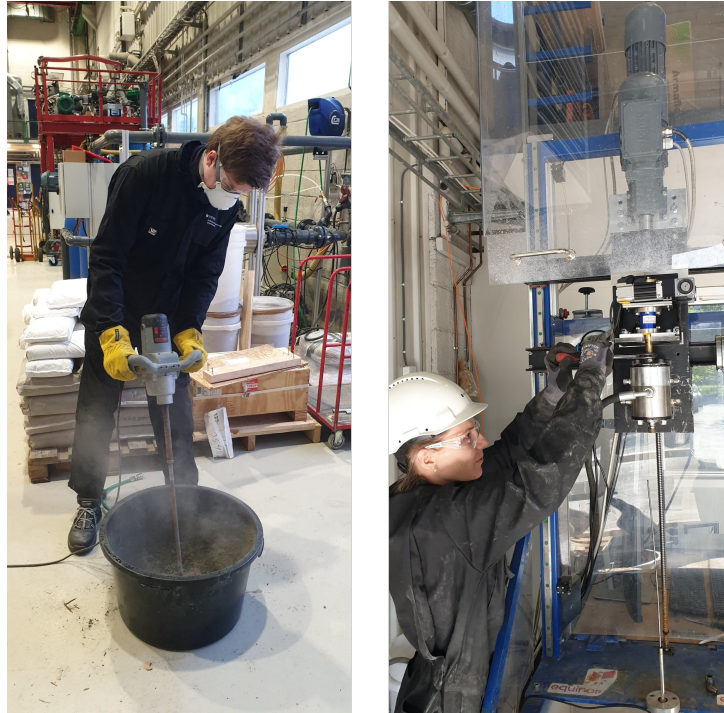


Figure 4.3: Correct PPE during cementing and rig maintenance.

If other large scale operations are occurring in the workshop, further compulsory PPE such as helmets and hearing protection is displayed on the safety board. The workshop's safety board is shown in Figure 4.4.



Figure 4.4: Safety Board.

Personnel are prohibited from wearing loose clothing and long hair must always be tied back. This is a precaution taken against injuries related to entanglement in rig components.

4.3.2 Ergonomic Protective Measures

The team will use a hydraulic jack trolley to transport the large and heavy rock sample to mitigate ergonomic-related injuries. However, fine-tuning the rock sample beneath the drill floor is sometimes necessary. In such cases, the correct lifting technique and posture

are required. Each team member is responsible for assisting and correcting an individual if this is not performed correctly. The same applies when lifting the heavy acrylic protective glass during rig maintenance.

4.3.3 Mechanical Protective Measures

The protective measures used to mitigate the mechanical hazards on the rig include the protective cabinet, drilling constraints and emergency stop switch.

The protective cabinet shown in Figure 4.5 is made of acrylic glass and consists of two sections. The upper section encases the mechanical rig components above the drill floor and can be lifted for rig maintenance. Meanwhile, the lower section surrounds the rock sample and drill string below the drill floor. It can be opened on one side to insert the rock sample.



Figure 4.5: Protective cabinet encasing the drilling rig.

Both sections of the protective cabinet must remain closed during operations to serve as a safety barrier between the rig and personnel. The upper part is held down by its own weight, while the lower section is equipped with a lock. These protective measures eliminate the team's direct exposure towards hazards related to the moving rig components, drilling fluid and rock cuttings.

To further mitigate the mechanical hazards, the team must ensure the rig is kept within its operational limits while drilling. Drilling constraints such as maximum allowable Weight On Bit (WOB), torque and hydraulic pressure have been calculated with a safety factor and added to the control script. This will reduce the vibrations and risk of drill string failures such as buckling, twist off and burst which can send projectiles and cause impact injuries.

The emergency stop switch shown in Figure 4.6 is a safety mechanism used to terminate all operations instantly by breaking the electric circuit to the rig components. One team member must always be near the switch, and there is a low threshold to press it if a situation is perceived as unsafe. Since the emergency stop switch is a critical element in preventing mechanical safety hazards, it is large in size and placed in an easily accessible location by the electrical cabinet.



Figure 4.6: Emergency stop switch.

4.3.4 Electrical Protective Measures

The drilling rig consists of multiple electrical components that present electrical fire hazards. As a protective measure, only qualified personnel are allowed to install, modify and maintain the complex electrical system. In the event of a fire, the team is aware of the proper procedures and know where to find and how to use the various types of fire hoses and fire extinguishers. The electrical cabinet is positioned on the opposite end of the hydraulic system on the miniature drilling rig as an additional control to mitigate the electrical hazards.

4.3.5 Chemical Protective Measures

Cement during the production of rock samples and management of rock cuttings poses a health risk to the team. As mentioned, a general protective measure against the exposure to cement dust during these operations is wearing the proper PPE such as overalls, dust masks and disposable gloves. The team also designed and implemented a diverter to

further mitigate the chemical hazards associated with this project. The diverter eliminates the team's direct contact with the return fluid and rock cuttings by diverting them in a controlled manner from the drilling site and directly to the drain. Additional benefits with the diverter are that it reduces the time spent cleaning the workshop floor and prevents slips and falls due to wet surfaces.

4.4 HSE Learnings

The key to improving HSE is to document and analyze unsafe situations related to the project. Reviewing these occurrences is a great way to learn and determine what procedures are working and what methods need to be implemented or reconsidered to increase the overall safety.

The team created safety cards to register unsafe acts, unsafe conditions and general safety observations that may lead to incidents if ignored over a long period of time. The observation, the action taken due to the observation and the learning outcome must be registered. An example of an incident that occurred during rig maintenance is shown in Figure 4.7. These cards are all stored in a large excel bank which allows the team to easily access the information and avoid similar situations.



 Drillbotics 2022 Safety Card 	
Date: 07.02.22	Observers: Henrik & Mikaela
Safety observation	<input type="checkbox"/> Planning
PPE	<input type="checkbox"/> Procedures <input checked="" type="checkbox"/>
Tools and equipment	<input type="checkbox"/> Unaware <input checked="" type="checkbox"/>
Untidy workplace	<input type="checkbox"/> Body posture
Communication	<input checked="" type="checkbox"/> Other <input type="checkbox"/>
What did you observe? Drill pipe buckled while the team was working on the rig. It happened because the hoisting motor was on without knowing about it. The protective glass was in upright position, could have caused injury to people.	
What action did you take? The people stepped back, took the protective glass down and released the tension in the drill pipe by hoisting upwards. Then all components were removed carefully. No damage on other components except drill pipe and rod.	
Learning outcome Always turn off all motors when doing maintenance on the rig. Reduce the amount of people around the rig to avoid misunderstandings between the operators.	

Figure 4.7: Safety card example from a real incident.

Human Factors

In one way or another, humans will always be involved in automated complex engineering projects. However, the degree of involvement will vary greatly depending on the need and scope of the system. If a system is completely dependent on humans to function optimally, the probability of failure over time is very high. This can be justified knowing that when humans are put to monitor systems, it often leads to errors due to deviant behavior. In a situation like this, humans tend to make unwise decisions that lead to failure. In addition, a human's ability to make decisions can also be influenced by external factors, which in some cases also can be the origin of the failure [24].

With the constant advancements in complex engineering technology, human interaction concerns become increasingly relevant in today's industry. As the tasks become more and more complex, those that are suitable for it should be allocated to automation [90]. This chapter will cover basic theory about automation in general and the importance of human factors in automated systems. Furthermore, human factors in the oil and gas industry will be presented. In the end, the implementation of human factors in the Drillbotics 2022 rig is discussed.

5.1 Human Factors Theory

High demands are placed on systems that must be both safe, efficient, and reliable. The constant technological development has made it possible for humans to be replaced by machines to automate processes. Autonomy is defined as the capability of a system to perform decisions in processes and that works independently of humans or external systems [26].

The degree of autonomy in a system varies from manual human control to fully autonomous. It is common to divide the degree of autonomy into different levels, as presented in Table 5.1. The table describes the roles of the operator for the corresponding level of automation. As the automation increases, the human plays less of a role and the com-

puter has more or less all responsibility. At the stage where the operator is considered in the loop means that the human still has a contributing role, and out of the loop means that the system operates fully without human interaction [26].

Table 5.1: Five levels of automation [15].

Level	Automation	Operator	System
1	No automation	All operations	Warns, protects
2	Limited support	Controls "In-the-loop"	Guides, supports
3	Tactical, monitors	Involved - continually monitors "On-the loop"	Controls within well-defined boundaries
4	Automated support Strategic	"Out -of-loop" interruption-determined, prompted by the system	Operates independently, but can hand back control
5	Autonomous	Fully "out-of-loop"	Operates independently - switches to safe state itself

Several of the previous mentioned levels can be used in one and the same system. For example, data collection, analysis and the decision making implementation part of a system may require different degrees of autonomy [15].

Both the constraints and advantages of human factors must be taken into account to determine the most suitable level of automation in any system.

One definition of human factors is "the scientific discipline concerned with the understanding of interactions among humans and other elements of a system in order to optimize human well-being and overall system performance" [26].

Paul Fitts was a psychologist that wrote a set of elements which described the relationship between computers and humans [11]. Although Fitts list dates back to over 70 years ago, it is possible to draw parallels and find points that are also relevant today. "Ability to handle highly complex operations, i.e to do many different things at once" is one of the points that is still highly relevant. In the past and in the foreseeable future, computers will always be able to handle complex operations better than humans, and Fitts predicted this already 70 years ago. Figure 5.1 presents the original Fitts list.

Humans appear to surpass present-day machines in respect to the following:	Present-day machines appear to surpass humans in respect to the following:
1. Ability to detect a small amount of visual or acoustic energy	7. Ability to respond quickly to control signals and to apply great force smoothly and precisely
2. Ability to perceive patterns of light or sound	8. Ability to perform repetitive, routine tasks
3. Ability to improvise and use flexible procedures	9. Ability to store information briefly and then to erase it completely
4. Ability to store very large amounts of information for long periods and to recall relevant facts at the appropriate time	10. Ability to reason deductively, including computational ability
5. Ability to reason inductively	11. Ability to handle highly complex operations, i.e. to do many different things at once
6. Ability to exercise judgment	

Figure 5.1: Original Fitts list [11].

The validity of Fitts list today has been questioned by critics due to the long time that has passed since it was published. To further analyze this, two surveys were in 2015 conducted that addressed the question of whether computers surpass humans or vice versa. The surveys addressed the same question for all the elements in Fitts list and the results are shown in Figure 5.2.

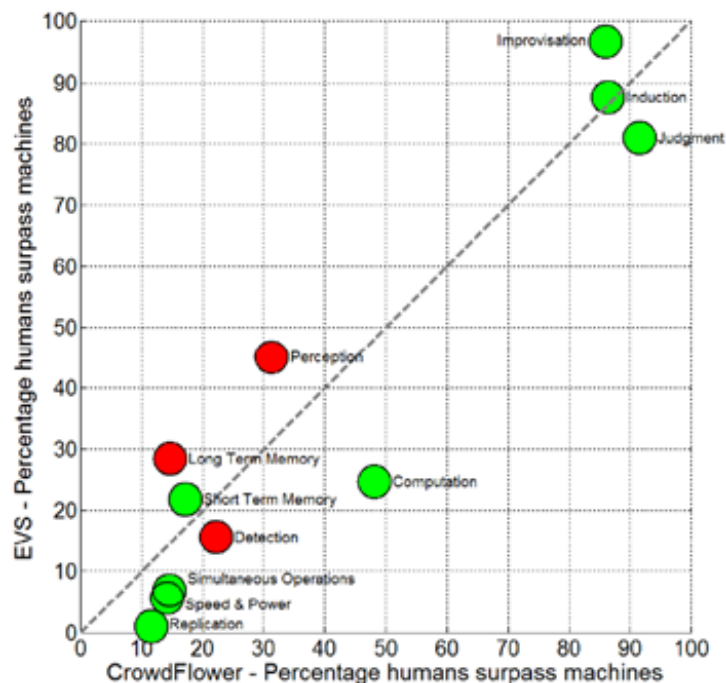


Figure 5.2: Present day survey results of Fitts list [11].

From the result it appears that there is not a full correspondence with the original Fitts list. The results illustrate that computers today also outcompete humans on long term memory, perception and detection. This is due to several reasons, but the most important is due to the rapid technological advancements that have taken place recently within storage capacity and artificial intelligence [11]. Overall, the results clearly show that computer machines surpass people at 8 out of 11 points.

Considering the above results and statistics in which human factors account for the majority of the incidents, it appears that automation has the potential to minimize human errors. While the use of automation is a useful tool, it does not always provide the desired outcomes. It may in some cases even contribute to additional human performance problems. These drawbacks are commonly referred to as the “Ironies of Automation” [1].

The design induced error is regarded as one of the main ironies in automation and it suggests that it is impossible to completely eliminate the human error in any automated system. This is due to the fact that the designer is human as well. In the efforts to eliminate the potential manual human errors, new errors in the automated system are created. The human imperfections will therefore always remain in the automated system to some degree.

Another irony stems from the shift of the human role in the system. As the system becomes automated, the human responsibility changes from executing an operation to monitoring it and ensuring it functions correctly. Therefore, it is of the highest importance that the operator maintains complete Situational Awareness (SA) to prevent system failure. This is essential for the operator to safely and efficiently regain control of the system if it starts to behave inconsistently.

Endsley classified situational awareness into three distinct stages. The first stage refers to a human who can recognize the system’s current state and perceive what is occurring. The second stage relates to the comprehension of the system through interpretation and evaluation. Lastly, the final stage of situational awareness relates to predicting future states of the system by extracting information and extrapolating data forward in time. The operators of automated systems must receive tailored training in order to ensure the highest stages of situation awareness is reached. This is necessary to avoid catastrophic consequences [26].

In conclusion, choosing a suitable level of autonomy for a system requires careful consideration. The ability to understand human factors becomes increasingly important as the design becomes more autonomous. Thus, the challenge is to create a safe, reliable and efficient system of high autonomy while the operator maintains a high stage of situational awareness [1].

5.2 Automation and Human Factors in the Drilling Industry

Among the most important advantages that automated systems can offer in the oil and gas industry is the improvement of operations, making them more efficient and reducing risks. In terms of cost reduction, it is important to highlight that the most expensive and dangerous operation in the oil and gas industry is drilling. For this reason, great efforts have been performed to apply automation in the drilling industry.

5.2.1 Advantages of Automation in the Drilling Industry

There are several domains where the application of automation can improve processes in the drilling industry. One of the most relevant is the replacement of heavy duty work done by people, generally in dangerous zones such as the drill floor, and replacing them with machines and automated systems. This change will increase the productivity of the process, since machines can withstand heavier loads, longer working hours and are more precise and reliable. In addition, by taking humans away from the red zones, the process becomes safer [6].

The transfer of tasks from humans to machines also allows individuals to take on a monitoring role rather than an operating role. This frees up time and allows the human to focus on more rewarding tasks [6].

Furthermore, given that automated processes diminish the direct involvement of humans into the operations, especially in repetitious, tedious labors, the human error is also reduced [6]. The human factor plays an important role in the generation of Non Productive Time (NPT) which normally accounts for 15 % of the total drilling time [33]. Therefore, when the human involvement is reduced, its repercussions on NPT is also reduced and the efficiency increases.

Another beneficial aspect of the application of automation in drilling is the opportunity for accurate surveillance and prediction of future events. If the parameters of drilling operations can be monitored in real life and modelled into standard conditions, then a projected behaviour of these variables can be predicted [105]. If in any case, these parameters start to deviate from the anticipated behaviour, then it is possible to identify upcoming complications such as stuck pipe or kick events on beforehand. Since the detection of these problems is done at an early stage, preventive actions can be taken, avoiding the problem itself before it happens. This results in a preventive culture, where the problem is identified and avoided instead of a current corrective culture, where the event is solved after it has manifested. This change in culture can contribute to the reduction of time, cost and risk [105].

5.2.2 Implementation of Automated Systems with Respect to Human Factors

In order to apply automated processes into the oil industry, it is essential to get a proper insight into the human-machine interaction and the role of human factors in automation. Thus, a review of procedures, experiences and learnings from past incidents is beneficial.

Following a thorough report prepared by Sintef about automation in other industries, it is possible to observe that the aviation industry is one of the most matured in this subject, given their approach of implementing automation in a gradual and safe way. Their strategy to achieve this was to involve the user or operator at very early stages

of the design and implementation of automated systems, making these processes user-centered. In addition, they continuously trained their personnel to regain control over the operations at any point of the process, even if the situation is out of normal circumstances. Thus, situational awareness is maintained and a safe operation is ensured [26]. Moreover, the change between manual and automated control should be facilitated and solicited by the system itself [47].

Another useful learning is that the user needs to maintain the situational awareness throughout the whole process. If this is not guaranteed, the operator can be overconfident with the autonomous system, which can lead to miss-perception of risk and subsequently accidents. A relevant example for this happened in the Gulf of Mexico in 2010 with the Macondo blow out. In this catastrophe, a "general miss-understanding of critical signals and mental models by the operators in charge" were identified as root source for the event [16]. In addition, in the report by Sintef it was stated that it is possible to correlate the level of situational awareness and the generation of accidents in the drilling industry. The lower the level of situational awareness in the operators, the greater the number or related events [26]. Among the reasons for low situational awareness in drilling operations are fatigue and high stress [4].

In a discussion presented by Iversen, it is stated how important it is for the people involved in a process to have a complete comprehension of the autonomous operation. This was proved by preparing an experiment where researchers gave a simulated semi-autonomous system for drilling to the drilling crew. Due to the competence gap of the personnel regarding automation, the operators fell into the denominated "mode confusion", where they did not completely comprehend what to expect from the automated system. This may induce the personnel involved into committing errors and making wrong choices [8].

The Human Machine Interface (HMI) is another element that is relevant for a safe and satisfactory application of automation into a process. This interface provides the inter-communication that exists between the signals provided by the system and the perception, understanding and interaction that the user has with them [17]. In order for the operator to make decisions in a efficient way, it is critical that the information provided by the HMI is effective and easy to understand and interpret [47].

The use of visual and auditory signals and alarms is another exemplification of the aforementioned communication between the automated system and the user [17]. Searching to help the operators to make quick, effective and practical decisions, it is essential for the operator to be fully prepared in the detection and comprehension of alarms, as well as their significance in the system [17]. On the other side, the excessive use of alarms can lead to accidents due to misinterpretation [20].

5.3 Human Factors in the Drillbotics Competition

As discussed, human factors play a key role in the successful and safe implementation of an automated process to the drilling operations. Therefore, the team has implemented some of the lessons learned and good practices on how to apply human factors into the automated system of the drilling rig for the Drillbotics competition. A thorough discussion about this application and further details will be presented in this section.

5.3.1 Improve Situational Awareness

One method used to account for human factors in the automated system is to improve the situational awareness of both the designers and operators of the automated process. As a result, the team proposed a series of strategies to improve situational awareness in every member of the team, as well as integrating everyone into a more active role in the design, implementation and operation of the automated drilling control. Following, these strategies will be explained.

5.3.1.1 Situational Awareness Training

The first strategy to improve the situational awareness of the team was to take a series of training sessions for both the petroleum engineers in coding and programming, as well as some basic drilling training for the cybernetics student.

On one hand, the petroleum engineering students got involved in the control system from an early stage of the development of the project. Even though the petroleum students did not design the control system, it was important to understand the algorithms and coding behind the system. In order to achieve this, the petroleum engineering students assisted to several workshops and training sessions organized by the faculty of cybernetics, and by the hardware and software suppliers of the different rig components.

Additionally, the whole team showed a commitment to better understand not only the software to control the rig, but also the hardware itself. As a result, the team gained a better understanding of the relationship between the hardware and software as well as the communication protocols used.

On the other hand, the drilling student taught the cybernetics student the main principles of drilling and how they are applied to the miniature rig and competition. Close collaboration and continuous communication was necessary between the team members in order for the cybernetics student to successfully design and improve the autonomous control system. Consequently, the team ensured the control system was user friendly and compliant with the drilling requirements of the competition.

As a result, the synergy created in the group offered an opportunity for all members to have

open conversations to solve doubts or provide suggestions. This allowed close collaboration and support throughout the different stages of the system design and implementation. In addition, all operators were fully aware of the system's behaviour and also understood which components were most likely to malfunction, as well as possible solutions to solve the problem.

5.3.1.2 Computer screen positioning arm

Another useful strategy to improve situational awareness of the system was to upgrade the rig with an adjustable positioning arm for better placement of the computer screens. As seen in Figure 5.3, last year's set up was not ideal [9].



Figure 5.3: Computer screen setup NTNU Drillbotics 2021.

From the image, it can be seen that the second monitor is positioned at an angle from the main screen. This makes it difficult and inconvenient to consult all the information as the operator can't see both screens simultaneously. As a result, the operator may lose valuable information that can in worst case lead to damage of the system or environment. As an improvement for this situation, an adjustable arm was installed for the second monitor to make both screens visible to the operator. This enabled the operator to inspect both screens simultaneously. The new implemented set up is shown in Figure 5.4:



Figure 5.4: Adjustable arm for second monitor

5.3.1.3 Distance to Next Target Point

A further idea implemented to help the operator to keep a high level of awareness during drilling operations is to introduce a section in the GUI where the distance to the next target points is shown at all times. This can be seen on Figure 5.5:

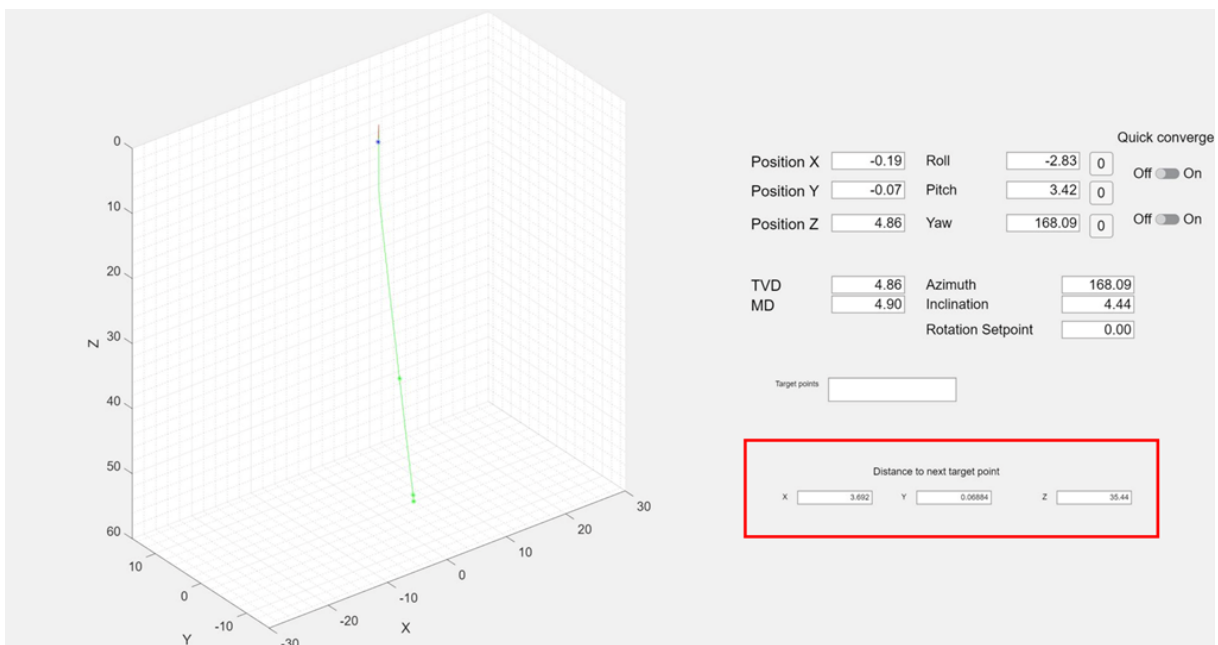


Figure 5.5: GUI with the distance to next target point marked with a red square.

This new feature allows the operator to keep better track of target objectives. This is

important because hitting the target points is an essential part of this project.

5.3.2 Bow Tie Risk Assessment

The bow tie risk assessment is a methodology used to easily visualize the cause and effects of a potential risk [99]. It is commonly used in the oil and gas industry to produce safe procedures and action plans which will protect the company's personnel, reputation, assets and environment. The bow tie diagram with its characteristic shape is presented in Figure 5.6:



Figure 5.6: Bow tie analysis diagram [99].

The diagram is divided into three main sections. The prevention segment which is composed of potential causes and control measures, the hazardous event, and the recovery segment consisting of recovery measures and potential outcomes. These are shown from left to right in the diagram and will be described below.

5.3.2.1 Bow Tie Sections

At first, a risk that is considered a potential threat to the project must be identified. The next step is to pinpoint the potential causes that can result in this hazardous event. In order to reduce the risk of these threats evolving, control measures are introduced as preventive barriers. In the case that these prevention methods do not work, it is important to reduce the impact of the hazardous event. This is done by establishing recovery measures. These will protect the system from negative potential outcomes such as equipment damage or personnel injuries.

Several parameters are important to take into consideration when applying the bow tie risk analysis. The first factor is that the bow tie should be performed by a group of people with different backgrounds and views. This will broaden the variety of mindsets used to identify, analyze and finally plan a prevention and recovery scheme for different hazardous scenarios.

A second aspect that is crucial for an effective bow tie analysis is to be explicit in the description of each section. This will allow for more detailed planning of both preventive and recovery methods which will increase the situational awareness of the individuals involved.

5.3.2.2 Bow Tie Analysis for Drillbotics

The team worked together and performed multiple bow tie analysis for different hazardous events identified in regard to the miniature rig. Four major risks were identified. An example of the team’s bow tie analysis for a projectile hazard is shown in Figure 5.7. The remaining diagrams are found in Appendix B.

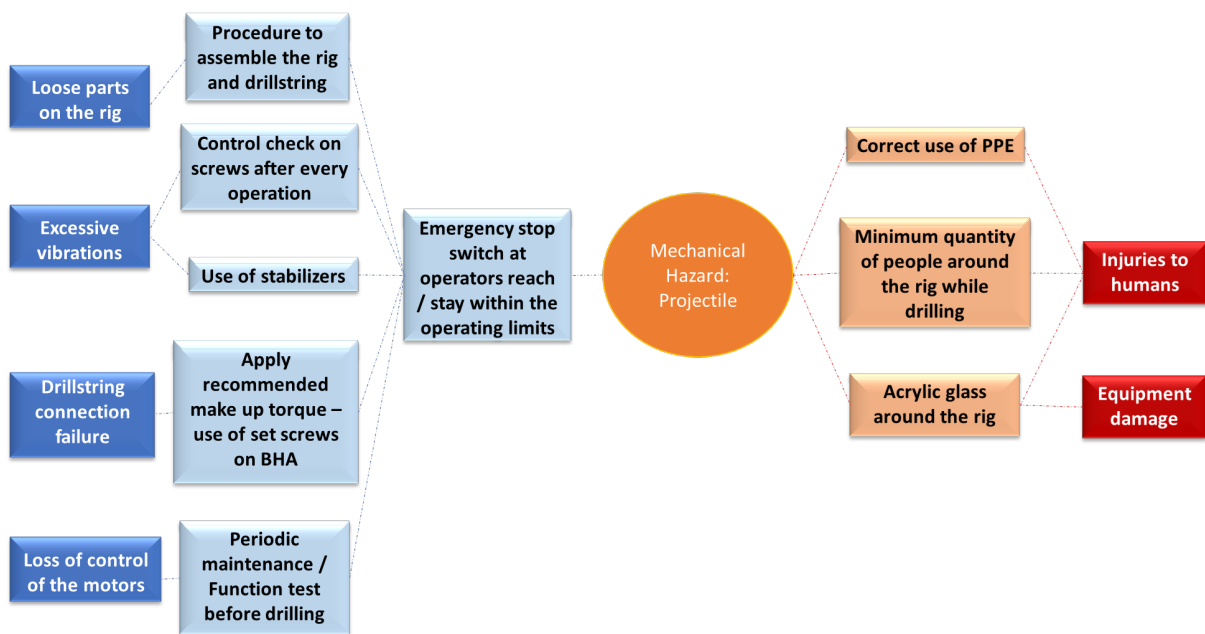


Figure 5.7: Bow tie analysis for a projectile event.

Getting familiar with this risk assessment tool was incredibly beneficial for the team to get a better understanding of the potential risks and to improve the situational awareness.

Theoretical Background

The theoretical research was performed in phase I of the competition. Therefore, the contents in this section will be similar to the project report that was submitted as the specialization project fall 2021 [24].

In this section, the theoretical background of the project will be reviewed and presented, as a mean to have a better understanding of the mathematical framework used for the correct selection of materials, equipment and parts to accomplish the design and implementation of the drilling rig.

6.1 Directional Drilling

As presented in the project guidelines, the target points given on the competition day will require the well to be directional. This means that there will be changes in inclination and azimuth to meet the objectives [90]. The use of directional drilling has been an innovative solution in the recent decades due to its versatility and applicability to solve complex drilling challenges. Among these challenges, there are [23]:

- *Drilling single wells to inaccessible areas.*
- *Drilling to connect multiple targets using the same well.*
- *Drilling of relief wells.*
- *Geo-steering.*
- *Drilling away / around problematic zone like salt domes.*
- *Drilling multiple wells from a single location offshore.*
- *Drill multiple wells from the same main wellbore.*

6.1.1 Types of Directional Wells

There are several factors and parameters in drilling that are highly dependable on the type of directional well. Some of these factors are the design of the drill string and BHA, as well as hole cleaning strategies with hydraulics and fluid additives. Different types of directional wells include [23]:

- *Extended Reach Drilling, ERD (horizontal section is 2 times or more the vertical section.)*
- *Conventional directional wells.*
- *High inclination wells (60° - 85°).*
- *Horizontal wells (85° - 115°).*

6.1.2 Well Path Geometry

The well path geometry is highly dependent on the characteristics mentioned in the sections above. As an example, some well path geometries are illustrated in Figure 6.1:

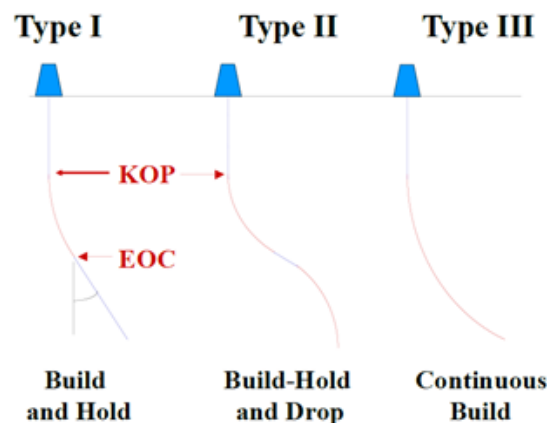


Figure 6.1: Types of well paths [23].

Following the previous figure, it is important to highlight that the team will design the rig so it can drill any type of well path, since the final target points will be disclosed only on the day of the competition. Nevertheless, efforts will be centered to prepare the system for a well path of type III.

6.1.3 Well Profile Terminology

There are some key parameters that describe the well path profile. The most important are presented in Figure 6.2.

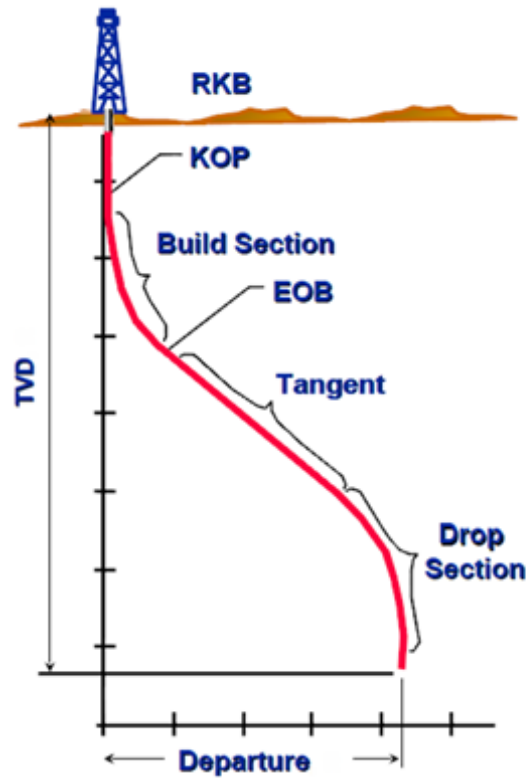


Figure 6.2: Deviated well terminology [23].

These parameters are explained in more detail [23]:

- *TVD: True Vertical Depth. distance between the reference point and the bit only in the vertical axis.*
- *MD: Measured Depth. Actual distance between the reference point and the bit.*
- *KOP: Kick Off Point. Point in the well where there is a build up in its inclination.*
- *Build Section. Section of a well where the wellpath has an increment in inclination.*
- *EOB: End of Build. Last point where the inclination is increased.*
- *Tangent. Section where the inclination is held.*
- *Drop Section. Part where the inclination is reduced.*

In order to locate any position downhole while drilling a directional well, a convention of coordinates has been widely used in the industry. In this framework, there are three axis $\{X,Y,Z\}$ represent the $\{N,E,D\}$ coordinates system, respectively. Here the axis denote the North component N, East component E, and Down component D, otherwise known as True Vertical Depth (TVD). Furthermore, the starting point of any well is at the origin $\{0,0,0\}$. Afterwards, any other position will be described as the distance from this origin on the tri-axial framework [23].

Since the competition guidelines state that the objectives may be within a certain inclination and azimuth [90], these terms need to be explained further with the help of Figure 6.3 [23]:

Azimuth: The angle between the well path and the North axis (true or magnetic) measured in the plane and clockwise from North [23]. This change will only affect the X and Y axis on the tri-axial system of coordinates, equivalent to the North and East components.

Inclination: The angle between a tangent of the current well path and a vertical plane through the reference point [23].

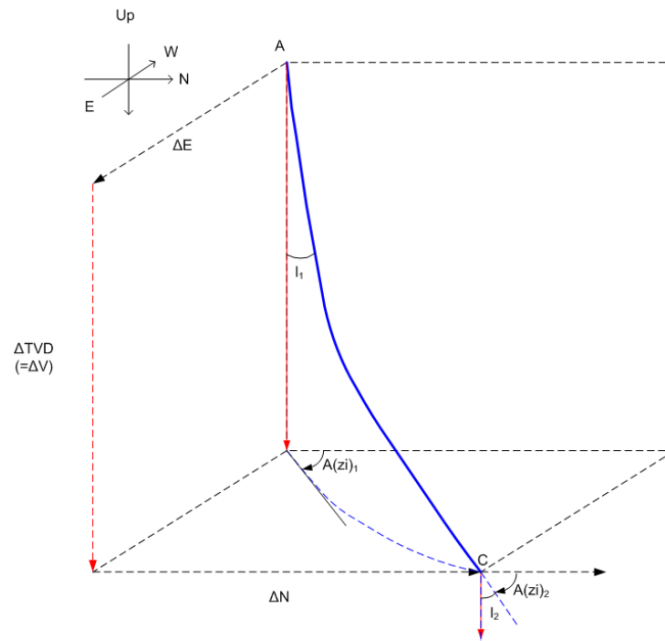


Figure 6.3: Inclination (I) and azimuth (A) [23].

A change in both azimuth and inclination implies a turn in a three-dimensional space, which results in a 3D well path. In drilling, such a change of direction in the well profile is called dogleg angle (ϕ), depicted in Figure 6.4. When this change in direction is normalized per curve length, it is known as Dogleg Severity (DLS) [$^{\circ}/m$] and can be obtained with the following equation [23]:

$$DLS = \frac{\phi}{CL} \quad (6.1)$$

Where $\phi[^{\circ}]$ is the dogleg angle and $CL[m]$ is the course length [23].

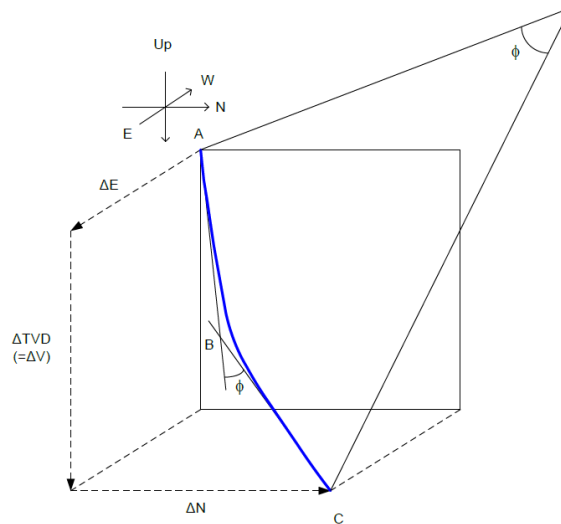


Figure 6.4: Dogleg Angle (ϕ) [23].

6.1.4 Survey Calculation Methods

In the drilling industry, it is possible to estimate the position of the well from the origin with the use of different survey methods. Furthermore, these methods are also important in the calculation of the dogleg angle. In the following section, the most important survey calculation methods will be described, from the least to the most accurate [23]:

Tangential method: This method assumes the wellbore is a straight line from the tangent of the lower survey point. This method is highly inaccurate because it ignores the upper survey point, as illustrated in Figure 6.5 [23].

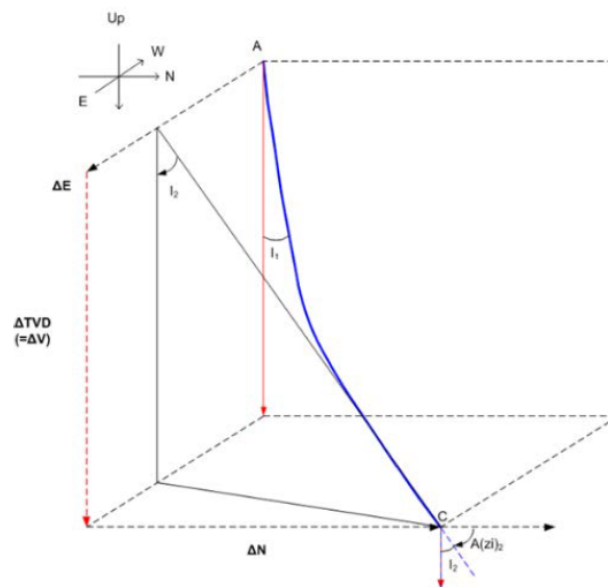


Figure 6.5: Tangential method [23].

Average angle method: Figure 6.6 shows this method uses a straight line to connect the upper and lower survey stations. It provides reasonable projections of the well path, as long as it does not have a high curvature or that the survey points are not far from each other [23].

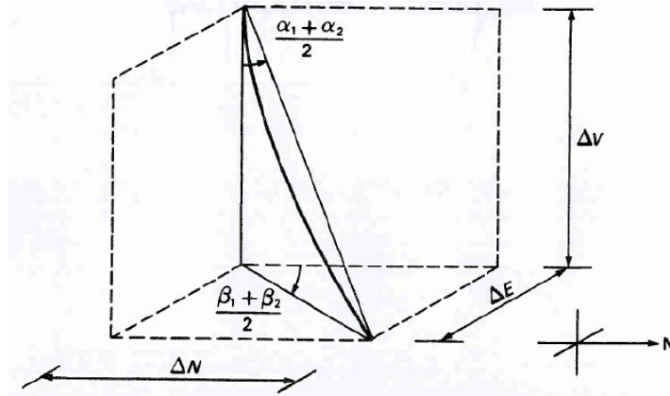


Figure 6.6: Average angle method [23].

Radius of curvature method: In Figure 6.7, it can be observed that the well path between two points is calculated with the use a cylindrical curvature [23].

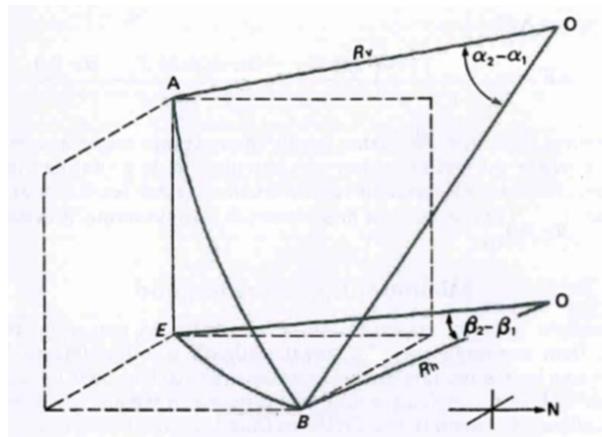


Figure 6.7: Radius of curvature [23].

The radius of the curvature $RC[m]$ is calculated using the angle AOB.

$$RC = \frac{180CL}{\pi(\alpha_2 - \alpha_1)} \quad (6.2)$$

Where $\alpha_1[^\circ]$ and $\alpha_2[^\circ]$ refer to the inclination at the first and the second survey point, respectively. This equation can be rearranged to obtain the course length $CL[m]$.

$$CL = \frac{RC\pi(\alpha_2 - \alpha_1)}{180} \quad (6.3)$$

Balanced tangential method: This method assumes the well path is approximated with two tangents of equal length from the upper and lower points of survey, as depicted in Figure 6.8 [23].

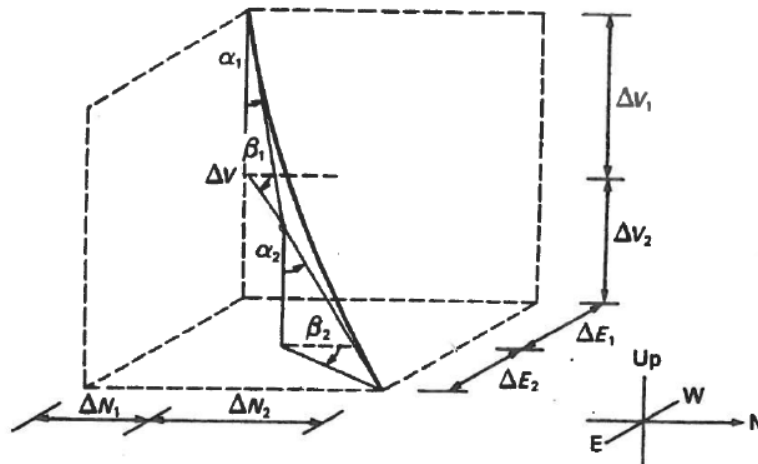


Figure 6.8: Balanced tangential method [23].

Minimum curvature method: This method is an improved version of the balanced tangential method, where the tangents are replaced with a circular arc to estimate the well path. The method is shown in Figure 6.9. The ratio factor F is used to apply this correction and is a function of the dogleg angle [23]. Since this method is considered to be the most accurate, the Drillbotics guidelines state that this survey method should be used for the competition.

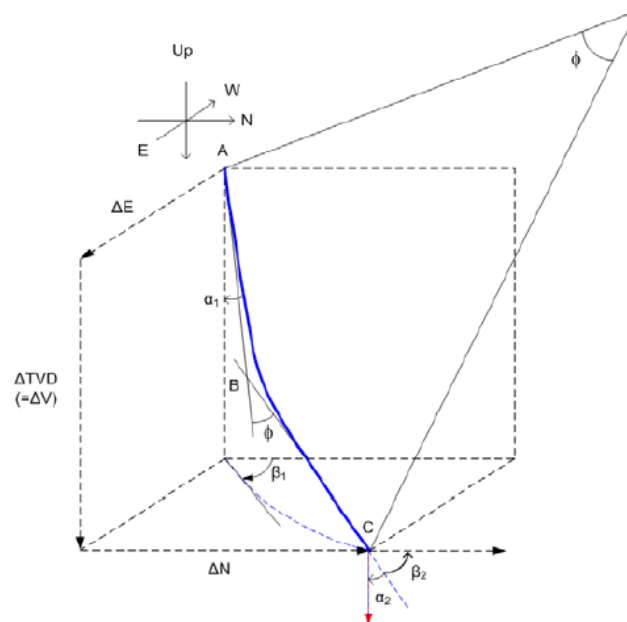


Figure 6.9: Minimum curvature method [23].

The derivation of the the minimum curvature method is presented below [23].

The dogleg angle ϕ [°] is found by:

$$\phi = \arccos [\cos \alpha_1 \cos \alpha_2 + \sin \alpha_1 \sin \alpha_2 \cos (\beta_2 - \beta_1)] \quad (6.4)$$

Where α_1 [°] and α_2 [°] refer to the inclination at the first and the second survey point, respectively. β_1 [°] and β_2 [°] refer to the azimuth at the first and the second survey point, respectively.

The ratio factor F [-] is derived and calculated as follows:

$$\begin{aligned} F &= \frac{AB + BC}{AC} \\ AB = BC &= RC \tan\left(\frac{\phi}{2}\right) \\ AC &= \frac{\pi RC \phi}{180} \\ F &= \frac{2 \cdot 180}{\phi \cdot \pi} \tan\left(\frac{\phi}{2}\right) \end{aligned} \quad (6.5)$$

Where AB [m] and BC [m] are the distances of the tangent lines, used to build the arc length AC [m].

At last, the changes in the North ΔN [m], East ΔE [m] and Vertical ΔV [m] components are calculated, respectively:

$$\Delta N = \frac{FAC}{2} (\sin \alpha_1 \cos \beta_1 + \sin \alpha_2 \cos \beta_2) \quad (6.6)$$

$$\Delta E = \frac{FAC}{2} (\sin \alpha_1 \sin \beta_1 + \sin \alpha_2 \sin \beta_2) \quad (6.7)$$

$$\Delta V = \frac{FAC}{2} (\cos \alpha_1 + \cos \alpha_2) \quad (6.8)$$

6.2 Bottom Hole Assembly (BHA)

The Bottom Hole Assembly (BHA) design is of uppermost importance because it is essential in having a fully functioning and efficient drilling system. This chapter presents basic theory about the BHA, which is the foundation of the final BHA design in this project.

6.2.1 Directional Steering

Different BHA assemblies exist to obtain directional steering in the drilling industry [23]:

- Traditional assemblies
- Steerable motor assemblies
- Rotary steerable systems (RSS)

The traditional assemblies consist of a bent sub and a straight motor. When a straight motor is used, the drill string cannot rotate while drilling. Furthermore, the bent sub restricts the system to only build a well trajectory with constant curvature. Due to these constraints, traditional assemblies can only be applied to large hole sections of a well, which is why they are rarely used in the industry today [41].

The Positive Displacement Motor (PDM) is an example of a steerable motor assembly that uses a bent sub or bent housing in combination with a mud motor to provide directional control. In contrast to traditional assemblies, steerable motors are more versatile since they can kick off, build angle and drill tangents [41]. For this reason, these types of assemblies offer a more accurate drilling steerability of the system.

In order to meet the demands of more challenging well trajectories, Rotary Steerable System (RSS) was developed as an innovative solution and is frequently used in the oil and gas industry today. The advantage with RSS is that while drilling, the drill string can be both rotated and steered at the same time.

6.2.2 Positive Displacement Motor (PDM)

Steerable motor assemblies consist of two key components which are bent housings and a mud motor. There are two different types of mud motors. It can either be a Positive Displacement Motor (PDM) or a Downhole Turbine Motor (DTM) [23]. Out of these two, PDMs are the most used motors for this application. Figure 6.10 shows that the major components of a PDM are power section, adjustable bend and bearing section.

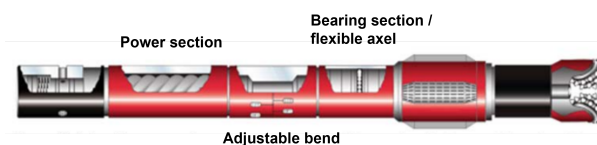


Figure 6.10: Standard PDM showing main components [23].

6.2.2.1 Power Section

The PDM is driven by drilling fluid circulating through the motor section to provide hydraulic power that induces rotation to the system. A rotor and stator are combined to form the power section of the unit. In this design, both the rotor and stator have a helical shape. However, the stator has an additional lobe compared to the rotor as shown

in Figure 6.11. During operation, cavities are generated in the seal between the rotor and stator. Fluids pushed through these cavities cause rotation of the rotor inside the stator, and as a result the drill bit is forced to rotate [23].



Figure 6.11: Rotor and stator combination [23].

The number of lobes can vary, affecting both the provided RPM and torque. According to Figure 6.12, a larger number of lobes increases torque, but the resulting RPM will decrease. Consequently, a trade off will need to be made between the output torque and RPM when choosing the amount of lobes in a PDM.

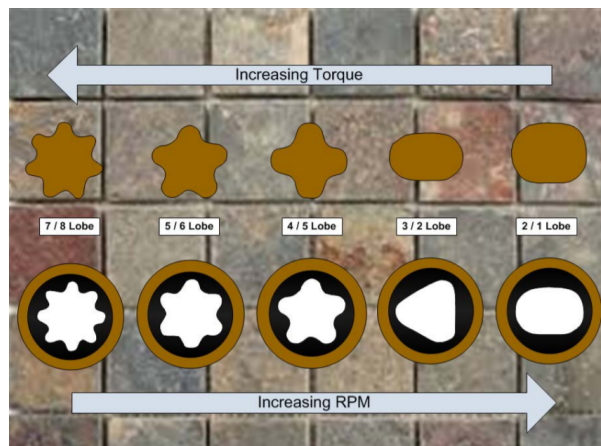


Figure 6.12: Lobe arrangement [23].

6.2.2.2 Bent Housing

The bit tilt can be achieved by using a bent housing. A bent housing can either be fixed at a given angle, or it can be adjustable which gives the ability to change angle if necessary. Figure 6.13 shows a bent sub made of steel with a fixed angle.

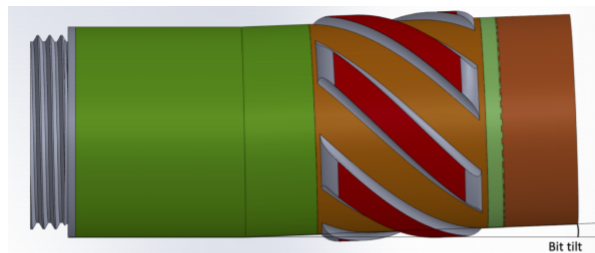


Figure 6.13: Bent housing [10]

However, a surface adjustable bent sub is a more flexible solution. Double pin, lock

housing, adjusting sleeve and offset housing are the main components. The adjusting sequence and process is shown in Figure 6.14 and is performed as following [38]:

1. Break out the lock housing by unscrewing it.
2. Remove the adjusting sleeve from the gear teeth.
3. The sleeve can then be adjusted to the preferred angle.
4. Reengage the gear teeth with the sleeve.
5. Maintain the selected angle by tightening the lock housing.

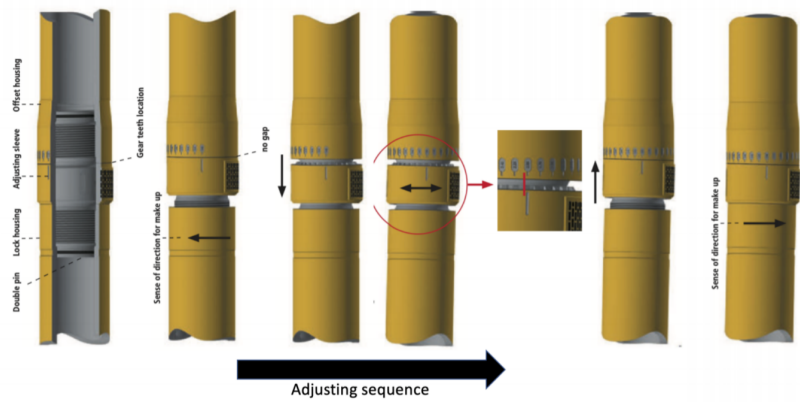


Figure 6.14: Adjustable bent sub connection procedure [38].

6.2.2.3 Transmission Section

The axis of rotation of the eccentric rotor is often misaligned with the drill bit's axis of rotation in a PDM. For that reason, a transmission section can translate the eccentric rotation to concentric rotation [23]. Flexible rods and U-joints can both be utilized for this purpose. The main advantage of the flexible rods is that they not require lubrication or rubber sleeve. Additionally, they do not bend as much laterally as U-joints. Compared to U-joints, flexible rods usually have lower maintenance costs. Figure 6.15 illustrates the differences between flexible rod and U-joint.

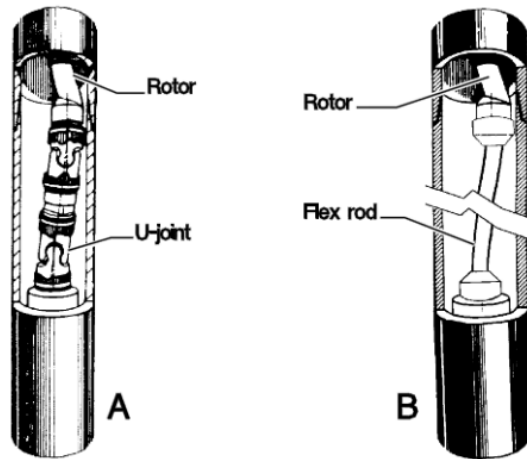


Figure 6.15: U-joint and flexible rod [23].

6.2.2.4 Bearing Section

The bearing section is responsible for that torque and rotation is transmitted from the transmission shaft and all the way to the drill bit. Support is primarily provided by three sets of bearings: two set for radial support, and one set for axial support [23]. In addition, the axial bearings support the load that is induced when the drill string is taken on and off the bottom of the well. Figure 6.16 illustrates the diversion of a small portion of drilling fluid through the bearings for lubrication and cooling purposes. The major part of the fluid is led through the drive shaft of the section and then continuing through the bit nozzles.

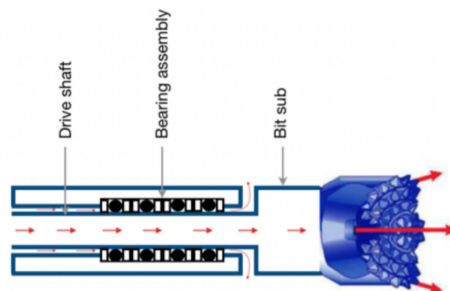


Figure 6.16: Different flow paths [25].

6.2.3 Rotary Steerable System (RSS)

Baker Hughes first established the Rotary Steerable System (RSS) in 1995 as a new and novel technology in the industry [23]. As illustrated in Figure 6.17, there are two types of RSS systems: push the bit and point the bit.

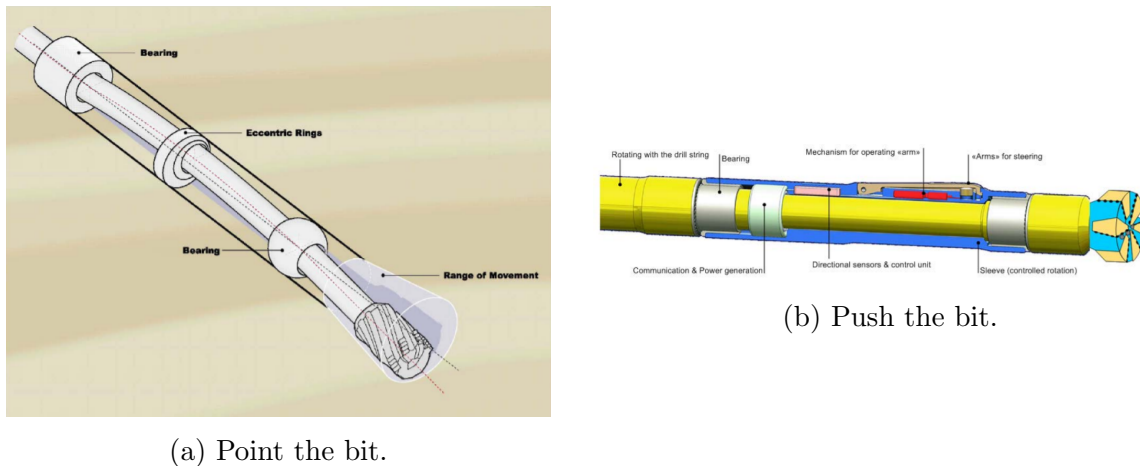


Figure 6.17: RSS variants [23].

In order to steer the bit in the desired direction, the concept of push the bit method laterally forces the bit into the side wall of the well [23]. In contrast, point the bit means that the bit is tilted a small distance from the center axis, thereby orienting the bit in the desired direction. The drive mechanism for this to happen is a mechanical system that consists of eccentric rings causing the drill string to deflect.

RSS provides better hole cleaning than non-rotating systems due to the rotation of the pipe. When the drill string rotates, cuttings are easily removed from the borehole wall and rise because of the flow pattern. Moreover, RSS has more constant drilling parameters compared to other systems. For example, wellbore tortuosity is less common when using RSS, which creates a smoother well path. In addition, vibrations are expected to be lower and WOB is easier controlled with RSS [23].

6.2.4 Dog Leg Severity (DLS) based on BHA Specifications

The following equation illustrates an alternative way to calculate the DLS acquired from the specifications and properties of the BHA [23].

$$DLS = \frac{2\theta}{L_1 + L_2} \quad (6.9)$$

In this equation, θ [°] is the bit tilt, L_1 [m] is the interval from the upper stabilizer to the bending point, and L_2 [m] is the interval from bending point to the bit. Figure 6.18 shows all of these parameters.

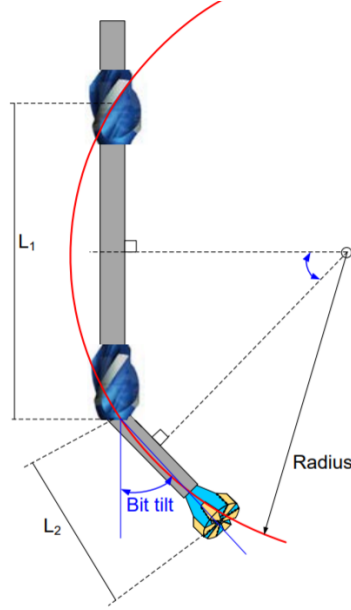


Figure 6.18: Parameters for Equation 6.9 [23].

6.3 Drill String Mechanics

A thorough understanding of drill string mechanics is essential to ensure safe drilling operations. Therefore, it is important to determine the mechanical limits of the drill string to avoid operating outside these values. In worst case if these values are exceeded, drill string failure can happen which may not only damage the miniature drilling, but also be hazardous for the environment and the operators.

6.3.1 Pipe Twist Off

Drill pipe twist off is a failure that occurs when the torque induces shear stresses that exceed the pipe's shear strength. A constraint must therefore be set for the torque applied while drilling. Equation 6.10 is used to calculate the maximum allowable torque T_{max} [Nm] under the thin wall assumption, which assumes the radius and shear stress to be constant [23].

$$T_{max} = \tau_{max} \frac{\pi}{16} (OD^2 - ID^2) (OD + ID) \quad (6.10)$$

The maximum shear stress that the drill pipe can withstand is found by Von Mises criterion using Equation 6.11. This criterion assumes that $\sigma_{23} = \sigma_{31} = 0$ and $\sigma_{12} = \tau_{max}$.

$$\tau_{max} = \sqrt{\frac{2\sigma_{ys}^2 - [(\sigma_z - \sigma_\theta)^2 + (\sigma_\theta - \sigma_r)^2 + (\sigma_r - \sigma_z)^2]}{6}} \quad (6.11)$$

The above equation includes the following variables: radial stress $\sigma_r[Pa]$, tangential stress $\sigma_\theta[Pa]$, axial stress $\sigma_z[Pa]$ and the yield strength of the pipe $\sigma_{ys}[Pa]$. Figure 6.19 shows these stress components acting on the drill pipe.

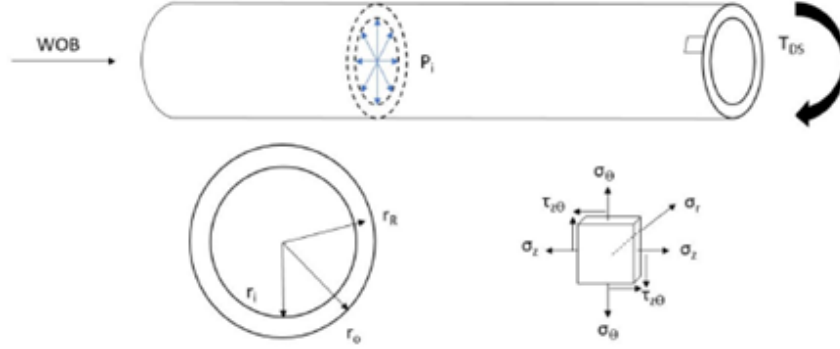


Figure 6.19: Stress components acting on the drill pipe [55].

Aside from the pipe dimensions, the radial and tangential stresses are solely affected by internal pressure. To calculating these stresses, Equation 6.12 and 6.13 are used, respectively. In contrast, the total axial stress is determined by the contributions from the internal pressure, WOB and bending stress. Equation 6.14, 6.15 and 6.16 must therefore be summed up to calculate this stress [64].

$$\sigma_r = \frac{\left(\frac{ID}{OD}\right)^2 - \left(\frac{ID}{2r}\right)^2}{1 - \left(\frac{ID}{OD}\right)^2} p \quad (6.12)$$

$$\sigma_\theta = \frac{\left(\frac{ID}{OD}\right)^2 + \left(\frac{ID}{2r}\right)^2}{1 - \left(\frac{ID}{OD}\right)^2} p \quad (6.13)$$

$$\sigma_z^p = \frac{\left(\frac{ID}{OD}\right)^2}{1 - \left(\frac{ID}{OD}\right)^2} p \quad (6.14)$$

$$\sigma_z^{WOB} = \frac{WOB}{A_{cs}} \quad (6.15)$$

$$\sigma_z^b = \frac{E}{RC} r \quad (6.16)$$

In the above equations, $r[m]$ is the distance from the centre of the pipe to the point of interest, $A_{cs}[m^2]$ is the cross sectional area of the pipe, E is the elastic modulus and $RC[m]$ is the radius of curvature.

6.3.2 Pipe Bending

Drill pipe bending occurs when an applied axial force results in a bending moment. Realistically, the pipe wall thins out on the stretched side and thicken on the compressed side. However, an estimate of the bending stress can be made using Equation 6.16 when assuming a constant drill pipe cross section [64].

6.3.3 Rod Stresses

The rod is a compact and cylindrical shaft that must withstand shear and bending stresses while drilling. The combination of these stresses acting simultaneously can be defined by the comparative stress using Equation 6.17. To avoid failure, the comparative stress must not exceed the rod's yield strength, and it therefore becomes a limiting factor [65].

$$\sigma_c = \sqrt{\sigma_b^2 + 3\tau_s^2} \quad (6.17)$$

In the equation above, $\sigma_c[Pa]$ is the comparative stress, $\sigma_b[Pa]$ is the bending stress and $\tau_s[Pa]$ is the induced shear stress.

The bending stress is found by Equation 6.18, where $M_b[Nm]$ is the bending moment and $W_x[m^3]$ is the area resistance moment.

$$\sigma_b = \frac{M_b}{W_x}; \quad W_x = \frac{\pi}{32}d^3 \quad (6.18)$$

The induced shear stress is computed using Equation 6.19, where $M_s[Nm]$ is the applied torque, $W_p[m^3]$ is the polar area resistance moment and $d[m]$ is the rod diameter.

$$\tau_s = \frac{M_s}{W_p}; \quad W_p = \frac{\pi}{16}d^3 \quad (6.19)$$

6.3.4 Buckling

As a consequence of high drilling loads, a drill string tends to buckle because of elastic or plastic deformation of the pipe. A buckling process usually consists of two stages where sinusoidal buckling is followed by helical buckling [19]. The drill string undergoes sinusoidal buckling when the compressive forces exceed a certain limit. Due to the fact that the deformation occurs in the 2D-plane, sinusoidal buckling itself is not critical during operations. In contrast, the drill string takes on a helical shape when helical buckling occurs and should therefore be avoided. The reason is because drill string fatigue and WOB transfer can both become a problem since the contact forces between the wellbore and drill pipe are so high. Figure 6.20 illustrates the two stages of buckling.

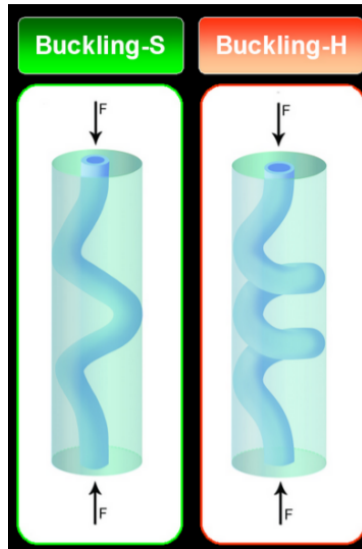


Figure 6.20: Helical and sinusoidal buckling [19].

It is likely that a drill pipe buckles when the axial compressive force in the pipe goes beyond the critical limit. Assuming central loading on the pipe, the critical buckling of long columns is given by Euler's equation [36].

$$\sigma_{cr} = \frac{F_{cr}}{A} = \frac{\pi^2 E}{\left(K \frac{L}{r_g}\right)^2} \quad (6.20)$$

In Equation 6.20, $\sigma_{cr}[Pa]$ is the critical load, $F_{cr}[N]$ is the critical force, $A[m^2]$ is the cross sectional area of the pipe, $E[Pa]$ is Young's modulus, $L[m]$ is the unsupported length of the pipe and $r_g[m]$ is the radius of gyration. In Table 6.1, different values of $K[-]$ are shown depending on the conditions at the end of the drill pipe.

Table 6.1: Different values for K based on end condition [36].

End condition	Pinned-pinned	Fixed-fixed	Fixed-pinned	Fixed-free
Illustrations				
Theoretical K	1	0.5	$1/\sqrt{2}$	2
Recommended K	1	0.9	0.9	2.1

The radius of gyration is the length from a given centroid where the whole area can be

concentrated around without affecting the moment of inertia [37]:

$$r_g = \sqrt{\frac{I}{A}} \quad (6.21)$$

$$I = \frac{\pi}{64}(OD^4 - ID^4) \quad (6.22)$$

In the above equations, $I[m^4]$ is the moment of inertia and $A[m^2]$ is the cross sectional area of the drill pipe. $ID[m]$ represents the inner diameter of the pipe and $OD[m]$ represents the outer diameter.

The slenderness ratio $R_s[m]$ is expressed by the following equation:

$$R_s = \left(\frac{L}{r_g}\right) \quad (6.23)$$

The term L/Rg can also be recognized in Equation 6.20. As Equation 6.23 shows, a longer drill pipe will result in a higher slenderness ratio. Hence, a longer segment of drill pipe is more vulnerable to pipe buckling compared to a shorter segment.

On the other hand, the critical buckling limit for a pipe column of intermediate length is calculated with Johnsons formula as follows [36]:

$$\sigma_{cr} = \sigma_{ys} - \left(\frac{\sigma_{ys}KL}{2\pi r}\right)^2 \left(\frac{1}{E}\right), \quad \text{if } \frac{L}{r_g} \leq \left(\frac{L}{r_g}\right)_{cr} \quad (6.24)$$

In this equation, $\sigma_{ys}[Pa]$ is the yield strength and $r[m]$ is the radius of the pipe.

The critical slender ratio determines whether Equation 6.20 (Euler's) or Equation 6.24 (Johnson) should be applied in order to calculate the critical buckling limit of the drill pipe.

$$\left(\frac{L}{r_g}\right)_{cr} = \sqrt{\frac{2\pi^2 E}{K^2 \sigma_{ys}}} \quad (6.25)$$

When all the above equations are taken into consideration, the maximum WOB that can be exposed to the drill pipe without buckling is calculated as follows:

$$F_{max \text{ WOB}} = \sigma_{cr} A \quad (6.26)$$

The given σ_{cr} in the equation above is calculated by Equation 6.20 (Euler's) or by Equation 6.24 (Johnson) depending on if the equation for long or intermediate drill pipe columns are to be used.

6.3.5 Burst

An internal pressure greater than the pipe's material strength can result in burst of the pipe. Barlow's equation has been used for a long time in the industry to calculate burst pressure. However, there has been discussions about the accuracy of this equation. According to research, the equation is found to be too conservative for thick walled pipes, but too little conservative for thin walled pipes. For this reason, the American Petroleum Institute (API) has modified Barlow's equation to include a factor of 0.875 to be on the safe side [22]:

$$P_{burst} = 2 \frac{0.875 \sigma_{ys} t}{OD SF} \quad (6.27)$$

In this equation $t[m]$ is the wall thickness and $SF[-]$ is the safety factor which is 3 for drilling and 2 for tripping [23].

6.3.6 Fatigue

Fatigue lowers the life expectancy of the drill string and is a common contributor to drill string failure. It is caused by dynamic loads and cyclic stresses such as rotation and vibration. When stresses like these act repeatedly over time, they will initiate microscopic fissures that eventually propagate into macroscopic cracks. Fatigue failure can occur even if the stresses acting over time are considerably lower than the material yield strength [3].

The drill string is most susceptible to fatigue when drilling deviated wells. This is because the bent and rotating drill string will experience repeated tension and compression in the pipe wall, as seen in Figure 6.21 [3].

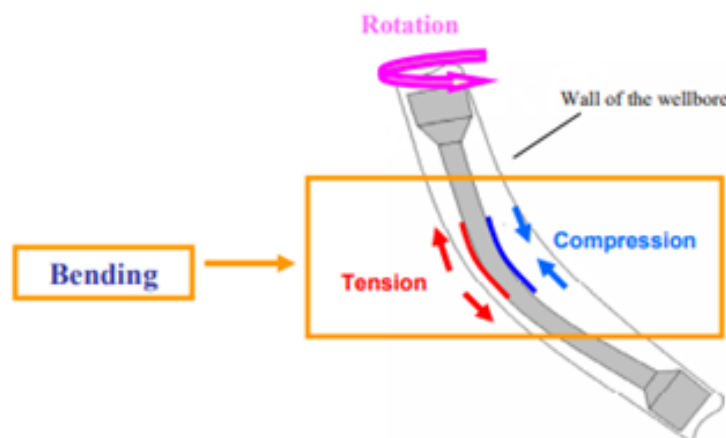


Figure 6.21: Cyclic stress in deviated wells [3]

An S-N curve shown in Figure 6.22 can help determine the fatigue life of a material. It indicates the number of stress cycles a material can endure at a specific stress level before

it fails. In addition, the graph provides a fatigue limit for certain materials. This limit is of utmost importance because it specifies the maximum stress amplitude under which fatigue failure will not occur. The bending stress will therefore need to be constrained to this amplitude [94].

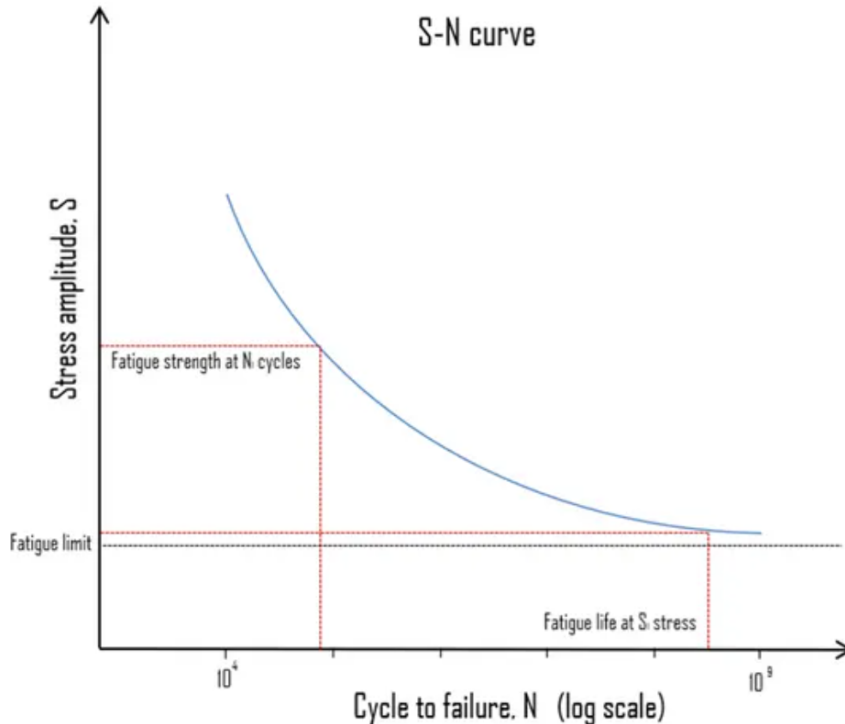


Figure 6.22: S-N curve [94]

6.3.7 Natural Frequency

A system's natural frequency is defined as the frequency at which it oscillates in the absence of a driving or damping force. These oscillations are also known as free vibrations. If an external force is applied to the system with a frequency equivalent to the natural frequency, resonance will occur. This is a phenomenon in which the amplitude of the vibrations increase drastically [108].

Resonance can be very destructive to the drilling equipment on the miniature rig. The intensified vibrations travel from the drill bit, through the BHA and up the entire drill pipe. They can cause bit bounce, bit whirl and stick and slip scenarios which may lead to wear, damaged drill bit cutters and broken drill string connections. Therefore, to protect and prolong the durability of the equipment, it is important to identify and avoid drilling at the Critical Rotary Speed (CRS) that results in frequencies close to the system's natural frequency [100].

During operation, the rod and drill pipe can vibrate both laterally and longitudinally. The CRS [*RPM*] that gives rise to amplified vibrations in the lateral direction is estimated

within 15% accuracy by Equation 6.28 [23].

$$CRS = 4760000 \frac{\sqrt{D^2 + d^2}}{l^2} \quad (6.28)$$

Where $D[in]$ is the outer diameter, $d[in]$ is the inner diameter and $l[in]$ is the length of the rod or pipe.

Meanwhile, the CRS that causes resonance in the longitudinal direction of the rod and drill pipe is approximated using the following set of equations [96].

$$\beta = \frac{m}{M} \quad (6.29)$$

$$\alpha_n \tan(\alpha_n) = \beta \quad (6.30)$$

$$CRS = \frac{60\alpha_n c}{2\pi l} \quad (6.31)$$

Where $m[kg]$ is the mass of the rod or drill pipe, $M[kg]$ is the mass of the BHA, $c[m/s]$ is the sound velocity of the material and $l[m]$ is the length of the rod or drill pipe.

Like the rod and drill pipe, the BHA is also subjected to free vibrations. The CRS that should be prevented for a BHA without a shock sub is calculated using the following equation [23].

$$CRS = \frac{84240}{l_{BHA}} \quad (6.32)$$

Where $l_{BHA}[in]$ is the length of the BHA.

6.4 Drill Bit

The drill bit is crucial to any drilling operation as it cuts or crushes the rock to remove the formation. In order to increase the drilling performance and borehole quality, it is essential to select a durable drill bit that provides a high Rate Of Penetration (ROP), good steerability, and can drill a full gauge hole. These properties are attained by carefully considering particular characteristics such as the drill bit type, bit profile, cutter layout and orientation and force balance when designing the drill bit [23].

6.4.1 Types of Drill Bits

The two main classifications of drill bits used in the industry are roller cone bits and fixed cutter bits. Roller cone bits date back to the early 1900s and are typically composed of three independent cones that rotate on lubricated bearings. The main components of roller cone bits are seen in Figure 6.23. In addition, depending on how the teeth are manufactured, these bits are further categorized as either milled tooth bits or insert bits [23].

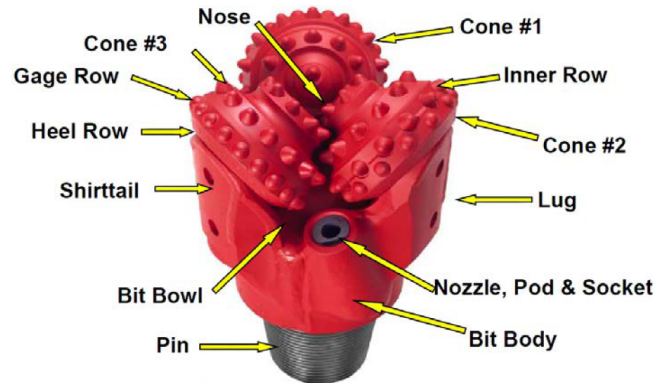


Figure 6.23: Components of a roller cone bit [23].

Since the late 1900s, fixed cutter bits such as Polycrystalline Diamond Compact (PDC) bits have become increasingly popular due to their cost-effective design. These bits are fixed since they do not have any moving components. Instead, the cutter blades are integrated into the stainless steel or tungsten carbide bit body, which provides the drill bit with its solidity and strength. The cutters are made by a bonded layer of polycrystalline or tungsten carbide and are soldered onto the inner and outer rows of the bit body. The cone, nose, shoulder, gauge, and nozzle are additional components of the PDC bit and are shown in Figure 6.24 [23].

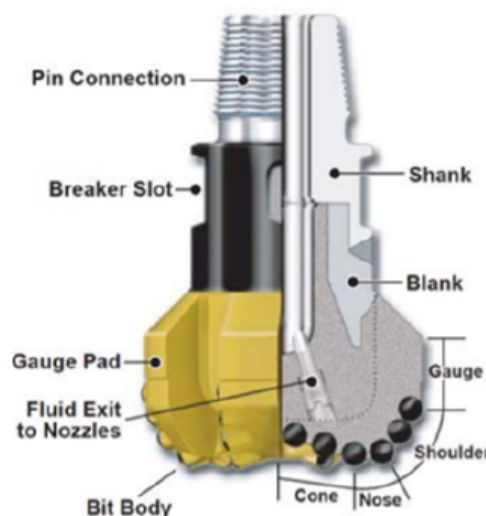


Figure 6.24: Components of a PDC bit [23].

Roller cone bits and PDC bits use different mechanisms to drill the formation. The roller cone bit crushes the rock by inducing a compressive shear failure, whereas the PDC bit cuts the rock by creating a shear stress failure. Generally, drilling using shear stress is more efficient than compressive stress since it requires less energy to reach the formation's plastic rupture limit. This is clearly illustrated in Figure 6.25 when drilling through shale. As a result, PDC bits require less WOB to drill than roller cone bits [23].

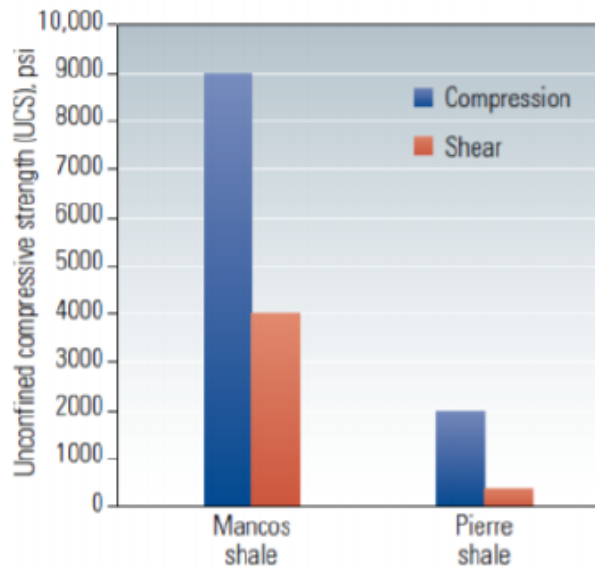


Figure 6.25: Drilling shale using shear and compressive stress [23].

Overall, the PDC bit is the superior drill bit for the Drillbotics competition. Its solidity will significantly reduce the potential risk of bit failure and eliminate dropping internal moving components into the borehole. In addition, buckling the drill pipe can be avoided due to its low WOB requirement. Hence, the following sections will focus exclusively on the PDC bit design.

6.4.2 Bit Profile and Cone Angle

The bit profile and cone angle are fundamental features of the PDC drill bit. They affect a variety of drilling parameters such as stability, steerability, aggressiveness and hole cleaning [43].

Bit profiles are categorized according to their shape. The four general classes are flat, short parabolic, medium parabolic and long parabolic, and their respective design and characteristics are illustrated in Figure 6.26. A flat profile has a nose located close to the gauge, which increases the load distribution on the bit face. This results in a high nose durability, strong directional capability and makes it suitable for hard and non-abrasive formations. A long parabolic profile, on the other hand, has a nose closer to the centre of the bit, which increases the cutter density on the shoulder. This reduces the drill bit's steerability, but increases the shoulder durability and makes it favourable for soft and

abrasive formations. Essentially, no bit profile is fitting for all drilling operations and a trade-off between the desired properties must be made. As a compromise, a short or medium parabolic profile is typically selected to benefit from the advantages of both sides [43].

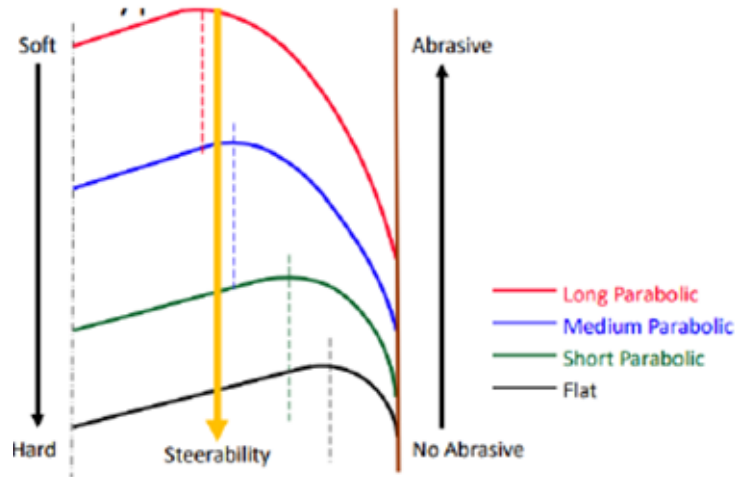


Figure 6.26: Bit profile shape and characteristics [43].

The cone angle described by the cone's included angle is classified as deep (90°), medium (120° - 140°) or shallow (150°). A deep cone angle, as shown to the left in Figure 6.27, has an increased diamond volume in the centre and creates a cone-like structure when drilling. This leads to the drill bit having a high degree of stability. On the contrary, the flatness of the shallow cone angle provides less stability, but an increased steerability, aggressiveness and hole cleaning efficiency. Consequently, stability comes at the expense of the other desired properties. This is why selecting the cone angle will require a similar compromise as when choosing the bit profile [43].

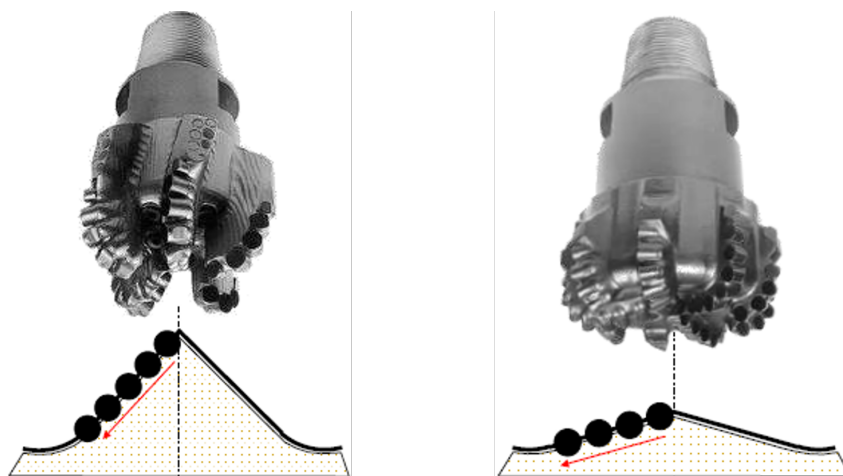


Figure 6.27: Deep and shallow cone angle [43].

6.4.3 Cutter Layout

The cutter layout is a crucial design aspect for increasing the drilling efficiency and bit durability. The cutters should be strategically placed from the cone's apex to the gauge of the bit to guarantee complete bottom hole coverage. This will ensure that no formation remains uncut, and thereby significantly reduces wear to the bit body [42].

The cutter's radial distance from the centre axis will affect its linear velocity. This relationship can be expressed as follows:

$$v = \omega \cdot r \quad (6.33)$$

In this equation, $v[m/s]$ is the linear velocity, $\omega[m/s]$ is the angular velocity and $r[m]$ is the radial distance from the centre axis [44].

A cutter at the gauge of the bit will experience a higher linear velocity than a cutter at the cone's apex. It will also cover a greater circumference in one revolution and have to remove more cuttings, resulting in additional wear. To achieve uniform wear, a cutter layout with a cutter density increasing towards the gauge is typically selected. This increases the durability and reduces the torque experienced by the drill bit. [42]. Such a cutter layout is shown in Figure 6.28.

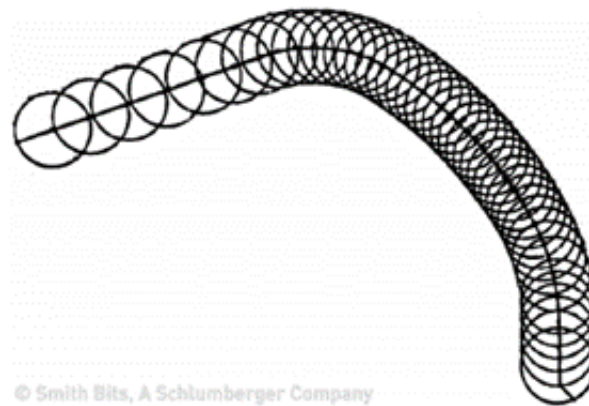


Figure 6.28: Cutter layout with cutter density increased towards the gauge [42].

Increasing the cutter density on the bit face does not come without a cost. The Depth of Cut (DOC) and ROP will consequently decrease. Additionally, the hole cleaning will become less efficient since the cuttings have less space to flow out of the structure [43].

It is possible to manipulate the cutter density by how the cutters overlap. A cutter layout is generally classified as a single set layout or a track set layout, and their respective configurations are shown in Figure 6.29. Cutters of a single set layout experience the same work load because every cutter is placed at a different radial and axial position. As a result, the drilling efficiency is increased. On the contrary, a track set layout consists of cutters on different blades that overlap the same cutting area. This arrangement generates

more pronounced ridges when drilling, which increases the bit stability but decreases the ROP [43].

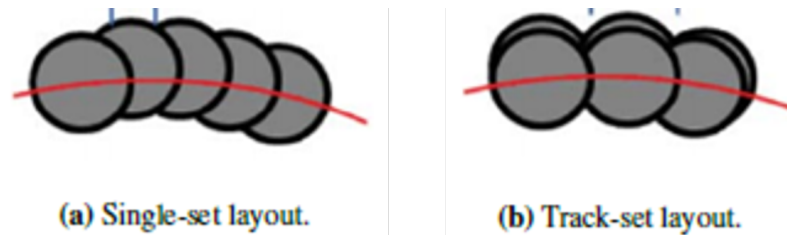


Figure 6.29: Two types of cutter layout [18].

6.4.4 Cutter Orientation

The cutter orientation is defined by its back rake and side rake angle. These angles significantly impact the drill bit's interaction with the formation and affect the bit's aggressiveness, durability, DOC and hole cleaning efficiency. Therefore, it is important to mount the cutters with the appropriate orientation to achieve the desired drilling properties.

The back rake angle is measured between the cutter's face and the line perpendicular to the drilled formation. It is shown in Figure 6.30 and describes the angle at which the cutter attacks the formation. Smaller back rake angles force the cutters deeper into the formation, resulting in a higher DOC and a more aggressive drill bit. This is suitable for maximizing the ROP in softer formations. On the contrary, larger back rake angles reduce the DOC, bit aggressiveness and induced vibrations, resulting in a more durable drill bit which is beneficial for harder formations [42].

Individual cutters are typically given varying back rake angles to attain the correct drilling parameters. A back rake angle of 15° is common for cutters on the inner rows, whereas 30° is normal for the outer rows [43].

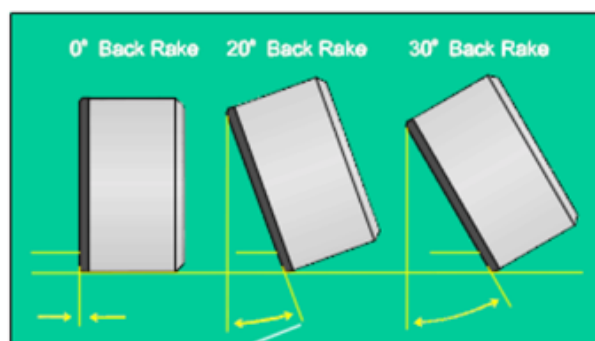


Figure 6.30: Cutter back rake angle [23].

The side rake angle is measured between the cutter's face and the line perpendicular to the rotational direction. It is illustrated in Figure 6.31. Like the back rake angle, a less

aggressive drill bit is attained by a larger side rake angle. In addition, the hole cleaning efficiency is affected by the side rake angle. A larger angle will result in the cuttings curling away from the cutter's face to the outer periphery of the drill bit, and it thereby increases the hole cleaning efficiency [23].

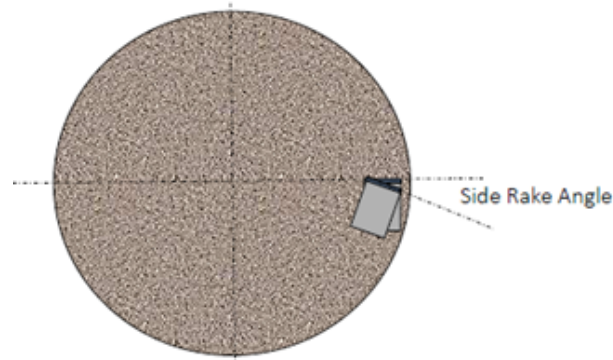


Figure 6.31: Cutter side rake angle [43].

6.4.5 Force Balance

A balanced force design will enhance bit stability and lead to efficient drilling. It is achieved by arranging the cutters so that the lateral forces do not offset the drill bit [18].

Traditionally, the cutters are arranged in a spiral pattern from the centre of the bit face to the gauge, as shown in Figure 6.32. In this example, cutters 1 and 2 drill the rock's inner ring, whereas cutters 3, 4 and 5 drill the rock's outer ring. After the drill bit makes a complete revolution in an anticlockwise direction, cutter 2 will have removed considerably more rock than cutter 1. Likewise, cutter 5 will have removed significantly more rock than cutters 3 and 4. This occurs because the cutters are located on the same side of their respective rings. As a result, an imbalanced force arises, leading to uneven cutter wear and inefficient drilling [18].

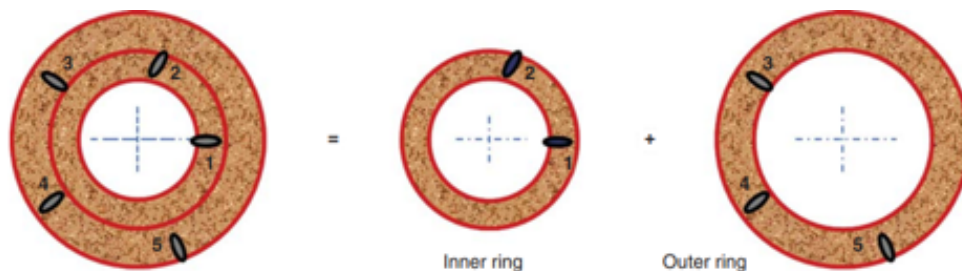


Figure 6.32: Traditional cutter layout leading to inefficient drilling [18].

However, the cutters in each ring will drill the same volume of rock per revolution if the cutters are rearranged angularly, as shown in Figure 6.33. In this way, a balanced force design is achieved and the drilling performance is enhanced [18].

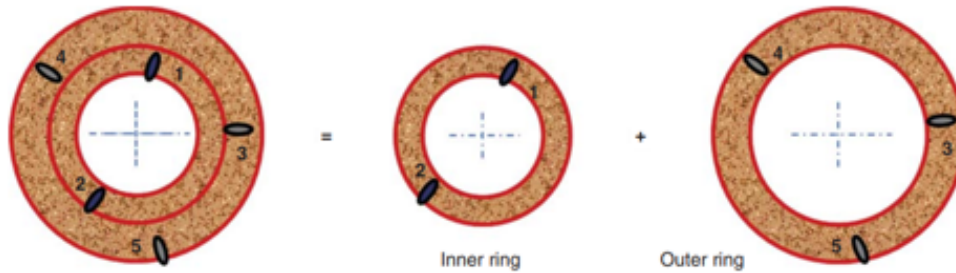


Figure 6.33: Rearranging the cutter layout angularly leading to efficient drilling [18].

6.5 Drilling Hydraulics

The main functions of the hydraulic system on a drilling rig are to ensure efficient hole cleaning and maintain wellbore stability. The most important part of the system is the drilling fluid, which is a mix between a base fluid, normally water or oil, and additives. A more detailed list of the main functions of the drilling fluid is presented [23]:

- Provide stability to the hole through different mechanisms such as mechanical stability with the hydrostatic pressure, chemical stability and filtration control.
- Remove cuttings originating from the drilling operation out of the well.
- Provide hydraulic power to the downhole tools.
- Lubricate and cool the bit and drillstring.
- Be a mean for the telemetry communication system.

6.5.1 Hole Cleaning

Hole cleaning is necessary to drill a well in an efficient and safe manner. The main point is to remove any kind of cuttings, cavings or debris out of the well. Poor hole cleaning can result in downhole problems such as stuck pipe or bit balling, which may have heavy consequences on the drilling performance. In order to secure sufficient hole cleaning, two main parameters must be calculated: flow velocity and flow regime [23]. These parameters are heavily affected by the inclination of the well. Segments of a well can typically be characterized by its inclination [23].

- Vertical section ($0^\circ - 30^\circ$)
- Tangent section ($30^\circ - 65^\circ$)
- Horizontal section ($65^\circ - 90^\circ$)

Each section will have a different flow regime and should therefore be analysed separately. Following the guidelines presented by Drillbotics for this year competition, the inclination of the well will not exceed 30°. For this reason, the analysis for the hole cleaning and flow regime of the vertical section of a well will be presented.

The key parameter to secure proper cleaning in the vertical section is the fluid velocity. This has to be high enough to overcome the gravitational pull and slippage that forces the cuttings down. A detailed explanation and derivation of cutting transport and slip velocity is found in Appendix C. In this section, only the key points and equations will be presented.

The slip velocity $v_{sl}[m/s]$ for a body with a spherical shape present inside a laminar flow regime is given by [40]:

$$v_{sl} = \frac{d_s^2 g (\rho_s - \rho_f)}{18 \mu_f} \quad (6.34)$$

Where $d_s[m]$ is the diameter of the sphere, $g[m/s^2]$ is the gravity, $\rho_s[kg/m^3]$ is the density of the cuttings, $\rho_f[kg/m^3]$ is the fluid density and $\mu_f[Pa \cdot s]$ is the fluid viscosity. Since it is not reasonable to assume that the entire system is under the laminar flow regime, the slip velocity must be expressed for all the different flow regimes [40].

$$v_{sl} = \sqrt{\frac{4(\rho_s - \rho_f)gd_s^2}{3f\rho_f}} \quad (6.35)$$

$$Re = \frac{\rho_f v_{sl} d_h}{\mu_f} \quad (6.36)$$

Where $f[-]$ is the friction factor obtained from Figure 6.34.

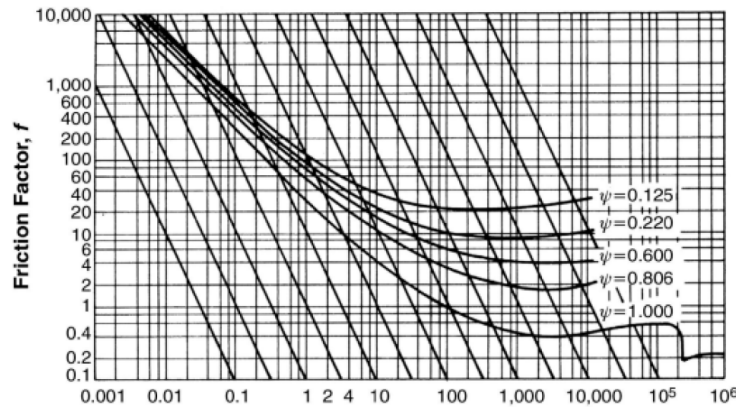


Figure 6.34: Interaction between friction factor f and Reynolds Number Re for the interaction between a particle in the Newtonian fluids [22].

The steps needed to obtain the final slip velocity v_{sl} are:

1. Estimate v_{sl} for a laminar flow regime with Equation 6.34.
2. Calculate Reynolds Re number using Equation 6.36.
3. Find the friction factor f graphically using Figure 6.34.
4. Calculate the final v_{sl} for any flow regime with Equation 6.35.

Once the final slip velocity is calculated, the final flow rate can be calculated with Equation 6.37:

$$q = A_{cs} \frac{v_{sl}}{1 - R_t} \quad (6.37)$$

Where R_t is the expected transport ratio and $A_{cs}[m^2]$ is the cross sectional area of the pipe being analyzed.

6.5.2 Pressure Losses

As the fluid becomes dynamic, it will experience friction against the surrounding media and result in pressure losses. In order for the fluid to flow through the system, the pump output must be greater than the pressure losses experienced [23]. For a detailed examination and modelling, the whole system can be analysed in their different sub sections. The sum of the individual pressure losses from each sub section will be the required pump pressure. This can be observed in Equation 6.38:

$$P_{req} = \Delta P_{hose} + \Delta P_{swivel} + \Delta P_{DP} + \Delta BHA + \Delta P_{nozzle} + \Delta P_{ann} \quad (6.38)$$

Where

- $P_{req}[bar]$ is the outlet pump pressure
- $\Delta P_{hose}[bar]$ is the pressure losses in the hose
- $\Delta P_{swivel}[bar]$ is the pressure losses in the swivel
- $\Delta P_{DP}[bar]$ is the pressure losses in the drill pipe
- $\Delta BHA[bar]$ is the pressure losses in the BHA
- $\Delta P_{nozzle}[bar]$ is the pressure losses in the nozzles of the bit
- $\Delta P_{ann}[bar]$ is the pressure losses in the annular space

In addition, a safety factor is used to avoid problems related to the uncertainty of calculations.

6.5.2.1 Pipe Pressure Losses

Pressure losses associated with the drill pipe occur when the fluid flows through the pipe from surface to bottom and up the annulus. These pressure losses can be obtained with Equation 6.39:

$$\Delta P_i = f_i \frac{L_i}{dh_i} \frac{\rho_f v_i^2}{2} \quad (6.39)$$

Where $\Delta P[\text{bar}]$ is the pressure losses, $L_i[\text{m}]$ is the length of the section being analyzed, $\rho_f[\text{kg}/\text{m}^3]$ is the fluid density, $v_i[\text{m}/\text{s}]$ is the velocity of the fluid and $dh_i[\text{m}]$ is the hydraulic diameter. The hydraulic diameter is defined as the ID of the drill pipe when calculating pressure losses inside the drill pipe, and the difference between the hole size and OD of the drill pipe for pressure losses in the annular space.

Reynolds number is calculated with Equation 6.36. The friction factor f_i will change depending on the flow regime. If the Reynolds number $Re[-]$ is less than 2300, the flow regime is laminar. Then, the friction factor can be calculated using Equation 6.40. This equation is only valid if the roughness of the pipe is not severe [40].

$$f = \frac{64}{Re} \quad (6.40)$$

On the other hand, if Reynolds number is above 2300, the flow regime in the system is turbulent. Equation 6.41 and 6.42 are used to calculate the friction factor. The final value of f will be the average of these two [40].

$$\frac{1}{\sqrt{f}} = -1.8 \log \left[\left(\frac{\epsilon/D}{3.7} \right)^{1.11} + \frac{6.9}{Re} \right] \quad (6.41)$$

$$f = \frac{0.25}{\left[\log \left(\frac{\epsilon/D}{3.7} + \frac{5.74}{Re^{0.9}} \right) \right]^2} \quad (6.42)$$

$\epsilon[\mu\text{m}]$ is the material roughness and $D[\text{m}]$ is the internal diameter of the pipe.

6.5.2.2 Bit Pressure Losses

A high pressure drop is favorable across the drill bit to maximize the cuttings removal. For this reason, the bit nozzles normally have a small cross sectional area. This pressure drop typically represents more than half of the total pressure losses of the entire system. The fluid velocity through the nozzles $v_n[\text{m}/\text{s}]$ can be calculated with Equation 6.43 in order to obtain the nozzle pressure losses [23].

$$v_n = C_d \sqrt{\frac{2\Delta P_{nozzle}}{\rho_f}} \quad (6.43)$$

Where $C_d[-]$ is the discharge coefficient, which is usually set to 0.95. By rearranging the formula and expressing v_n as a function of flow rate and nozzle area, the pressure losses from the nozzles can be calculated by [23]:

$$\Delta P_{nozzle} = \frac{\rho_f q^2}{2A_n^2 C_d^2} \quad (6.44)$$

Where $q[m^3/s]$ is the flow rate and $A_n[m^2]$ is the total flow area through the nozzles.

6.6 Mechanical Specific Energy (MSE)

Mechanical Specific Energy (MSE) is a measure of how much energy is required to remove a certain volume of rock from the bottom of the wellbore [104]. Mathematically, it is given by units of energy per units of volume, which represents a stress in psi or MPa. MSE is calculated with conventional drilling parameters such as WOB, RPM, ROP and torque [54].

The general definition of MSE is given by Equation 6.45.

$$MSE = \frac{\text{Total Energy Input}}{\text{Volume removed}} \quad (6.45)$$

Since MSE permits an objective comparison between different drilling tools and techniques to remove a given quantity of rock, this value is used as an operational efficiency criteria for optimizing drilling strategies [34].

During drilling operations, both vertical and rotational energies are acting in the bottom of the well. Equation 6.45 can therefore be split into two terms which represent the two energies, respectively [54].

$$MSE = \frac{\text{Axial Energy Input}}{\text{Volume removed}} + \frac{\text{Rotational Energy Input}}{\text{Volume removed}} \quad (6.46)$$

The vertical energy input can be expressed as the axial force WOB multiplied by the distanced drilled Δh . On the other hand, the rotational energy input is described by the torque T applied while drilling multiplied by the distance rotated. This distance is expressed as $2 \cdot \pi \cdot n$, where n is the number of rotations of the drill bit. These relationships are shown in Equation 6.47 [54]:

$$MSE = \frac{WOB \cdot \Delta h}{Area \cdot \Delta h} + \frac{T \cdot 2\pi \cdot n}{Area \cdot \Delta h} \quad (6.47)$$

Equation 6.47 can be further modified by dividing the second term by a time unit. As a result MSE can be expressed as [54]:

$$MSE = \frac{WOB}{Area} + \frac{T \cdot 2\pi \cdot RPM}{Area \cdot ROP} \quad (6.48)$$

A smaller MSE requires less energy to remove a rock volume and results in a more efficient operation. The relationship between MSE and WOB is shown in Figure 6.35 [104].

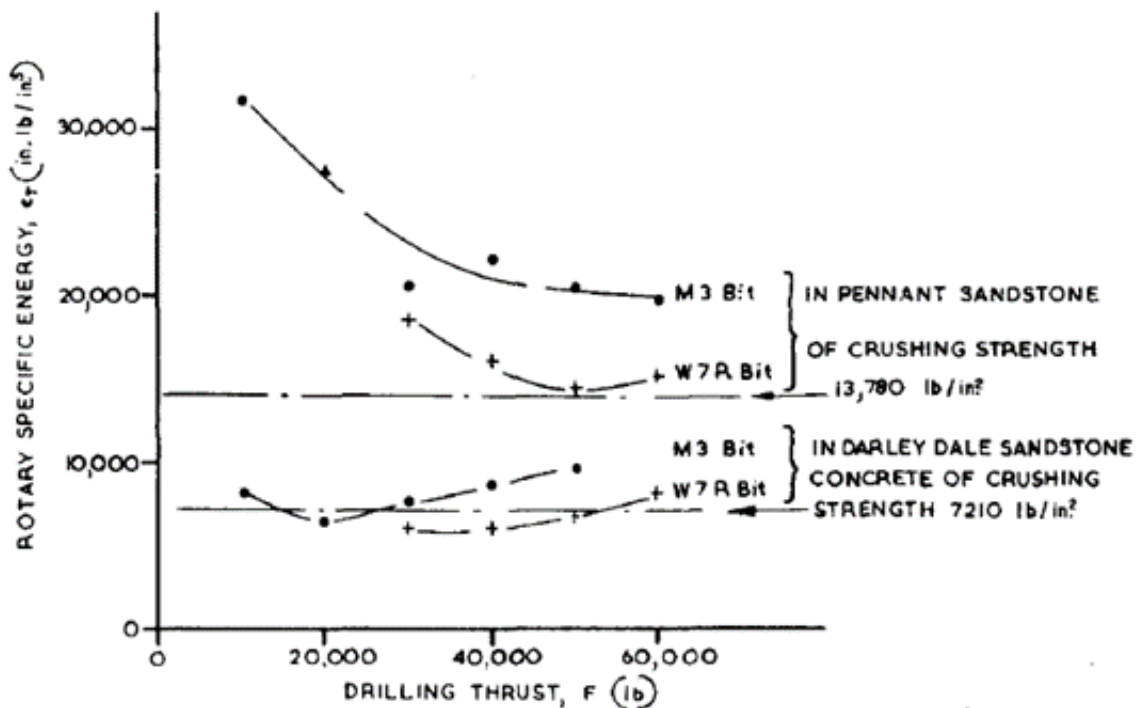


Figure 6.35: Plot presenting relationship between MSE and WOB [104].

The efficiency of the energy spent to remove the cuttings from the rock is directly proportional to the size of the cuttings and the depth of cut [54]. At very low values of WOB, the cutters do not have enough vertical thrust to penetrate the rock. As a result, the input energy is dissipated into friction and the MSE tends towards infinity [104]. However, once the WOB is sufficient, the cutters are able to penetrate the rock. This results in more efficient drilling with a lower MSE, since the energy previously lost to friction is used to remove the rock. The MSE will continue to decrease with an increasing WOB since the depth of cut and cutting size increases [104].

This principle is clearly illustrated Figure 6.36. In the left figure, the WOB is so low that there is almost no depth in cut, making the system highly inefficient. The right figure shows an example of when the WOB starts to increase. The depth of cut becomes greater and generates larger cuttings which reduces the MSE [104] [54]:



(a) Small depth of cut [54].



(b) Big depth of cut [54].

Figure 6.36: Effect of the WOB on the depth of the cut.

As the WOB continues to increase, the MSE will stabilize, and may even start to increase. This occurs since the cutters are dug further into the rock, exposing them to increasing loads which may eventually stall the bit [104].

The maximum efficiency is obtained where the MSE is minimized with an optimum combination of WOB, torque, RPM and ROP [104].

The minimum MSE coincides with the confined compressive strength of the rock that is being drilled [104]. An estimate of the optimal MSE can therefore be obtained if the strength of rock is found from lab testing. Since the rock sample used for the Drillbotics competition is not exposed to pore pressure, the unconfined compressive strength of the cement block can be used as the reference for the optimized MSE value.

Mechanical Rig Design

This chapter covers the evolution of the NTNU Drillbotics rig and describes all the mechanical components associated with the miniature drilling rig in this project. A robust design is important to ensure sustainable and safe drilling operations. All components are ensured to withstand high loads during drilling operations.

7.1 Drillbotics Rigs 2017-2021

A brief description of the previous year’s designs will be presented in this section since many of the components and concepts will be reused in this year’s design. When NTNU participated in the Drillbotics competition for the first time in 2017, the competition objectives were as follows: “Design a fully automated drilling rig that can autonomously drill a vertical well as quickly as possible while maintaining rig and drill string integrity” [5]. Since then, every team has utilized the framework of the rig that was created by the 2017 team. The drilling concept back then was based on having a top drive motor that provided rotation and torque to the drill bit. In addition, a hoisting motor with a ball screw enabled vertical movement of the drill pipe. As a result of very good work throughout the semester, the 2017 team ranked second in the competition.

The 2018 team further developed and built on the design from 2017. New protective glass, solutions for fluid returns and solutions for drill string alignment were the main improvements for the rig that year. These contributions combined with efficient work resulted in the first place of the competition [55].

In 2019 the competition objectives were shifted to involve autonomous directional drilling. The team implemented a new PDM motor including a bent sub which enabled to drill deviated well paths [57]. However, the team was not able to compete in the competition because the drilling rig did not pass the toll customs.

Because of Covid-19 pandemic, the 2020 team got all their activities related to Drillbotics

cancelled [58].

The competition objectives in 2021 were the same as in 2020, which involved drilling a deviated well with a maximum inclination of 30° and a maximum change in azimuth of 15° . The team abandoned the earlier used PDM and replaced it with a rotating rod to power the bit instead. To obtain directional steering, an azimuth control motor was implemented [9]. After these rig modifications, the team placed first in the competition with the new design.

7.2 Rig Framework

The original rig framework dates back to 2017 when NTNU joined the competition for the first time. Every year new teams have inherited the rig and further improved and developed it to fit the new competition objectives. The rig framework is primarily made of steel, and consists of beams that are both welded and screwed together with nuts. The general framework is made up of the derrick, drilling floor, computer table and rock sample space as shown in Figure 7.1. In the rig set up, drilling and electrical components are implemented to the framework. The total height of the rig is 2.85 m, the width is 0.75 m and the length is 1.65 m. Including all components on the rig, the total mass of the miniature drilling rig is around 170 kg. The rig is capable of drilling rock samples with maximum dimensions of 0.85m x 0.6m x 0.6m (H,W,L).

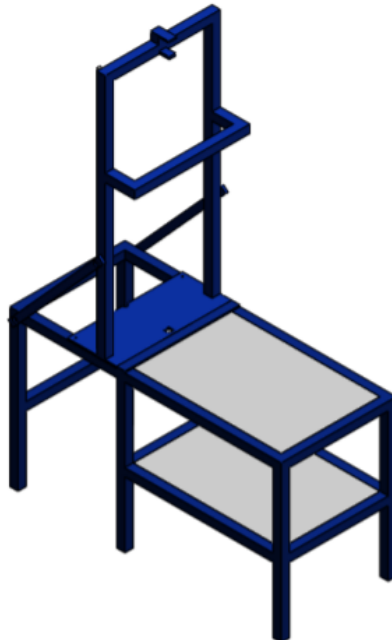


Figure 7.1: Rig framework without components.

There is an acrylic glass cover for the derrick as well as the drilling system to protect the

operator and the environment. Several hazards are associated with rotating objects in this system and the protection glass therefore acts as a barrier to avoid potential flying objects. The protective glass shown in Figure 7.2, is connected to the rig framework with bolts. In case of maintenance work or intervention on the drilling system, the glass cabinet can easily be lifted on expansion slides to access the system.

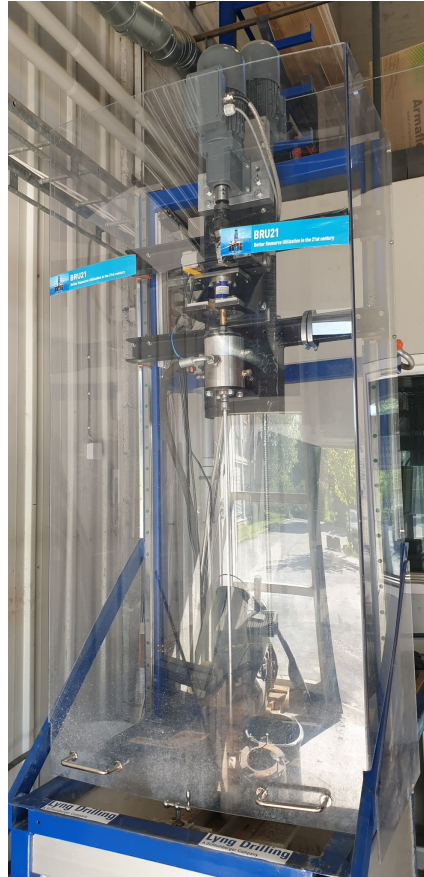


Figure 7.2: Acrylic glass cover.

7.2.1 Chargeable Weight Calculations

The Drillbotics guidelines requires all teams to compute the chargeable weight of the rig in case of it must be shipped where the competition takes place [90]. It is beneficial that the derrick can be folded down which reduces the effective height of the rig as shown in Figure 7.3. Either the gross or volumetric weight will be considered as the chargeable weight, depending on which one of them is the largest. According to the method proposed by the guidelines, the volumetric weight is computed to 437 kg. On the other hand, the gross weight of the miniature drilling rig is measured to be 170 kg. Hence, the chargeable weight of the rig is volumetric weight of 437 kg. This weight will however not be relevant since the competition will be held virtually at NTNU, but the calculations are presented for the benefit of future NTNU Drillbotics teams.

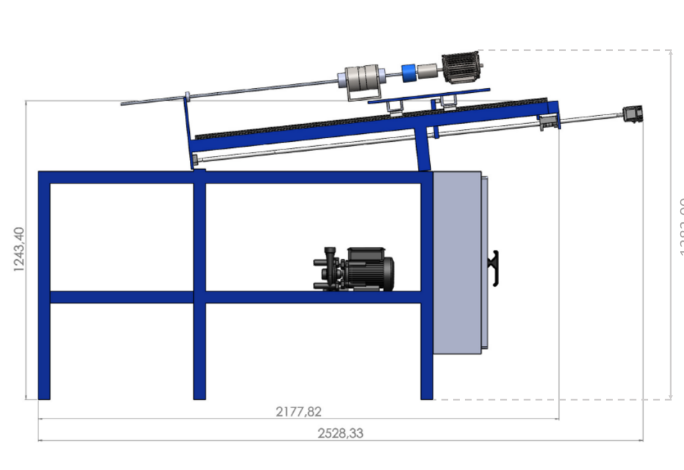


Figure 7.3: Rig in folded position.

7.3 Drillbotics 2022 Rig

The NTNU rig performed excellent in the 2021 Drillbotics competition. For that reason, this year's team aimed to further develop the design and enhance its capabilities. Overall, the main components on the rig will be kept the same as earlier since they have proven to work efficiently.

The rig has several different systems that work together to perform safe and efficient drilling operations. The various systems include the hoisting system, drilling system, azimuth control system, circulation system and electrical system. The rig systems are shown in Figure 7.4. They are all equally important and if a system does not work it results in the rig not being able to perform operations.

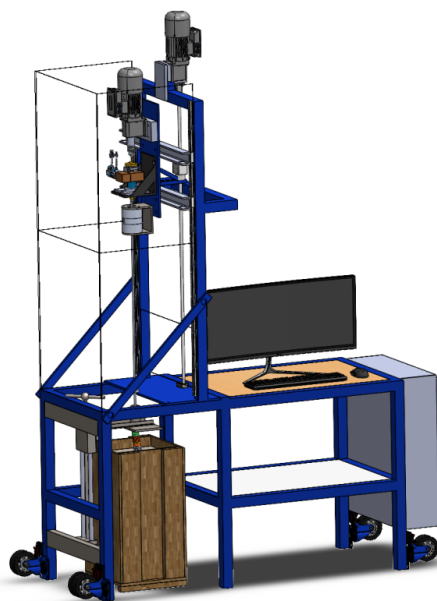


Figure 7.4: NTNU Drillbotics 2022 rig.

The drilling concept is having a rotating rod inside a drill pipe which transfers torque and RPM to the bit. The drill pipe is not rotating while drilling, but it transmits the WOB from the hoisting system to the bit at the bottom. In addition, a fixed bent sub allows the BHA to kick off and build a deviated well path with inclination. The azimuth control system allows for azimuth changes in the formation plane by orienting the drill pipe and BHA.

Several possibilities for alternative steerability options were reviewed in phase I of the competition to enhance and advance the rig performance. After thorough analysis and discussions with the lab engineers, the team chose to keep the fixed bent sub combined with the azimuth control motor because of complex solutions restricted by small dimensions. The reader is encouraged to review the project report submitted in the fall 2021 for further details about the steerability options [24].

A new diverter has been designed and implemented into the system to ensure a semi-closed circulation system that allows returns from the well to be controlled in a safe manner. Further, development and research has been performed on the drill bit design, resulting in a ranking of the best available drill bits available for the competition day. In addition, a new drill chuck has been installed on the rig to further improve the transmission of torque and RPM to the drill bit. Moreover, the team has performed an overall optimization of the rig by tuning drilling parameters and improving the mechanical components.

Several wireless communication options for the sensor were explored. The BHA had to be redesigned to fit the sensor card and batteries. However, the Bluetooth communication proved to not work, and the team was forced to use the original BHA design.

7.4 Hoisting System

At large-scale drilling in the industry, WOB is mainly obtained by the self-weight of drill pipes, heavy weight drill pipes and drill collars. Vertical movement of the drill string is a separate system which includes draw-works and travelling blocks. On the other hand, the rig in this project has a combined system for providing WOB and hoisting of the drill string.

The hoisting system converts rotational movement provided by the hoisting motor into vertical displacement. This is done by having a nut and bracket moving vertically on a ball screw. In addition, two linear roller guides are mounted on each side of the framework which enables the system to slide up and down vertically while having the horizontal position fixed. The carriage mount is connected to the ball screw with a steel beam, ball screw nut and bracket. When the hoisting motor provides rotation, the ball screw is forced to rotate, and the system can be lowered into the well while drilling. Figure 7.5 shows the main principle and components of the hoisting system.

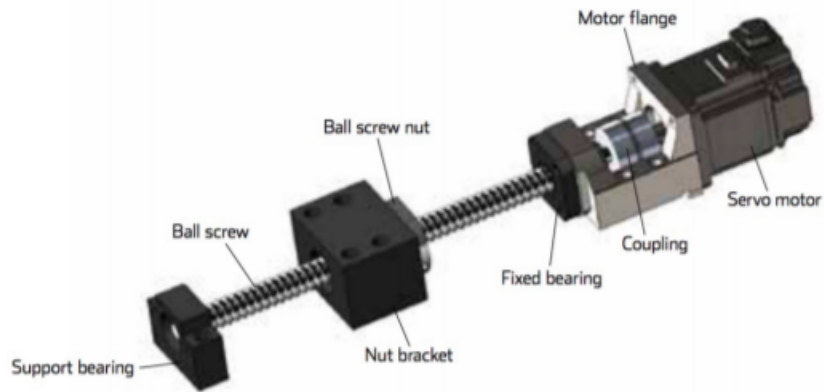


Figure 7.5: Principle that the hoisting system builds on [25].

7.4.1 Hoisting Motor

The hoisting motor is the tallest placed component on the miniature drilling rig. The supplier of the motor is Lenze and the model number is GST03-2M VBR 063C42. The motor's primary function is to provide rotation to the previously mentioned ball screw so that the drill pipe can move up and down. There is a gear ratio between the ball screw and the hoisting motor which is set to be 1:8.935 [83]. The maximum value for RPM output is 3400 and 45 Nm for torque, respectively [67]. The hoisting motor is shown in Figure 7.6. Further motor specifications are found in Appendix E.



Figure 7.6: Hoisting motor.

7.4.2 Carriage Mount

The carriage mount is a steel frame where all the drilling components are placed. The back is connected to the nut and bracket which enables the system to be moved vertically. Channel struts are used in combination with roller guides to ensure a safe and precise displacement. The roller guides main function is to make sure that the system only moves against the same axis. The carriage mount with all mounted equipment has a total mass of 50 kg.

7.4.3 Load Cell

A cylindrical load cell manufactured by APE Transducer is used to measure and control the WOB during drilling. The specific model is TC4-AMP and is depicted in Figure 7.7a [106]. The load cell is located behind the carriage mount and just below the nut bracket as shown in Figure 7.7b. While drilling, the load cell generates voltage outputs which can be converted into force and WOB. Voltage outputs are in the range of $[-10V, 10V]$ which corresponds to a force range of $[-2500N, 2500N]$. To translate the readings into WOB, the following equation can be applied:

$$WOB = V \frac{F_2 - F_1}{g(V_2 - V_1)} - m_{offset} \quad (7.1)$$

In this equation $V[V]$ is the measured voltage given by the load cell. $F_2[N]$ and $F_1[N]$ are the upper and lower force limits that can be measured by the load cell. $V_1[V]$ and $V_2[V]$ give the corresponding voltage range, and $m_{offset}[kg]$ is a constant which is used to account for the weight of the carriage mount and its drilling components.



(a) TC4-AMP [106].



(b) Installed on rig

Figure 7.7: Load cell.

7.4.4 Safety Limit Switches

As a risk reducing measure, two safety limit switches are located on the rig to shut off the hoisting motor if the carriage mount operates beyond its operating window. They are placed on the roller guides which is the axis the system moves along. There is one at the top of the derrick to prevent the system from being hoisted over the top and avoid the BHA from hitting the derrick floor. This switch can be seen in Figure 7.8.

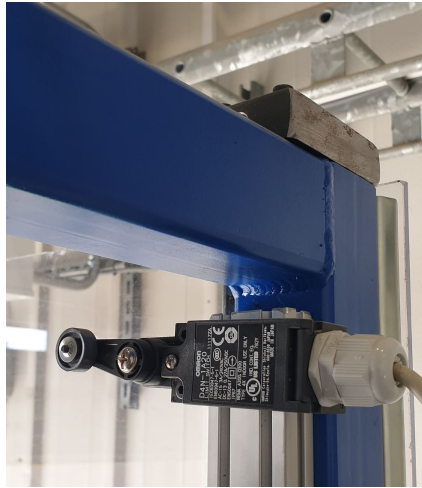


Figure 7.8: Upper safety limit switch.

On the other hand, the lower switch is placed close to the drill floor to avoid the drilling system from interfering with the upper stabilizer.

7.5 Drilling System

The complete drilling system shown in Figure 7.9, provides the rotation and stabilization required to drill the formation successfully. The miniature rig's drilling concept is based on slide drilling, which entails independent drill bit and drill string rotation. The top drive motor drives the drill bit by transmitting torque through the rod located inside the drill pipe. The drill pipe will slide along the borehole while drilling and will only be rotated by the azimuth system if an azimuth change is necessary. The drilling system also consists of two stabilizers that enhance the drilling performance by increasing workload limits and reducing lateral vibrations.

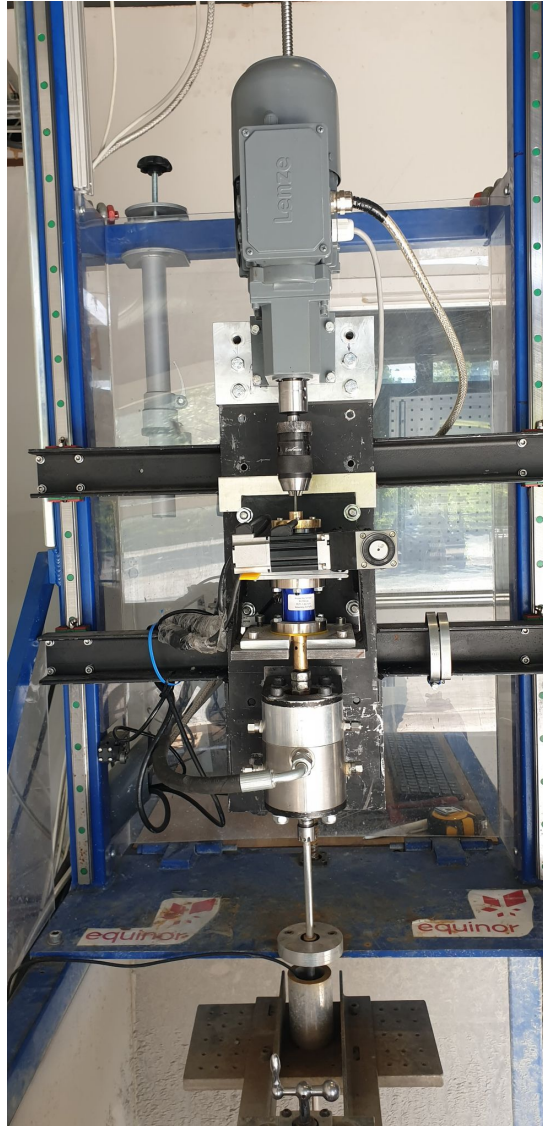


Figure 7.9: Drilling system.

7.5.1 Top Drive Motor

The top drive motor is located at the top of the drilling system and is fixed to the carriage mount via an adaptor plate as shown in Figure 7.9. The motor delivers the torque required to drill the formation by transmitting the rotational force through the rod and universal joint before reaching the drill bit.

The G500-H45 MF 063-42 Lenze motor and gearbox has a 1:2.597 gear ratio. It provides the drilling system with a rotational velocity of 1309.2 RPM and a maximum output torque of 5 Nm. Further specifications of the top drive motor are presented in Appendix F.

7.5.2 Top Drive Connection and Drill Chuck

A new top drive connection and drill chuck, seen in Figure 7.10a, fasten the rod to the top drive motor. The connection is made of stainless steel and acts as an adaptor between the motor and drill chuck.

The drill chuck has been upgraded to one that is much stronger and tightens better around the rod while drilling. The drill chuck is locked in place and consists of three jaws that grasp the rod. A unique tool seen in Figure 7.10b is used to tighten these jaws to make sure the rod remains secure and stable while experiencing rotation and vibrations during drilling. This is a cheap and effective technique as it allows for a quick and safe rod replacement in case of failure. Further drill chuck specifications are found in Appendix G.



(a) Top drive connection fastening the drill chuck to the top drive motor.



(b) Drill chuck with unique tool.

Figure 7.10: Top drive connection and drill chuck.

7.5.3 Rod

The titanium rod seen in Figure 7.11 is a compact cylindrical shaft with a length and diameter of 1.42 m and 4 mm, respectively. It extends from the drill chuck jaws down to the universal joint in the bent housing, and is used to transfer torque to the drill bit. The advantages of using titanium as the rod material are discussed in Section 8.1.3 and 8.1.6.



Figure 7.11: Titanium rod.

7.5.4 Drill Pipe

The Drillbotics guidelines predetermine the drill pipe specifications. It has a length of 91 cm and an inner and outer diameter of 7.04 mm and 9.53 mm, respectively. The hollow cylindrical drill pipe is seen in Figure 7.12. The making and breaking of drill pipe connections are not essential for the competition, and the miniature drilling rig is therefore designed to drill with the drill pipe's entire length in one run.



Figure 7.12: Aluminium drill pipe.

The guidelines permit aluminum or stainless steel as the drill pipe material. Careful considerations and calculations were made in Section 8.1.2 to select the material that can operate within its elastic limits. In conclusion, the aluminum alloy 7075-T6 was chosen as it meets all the competition requirements and will not undergo plastic deformation when subjected to the most critical bending stress.

7.5.5 Stabilizers

The miniature drilling rig has an upper and a lower stabilizer as shown in Figure 7.13. Both stabilizers increase the workload limits such as the critical buckling limit, by reducing the unsupported length of the drill pipe. They also improve the overall drilling performance by stabilizing the system and minimizing lateral vibrations.



Figure 7.13: Upper and lower stabilizer with manual hoisting mechanism.

The upper stabilizer is a 10 cm wide disc secured to the drill floor using three socket screws. The roller bearing in the disc's centre has an inner diameter that matches the drill pipe's outer diameter. It provides stability to the system by decreasing the rotational resistance while reducing the lateral vibrations of the drill pipe.

The lower stabilizer, also known as the riser, is a hollow aluminum cylinder mounted to an aluminum plate under the drill floor. Its inner diameter is marginally larger than the BHA's outer diameter so that it can efficiently stabilize the BHA during top hole drilling. Figure 7.13 also shows the manual hoisting mechanism consisting of a ball screw system and lever, which is used to position the lower stabilizer at its most effective height.

7.6 Azimuth Control System

The azimuth control system is crucial to the closed-loop steering mechanism. It is used to orient the drill string precisely and estimate the position of the drill bit accurately.

The complete azimuth control system is shown in Figure 7.14. The hollow shaft gearbox with a rotary table is located directly under the brass T-shaft's upper plate. Attached to it are the two right angled gearboxes and the azimuth servo motor. The blue torque sensor is positioned under the hollow shaft gearbox.

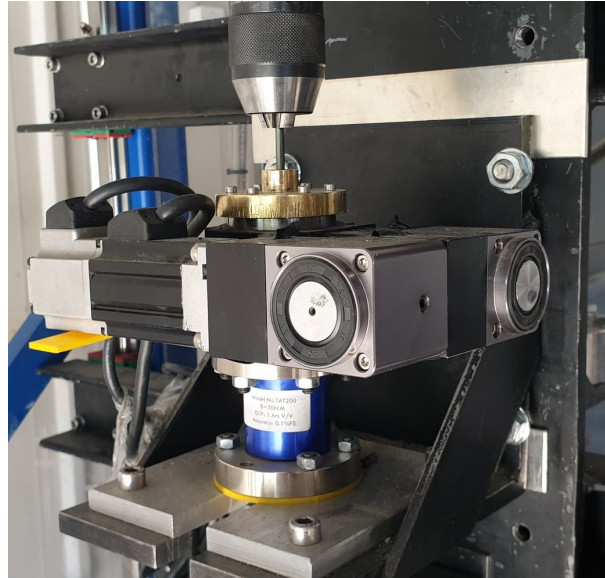


Figure 7.14: Azimuth control system.

7.6.1 Hollow Shaft Gearbox with Rotary Table

The hollow shaft gearbox with a rotary table is a Hypoid GSH 60-30K-SV1 and is shown in Figure 7.15. It permits the drill string to be oriented accurately while the rod rotates independently inside the drill pipe. The hollow shaft gearbox has a 1:30 gear ratio and can deliver the azimuth control system with a rotational velocity of 2500 RPM and a maximum output torque of 30 Nm. Further specifications of the hollow shaft gearbox are found in Appendix I.

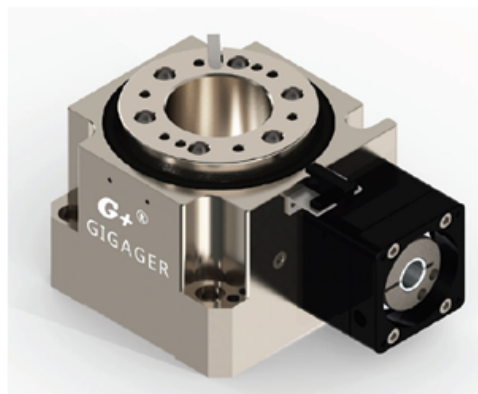
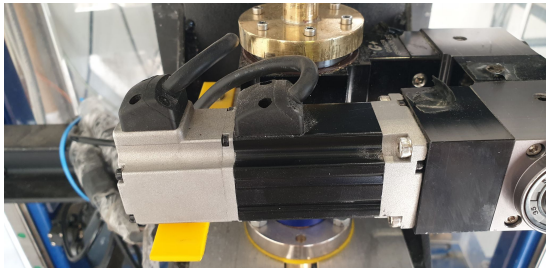


Figure 7.15: Hollow shaft gearbox with a rotary table [51].

7.6.2 Azimuth Servo Motor and Right Angled Gearboxes

The azimuth servo motor by Moons' Industries seen in Figure ??, delivers torque to the hollow shaft gearbox. It has a maximum power output of 0.1 kW and delivers the azimuth control system with a rotational velocity of 3000 RPM and a rated torque of 30

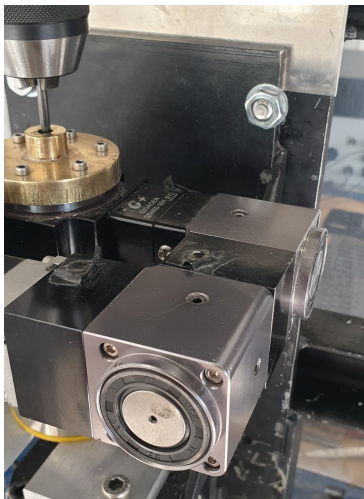
Nm. The motor and its corresponding drive support Modbus communication and are of the model SM0402AE4-KCD-NNV and M2DV-1D82IP, respectively. They are shown in Figure 7.16a. Further specifications of the hollow shaft gearbox are found in Appendix J.



(a) Azimuth servo drive and motor [82]

Figure 7.16: Azimuth servo motor components.

The azimuth motor cannot provide the low rotational velocity required for precise drill string orientation. Therefore, two right angled gearboxes with a 1:3 gear ratio are positioned between the azimuth servo motor and the hollow shaft gearbox, as seen in Figure 7.17. These GSZ042-03K-SV gearboxes from Gigager have a permissible input velocity of 2500 RPM and an allowable torque of 12 Nm. Further specifications of the right angled gearboxes are found in Appendix K.



(a) Right angled gearboxes located between the hollow shaft gearbox and azimuth servo motor.



(b) Right angled gearbox [52].

Figure 7.17: Gearbox.

As a result, the complete azimuth control system obtains a 1:270 gear ratio. This provides adequate accuracy of the drill string orientation for the competition.

7.6.3 T-shaft

The hollow brass T-shaft transfers rotation from the azimuth motor to the drill pipe, while permitting internal rotation of the rod. At the top, the T-shaft is attached to the gear box, passing through the rotary table and the torque sensor. At the bottom, the T-shaft is screwed onto the hollow shaft on the hydraulic swivel. It has a small inner channel of 4 mm where the rod can freely rotate, while preventing any water from migrating upwards from the hydraulic swivel. The hollow brass T-shaft can be seen in Figure 7.18. The complete dimensions are given in Appendix L.



Figure 7.18: Brass T-shaft [9].

7.6.4 Torque Sensor

An external torque sensor is used as part of the azimuth system. The model TAT200 is a hollow torque sensor produced by HT Sensor Technology. It measures the torque applied to the drill pipe by the azimuth motor, in the range of 0-30 Nm. The torque sensor is positioned using two adaptor plates along the T-shaft, and is displayed in Figure 7.19. Specifications of the torque sensor are given in Appendix M

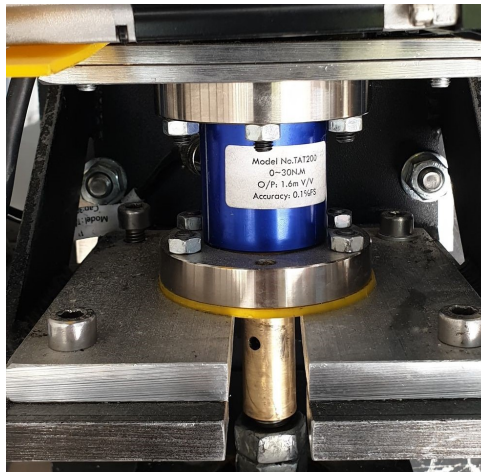


Figure 7.19: Torque sensor installed.

7.7 Circulation System

The circulation system is responsible for providing drilling fluid to the rig. Among the most important functions that this system provides are cutting removal from the wellbore, as well as lubrication and cooling of the bit.

The circulation system has been upgraded from an open system to a semi-closed system. This was achieved by introducing a new diverter. This allows the returns to be controlled and handled in a safe manner.

7.7.1 Hydraulic Swivel

The hydraulic swivel allows water to be supplied to the rig, while permitting the internal azimuth system to rotate freely. The swivel has five major components: swivel house, hollow swivel shaft, roller bearings, seal section and drill pipe connector. It is fixed to the carriage mount as seen in Figure 7.20.

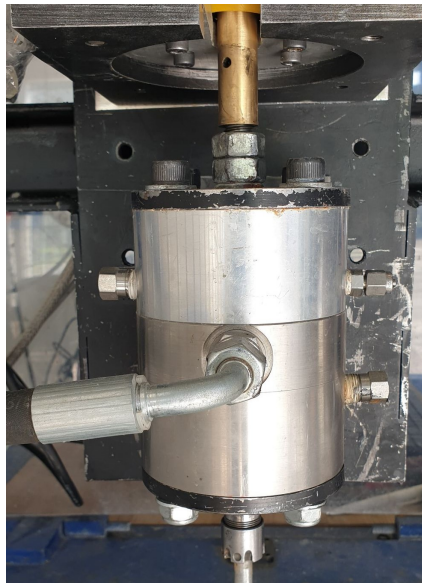
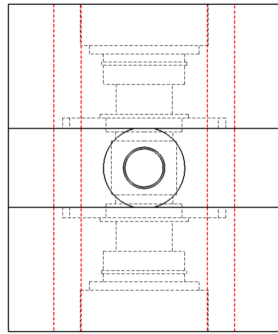


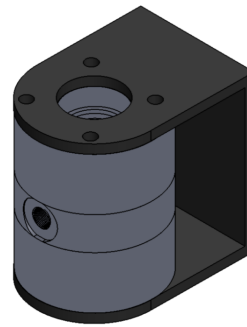
Figure 7.20: Hydraulic swivel fixed on the carriage mount [9].

7.7.1.1 Swivel House

The swivel house consists of a top, middle and bottom section. These components are made of stainless steel and are held together by an iron cast holder, using four iron bolts. These bolts go through the housing and the holder, and are secured at both ends with insert lock nuts. This concept is shown in Figure 7.21



(a) Swivel house cross section.



(b) Iron cast holder.

Figure 7.21: Swivel house.

7.7.1.2 Hollow Swivel Shaft

The hollow swivel shaft is used to transmit torque between the T-shaft and drill pipe. It has a 10 mm orifice which allows water to enter the drill pipe. The 4 mm inner diameter above the orifice prevents water from migrating up towards the azimuth system. On the other hand, the lower end of the swivel shaft has a diameter of 7mm, which results in a smaller pressure drop. Thus, the water is favoured to travel down the drill pipe. This principle is seen in Figure 7.22.

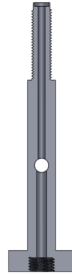


Figure 7.22: Swivel shaft cross section [9].

The outer diameter of the swivel shaft remains constant. This allows for a proper seal in the swivel housing. The swivel shaft is connected to the T-shaft using three nuts as shown in Figure 7.23. This prevents the system from unscrewing if it is rotated in a counter-clock wise direction.

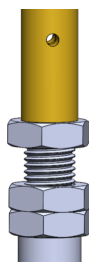


Figure 7.23: Connection between the swivel shaft and brass T-shaft [9].

7.7.1.3 Roller Bearings

The roller bearings permit a firm grip between the swivel housing and the swivel shaft. Additionally, the swivel shaft is allowed to rotate freely both in both directions with reduced friction. The roller bearings design and position inside the swivel housing can be observed in Figure 7.24.

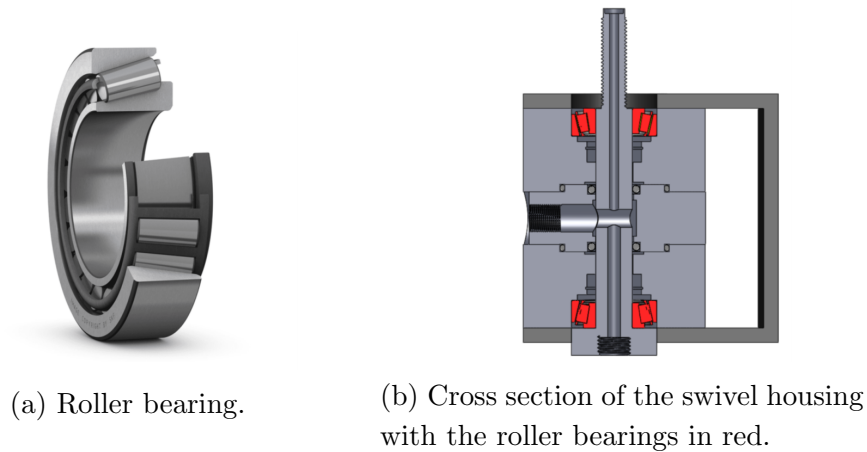


Figure 7.24: Roller bearings in the swivel housing [9].

7.7.1.4 Sealing Section

The sealing section in the swivel housing consists on four concentric O-rings, placed as a way to avoid any water leakage from the housing. The four O-rings are located in circular-shaped grooves between the sections of the swivel housing. This can be observed in Figure 7.25.

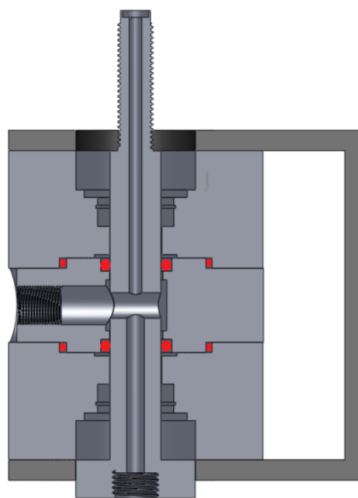


Figure 7.25: Housing cross section with O-rings marked in red [9].

7.7.1.5 Drill Pipe Connection

The drill pipe is attached to the swivel shaft using a drill pipe connector. The connector consists of a nipple, spring collet and cap as shown in Figure 7.26. The nipple is hollow and is screwed onto the lower end of the swivel shaft. The spring collet tightens around the drill pipe and an O-ring is placed as an extra measure to avoid leakage.



Figure 7.26: Drill pipe arrangement from top: nipple, drill pipe, O-ring, spring collet and collet nut.

This connection is designed to withstand a maximum torque of 17 Nm. Given that the maximum expected torque when drilling will be around 4.5 Nm, the connection should be able to withstand the loads.

7.7.2 Diverter

A new diverter was designed and implemented to the miniature rig to create a semi-closed circulation system. The top of the diverter is screwed into the lower stabilizer. The bottom end has a rubber seal that is compressed using the manual hoisting mechanism and prevents leakage. The inner diameter was designed to allow the BHA to rotate freely while drilling the top hole section.

The lower end of the diverter is equipped with a bell nipple. A hose can be easily attached to guide the returning water and cuttings to the drain. This significantly improved the HSE since the returns are disposed in a controlled manner and toxic chemicals are not left exposed to the air. Additionally, slippery surfaces in the working area are prevented which further reduces potential injuries to personnel. The diverter was manufactured in the workshop and the final result is shown in Figure 7.27. Further details of the diverter and dimensions are found in Appendix O.



Figure 7.27: Diverter.

7.8 Electrical System

The electrical system of the miniature rig is responsible for sensor data acquisition and control of different motors.

7.8.1 DAQ

Several of the sensors on the rig can only send analog signals, and a Data Acquisition (DAQ) is therefore used to convert to digital signals which can be further processed in the control system. A DAQ has been used in the electrical system since 2018, and it is manufactured by National Instrument with model name USB-6212 as seen in Figure 7.28. The sampling rate is maximum 400 kS /s [63]. The load cell and the torque sensor are the only components that are connected to the DAQ.



Figure 7.28: USB-6212 DAQ [63].

7.8.2 Downhole Sensor

The use of downhole sensor data in the control algorithms of the rig has been a competition requirement since 2019. The sensor used in this system is an Arduino Nano 33 BLE which is the same sensor used last year. It has the dimensions of 18 x 45 x 7 mm (W x L x H) and is shown in Figure 7.29. The sensor card has a gyroscope, tri-axial accelerometer and magnetometer that can be used to estimate the inclination, azimuth and the position of the drill bit and BHA. It is powered and communicates with the computer through a USB cable.



Figure 7.29: Arduino Nano 33 BLE [28].

7.8.3 Overview Electrical System

A simple overview of the electrical system is presented in Figure 7.30. As the figure shows, the load cell and torque sensor are connected to the DAQ, which is further connected to one of the computers. Furthermore, the sensor card data acquisition takes place through a standard USB cable that transfers data directly to the computer. All the different motors on the rig are operated and controlled from the control system via Modbus TCP communication technology.

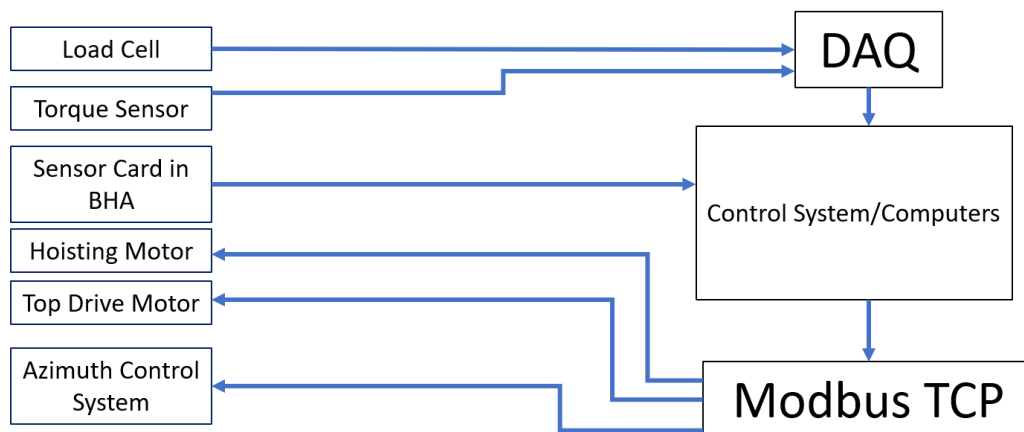


Figure 7.30: Overview electrical system.

7.9 Wireless Communication Options

Wireless communication options were researched with the aim to get rid of the USB cable. Although functional, the cable restricts large azimuth changes as it can become tangled around the drill string and break. As a solution, the team reviewed different options to establish wireless communication between the downhole sensor and the computer. The first option was to use Bluetooth as this was already a built-in function in the downhole sensor card. Unfortunately this method proved to not work and alternative wireless options had to be explored. Communication through radio waves and magnetic fields were also explored, but ended with unsuccessful results. Details about these options are presented in this section.

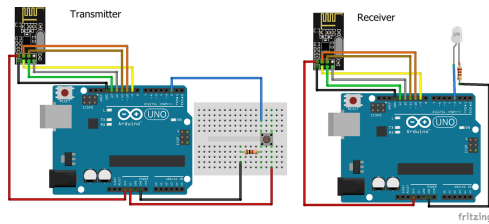
7.9.1 Bluetooth Communication Option

The Arduino Nano 33 BLE sensor card was programmed to transfer data and communicate through Bluetooth. Several tests were conducted at surface and a stable connection between the sensor card and the computer was established. However, when the sensor card was placed inside a pre-drilled well in the rock sample, it was difficult to maintain communication. Several attempts were performed with different settings, but ended unsuccessfully as well. The team discussed this issue with a Bluetooth expert who explained the method was impractical due to the large rock density. For this reason, the team discontinued the Bluetooth option.

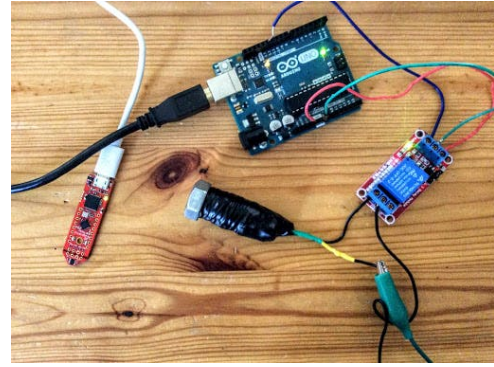
7.9.2 Wireless Communication Alternatives

Additional research led the team to believe that communication through radio waves or magnetic fields could be viable options. However, since these were not supported by the current sensor card, the team had to look for sensors in the market using these communication methods.

The team found affordable sensor cards produced by Arduino for both options. The sensor card supporting radio wave communication is shown to the left in Figure 7.31a, while the magnetic field option is shown to the right. Both sensors consist of a receptor and transmitter array [59] [60].



(a) Radio waves data transfer [59].



(b) Magnetic field data transfer configuration [60].

Figure 7.31: Wireless data transfer options.

Unfortunately, neither of the sensor cards were suitable options due to the large size. They would not be able to fit inside the BHA. As a result, the wireless communication was discontinued, and the cable will be used to transfer data from the downhole sensor.

7.10 Bottom Hole Assembly Design

The original plan this year was introduce wireless communication and avoid having a cable downhole as it did not allow for continuous rotation of the BHA when drilling the vertical section with the bent sub. To achieve this goal, the BHA needed to be redesigned to make space for the batteries that would power the sensor card. A wireless connection would also make it possible to move the sensor card closer to the drill bit, which would decrease the uncertainties in the position estimation of the drill bit in the well.

The team completed a BHA redesign in parallel to testing the wireless Bluetooth communication. Unfortunately, the Bluetooth communication was unsuccessful and the wireless BHA design could not be implemented. For that reason, the BHA from last year had to be reintroduced and is presented in this section. The work related to the wireless BHA design will also be covered in this section in case later NTNU teams should benefit from it.

7.10.1 Original BHA Design

The original BHA inherited from last year is shown in Figure 7.32. It was designed to provide stability and steering capability while drilling. It also houses the sensor card and transmits torque from the rod to the drill bit. From top to bottom, the BHA is composed of an upper stabilizer, sensor housing, bent sub, lower stabilizer, wear plate and a bit sub. The design also includes a universal joint and drive shaft within. All these components will be described in further detail below.

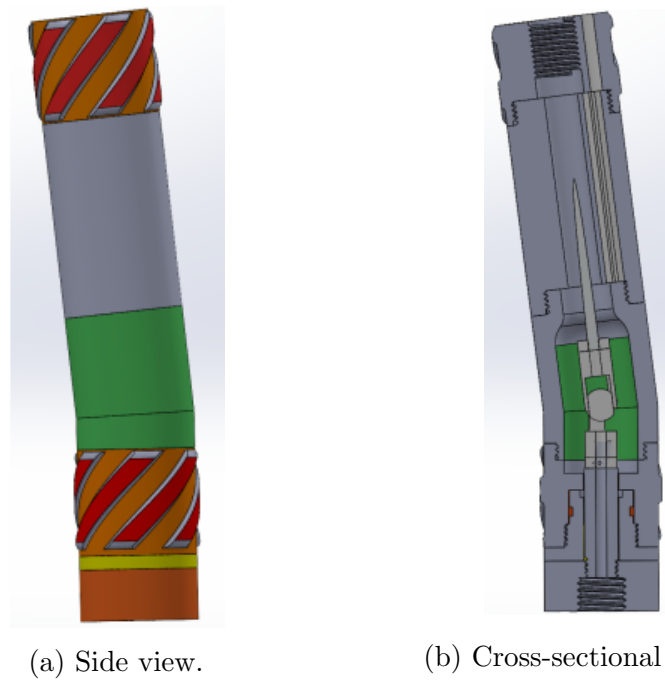


Figure 7.32: Original BHA design showing all components [9].

7.10.1.1 Stabilizers

The responsibility of the stabilizers is to ensure a stable BHA while drilling. In addition, they counteract vibrations and make the BHA easier to steer in the desired direction. The stabilizers are manufactured using thick-walled steel which makes them strong enough to withstand loads experienced during drilling operations.

Figure 7.33 shows the design of the upper stabilizer. It is located at the top of the BHA and connects to the drill pipe. The lower stabilizer has a similar design, but without a drill pipe connection. It is positioned between the bent sub and wear plate.

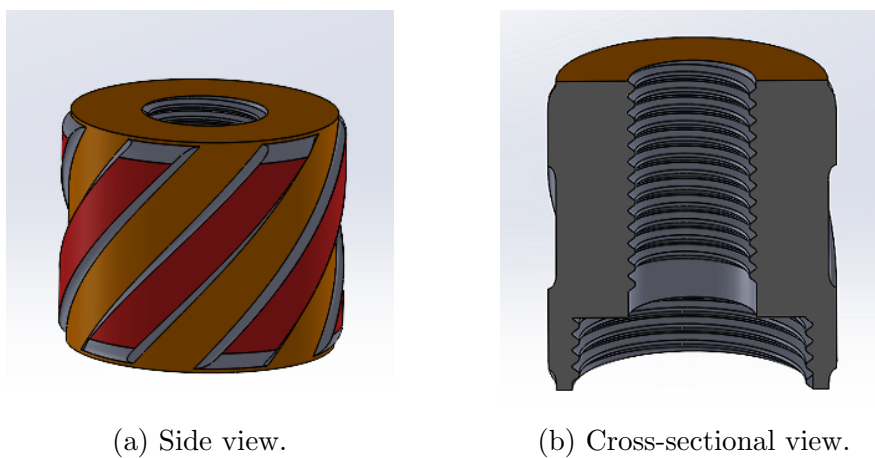


Figure 7.33: Upper stabilizer design.

7.10.1.2 Sensor Housing

The sensor housing is located between the upper stabilizer and bent sub. It is a thick-walled cylinder that contains a compartment to hold the sensor card. The design is shown in ???. The compartment protects the sensor card from water and mechanical stresses which permits stable power and communication between the sensor card and computer.

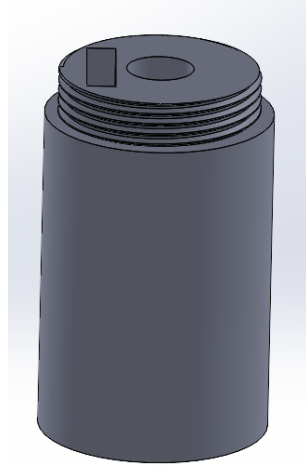


Figure 7.34: Sensor housing.

7.10.1.3 Bent Sub

The bent sub is located below the sensor housing and is shown in Figure 7.35. The fixed angle on the bent sub enables the BHA to kick off and build a deviated well path. The angle is determined using the DLS that is required to reach the maximum inclination that is specified by the guidelines. The bit tilt required to drill a 30° inclination is 6.91° .

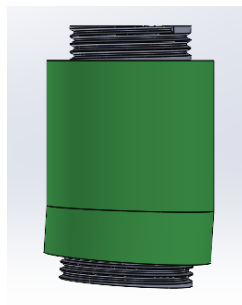


Figure 7.35: Bent Sub.

The bent sub also houses the transmission section with the universal joint welded to the drive shaft. The rod extends halfway through the sub where it is connected to the universal joint that transfers torque and rotation to the drill bit.

7.10.1.4 Wear Plate

There is friction in the connection between the bit sub and the lower stabilizer. During drilling operations, the bit sub rotates against the stabilizer and together with cuttings, the components wear down over time. To prevent this happening, a wear plate in peak is utilized. Instead of damaging the component, the wear plate will wear down over time, so it needs to be replaced after some period of time.

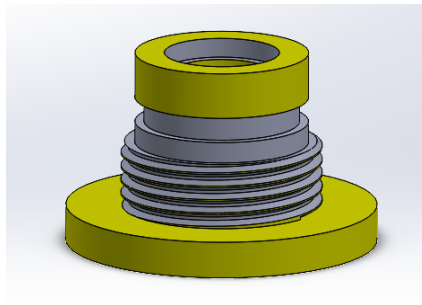


Figure 7.36: Wear plate.

7.10.1.5 Bit Sub

The bit sub shown in Figure 7.37 is located below the lower stabilizer acts as the connection between the drive shaft and drill bit. It is manufactured in steel and is able to withstand high loads during drilling. Based on previous experiences, the bit sub has proven to work well and does not need to be upgraded or redesigned.

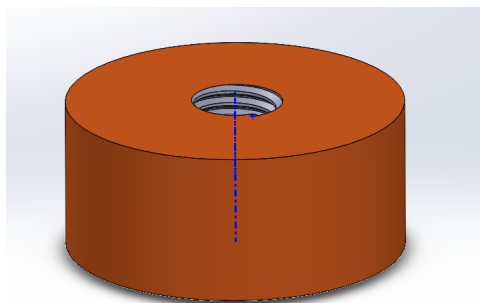


Figure 7.37: Bit sub design.

7.10.2 Wireless BHA Design

The wireless communication required a redesign of the original BHA design. The new design is shown in Figure 7.38. Although not implemented, it would potentially be able to increase the control and steerability of the BHA. The modifications made to the original design are presented in the following sections.

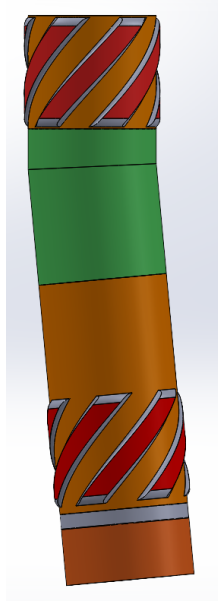
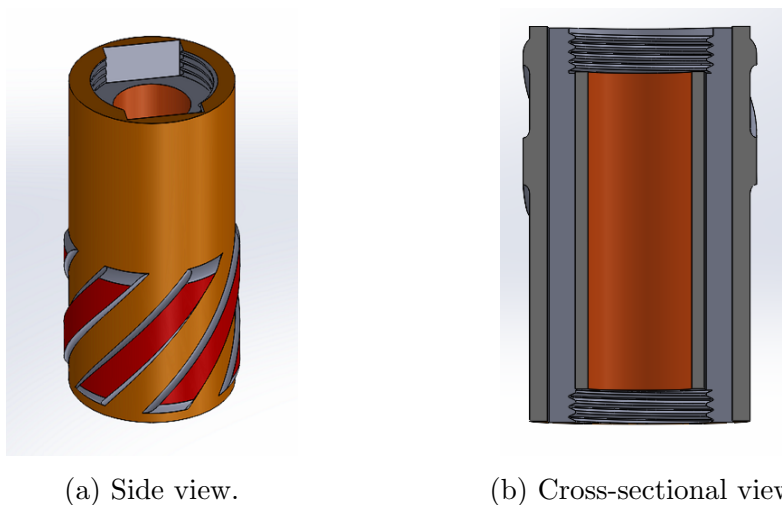


Figure 7.38: BHA design wireless solution.

7.10.2.1 Combined Sensor Housing and Lower Stabilizer

Compared to the original design, the redesign combines the lower stabilizer and sensor housing into one component. In this way, the total length of the BHA is shortened by 3.9 cm as one coupling point is removed. This will increase the steerability and also make the design more robust.

The combined sensor housing and stabilizer is located below the fixed bent sub, which also makes the position estimation more accurate since the sensor card is placed closer to the bit. As shown in Figure 7.39, two compartments are present which house the sensor card and batteries required for wireless communication.



(a) Side view.

(b) Cross-sectional view.

Figure 7.39: Lower stabilizer design.

7.10.2.2 New Wear Plate

The BHA design that allows for wireless communication will need a redesign of the wear plate to fit properly. The wall thickness has to be reduced and the length had to be increased to fit it through the combined lower stabilizer and sensor housing. The new design of the wear plate is presented in Figure 7.40

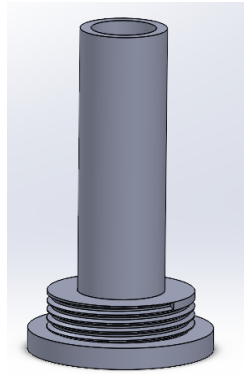


Figure 7.40: Redesigned wear plate.

7.11 Drill Bit

The drill bit is a small but essential component on the rig as it greatly affects drilling performance. With the correct specifications, drill bit stability, steerability and durability are increased which enhances drilling parameters such as ROP and hole quality. Therefore, the team aimed to find the optimum drill bit design to achieve the best results for the Drillbotics competition.

DSATS supplies all teams with a PDC drill bit that can be used for the competition day. However, the guidelines state that the teams also have the option to design and produce their own drill bits. Experiences from previous NTNU Drillbotics teams found that the custom designed drill bits manufactured by Lyng drilling performed better than any other tested bits. Therefore, this year's team decided to solely focus on a custom design.

The team last year designed and optimized two drill bits in accordance with the competition requirements. Since this year's competition objective and required drill bit dimensions are identical, this year's team opted to use these drill bits as a starting point. Last year's team did not have enough time to perform a thorough analysis on these drill bits. Therefore, this year's team originally sought to test, evaluate and compare their performance before further optimizing the drill bit designs using the theory presented in Section 6.4. However, due to the long manufacturing process and busy schedule of Lyng drilling, the new drill bits had to be designed and ordered immediately. After performing a qualitative evaluation and receiving feedback from last year's team and Lyng drilling, four new drill bits were designed in Solidworks and manufactured.

This section will present the design of both the old and new drill bits and give an overview of their specifications. Finally, the general modelling process in Solidworks will be shown.

7.11.1 Old NTNU Drill Bits

Last year's team designed and manufactured NTNU Bit 1 and NTNU Bit 2 in collaboration with Lyng Drilling. Achieving a high ROP was not their primary focus when creating the drill bit designs since a generous three hours was given to drill the well on the competition day. On the other hand, they aimed to design a steerable drill bit with a high degree of stability that would give minimal torque and vibrations, as this would be required to drill a directional well effectively. Two different designs were produced due to the trade-off between steerability and stability. NTNU Bit 1 was intended to be more stable, while NTNU Bit 2 focused on the steering capability. The drill bits are seen in Figure 7.41 and the designs differ in the cone angle, blade layout and cutter number [9].

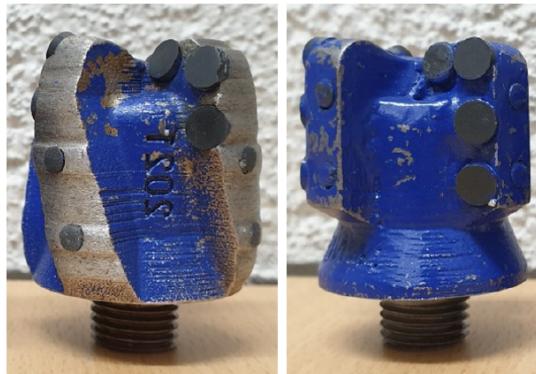


Figure 7.41: NTNU Bit 1 and NTNU Bit 2.

NTNU Bit 1

The main objective of NTNU Bit 1 was to increase the stability of the drill bit and reduce its lateral vibrations. This was achieved by designing the bit with a short parabolic profile and a medium cone angle. In addition, the bit had a long gauge pad and spiraling blades, which maximized the surface area of the gauge pad and thereby reduced the gauge stresses.

The bit body consisted of 12 integrated cutters with a 6 mm diameter arranged in a single set layout. Only one cutter was placed on the gauge of the drill bit to decrease the side aggressiveness and reduce the lateral vibrations. To further increase the stability, the DOC on the bit face and gauge were limited to 0.75 mm and 0.1 mm, respectively. This also has a positive effect on the durability of the drill bit by preventing cutter failure.

To ensure efficient drilling with a high ROP, the bit face cutters were designed with 15° back rake angles. In contrast, the gauge cutters were set to 25° to reduce the bit aggressiveness and maintain the bit stability. High hole cleaning efficiency was ensured with 4 nozzles and enhanced by setting all cutter side rake angles to 10° . Lastly, the gauge of

each blade contained two Thermally Stable Polycrystalline (TSP) diamond inserts which produced low friction surfaces and increased lateral stability [9].

NTNU Bit 2

NTNU Bit 2 was designed with the primary focus of increasing the steerability of the drill bit. It had four major differences compared to NTNU Bit 1.

Firstly, as opposed to using a medium cone angle, a shallow cone angle was used to increase the drill bit's steering capability. The length of the gauge pad was reduced to make it more passive and prevent the drill bit from going straight when trying to build angles. Straight blades were also implemented instead of spiral blades to increase the side aggressiveness by allowing the cutter radial forces to be summed up on the gauge. Finally, 16 cutters were integrated into the bit body instead of 12, which allowed for 2 cutters to be placed on the gauge and increase the steerability of the bit [9].

7.11.2 New NTNU Drill Bits

The team analysed the two drill bits from last year before attempting to create a new optimized drill bit design. Since there was not any quantitative data available from drill bit testing last year, the team had to rely on verbal feedback, qualitative observations and simulations performed in collaboration with Lyng drilling.

Last year's team expressed that both drill bits performed well and were sufficient for the Drillbotics competition. However, vibrations were the largest issue experienced while drilling and they recommended to use NTNU Bit 1 due to its extra stable design. Therefore, the team ruled out NTNU Bit 2 and chose to further investigate methods to enhance the design of NTNU Bit 1.

Next, the team performed a qualitative evaluation of the drill bit. NTNU Bit 1 indicated some overall wear on the bit body and had experienced impact damage on two of the cutters as seen in Figure 7.42. The cutters affected were located on the nose / shoulder of blades 2 and 4. The cause is unknown but was most likely due to high loads sustained while drilling.

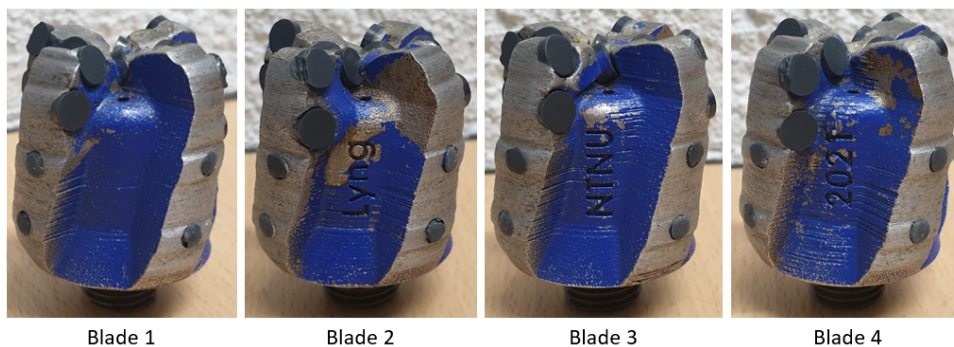


Figure 7.42: Qualitative evaluation of NTNU Bit 1.

Figure 7.43 demonstrates the cutter distribution of NTNU Bit 1 more clearly. From the figure it can be seen that the two damaged cutters were the most exposed and will therefore have endured the highest loads while drilling. This is an issue the team decided to focus on when optimizing the drill bit design.

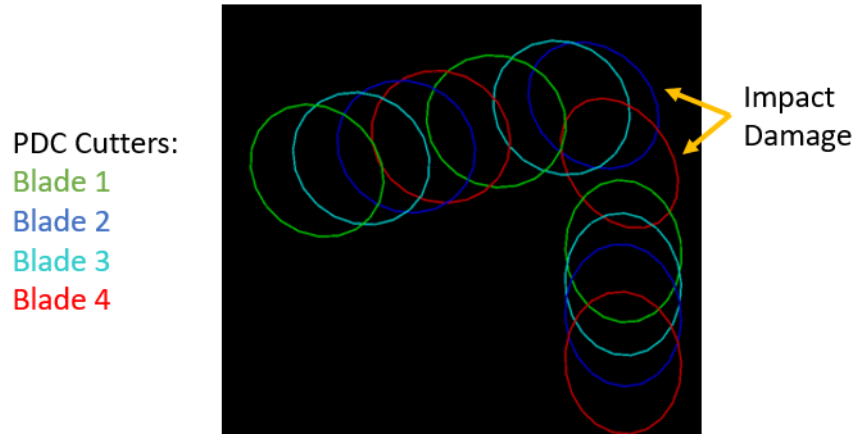


Figure 7.43: NTNU Bit 1 cutter distribution.

The drill bit simulation performed with Lyng drilling showed that the drill bit was around 27% out of balance while drilling which would have led to wasteful energy and inefficient drilling. Therefore, to improve the drill bit performance, the team also wanted to create a design with a higher force balance.

Based on the feedback, observations and simulations, the team decided to create several new designs built on NTNU Bit 1, which will all be tested in order to find the optimal drill bit for the competition.

NTNU Bits 3 and 4

NTNU Bits 3 and 4 are constructed with the same design as NTNU Bit 1. The reason for this is due to the unspecified cause of the cutter impact damage. The team wants to perform further testing and analysis to determine whether the damage was a cause of excessive drilling loads or inadequate drill bit design.

However, the two drill bits differ slightly from NTNU Bit 1 as the sharp cutters used were no longer available. Instead, NTNU Bits 3 and 4 are manufactured with $0.3 \times 45^\circ$ bevel cutters. The difference in cutter shape is shown in Figure 7.44. The effect the new design is unknown and will be investigated during testing.



Figure 7.44: Sharp and bevel cutters.

Since the bit body of NTNU Bit 1 experienced some wear, the team also wanted to investigate whether a new material could increase the drill bit durability. Therefore, NTNU Bit 3 will be made of the original X1 Metal 420i steel infiltrated with bronze, while NTNU Bit 4 will be hard-faced with the stronger 17-4PH stainless steel. More detailed material specifications are found in Appendix Q.

The final product of NTNU Bits 3 and 4 are shown in Figure 7.45.

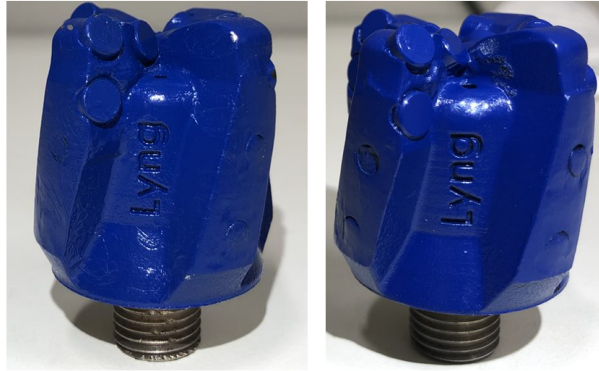


Figure 7.45: NTNU Bit 3 and NTNU Bit 4.

NTNU Bits 5 and 6

The design of NTNU Bits 5 and 6 was created based on the observations and simulations performed on NTNU Bit 1. Various modifications were made to last year's design to enhance the bit durability and drilling performance.

First of all, the cutting structure was altered slightly as seen in Figure 7.46. The cutter density on the nose / shoulder was increased to limit the exposure of high drilling loads that may result in impact damage. Several cutters on the gauge were also adjusted to improve the force balance of the drill bits. According to simulations performed with Lyng drilling on this new bit design, the unbalanced forces while drilling have decreased from 27% to 16%, which should generate an increase in drilling efficiency.

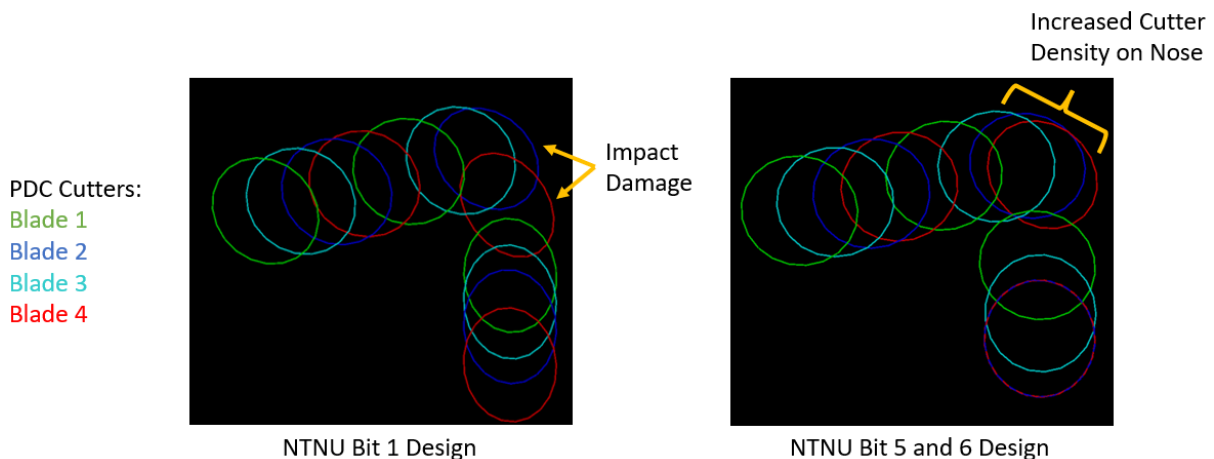


Figure 7.46: Cutting distribution of NTNU Bit 1 and NTNU Bit 5 and 6.

Figure 7.47 displays the alterations made to the bit body. The width of the blades on the face and gauge were increased to enhance the drill bit stability and lessen the vibrations experienced during drilling last year. Two additional wear protecting TSP inserts were implemented to each gauge pad to produce low friction surfaces and improve drill bit durability. An extra TSP insert was added to the nose of the bit as re-enforcement and as a DOC limiting feature. Lastly, space was also opened up in the centre of the drill bit to add an extra nozzle for improved cutting removal.

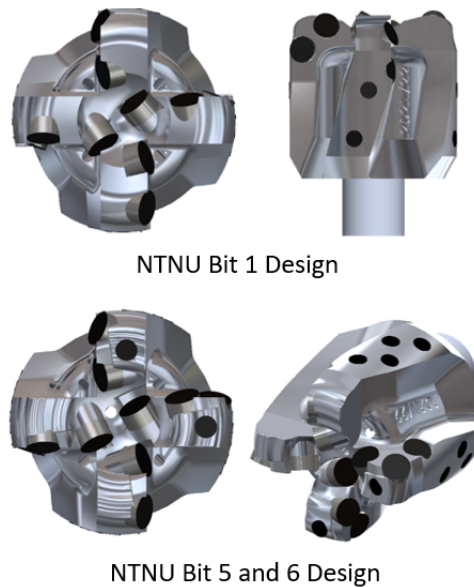


Figure 7.47: Bit body of NTNU Bit 1 and NTNU Bit 5 and 6.

NTNU Bits 5 and 6 differ in two ways. Firstly, as mentioned previously, the team wants to examine the effect of the bit body's material on the drill bit durability. Therefore, NTNU Bit 5 is composed of the original X1 Metal 420i, while NTNU Bit 6 is hard-faced with 17-4PH stainless steel. Secondly, Lyng drilling had 7 sharp cutters left over from previous years. The team decided to use these cutters on the bit face of NTNU Bit 5 while the outstanding cutters remain bevel shaped. NTNU Bit 6 is only arranged with bevel shaped cutters. The final products of these drill bits are shown in Figure 7.48.

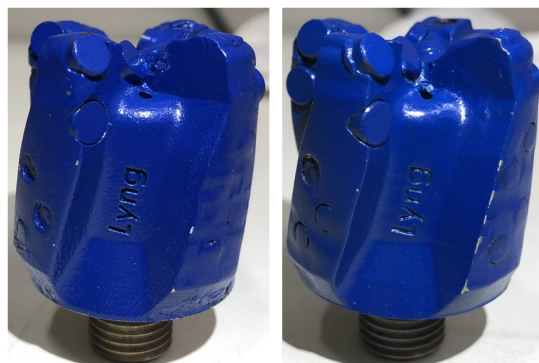


Figure 7.48: NTNU Bit 5 and NTNU Bit 6.

7.11.3 Drill Bit Specifications

The various drill bit designs that will be tested and evaluated in this project are displayed in Figure 7.49.



Figure 7.49: NTNU drill bits.

Table 7.1 shows an overall comparison of the NTNU bit specifications. The differences in bit body material and cutter shape, as well as the number of TSP inserts and nozzles are clearly presented. Additional information of the various drill bit designs is found in Appendix Q.

Table 7.1: Drill bit specifications.

Bit Type	NTNU Bit 1	NTNU Bit 2	NTNU Bit 3	NTNU Bit 4	NTNU Bit 5	NTNU Bit 6
Bit diameter	1.5"	1.5"	1.5"	1.5"	1.5"	1.5"
Length	1.8"	1.8"	1.8"	1.8"	1.8"	1.8"
Bit body material	X1 Metal 420i	X1 Metal 420i	X1 Metal 420i	17-4PH Steel	X1 Metal 420i	17-4PH Steel
Blade number	4	4	4	4	4	4
Sharp cutter number	12	16	0	0	7	0
Bevel cutter number	0	0	12	12	5	12
Cutter diameter	0.236"	0.236"	0.236"	0.236"	0.236"	0.236"
TSP inserts number	8	8	8	8	17	17
Nozzle number	4	4	4	4	5	5

7.11.4 Drill Bit Modelling Process

NTNU Drillbotics has had a longstanding collaboration with Lyng Drilling. The team is responsible for designing and modelling the drill bit, while Lyng Drilling manufactures the final product. Continuous communication between the two parties is essential to successfully create the optimal drill bit for the competition.

The drill bit modelling process begins with identifying the necessary bit properties for an operation. Based on the theory and design considerations developed in Section 6.4, a 2D sketch is prepared as a foundation for the final bit design. The purpose of the 2D sketch is mainly to present the bit and blade geometry, as well as specify parameters such as

bit diameter, bit profile, cone angle and cutter distribution. The 2D sketch for the new NTNU Bits 5 and 6 is seen to the left in Figure 7.50.

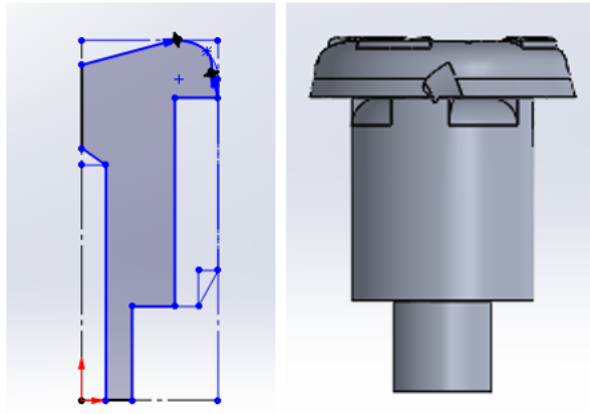


Figure 7.50: 2D sketch and basic 3D model of the drill bit body.

Based on the 2D sketch, a basic 3D model of the drill bit's body is developed in SolidWorks, as seen to the right in Figure 7.50. This is achieved using the revolve boss/base application in the modelling program.

The next step is to determine the cutter geometry and orientation, which includes the back rake and side rake angles. Once established, the cutter structure is modelled in SolidWorks as seen in Figure 7.51. These cutters will be used as placeholders when creating the bit body.

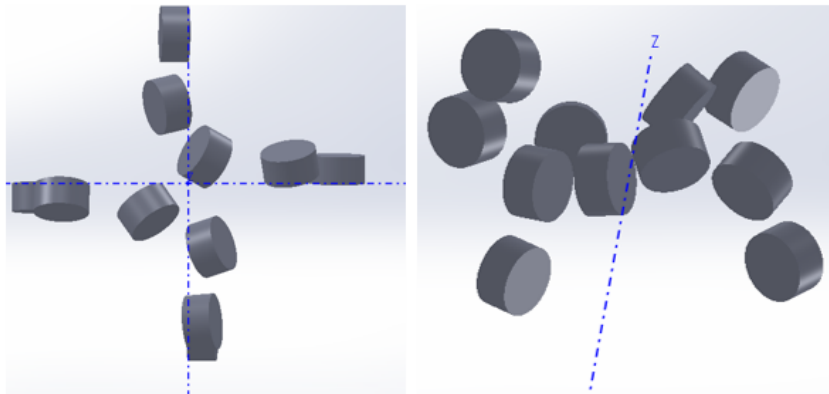


Figure 7.51: Top and side view of 3D cutter structure.

Thereafter, the complete bit body shown in Figure 7.52 is modelled by inserting the bit blades, creating the cutter sockets and extruding the nozzles.

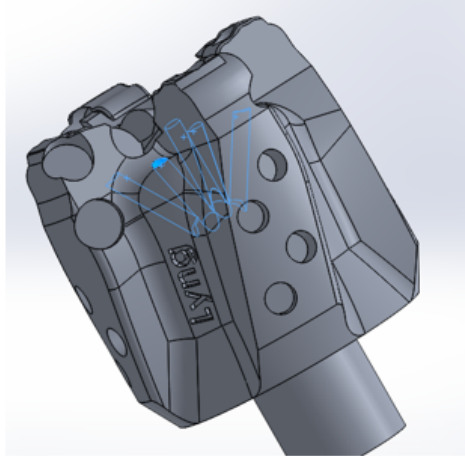


Figure 7.52: Final bit body.

Finally, the SolidWorks drill bit model is sent to Lyng drilling for feedback and approval. Once both parties are pleased with the design, it is 3D printed and sent to Lyng Drilling where they add the finishing touches. Threads are created and the cutters and inserts are integrated into the bit body using silver which has a melting point of 700° . The 3D printed drill bit mould and final product are shown side by side in Figure 7.53.

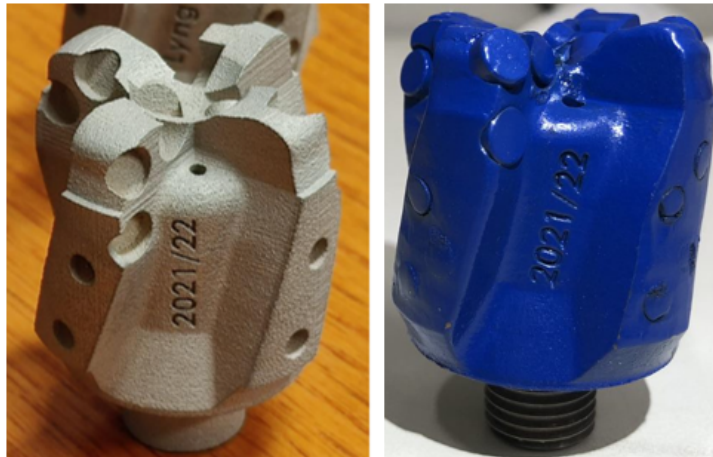


Figure 7.53: 3D printed drill bit mould and final product.

Design Limits and Constraints

The Drillbotics guidelines provide certain constraints that must be followed for the competition. These include both restrictions to the mechanical components and rig power consumption. Analysis and results regarding these two topics will be discussed in this chapter.

8.1 Mechanical Limitations

Mechanical and operational limitations are essential for the miniature drilling rig to function correctly and safely. Exceeding these limitations will lead to failure and a hazardous environment. The Drillbotics guidelines provide several constraints, which will be assessed in this section to justify the implementation of various rig components. Table 8.1 contains the design parameters for evaluating the design limits.

Table 8.1: Design parameters.

Variable	Symbol	Value	Unit
OD Drill Pipe [90]	OD_{DP}	9.53	mm
Wall Thickness Drill Pipe [90]	t_{DP}	1.24	mm
Length Drill Pipe [90]	m_{DP}	0.06	kg
Mass Drill Pipe	L_{DP}	91.44	cm
Diameter Rod	d	4.00	mm
Length Rod	L_{rod}	1.42	m
Mass Rod	m_{rod}	0.078	kg
Speed of sound Aluminium [61]	c	3100	m/s
Speed of sound Titanium [61]	c	3125	m/s
Elasticity Modulus - Stainless Steel 316 [78]	E	200	GPa
Elasticity Modulus - Aluminium 6061-T6 [79]	E	68.90	GPa
Elasticity Modulus - Aluminium 7075-T6 [80]	E	71.70	GPa
Elasticity Modulus - Grade 5 Titanium [89]	E	114	GPa
Shear Modulus - Stainless Steel 316 [27]	G	74	GPa
Shear Modulus - Aluminium 7075-T6 [27]	G	26.9	GPa
Shear Modulus - Grade 5 Titanium [27]	G	44	GPa
Material Yield Strength - Stainless Steel 316 [78]	σ_{ys}	290	MPa
Material Yield Strength - Aluminium 6061-T6 [79]	σ_{ys}	276	MPa
Material Yield Strength - Aluminium 7075-T6 [80]	σ_{ys}	503	MPa
Material Yield Strength - Grade 5 Titanium [89]	σ_{ys}	1100	MPa
Fatigue Strength - Aluminum 7075-T6 [80]	σ_{fat}	159	MPa
Fatigue Strength - Grade 5 Titanium [89]	σ_{fat}	700	MPa
OD BHA	OD_{BHA}	36.07	mm
ID BHA	ID_{BHA}	26.42	mm
Length BHA	L_{BHA}	20.5	cm
Mass BHA	m_{BHA}	1.5	kg
ID Swivel + Hose	ID_{S+H}	11.94	mm
Length Swivel + Hose	L_{S+H}	2.50	m
Roughness - Aluminium 7075-T6 [35]	ϵ_{DP}	$1.30 \cdot 10^{-6}$	m
Roughness - Grade 5 Titanium [13]	ϵ_{rod}	$1.50 \cdot 10^{-5}$	m
Fluid Density	ρ_f	1000	kg/m ³
Solid Density	ρ_s	2650	kg/m ³
Fluid Viscosity	μ_f	1	cP

8.1.1 Well Path

A well path must be smooth and efficient to precisely hit the given targets in the shortest possible time. The directional requirements given by the Drillbotics guidelines are as follows:

- *Hit one or more targets at one or more vertical depth(s) and X/Y coordinates.*
- *For the Group B competition, the starting directional plan to hit the targets will not require wellbore inclinations in excess of 30° from vertical, 15° change in azimuth, or 10" displacement (departure from the vertical axis at well center). The max displacement / inclination / azimuth are total / accumulated from the start to the end of the well path.*

The well path is constrained by either a 30° inclination or a 25.40 cm (10 in) horizontal displacement from the vertical axis. To create the best possible rig design, the team has evaluated which of these restrictions limit the well path.

The well will be drilled in a rock sample provided on the competition day with dimensions of 30 x 61 x 61 cm (12 x 24 x 24 in). First, a vertical pilot hole must be drilled to the kick off point, which is located at a depth equal to or greater than 10.16 cm (4 in). This leaves a maximum vertical section of 50.80 cm (20 in) available for the directional well path.

Restricting the directional well path to a 30° inclination while assuming a constant build rate, results in a maximum horizontal displacement of 13.59 cm as shown in Figure 8.1. This corresponds to a well path with a Radius Of Curvature (RC) of 1.02 m. Since the horizontal displacement is less than the second restriction of a 25.40 cm horizontal displacement, the 30° inclination becomes the limiting constraint to the final well path. As a result, all the potential targets given on the competition day will be found within a 13.59 cm horizontal displacement from the vertical axis.

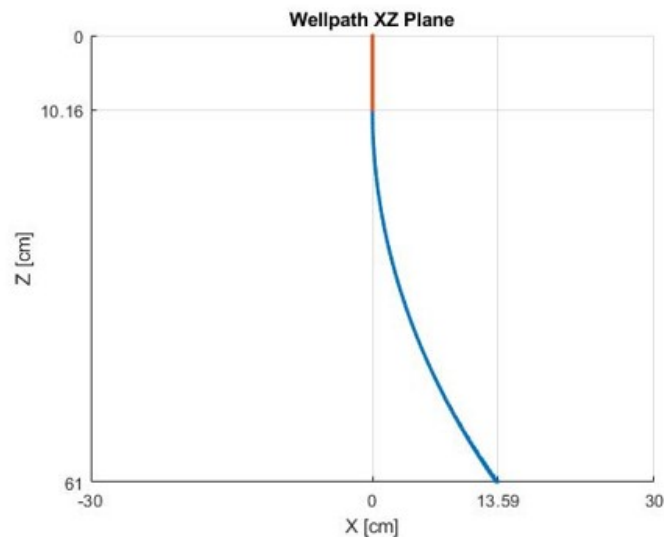
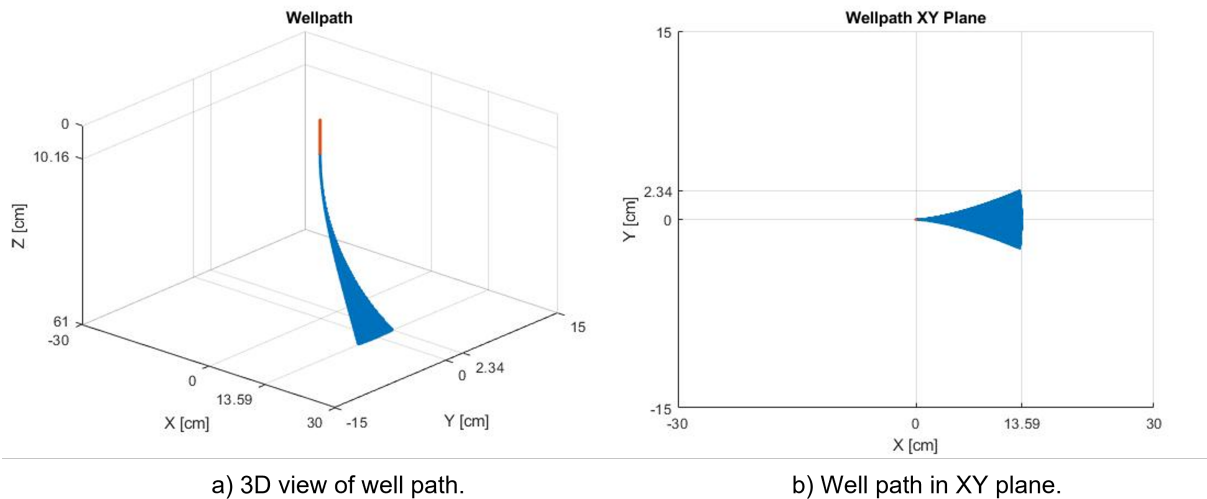


Figure 8.1: Well path restricted by a 30° inclination while assuming a constant build rate.

The final well path restriction of a 15° azimuth change results in a 2.34 cm maximum displacement in the horizontal plane. This is shown in Figure 8.2.

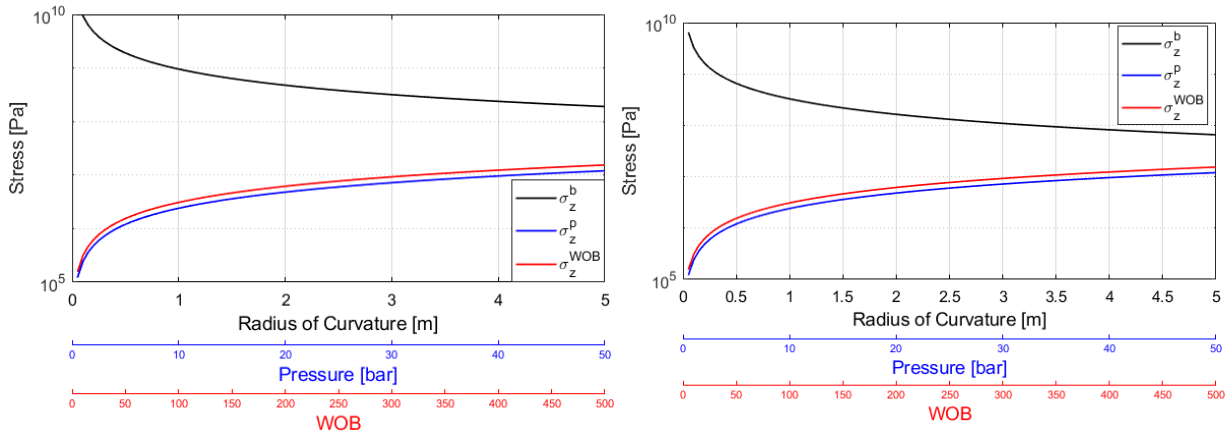
Figure 8.2: Well path with a 15° azimuth change.

8.1.2 Pipe Bending

The drill pipe must always operate within its elastic limits when drilling an arbitrary deviated well path in the $\{X,Y,Z\}$ plane. A pipe tends to bend because of a sum of multiple axial stresses acting on it. This can in worst case result in the drill pipe being deformed or damaged if the sum of these stresses exceeds the yield strength. Therefore, to prevent bending problems, a material analysis has to be conducted to decide which pipe to use.

Further analysis was conducted to determine which specifications and properties of steel and aluminum are most appropriate since the guidelines allow either material to be used. This section will review the results from previous NTNU teams regarding the comparison between stainless steel of grade 316 and aluminum 6061-T6.

In this project, deviated wells are to be drilled with the miniature drilling rig. The stresses acting on the pipe will normally increase with complex and deviated well paths. By evaluating the stresses acting on the drill pipe for different values of radius of curvature, further analysis can be conducted. Figure 8.3 shows the resulting total axial stress that the pipe experiences by using Equation 6.14, 6.15 and 6.16. It appears from the results that the axial stress due to bending is commanding as compared to the contribution from pressure and WOB for both materials. The lower boundary of the RC that guarantees that the pipe operates within the operational window can be found by comparing the resulting bending stress acting on the pipe with the material yields strength.

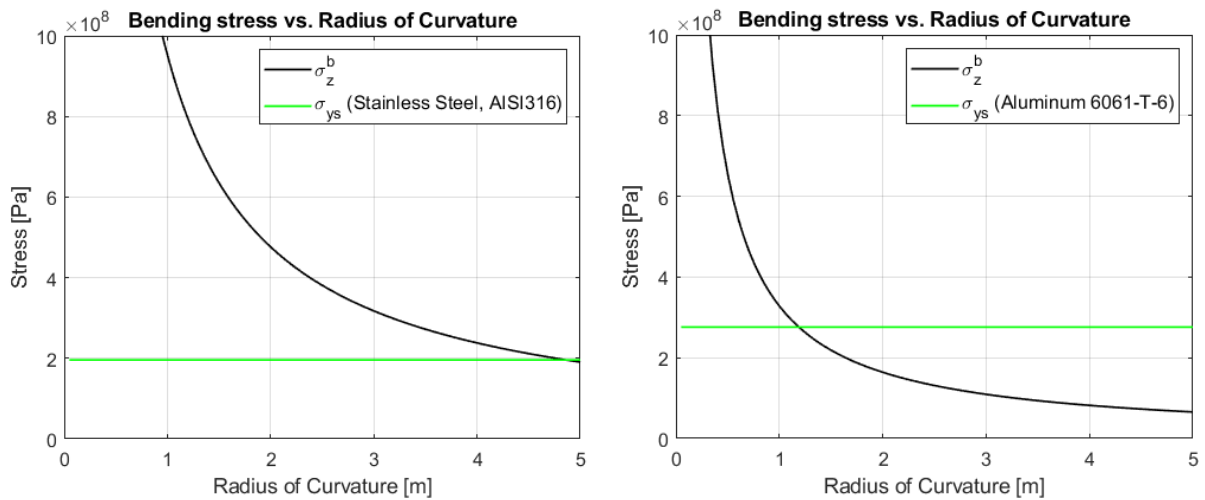


(a) Stainless steel pipe with grade 316.

(b) Aluminum pipe 6061-T6.

Figure 8.3: Various axial stresses plotted in function of RC , P , and WOB .

According to Figure 8.4a, the lowest RC that ensures that the steel pipe operates within the limit is 4.86 m that gives a horizontal displacement equal to 2.63 cm. Figure 8.4b indicates that the aluminum 6061-T6 provides a minimum RC of 1.19 m and a horizontal displacement of 11.22 cm. This clearly shows that the aluminum pipe is a better choice compared to the steel. Nevertheless, none of the pipes can meet the required horizontal displacement as earlier calculated to be 13.59 cm in Section 8.1.1. Therefore, previous NTNU teams explored the possibility of using another type of aluminum with stronger properties.



(a) Stainless steel pipe with grade 316.

(b) Aluminum pipe 6061-T6.

Figure 8.4: Axial bending stress plotted against RC .

Figure 8.5 is based on the same principle as presented earlier, but with aluminum 7075-T6 instead. This time as well, the dominating contribution will be from the bending stress. Aluminum of this type affords a minimum RC of 0.68 m, and the requirement of 30° inclination can be achieved within the dimensions of the given rock sample. As a

result, the findings show that aluminum 7075-T6 can withstand the loads during drilling operations, so that all the targets can be reached on the day of the competition.

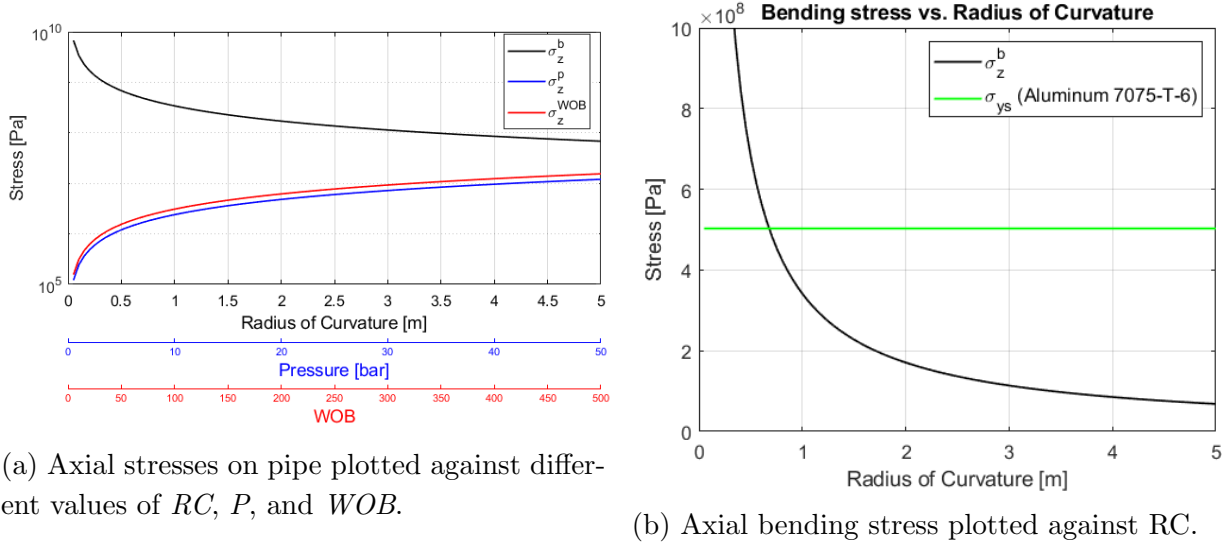


Figure 8.5: Aluminum pipe 7075-T6.

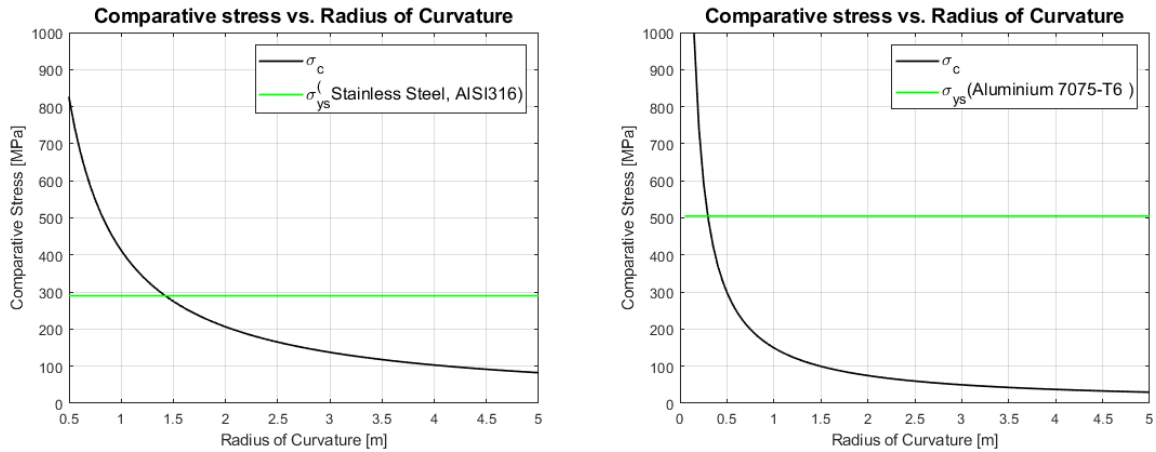
When assuming no azimuth change, and a final inclination of 30 degrees, the corresponding horizontal displacement is equal to 13.59 cm with a RC of 1.02 m. The bending stress at these conditions is calculated to be 322 MPa, and a safety factor can be found by comparing with the yield strength of the pipe:

$$SF_{Drillpipe} = \frac{503MPa}{322MPa} = 1.56$$

The safety factor ensures that the pipe is guaranteed to not exceed the elastic limit with an acceptable safety margin. As a result of the calculations in this chapter, the team chose to continue using aluminum 7075-T6 as the material for the drill pipe.

8.1.3 Rod Stresses

The rod experience much less stress due to the fact that all the weight is carried by the drill pipe. For this reason, the rod only experiences axial bending and shear stress during drilling operations with the miniature drilling rig. By using Equation 6.18 and 6.19 the axial bending stress and shear stress are calculated with input parameters from Table 8.1, respectively. As presented earlier, the comparative stress is a combination of these two stresses and is computed with Equation 6.17. Different materials such as steel, aluminum and titanium were previously explored as options for the rod material.



(a) Stainless steel pipe with grade 316.

(b) Aluminum pipe 7075-T6.

Figure 8.6: Comparative stresses as function of RC compared with the yield strength.

Figure 8.6 gives a comparison between the comparative stress and the yield strength of both stainless steel and aluminum 7075-T6. As Figure 8.6a shows, stainless steel will not work as intended since it will not provide a RC that can reach the wanted horizontal displacement of the rock. Moreover, the aluminum 7075-T6 pipe provides a sufficient RC to reach the inclination requirement of 30°. Nevertheless, based on testing conducted by last year’s team, the 7075-T6 rod did not work optimally due to several twist offs and other problems. As an alternative to find a stronger material, a titanium grade 5 rod was further investigated last year.

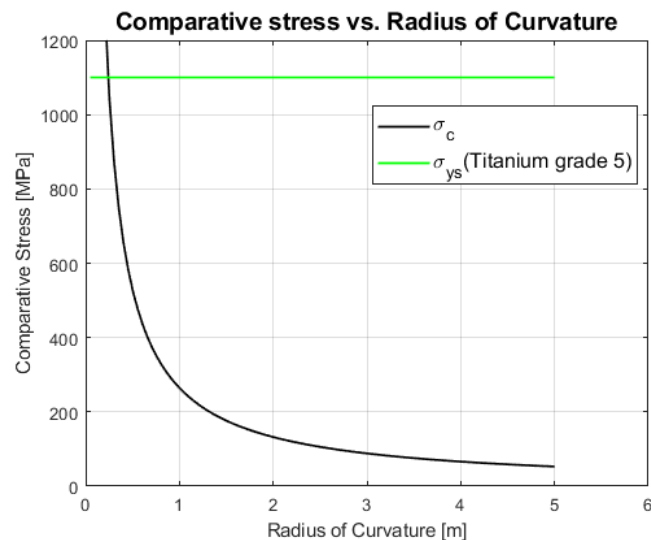


Figure 8.7: Comparative stresses plotted against RC and compared with material strength for titanium grade 5 pipe.

Figure 8.7 displays the comparative stress acting on the titanium rod with grade 5 as a function of RC. The titanium provides more than twice the strength compared to the aluminum 7075-T6 rod and should therefore be more robust and handle higher drilling

loads. After tests performed both last year and this year, the rod has proven to work sufficient and has not caused any severe problems. For this reason, the use of a titanium rod will continue in this year's design.

8.1.4 Pipe Buckling

A buckling analysis is performed only for the drill pipe as it bears all the load from the WOB. The aluminium 7075-T6 drill pipe has dimensions specified by the Drillbotics guidelines. It has a 9.53 mm (3/8 in) outer diameter, a 1.24 mm (0.0049 in) wall thickness and is 0.91 m (36 in) in length [90].

Equation 6.20 and 6.24 are used to calculate the critical buckling limit. They are both in function of the effective length factor K , which varies depending on the drill pipe's end conditions as shown in Table 6.1. The pinned-pinned end condition is not considered for the miniature drilling rig, as the drill pipe's top end is always fixed to the hollow swivel shaft.

The maximum allowable WOB to prevent a buckling failure during drilling operations is determined using Equation 6.26. Figure 8.8 shows the limiting WOB in function of the unsupported drill pipe length for the various end conditions.

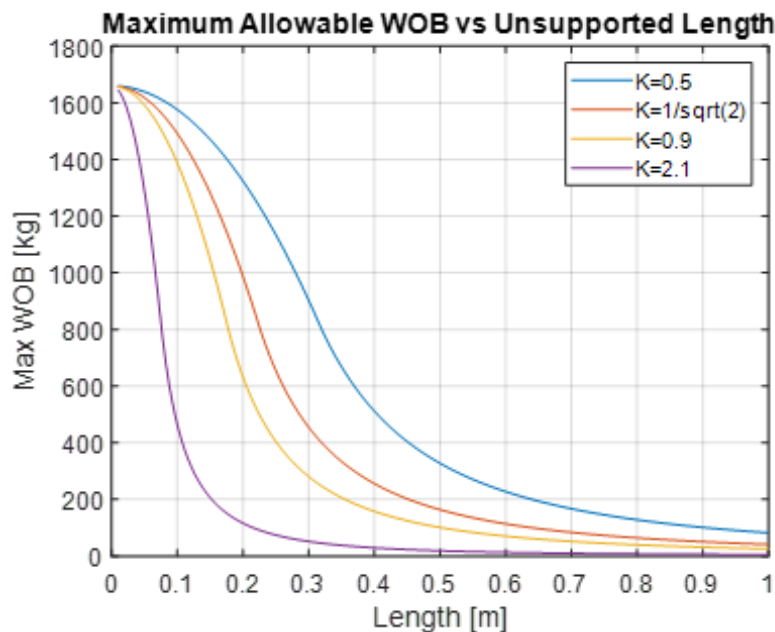


Figure 8.8: Maximum WOB versus the unsupported drill pipe length for different end conditions.

It can be seen that the maximum WOB increases as the unsupported drill pipe length decreases. Larger loads can also be applied for lower K values, representing more fixed end conditions. Therefore, the use of stabilizers becomes essential in maximizing the

allowable WOB, as they not only reduce the unsupported drill pipe length but also hold the drill pipe in place.

The rig has one stabilizer located on the drill floor that supports the drill pipe. The stabilizer is considered a fixed point as it restrains the lateral movement of the drill pipe. It also divides the drill pipe into two shorter unsupported segments. These are referred to as the top section and bottom section, respectively. The top section is fixed to the hollow swivel shaft and stabilizer, representing a fixed-fixed end condition. On the other hand, the bottom section represents a situation between a fixed-free and fixed-pinned end condition since the borehole wall offers some support to the drill pipe while drilling.

Calculations to determine the maximum WOB that the drill pipe can endure are performed for both top hole drilling and bottom hole drilling. These scenarios consist of the longest unsupported drill string lengths and represent the most conservative cases. The concepts of top hole and bottom hole drilling, as well as the drill pipe's top and bottom section for each scenario, are illustrated in Figure 8.9.

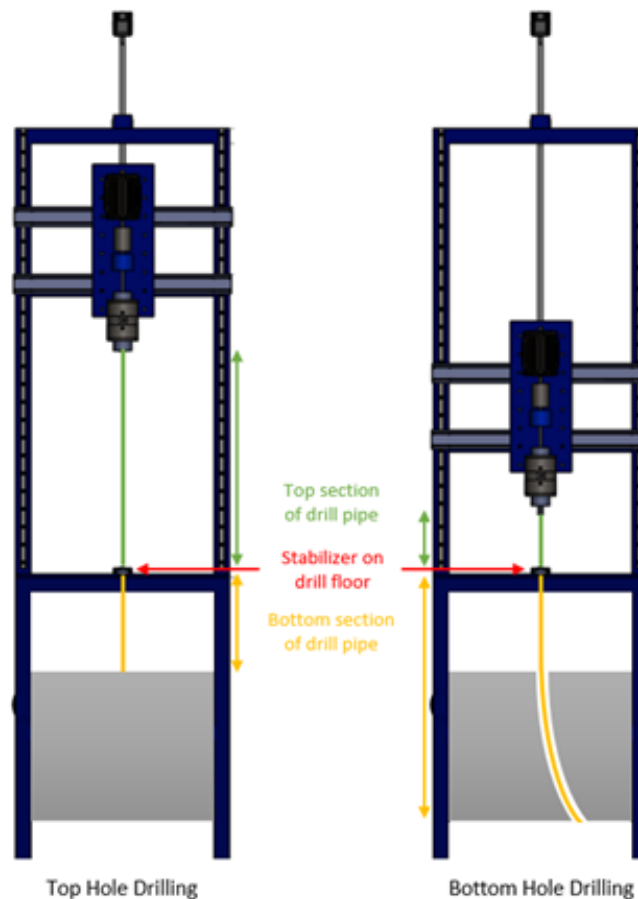


Figure 8.9: Top and bottom section of drill pipe for top and bottom hole drilling.

The limiting WOB when excluding the BHA from the drill string are presented in Table 8.2. These calculations were only performed with the recommended K values for each end condition found in Table 6.1.

Table 8.2: Maximum allowable WOB for the drill pipe excluding the BHA.

			Fixed-Fixed K	Fixed-Pinned K	Fixed-Free K
			0.9	0.9	2.1
		L [mMD]	Maximum Allowable WOB [kg]		
Unsupported drill pipe		0.91	30.5	30.5	5.6
Top section of drill pipe	Top hole drilling	0.69	53.1		
	Bottom hole drilling	0.06	1561.8		
Bottom section of drill pipe	Top hole drilling	0.22		521.1	95.7
	Bottom hole drilling	0.85		35.0	6.4

The results once again prove the importance of stabilizers, as a fully unsupported drill pipe restricts the maximum allowable WOB to 5.6 kg. With a stabilizer, the allowable load increases to 6.4 kg and is limiting by the bottom section of the drill pipe while drilling the end of the well bore. The results also show the general shift of the limiting WOB with the unsupported drill pipe length. For instance, the top section of the drill pipe tolerates an increasing WOB as drilling commences because the section length decreases. Similarly, the bottom section of the drill pipe withstands a decreasing load while drilling through the rock since its section length increases.

These results are however not entirely representative of miniature rig’s drilling system as the drill pipe is pinned to the BHA. The BHA has stabilizers with a diameter similar to the borehole and it covers a considerable length in the well which provides the drill string with extra stability. Therefore, to gain more realistic results, the bottom section of the drill string including the BHA should be regarded as a fixed-pinned scenario as the fixed-free end condition becomes too conservative. The maximum allowable WOB calculations with a drill string including a 20.5 cm BHA are presented in Table 8.3.

Table 8.3: Maximum allowable WOB for the drill string including the BHA.

			Fixed-Fixed K	Fixed-Pinned K
			0.9	0.9
		L [mMD]	Maximum Allowable WOB [kg]	
Top section of drill pipe	Top hole drilling	0.90	31.2	
	Bottom hole drilling	0.27	346.0	
Bottom section of drill pipe	Top hole drilling	0.01		1657.4
	Bottom hole drilling	0.64		61.8

Including the BHA in the drill string shortens the bottom section of the drill pipe and increases the unsupported length of the top section for both top and bottom hole drilling. Therefore, the bottom section no longer becomes the limiting case for the allowable load but rather the top section during top hole drilling. As a result, the maximum allowable WOB to prevent a buckling failure while drilling with the miniature rig is 31.2 kg.

8.1.5 Pipe Burst

The burst pressure of the aluminium 7075-T6 drill pipe is calculated under the thin wall assumption with Equation 6.27. To stay on the conservative side, a drilling scenario with a safety factor of 3 is used.

$$P_{burst} = 2 \cdot \frac{0.875 \cdot 503 \text{ MPa} \cdot 1.24 \text{ mm}}{9.53 \text{ mm} \cdot 3} = 382 \cdot 10^5 \text{ Pa} \quad (8.1)$$

The drill pipe is restricted to burst pressures of $382 \cdot 10^5$ Pa. This will not pose a problem because the miniature rig's hydraulic system uses low pressure tap water.

8.1.6 Twist Off

The maximum torque that the drill pipe and rod can withstand during drilling must be determined to prevent a twist off failure. The aluminium 7075-T6 drill pipe's twist off torque is computed using Equation 6.10 and 6.11. These equations consider the radial, tangential and axial stresses on the pipe's external wall which are calculated using Equation 6.12, Equation 6.13 and Equation 6.14–6.16, respectively.

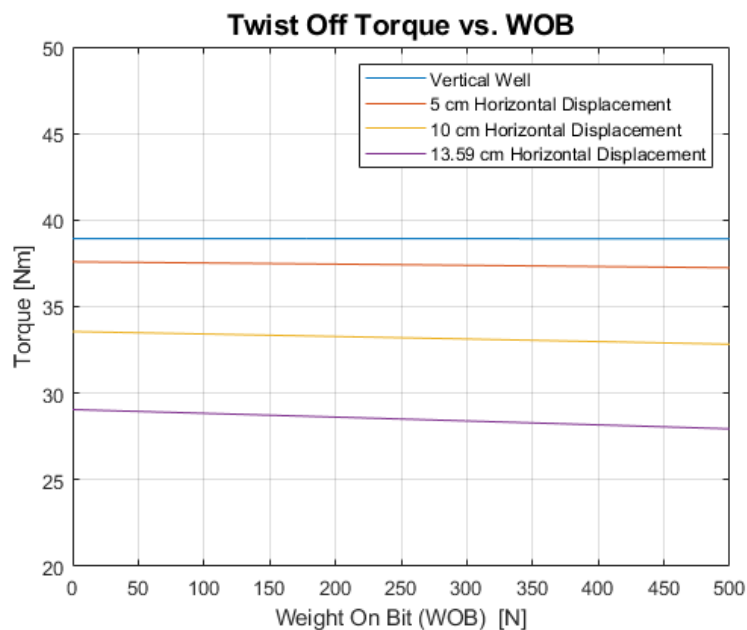


Figure 8.10: Drill pipe twist off torque versus WOB.

The drill pipe's twist off torque as a function of WOB is plotted in Figure 8.10 for four well trajectories with varying RC. The graph indicates that the maximum allowable torque reduces as the horizontal displacement of the well path increases. This is due to the increased bending stress experienced by the external wall of the drill pipe. The WOB and

pressure are insignificant factors in determining the limiting torque as seen in Figure 8.10 and Table 8.4, respectively.

Since the competition well path can have a horizontal displacement as high as 13.59 cm, the drill pipe's torque is restricted to 27.94 Nm. This limit is adequate based on previous experiences.

Table 8.4: Drill pipe twist off limit for several horizontal displacements.

Pressure [bar]	Horizontal Displacement [cm]			
	0	5.0	10.0	13.59
10	38.93 - 38.91 Nm	37.59 - 37.25 Nm	33.56 - 32.83 Nm	29.05 - 27.94 Nm
100	38.93 - 38.91 Nm	37.59 - 37.25 Nm	33.56 - 32.83 Nm	29.05 - 27.94 Nm
Twist off limit	38.91 Nm	37.25 Nm	32.83 Nm	27.94 Nm

The rod is a compact cylinder that transmits torque to the drill bit. The maximum allowable torque that the rod can withstand before twist off is determined using Equation 6.19. In this calculation, the induced shear stress is assumed to equal the material's shear strength. The twist off limit for three available materials is shown in Table 8.5.

Table 8.5: Rod twist off limit.

Material	Twist off limit [Nm]
Stainless Steel 316	4.32
Aluminum 7075-T6	4.16
Titanium Grade 5	9.55

The titanium rod has a maximum allowable torque of 9.55 Nm which is more than twice the limit of the stainless steel and aluminium rod. This torque restriction is considered to be adequate for the required drilling operations.

8.1.7 Drill Pipe and Rod Fatigue

Rotating the drill pipe can result in fatigue because of the induced cyclic stresses while drilling. The fatigue strength of aluminum 7071-T6 is 159 MPa, which is much lower compared to the earlier computed bending stress of 322 MPa. Since the drill pipe is not being continuously rotated, the drill pipe will not be exposed to fatigue from bending. However, after a long period of time, the bending stresses can result in fatigue failure that is not directly related to cyclic stresses. While the azimuth system rotates the drill pipe, wear may occur as a consequence of friction in the borehole wall and the titanium rod. These aspects can influence the fatigue strength of the pipe and potentially reduce it drastically.

On the other hand, the rod is being continuously rotated when drilling and is therefore more exposed for fatigue as a result of cyclic stresses. Earlier it was calculated that the highest comparative stress that the rod will experience is 238 MPa. The titanium rod has a fatigue strength equal to 700 MPa, which means that it has a sufficient safety margin included. When the same rod has been used for a long period of time, failure may happen because of fatigue related issues. It is however difficult to predict when it will fail.

8.1.8 Natural Frequency

Operations that produce a forced frequency equivalent to the natural frequency must be avoided to prevent amplified vibrations and damage to the drilling system. The Critical Rotary Speed (CRS) of the rod, drill pipe and BHA are calculated using the parameters in Table 8.1, to determine what top drive velocity should be avoided while drilling.

Rod

The CRS that induces intensified lateral vibrations in the titanium rod is predicted within 15% accuracy using Equation 6.28.

$$CRS = 4760000 \frac{\sqrt{(0.16in)^2}}{(0.56in)^2} = 243RPM \quad (8.2)$$

Meanwhile, Equation 6.29 - 6.31 are used to determine the CRS that causes resonance in the longitudinal direction.

$$\beta = \frac{0.078kg}{1.5kg} = 0.052 \quad (8.3)$$

$$\alpha_n \tan(\alpha_n) = 0.052 \rightarrow \alpha_n = 0.23rad \quad (8.4)$$

$$CRS = \frac{60(0.23rad)(3125m/s)}{2\pi(1.42m)} = 4833RPM \quad (8.5)$$

The results show the top drive should not be operated within a 15% range of 243 RPM, which corresponds to a range of 207 RPM and 279 RPM. Rod velocities of 4833 RPM should also be avoided, but is not a concern since the maximum top drive velocity is 1300 RPM.

Drill Pipe

Similar to the titanium rod, the CRS that causes natural lateral vibrations in the aluminium drill pipe is calculated using Equation 6.28.

$$CRS = 4760000 \frac{\sqrt{(0.38in)^2 + (0.28in)^2}}{(36in)^2} = 1734RPM \quad (8.6)$$

While, the velocity resulting in amplified longitudinal vibrations are estimated with Equation 6.29-6.31.

$$\beta = \frac{0.060kg}{1.5kg} = 0.04 \quad (8.7)$$

$$\alpha_n \tan(\alpha_n) = 0.04 \rightarrow \alpha_n = 0.20rad \quad (8.8)$$

$$CRS = \frac{60(0.20rad)(3100m/s)}{2\pi(0.9144m)} = 6475RPM \quad (8.9)$$

To prevent damage to the drilling system due to excessive drill pipe vibrations, the calculations show the rig is not to be operated between 1474 RPM and 1994 RPM and at 6475 RPM. These values are higher than the planned drilling range and should not pose a problem to the team.

BHA

The CRS producing free vibrations in the BHA is approximated by Equation 6.32.

$$CRS = \frac{84240}{8.07in} = 10439RPM \quad (8.10)$$

There should not be any issues related to BHA resonance since an angular velocity of 10439 RPM is far outside the operating range of the miniature drilling rig.

8.1.9 Drilling Rate

A time constraint of 3 hours is given to drill through the rock on the competition day. Several assumptions must be made in order to estimate a sufficient drilling rate. By assuming no azimuth change and a final inclination of 30°, the horizontal displacement will be 13.59 cm with a RC of 1.02 m. With these values, the length of the curved section will be equal to 53.2 cm. In addition, the 10 cm length from surface to the KOP has to be taken into consideration, which results in a total well path of 63.2 cm. Even though there are 3 hours given to drill through the rock, the team aims to complete the drilling within 2 hours to be on the safe side. With these assumptions, an average ROP of 0.53 cm/min is required.

8.1.10 Bit Tilt

To meet the maximum required inclination of 30° , the fixed bent sub angle has to be determined. To build a course length that is equal to 53.2 cm, the resulting DLS will be 56.4 deg/m. The bit tilt is computed by rearranging Equation 6.9 for θ and using the DLS together with the specifications of the BHA.

$$\theta = \frac{DLS(L_1 + L_2)}{2} = 5.78^\circ \quad (8.11)$$

Where $L_1 = 10.5$ cm and $L_2 = 10.0$ cm. Summing up, a bit tilt of 5.78° is necessary to achieve the final inclination of 30° . However, through testing, it was determined that a bit tilt of 6.91° was required to physically build this inclination.

8.1.11 Hydraulics

The hydraulic system plays a major role during drilling since it is the responsible for hole stability and cleaning. This is achieved by using the rheological properties of the fluid as well as its velocity to remove cuttings out of the well. The procedures used by the team to obtain the optimal values for the hydraulic variables in the system will be presented in this section.

8.1.11.1 Hole Cleaning

The drilling fluid used for drilling operations is water from the tap. The Drillbotics guidelines states that the rock sample provided will be a sandstone with homogeneous properties [90]. The density of the cuttings is assumed to be about $2650kg/m^3$. Another assumption is a perfect sphere with a diameter of $d_s = 2.4mm$ for the cutting geometry. Table 8.6 presents the relevant equations and results for the hole cleaning.

Table 8.6: Results of Hole Cleaning Calculations.

Parameters	Equations	BHA	DP
v_{sl} [m/s]	Equation 6.34	5.18	5.18
R [-]	Equation 6.36	10515 (Turbulent)	148009 (Turbulent)
f [-]	Figure 6.34	0.41	0.58
v_{sl} [m/s]	Equation 6.35	0.017	0.015
q [lpm]	Equation 6.37	2.24	0.09

To optimize the hole cleaning in the well, a transportation ratio of $R_t = 75\%$ should be used in Equation 6.37 [95].

The results in Table 8.6 show that the minimum flow rate obtained for the annulus between the open hole and BHA and open hole and drill pipe are 2.24 lpm and 0.09 lpm, respectively. If smaller flow rates are used in the system, then the risk of poor wellbore cleaning increases. The limiting flow rate is given by the BHA annulus. Including a safety factor, a minimum flow rate of 3 lpm was selected.

8.1.11.2 Pressure Losses

Once the minimum flow rate has been identified, the pressure losses throughout the system can be computed. Since the tap water has a pressure output of 7 bar and a flow rate of 3 lpm, Equation 6.38 provides the total pressure loss of the system. This result represents the sum of the different pressure losses experienced in each section of the hydraulic system. Equation 6.39 and 6.44 are used to calculate the pressure losses for the bit nozzles and pipe, respectively.

When a fluid flows through a system, it will experience friction caused by the contact and interaction with the surroundings. The pipe roughness affects the friction factor, and must therefore be considered when calculating the pressure losses in turbulent flow regime. This pipe pressure loss is calculated using Equation 6.39.

The water flows down the annulus between the inner rod and drill pipe. These components are made of different materials that have different roughness factors. Thus, it is necessary to quantify the water interaction with each material. This is done by estimating the surface area of the pipe and rod that will be in contact with the drilling fluid [10].

Since the water flows in the longitudinal direction of the rod and drill pipe, the fluid will have contact with the lateral surface area of the pipe and rod, as showed in Figure 8.11.

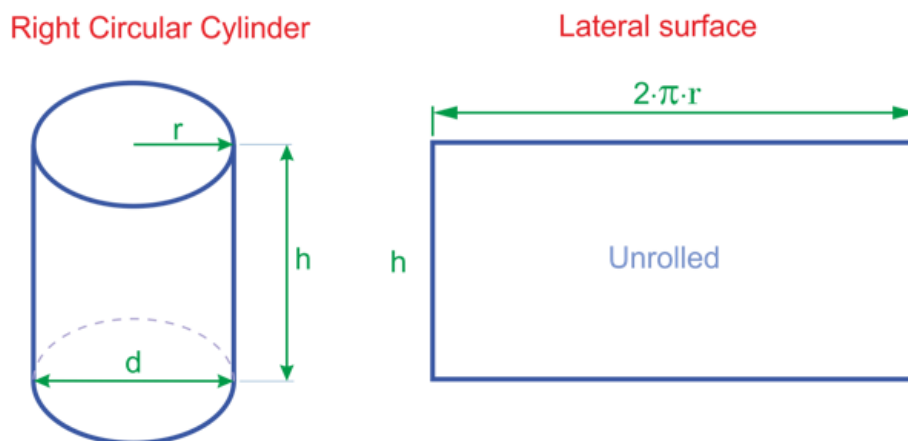


Figure 8.11: Cylinder lateral surface area [93].

Next, it is possible to determine the flow area:

$$A_{l_{flow}} = 2\pi r h \quad (8.12)$$

Where $A_{l_{flow}} [m^2]$ is the lateral surface area of flow, $r [m]$ is the hydraulic radius of flow in the rod or pipe and $h [m]$ is the section length.

The percentage of lateral surface area with which the water will be in contact is approximately 36% for the rod and 64% for the drill pipe.

After obtaining these proportions, the equivalent roughness factor $\epsilon_f [m]$ is computed for the whole length of the pipe. This is done by summing each material roughness multiplied by the corresponding lateral surface lateral percentage.

$$\epsilon_f = \epsilon_{DP} \cdot \frac{A_{l_{DP}}}{A_{l_{total}}} + \epsilon_{rod} \cdot \frac{A_{l_{rod}}}{A_{l_{total}}}$$

$$\epsilon_f = 1.3 \cdot 10^{-6} \cdot 0.64 + 30.1 \cdot 10^{-6} \cdot 0.36$$

$$\epsilon_f = 1.17 \cdot 10^{-5} m$$

Finally, the pressure losses for all the different sections can be computed for different flow rates. All the different contributions for a given flow rate are summed up, resulting in the total pressure loss of the system. The final results are presented in Table 8.7.

Table 8.7: Pressure losses in different sections of the system.

Rate	Pressure losses						
q	Swivel + hose	DP internal	BHA Internal	Bit nozzles	BHA annular	DP annular	Total
lpm	bar						
3	7.97E-03	2.35	3.35E-05	0.09	1.68E-05	6.71E-03	2.45
4	1.31E-02	4.06	5.44E-05	0.16	2.24E-05	8.95E-03	4.23
5	1.93E-02	6.21	7.94E-05	0.24	2.79E-05	1.12E-02	6.49
6	2.67E-02	8.82	1.08E-04	0.35	6.51E-05	1.34E-02	9.21

A tap water pressure of 7 bar, corresponds to a maximum flow rate of 5.2 lpm. For this reason, the operating window for the flow rate has been established to be between 3-5.2 lpm.

8.1.12 Overview of Mechanical Limitations

In the previous sections, various limits have been calculated that should not be exceeded when operating the miniature drilling rig. An overview has been created to emphasize

and highlight the most important mechanical limitations. This is presented in Table 8.8.

Table 8.8: Overview of Mechanical Limitations

Parameter	Value
Max. horizontal displacement	13.59 cm
Max WOB	31.2 kg
Max torque on rod	9.55 Nm
Minimum ROP	0.53 cm/min
Bit tilt	6.91°
Flow rate	3-5.2 lpm

8.2 Rig Power Consumption

The largest power consumer on the rig is the hardware such as hoisting motor, top drive motor, azimuth system, load cell and torque sensor. In addition, the computers are responsible for a high total power consumption. According to the guidelines, the total power consumption of the rig should not exceed 25 HP or 18.64 KW [90].

8.2.1 Top Drive Motor

The top drive motor provides torque and rotation to the bit through the rod and the drive shaft. For that reason, the power consumption of the motor is calculated as function of applied torque and RPM:

$$P = \frac{T\omega}{\eta} \quad (8.13)$$

$$\omega = \frac{2\pi N}{60} \quad (8.14)$$

In these equations $P[W]$ is the power consumption, $T[Nm]$ is the applied torque to the rod, $\omega[1/s]$ is the angular velocity, $N[RPM]$ is the revolutions per minute, and $\eta[-]$ is the motor efficiency.

The motor data sheet reports that the maximum output of the motor is 3400 RPM and a torque of 45 Nm. The motor efficiency is given as 0.96, so there are not any considerable effect losses through the motor. With these values as input, Equation 8.13 and 8.14 results in 16.7 KW consumption when it operates at maximum values. Nevertheless, the helical gearbox restricts the motor to operate at 1300 RPM with a torque of 5 Nm. The maximum power consumption of the top drive will therefore be 710 W. However, 900 RPM is mostly used for drilling operations which corresponds to a power consumption of 490 W.

8.2.2 Hoisting Motor

The hoisting motor transmits rotation to the ball screw so that the hoisting system can be lowered into the well. The torque output is a function of the weight of the rotary system and the lead of the ball screw, and can be determined with the following equation:

$$T = \frac{F \cdot l}{2\pi\epsilon} \quad (8.15)$$

Where $T[Nm]$ is the torque, $F[N]$ is force caused by the rotary system, $l[m]$ is the ball screw lead and $\epsilon[-]$ is the efficiency of the motor.

By inserting the rotary system weight, ball screw lead length and motor efficiency, the output torque from the hoisting motor becomes:

$$T = \frac{F \cdot l}{2\pi\epsilon} = \frac{490 \cdot 0.005}{2\pi \cdot 0.9} = 0.43Nm$$

Then the power consumption can be calculated the same way with the same equations as with the top drive motor. Table 8.9 shows the power consumption for different RPM values up to 1300 which is the highest RPM that can be used during operations.

Table 8.9: Estimates of the hoisting motors power consumption at different RPM values.

Rotary Speed N [RPM]	Power Consumption P [W]
100	5
300	14
600	28
900	42
1300	61

The maximum power consumption of the hoisting motor is 61 W. However, since the rig will operate at 900 RPM, the expected power consumption is 42 W.

8.2.3 Azimuth System

The hollow shaft gearbox, two right angled gearboxes and the azimuth servo motor make up the complete azimuth system with a 1:270 gear ratio. The azimuth servo motor's power consumption is computed with Equation 8.13 and 8.14. At its peak conditions and a 90% efficiency, the azimuth servo motor operates with a 3000 RPM velocity and a 0.92 Nm torque, resulting in a maximum power consumption of 321 W. However, the rotary table's turn rate is not expected to exceed 40 deg/min (1/9 RPM), which corresponds to a 30 RPM motor velocity. Therefore, the expected torque will be significantly lower than the peak torque. For instance, a 0.15 Nm torque will result in a power consumption 0.52 W for the azimuth servo motor.

8.2.4 Torque Sensor

The torque sensor has a maximum capacity of 50 Nm and measures the rotational force transmitted from the azimuth system to the drill string. Applying Equation 8.13 and 8.14, the maximum power consumption of the torque sensor is 5.8 W when assuming 90% efficiency and a rotational velocity of 360 deg/min (1 RPM) provided by the azimuth servo motor. However, the operating range for the torque sensor and azimuth servo motor is 5-10 Nm and 40 deg/min (1/9 RPM), respectively. Therefore, the anticipated power consumption of the torque sensor is around 0.13 W.

8.2.5 Computer

The control system for the drilling rig will be operated from two independent computers. The first is a Dell Optiflex 7060, which has a maximum consumption of 200 W [31]. The second computer is a Dell Optiplex 7090 with a maximum power consumption of 260 W [62].

In addition, two screens are used to monitor the operations. One is a Dell U2711B and has a maximum consumption of 140 W, while the other is a Dell U3415W with maximum power consumption of 130 W [32].

In conclusion, the total power consumption of the computers and screens are summed to 730 W. However, assuming the system runs at 70% capacity, the anticipated power consumption is 511 W.

8.2.6 Total Power Consumption

Table 8.10 summarizes the total power consumption calculations.

Table 8.10: Rig Power Consumption.

Rig Component	Expected Power Consumption [W]	Maximum Power Consumption [W]
Top Drive Motor	490	710
Hoisting Motor	42	61
Azimuth System	0.52	321
Torque Sensor	0.13	5.8
Computer	511	730
Total	1044	1828

The expected power consumption of the rig is 1044 W. This is well below the constraint of 18640 W given by the Drillbotics guidelines.

Risk Analysis for Rig Components

This chapter identifies the risks associated with the components of the drilling rig. The aim is reduce the overall impact in the event of components failing. Therefore, it is important to determine the components which pose the highest risk of reducing the progress of the project. Risk is defined as the following relationship:

$$Risk = Probability \cdot Consequence \tag{9.1}$$

Equation 9.1 can be used to organize the components into a risk matrix. This further helps to classify the components into low, moderate, high or extreme risk which is represented by the following colors.

	Low
	Moderate
	High
	Extreme

Figure 9.1: Colors for risk classification.

In the beginning of the project, the team considered the probability and consequence of the individual rig components failing and placed them into the risk matrix, as shown in Table 9.1

Table 9.1: Risk matrix before risk mitigation

		Probability				
		Rare	Unlikely	Possible	Likely	Almost certain
Consequence	Catastrophic	Load cell	Top drive motor Hoisting motor Computer	Hollow shaft gearbox Azimuth motor Right angled gearboxes		
	Extensive	Drill floor-stabilizer	T-shaft Hydraulic swivel Drill bit	USB cable BHA components Sensor card		
	Moderate					
	Minor		Top drive connection Drill chuck Riser and diverter	Drill pipe Universal joint	Rod Azimuth-torque sensor	
	Insignificant		Drill pipe connection			

The intention before starting the project was to reduce the number of components in the higher risk area using risk mitigation methods. These include acquiring spare parts of the most critical components and having a redundancy plan in the case of failure. Table 9.2 shows the new risk matrix after the risk mitigation was performed and clearly conveys that several components have moved toward lower risk areas.

Table 9.2: Risk matrix after risk mitigation

		Probability				
		Rare	Unlikely	Possible	Likely	Almost certain
Consequence	Catastrophic	Load cell	Top drive motor Hoisting motor Hollow shaft gearbox Azimuth motor Right angled gearboxes Computer			
	Extensive	T-shaft Drill floor-stabilizer	Hydraulic swivel	USB cable BHA components Sensor card		
	Moderate					
	Minor		Top drive connection Drill chuck Drill pipe Riser and diverter Drill bit	Rod Universal joint	Azimuth-torque sensor	
	Insignificant		Drill pipe connection			

A risk evaluation and the potential risk mitigation methods performed for each component are discussed in the following sections.

9.1 Top Drive Motor and Hoisting Motor

The top drive motor provides torque to the drill bit, while the hoisting motor supplies WOB to the system. Both the motors are essential for drilling operations. If one motor were to fail, the consequences would be catastrophic due to the long delivery time and high cost to acquire a new one. The team has chosen not to purchase backups since the motors have performed well for several years and the probability of one failing or not delivering the required power is unlikely. Hence, the top drive and hoisting motors are considered to be high risk components.

9.2 Drill Chuck and Top Drive Connection

The drill chuck is mechanically solid and transfers torque from the top drive motor to the drilling system by gripping the rod. In the unlikely event of failure, the drill chuck is cheap and easily acquired from a local store. The top drive connection which attaches the drill chuck to the top drive motor was quickly produced by the NTNU workshop. It is robust and has a low probability of failure. Hence, both the drill chuck and top drive connection are considered to be low risk components.

9.3 Rod

The rod transfers torque from the top drive motor to the drill bit. It will most likely fail due to bending or twist off. To limit the chance of the rod twisting off, the rod will be greased as a risk mitigation method to reduce the friction between the rod and the T-shaft, swivel and drill pipe. The team has many rods in backup and will acquire more to be on the safe side. Due to the abundance of available rods and simple replacement shall it fail, the rod is classified as a moderate risk component.

9.4 Hollow Shaft Gearbox, Azimuth Motor and Right Angled Gearboxes

The azimuth system which consists of the hollow shaft gear box, azimuth motor and right angled gearboxes, provides the rotation to the drill pipe. These components are essential to the drilling system because without them the team would not be able to hit the targets that require an azimuth change. They have a high cost and a long delivery time which makes the consequence of failure catastrophic. Although the components are robust, there is a possibility of the components failing as they have only been in use for a couple of months. However, as a risk mitigation method, the the hydraulic system will

be consistently checked for leaks and the components will frequently be wiped from dust particles. The hollow shaft gearbox, azimuth motor and right angled gearboxes remain as high risk components.

9.5 Azimuth Torque Sensor

The torque sensor measures the torque while changing the azimuth of the drill pipe. Without it, mechanical failure could occur as it could lead the team applying more rotation to the drill pipe than the system can handle. The consequence could therefore be severe as the delivery time is very long. Since the azimuth torque sensor has previously failed, a backup is already available which significantly reduces the consequence. Hence, the azimuth torque sensor is considered to be a moderate risk component.

9.6 Load Cell

The load cell is used to measure the WOB applied by the hoisting system. It is an essential component to the drilling system, and without it, mechanical failure could occur to several components on the rig. It is also expensive and has a long delivery time. Therefore, the failure of the load cell could give catastrophic consequences. The likelihood of the component failing is however rare, since it is very robust and has given no issues throughout the years. Hence, the load cell is classified as a moderate risk component.

9.7 T-shaft

The T-shaft was designed and implemented by last year's Drillbotics team. If the T-shaft should fail, there is no alternative method to change the azimuth while drilling, and the drilling rig will therefore not be able to hit all the required targets. The rotating rod can tend to wear down the T-shaft while drilling, and in worst case damage the component so that the sealing effect is broken. A mitigating measure is therefore to lubricate the rod with grease before drilling to reduce the risk of failure. If it should fail, the lab engineers can produce a new one, but it is a complicated production process and can take several weeks before the team has a functional rig again. With a low probability of failure, but an extensive consequence if it should fail, the T-shaft is considered as a moderate risk component.

9.8 Hydraulic Swivel

Ever since Drillbotics in 2017, the hydraulic swivel has been an important component on the rig. It ensures that the drilling fluid enters the system properly, and if it should fail the system will not have functional circulation system and leaks could damage electrical components on the rig. Without any drilling fluid, hole cleaning and bit cooling can become problems. The hydraulic swivel was originally produced by the lab engineers in the workshop. If something unexpected should happen it can be repaired by them. Based on this, the hydraulic swivel is classified as a moderate risk in this project.

9.9 Drill Pipe

The drill pipe carries all the WOB that is transferred from the hoisting system to the drill bit. If the WOB during operations gets too high, the drill pipe can bend and buckle. In worst case the drill pipe can fail, but it can be replaced quickly since the team has many drill pipes in spare. As a risk mitigation method, the maximum allowable WOB has been determined which reduces the probability of the drill pipe failing. As a result, the drill pipe is classified as a low risk.

9.10 Drill Pipe Connection

There are drill pipe connections both in the hydraulic swivel and BHA. Based on experience from previous teams, the connections have proved to work very well without breaking. Extra drill pipe connections are available and they can be replaced easily by the team if one should fail. The drill pipe connection is therefore considered as a low risk according to the risk matrix.

9.11 Drill Floor Stabilizer

The drill floor stabilizer has been used four years in a row and is still working well. Its main purpose is to avoid large vibrations and movements of the drill string. It has radial bearings to prevent movement in lateral directions. It is robust, but in case of failure a lot of unwanted vibrations are induced to the system that also can impact other components on the rig. There is no backup solution for the drill floor stabilizer, so it must be manufactured by the workshop in case it should fail. Based on this, the risk is moderate for this component.

9.12 Riser and Diverter

The design and implementation of the diverter was done by this year's team. It was manufactured by the workshop and is a very robust component made of aluminum. In case of a leakage, cuttings and drilling fluid can accumulate on the laboratory floor. It will not affect the drilling performance of the rig, but it can in worst case lead to a slippery floor or inhalation of toxic cement cuttings, which can be a danger for drilling personnel. Summing up, the diverter is considered a low risk component because of low impact on the system performance shall it fail.

9.13 USB Cable and Connections

The USB cable provides power and data to the downhole sensor. There is a possibility of the cable breaking while drilling with the azimuth system as it can get tangled around the drill string. Water damage is also likely if the connection between the cable and sensor card not properly sealed. These can both lead loss of communication between the sensor card and control system, making further drilling difficult. For this reason, the USB cable is classified as a high risk component. In case of failure, the team has spare cables as replacements on site.

9.14 BHA Components

The BHA components play a key role in drilling operations as they provide the stability and steerability to the drill bit. The components are exposed to large drilling loads during operations and therefore have a possible probability of failure. Damage to certain parts of the structure will make further drilling impossible. However, the consequence is not catastrophic as the workshop can produce new BHA components within several working days. These components are considered to be high risk components and need to be handled with extra care.

9.15 Sensor Card

The sensor card is used to estimate the position of the drill bit. It may be damaged if it is exposed to water from the hydraulic system. This would result in extensive consequences as the system loses all directional control. Several extra sensor cards have been acquired as a risk mitigation method. The sensor card is also sealed and protected with a water resistant material. However, due to the long sealing process, the sensor card is classified as a high risk component.

9.16 Universal Joint

The universal joint in the BHA permits the transmission of torque from the rod to the drill bit, allowing the system to drill through the rock. Since the connection is continuously exposed to loads during drilling, there is a possible chance of it breaking. However, the consequence of such a failure is considered minor as the universal joint can be easily replaced with the help of the workshop. Spare parts are also available. Thus, its been classified as a moderate risk component.

9.17 Drill Bit

The drill bit is essential in the drilling operations to reach the targets in the rock. Throughout the years, the different Drillbotics teams have collaborated with Lyng Drilling to manufacture custom drill bits. The company has proven to produce very robust bits, providing high performance, high durability and overall reliability. There is no record of any bit failure on duty. This year's team has designed and acquired several new drill bits which reduces the consequence if something were to go wrong. For this reason, the drill bit is considered a low risk.

9.18 Computers

The two computers are responsible for the autonomous control and position estimation of the drill bit. There is a low probability of failure as computers are typically long lasting components. However, a failure would result in catastrophic consequences, as a new computer is expensive and requires time to implement. Even though they are well protected from possible water sources, the computers are classified as high risk components.

Chapter 10

Control System Design

Autonomous directional drilling requirements were introduced in previous editions of the Drillbotics competition. Last year's team designed and implemented a control system for the rig that partially fulfilled these demands. Since the requirements for this year's competition are identical, the team decided to adopt this control system with the aim to develop and enhance the system's capabilities.

An overview of the control system will be presented in this chapter. It is mainly based on the work performed by last year's cybernetics student Magnus Steinstø who published the thesis "Implementation of a Miniature Autonomous Directional Drilling Rig With NMPC Positional Control" [12]. Additional modifications that were implemented to further develop the control system are found in Jarle Ness' thesis, called "Implementation of a Miniature Autonomous Directional Drilling Rig" [84]. For a deeper understanding of the entire control system, the reader is advised to review his master thesis.

Furthermore, the drilling engineer's performed a thorough research on the understanding of the downhole sensor, as well as in the implementation of a new well trajectory optimization strategy called 3D Dubin's curves. These topics are closely linked to the control system design, but are presented as separate chapters. More information about the downhole sensor is found in Chapter 11 and 3D Dubins Curves are presented in Chapter 12.

10.1 Matlab and Simulink

The control system used for the miniature drilling rig is designed and implemented using Matlab and Simulink. The following section will provide an overview of the capabilities and functionalities of the software.

Matlab is a programming platform provided by Mathworks specifically designed for engineering applications. Matlab can be used to develop control systems, robotics, algorithms, data analysis and machine learning [73]. Many million engineers utilize Matlab all around

the world both in the academia and industry due to the broad perspective of applications [77]. An important feature is that Matlab also supports the ability to combine code from Python, C++ and HTML.

Simulink is a block diagram environment interface provided by Matlab that is used to build and simulate complex systems [74]. A predefined library with blocks and toolboxes makes it easy to build dynamic systems [75]. In addition, there are blocks that allow code written in Matlab to be incorporated as part of a Simulink model. The GUI where Simulink models are developed is shown in Figure 10.1

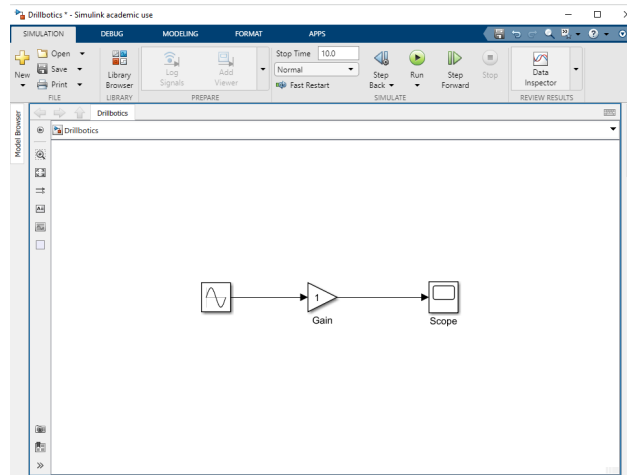


Figure 10.1: Simulink GUI Example.

10.2 Autonomous States

A requirement for the Drillbotics competition is to have a fully autonomous drilling rig. In full scale drilling operations, it is common to divide the drilling process into different stages. Also, the autonomous control system used in this project has multiple stages and is divided into different states. In total, there are 7 different states in the control system. For each state, there is a specific goal to be accomplished before moving to the next. The different states are presented graphically in Figure 10.2.

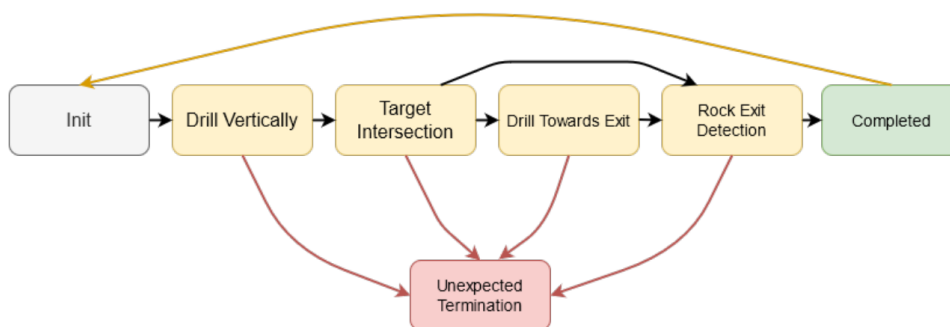


Figure 10.2: Overview autonomous states [12].

A summary of the different states are presented below [12].

Init

When the whole control system is executed from start, all motor actions are disabled by default and all set points are equal to zero. The autonomous operation must be physically initiated by an operator through the GUI.

Drill vertically

Vertical drilling takes place the first 4 inches until the kick off point. Because of the fixed bent sub, the system must rotate the azimuth system with a fixed set point equal to 540 deg/min. Because of the downhole sensor cable, the azimuth system works both clock-wise and anti clock-wise to avoid the cable winding up around the drill pipe. When the kick off point is reached, the system will continue to the next state.

Target Intersection

The target intersection state starts by the BHA orienting and steering towards the first target point. Every 5 cm of drilling, the system stops for a while to perform surveys. In between the survey stations, the azimuth system gains inputs from the NMPC controller in order to follow the reference path and thereby hit the targets. When all targets are reached, the system will continue either to Drill Toward Exit state, or to Rock Exit Detection state. The latter state will occur directly if the last target is close to one of the outer margins of the rock sample.

Drill Towards Exit

This state represents the drilled trajectory from the last target point towards the exit of the rock sample. To maximize the efficiency in this section, WOB is increased to maintain a higher ROP for this section because no azimuth change will take place. This state continues to the next state as the BHA approaches the outer limit of the rock sample.

Rock Exit Detection

This state is enabled when the drill bit is close to drill out of the rock sample. The WOB and ROP are lowered to avoid the system to continue out of the rock and potentially damage the system. The system will identify ROP changes when the bit goes from concrete to the rock sample container made of wood. When the wood is detected, the system will transition to the final state.

Completed

The completed state indicates that the autonomous operation has been executed successfully. All motors are stopped, and the system waits for the operator to determine what to happen next. The operator can reset the operation by pressing a button to take the system back to the init state.

Unexpected termination

Unexpected situations can occur at any time during autonomous drilling and can lead to damage to system and environment. The unexpected termination state ensures the system to fail in a safe manner. All motors and electricity will be turned off immediately if the system enters this state. The system can end up in this state from all the previously

mentioned states. If this happens, the system has to be reset after the operator has determined why the system failed.

10.3 GUI

The Graphical User Interface (GUI) ensures good communication flow in the transition boundary layer between the control system and the human operator of the rig. Large parts of the framework for the current GUI was developed in 2021 by last year's team [12]. Matlab has a dedicated app for easy creation and development of GUIs through an app called “App Designer”. The idea was to create a logical and as user-friendly GUI as possible so that the rig can be controlled in an appropriate way without having much background knowledge about the system.

The current GUI displayed in Figure 10.3 has two tabs; one for manual control of the rig and one for autonomous operation. The manual control tab allows the operator to run the rig manually which is appropriate for testing and verification of components and equipment on the rig. Regardless of autonomous or manual mode, important operational parameters will always be continuously displayed during drilling. These includes top drive torque, WOB and azimuth torque which all are displayed as live graphs at the left side of the GUI. In addition, top drive RPM, hoisting torque, hoisting position, and azimuth orientation are shown in dedicated boxes in the GUI.

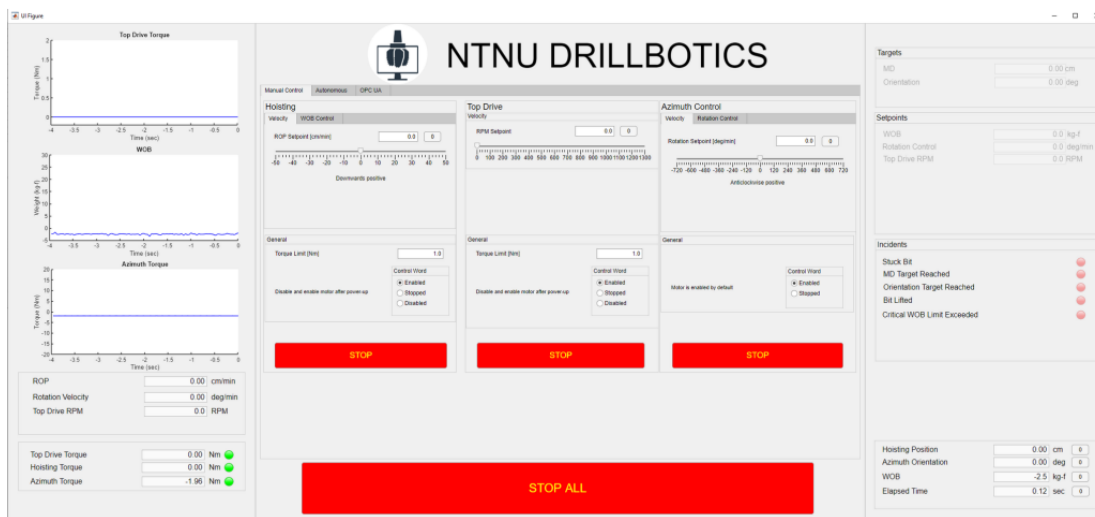


Figure 10.3: GUI for manual mode.

Furthermore, the appearance of the GUI in autonomous mode is shown in Figure 10.4. The “start state” and “end state” are chosen, and then the autonomous system will start the drilling process. During the process, the state progress is shown by a moving lamp with the different states as explained in Section 10.2. In addition, a list of incidents such as “Stuck bit” and “MD Target Reached” are displayed in the right side of the GUI.

If an unexpected incident occurs during drilling, the system will stop automatically. In addition, large stop buttons are placed easily visible so that the operator can intervene and shut down the system if necessary during autonomous operation.

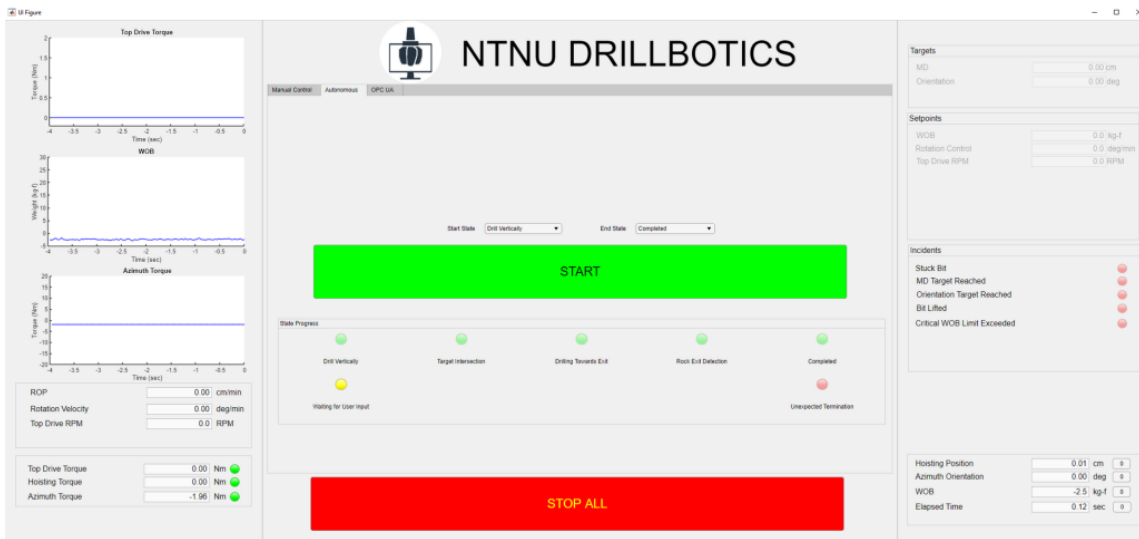


Figure 10.4: GUI for autonomous mode.

10.4 PID Controller

A Proportional Integral Derivative (PID) controller is a tool used to regulate a process variable, searching to drive the parameter from its current value towards a desired setpoint. The PID controller is based on a closed loop control system where an error value is constantly calculated, as the result of the difference between the variable that is measured, and the set point value assigned. With the constant adjustment of the process variable and reevaluation of the error, the convergence to the setpoint value is attained. Following, the mathematical expression for this procedure is represented by Equation 10.1. The PID controller consists of a proportional term, an integral term, and a derivative term [88].

$$u(t) = K_p e(t) + k_i \int_0^t e(\tau) d\tau + K_d \frac{de(t)}{dt} \quad (10.1)$$

Where:

- $e(t) = r(t) - y(t)$, where $e(t)$ is the error, given by the difference between the reference r and the output y .
- k_p is the proportional gain.
- k_i is the integral gain.
- k_d is the derivative gain.

The previous expression can be explained as a block diagram as shown in 10.5 [109].

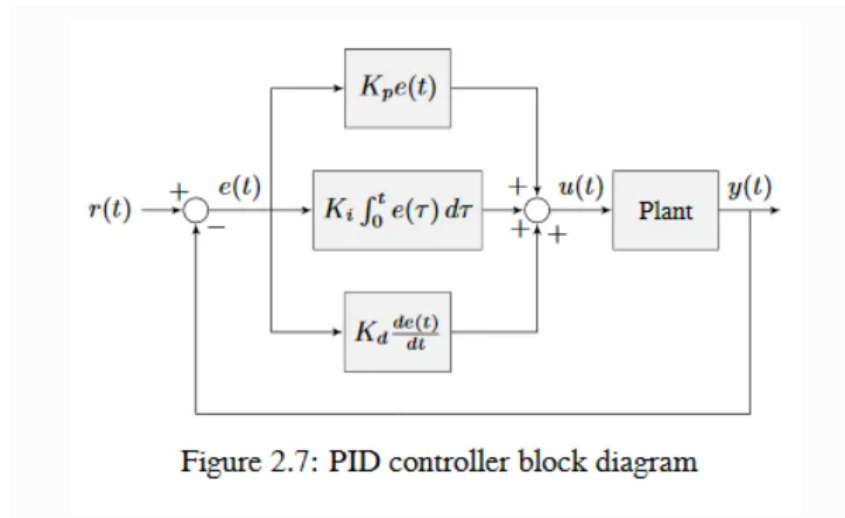


Figure 10.5: PID Controller block diagram [109].

It is important to highlight that the gain values K_x need to be individually tuned in order to make the process variable converge to the setpoint value [88].

- The **proportional gain** is the term which corrects the variable value proportionally to the current difference. If only this term is used in the system, the parameter value will not converge to the desired value, since the correction will tend to zero as the difference tends to zero.
- The **integral gain** is the term which corrects the variable value by accumulating the error from the first step, searching to increase the correction factor. If only this term is used in the system, the error value will be driven to zero, provoking an overshoot on the process variable.
- The **derivative gain** will try to minimize the overshooting caused by the integral gain by decreasing the correction factor when the process variable is close to converging to the setpoint.

The above constants can also be explained graphically for a deeper understanding. The three graphs presented show the process variable with a blue line and the set point with a green line.

The proportional error depicted in Figure 10.6, shows the difference between the process variable and the set point value.

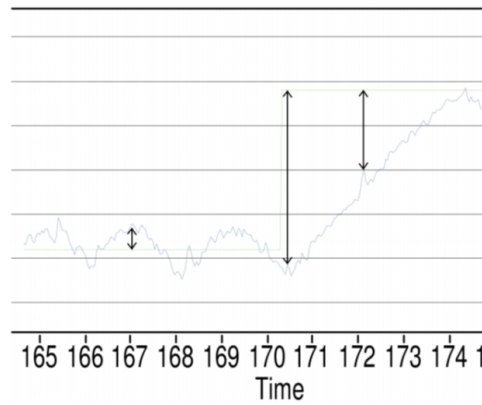


Figure 10.6: Illustration of the proportional error [57].

The integral error as a function of time, is shown in Figure 10.7. As seen, this is represented by the area under the curve.

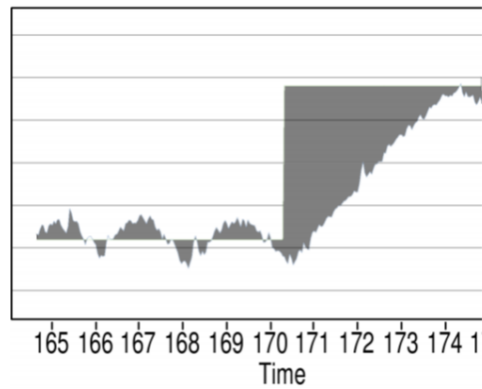


Figure 10.7: Illustration of the integral error [57].

Finally, the derivative error is evidenced in Figure 10.8. It is the derivative of the integral error.

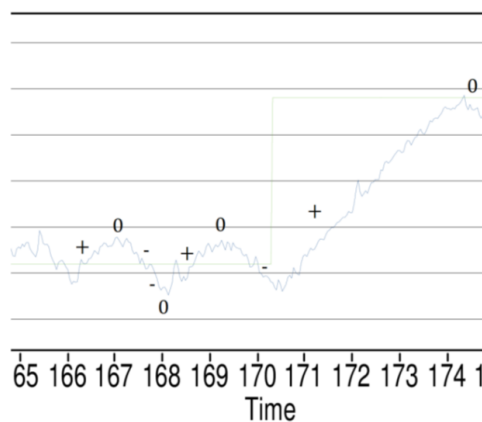


Figure 10.8: Illustration of the derivative error [57].

10.4.1 PID Tuning

The proper adjustment of the gains, K_p , K_i and K_d in Equation 10.1 used to optimize the PID controller performance is known as tuning. Once the gains are tuned, the PID controller is expected to be reliable and responsive while driving the process variable towards the setpoint [109].

Depending on the tuning of the gains, the type of response of the PID controller will vary. Thus, it is important to identify which type of response is required for the process to be controlled. The responses are characterized as underdamped, over-damped and critically damped and the concepts are seen in Figure 10.9. The underdamped response, typically oscillates around the set point before it stabilizes. The overdamped response rises closer to the set point at a slow rate, without the variable shooting beyond the set point. Finally, the critically damped response represents the fastest convergence time without overshooting [109].

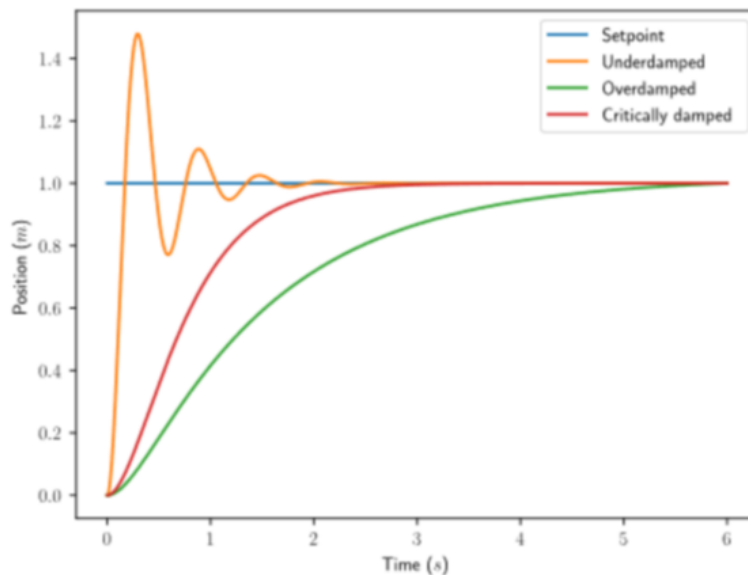


Figure 10.9: Types of responses for a PID controller [109].

A critically damped response is typically desired, as it avoids overshooting which can increase the time for the variable to stabilize at the setpoint. However, when the setpoint is changed from one value to another, a slight overshoot may be desired. Another feature that is common to have in a well-tuned PID controller is that the number of iterations that it takes for the system to converge and settle should be as low as possible. This minimizes wear and overuse of the actuators in the system [109].

The tuning of a PID controller can be achieved using different techniques. The individual gains in the control system are identified using the trial and error method. This method normally starts with setting the integral and derivative gains to zero. Next, the proportional term is increased gradually until the point where there are not excessive oscillations

around the set point, reaching a minimum steady-state error [66]. Once the proportional gain trend is attained and a fast response is achieved, the integral gain is raised which minimizing the steady state error. Finally, the derivative gain is increased to attain faster convergence to the set point value, while decreasing the overshooting of the integral gain. In an ideal scenario, these steps should be enough for the PID controller to be well tuned. However, the integral and derivative gains should be tuned individually to allow the system to converge towards the set point value. Likewise, it is important to consider system noise, which affects the correct tuning of the derivative term [9].

10.4.2 PID Implementation in the Control System

The trial and error method was applied by last year's cybernetics student to tune the PID controllers for different sensors on the rig.

Simulink contains a PID block that can be used for PID control and it supports both discrete and continuous systems. The component constants can also be dictated directly in the block by an external signal. This feature is seen in Figure 10.10. Since the control system works with discrete time-steps, it is necessary to choose the discrete implementation in the PID Block [9].

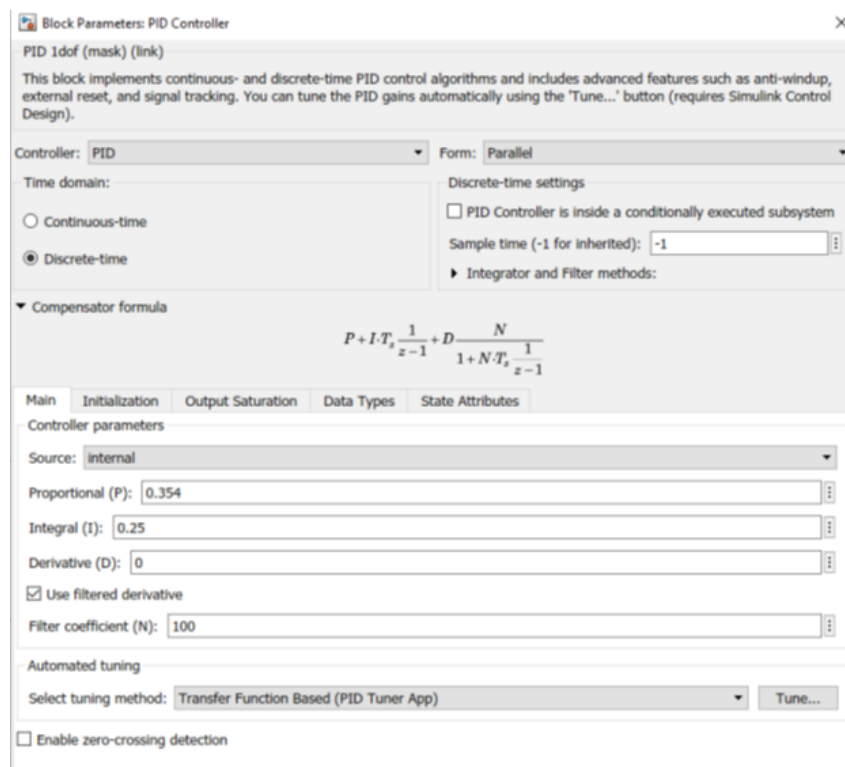


Figure 10.10: PID block in Simulink [9].

The formula used for the compensator in Simulink is shown in Equation 10.2. A large filter constant N is used to estimate the derivative term.

$$u[k] = \left(K_P + K_I \cdot T_s \frac{1}{z-1} + K_D \frac{N}{1 + N \cdot T_s \frac{1}{z-1}} \right) \cdot e[k] \quad (10.2)$$

A problem that may arise with this methodology is integral accumulation in the PID controller. To limit this issue, the anti-windup scheme option was activated in the system. Another key feature that is enabled in the PID block is the back-calculation method. This option is useful in preventing slow responses and accumulation by discharging the output from the integrator once the controller has reached its limit of saturation [69]. This can be done by feeding back the difference between the saturated and unsaturated control signal in the integrator [9].

10.4.2.1 PID Tuning Example for WOB

The optimal proportional, integral and derivative gains were obtained using the closed-loop PID auto-tuning tool in Matlab's Simulink [70]. On this software interface, the block used the output of the PID controller to evaluate the frequency of the response of the system and produced the PID controller coefficients in function of the target bandwidth and the phase margin [70]. It was possible to maintain the controller stable, since it was kept constant during the tuning process. The WOB PID Controller parameters were tuned and set in a pure PI-controller, where the proportional gain was $P = 0.354$ and the integral gain was $I = 0.25$. This example is observed in Figure 10.10 [9].

10.4.2.2 WOB PID Controller

Ensuring a constant WOB during drilling is of paramount importance. WOB impacts the ROP, vibrations and torque. If the WOB goes uncontrolled, it can lead to buckling of the drill pipe.

During drilling, the bit rock interaction can create different types of vibrations or changes in the torque, which can lead to the destabilization of the WOB. For this reason, the WOB PID controller must be quick and effective when keeping the WOB constant. The WOB is controlled by the hoisting velocity which is in function of the load cell readings. Since the WOB PID controller output is a fixed ROP set point, this signal is sent to the hoisting motor. As a preventive measure, this ROP output is given upper and lower limits. This is done with the objective of protecting the drill string and the system from uncontrollable acceleration of the hoisting system. It is especially useful when pulling out of hole to avoid excessive pulling forces in case of a stuck drill string or while tagging the rock just before drilling [9].

Figure 10.11 shows how the WOB controller is applied with a Simulink PID block in a sub-system. Here, the difference between the WOB estimated from the load cell readings and the WOB desired set-point is the error input [9].

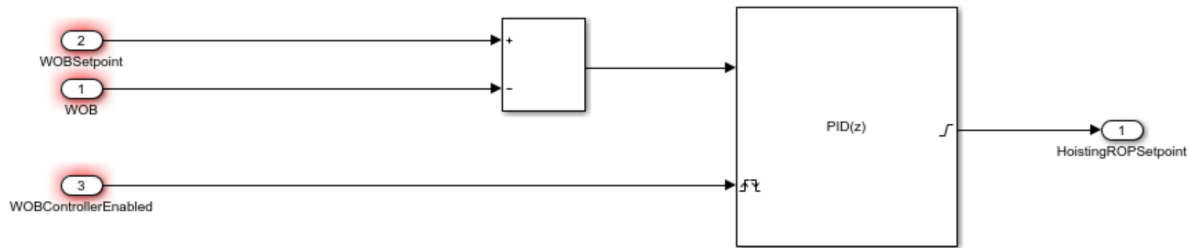


Figure 10.11: WOB PID controller in Simulink [9].

10.4.2.3 Azimuth Torque PID Controller

If the well path requires an azimuth change, the system has an implemented azimuth control system to orient the bit and drill string in the desired direction. The use of the azimuth system will result in friction since the bit is drilling both in the axial and lateral directions. Torque spikes may therefore occur, which can propagate from the bit through the drill pipe to the azimuth control system. If these torque spikes are left uncontrolled, the whole rig may suffer severe damage. For this reason, an azimuth torque PID controller has been applied to the system [9].

The azimuth torque PID controller applied in Simulink is presented in Figure 10.12. Since the rotation of the drill pipe from the azimuth motor can be both clockwise and counter-clockwise, the limit of the azimuth torque depends on the direction of rotation. The output from the azimuth torque PID controller is normalized which means the absolute value does not go above 1. Afterwards, it is multiplied by the absolute value of the desired set point [9].

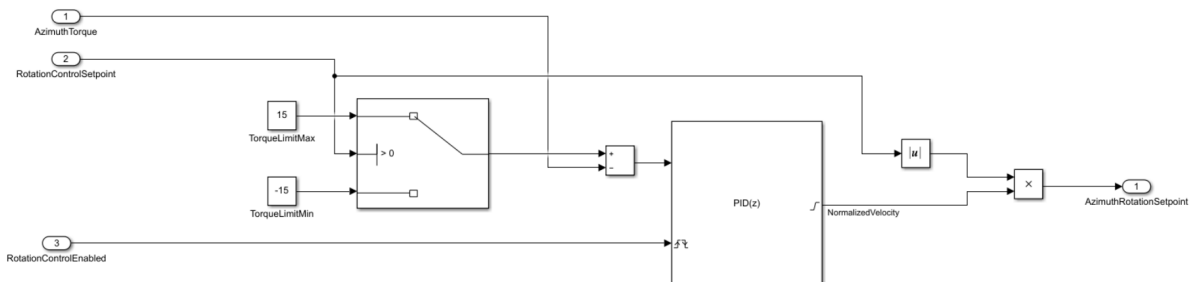


Figure 10.12: Azimuth torque PID controller in Simulink [9].

10.5 Kalman Filter

A Kalman filter is used to handle the uncertainty embedded in measurements from different sources, in order to provide an optimal, unbiased estimation of the system state [76]. This filter can combine and fuse readings from different sensors and weigh them in func-

tion of their co-variance. When Kalman filters are applied in a standardized manner, the measurements are assumed have a Gaussian distribution around their mean value. Therefore, the estimate with the lowest co-variance of the available options will be selected as the optimal state estimate [12].

10.5.1 Kalman Filter Theory

The Kalman filter compares the estimated model with the system's output using a linear state-space model. The optimal state is obtained by Equation 10.3 [12].

$$\hat{x}_k = A\hat{x}_{k-1} + Bu_k + K_k(y_k - C(A\hat{x}_{k-1} + Bu_k)) \quad (10.3)$$

The previous equation can be decomposed of the following equations.

The next state estimate is predicted by the Kalman filter using the prior estimate and current state [12].

$$\hat{x}_k^- = A\hat{x}_{k-1} + Bu_k \quad (10.4)$$

Since the co-variance of an estimate is susceptible to changes over time, the Kalman filter predicts the covariance of the current estimate by the use of the covariance of the prior estimate. This is done by weighing the current estimate against other predictions and taking the process noise covariance Q into account [12].

$$P_k^- = AP_{k-1}A^T + Q \quad (10.5)$$

The iteration of the Kalman filter algorithm will continuously update its estimate. It is common to calculate the Kalman gain, K_k , as a mean to minimize the variance of the optimal state estimate. This gain depends on R , which is the covariance of the measurement [12]:

$$K_k = \frac{P_k^- C^T}{CP_k^- C^T + R} \quad (10.6)$$

Then, a new state estimate can be obtained with the use of the Kalman gain, system output and the prior estimate [12].

$$\hat{x}_k = \hat{x}_k^- + K_k(y_k - C\hat{x}_k^-) \quad (10.7)$$

The new error covariance matrix of the optimal state estimate is useful for the monitoring of the anticipated deviation of the state estimate. This error covariance matrix can be

obtained in function of the Kalman gain, K_K , and prior estimate, \hat{x}_k^- , with the use of 10.8 [12]:

$$P_k = (I - K_k C) P_k^- \quad (10.8)$$

10.5.2 Extended Kalman Filter

Given the case that a system is not linear, the previously presented equations are not representative, since they describe a linear state space model. In addition, Kalman filters require to have all noise with a Gaussian distribution to provide optimal estimations. The problem with this requirement is that when noise values are put through a non-linear function, they will usually not result in a Gaussian distribution output. As a solution, it is proposed that while using Kalman filters, it is possible for the system to assume an approximately linear distribution of the noise, which is known as additive noise. This is shown by Equation 10.9 [9].

$$x_k = f(x_{k-1}, u_k) + w_k, \quad y_k = g(x_k) + v_k \quad (10.9)$$

Where x is the state, u the input and y the output. The variables w_k and v_k are noise values at a given time step for the states and output.

If a non-linear system behaves linearly within a small area, the system can be estimated with a linear approximation. For example, in the case of the prior predictions, a linear state-space model can be used by the Kalman filter [12]:

$$f(x) \approx f(\hat{x}) + f'(x)(x - \hat{x}) \quad (10.10)$$

The state and output function's Jacobians are applied directly for the linear approximation of the Kalman filter using Equation 10.11 [12]:

$$F = \left. \frac{\partial f}{\partial x} \right|_{\hat{x}_{k-1}, u_k}, \quad G = \left. \frac{\partial g}{\partial x} \right|_{\hat{x}_k} \quad (10.11)$$

If the output or the state function is linear, then it is possible to use the state-space matrix in exchange for the Jacobians. In Equation 10.12 the nonlinear approximations for a Kalman filter is presented [12]:

$$\Delta x_k \approx F \Delta x_{k-1} + w_k, \quad \Delta y_k \approx G \Delta x_k + v_k \quad (10.12)$$

10.5.3 Kalman Filter Implementation

In Simulink, there is a dedicated option which allows the user to implement Kalman filter blocks in the control system. Within these blocks, it is possible to implement linear state-space filtering, extended filtering, and unscented filtering. The fact that the system has a non-linear behavior, implies that the use of extended Kalman filter is mandatory for a correct approximation. Figure 10.13 shows the extended Kalman filter block which has one input y_1 and one state estimate output \hat{x} [72].

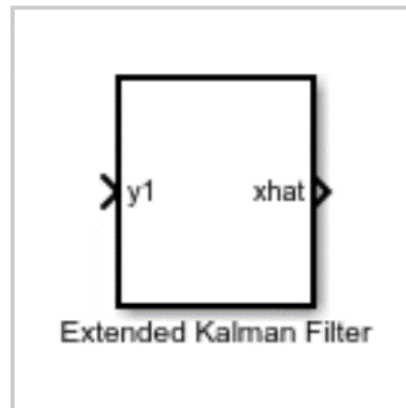


Figure 10.13: Extended Kalman Filter block in Simulink [72].

10.5.3.1 Hoisting velocity estimation

For correct control, positioning and steering of the system while drilling, an accurate ROP must be estimated. Since ROP is in function of the actual velocity of the hoisting system, then its estimate must be responsive when there is a sudden change. In addition, it must be consistent during constant velocities. This velocity is in function of the change in position of the hoisting motor. This ROP estimation process is implemented and observed in 10.14 [9].

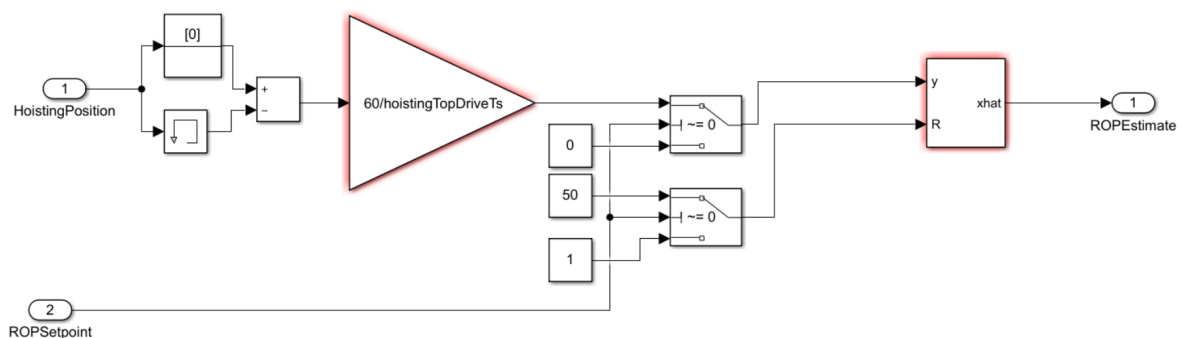


Figure 10.14: ROP estimation using a Kalman state observer in Simulink [9]

These estimations must be filtered because the velocity calculation between time-steps may change given a non-optimal encoder resolution. The solution for this is to adjust the process and measurement noise with the use a Kalman state observer filter [9].

10.5.3.2 Azimuth Rotation Velocity Estimation

Given the high frequency of the azimuth motor output, it is possible to filter the estimation of azimuth rotation velocity with a Kalman state observer filter. This tool provides an accurate estimate of the azimuth rotation velocity once the filter has adjusted the noise from the measurement and the process. Figure 10.15 portraits the complete process of the azimuth rotation velocity estimation using the Kalman filter in Simulink [9].

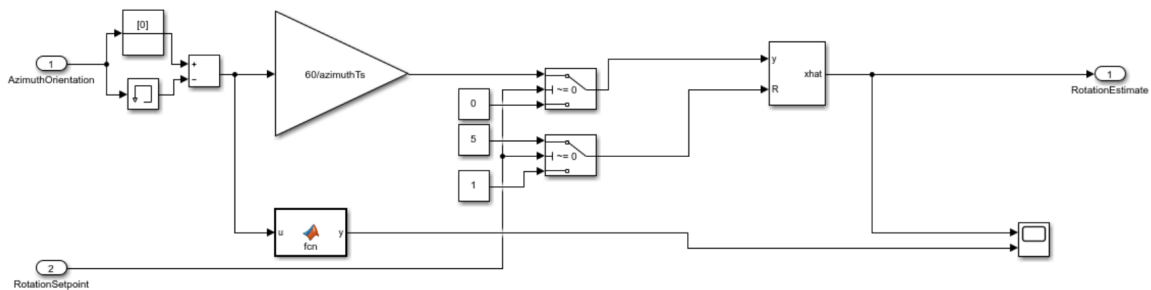


Figure 10.15: Azimuth velocity estimation using a Kalman filter in Simulink [9]

10.6 Position Estimate

In order to successfully reach the target points on the competition day, the system must know the position and orientation of the bit downhole at all times. This requirement has proven to be challenging due to the harsh conditions that the sensor must withstand while drilling. Therefore, the position downhole is based on the BHA orientation in combination with vertical displacement on surface. This methodology will be presented in this section.

10.6.1 Model Methodology

Since the data provided by the downhole sensor card is given in discrete time intervals, a discrete time model has been applied to the system. In this model, the inertial frame position is estimated based on a continuous time model. The core of the methodology assumes the angular velocity between the center of the BHA and the center of the bit will be in function of the BHA's bent orientation and the hoisting system velocity in the vertical axis displacement [12].

The location of the sensor card in the BHA is the reference point for the orientation estimate. The BHA has its own reference frame, known as body frame, where the BHA orientation will be estimated. This orientation is determined by the bent sub angle and the azimuth rotation of the drill pipe. It is assumed that the surface rotation of the azimuth control system is the same as the bottom rotation of the BHA body frame. The estimated rotation will then be translated into the inertial frame, and is further translated to displacement in the rock [12].

As a way to measure and describe the rotation of the BHA, body frames are used for each axis. The use of Euler angles can represent the frame orientation with roll, pitch, and yaw.

$$\hat{\phi}_{BHA}[k+1] = \hat{\phi}_{BHA}[k] = 0 \quad (10.13a)$$

$$\hat{\theta}_{BHA}[k+1] = \Delta t \cdot DLS \cdot \dot{d}[k] \hat{\theta}_{BHA}[k] \quad (10.13b)$$

$$\hat{\psi}_{BHA}[k+1] = \Delta t \cdot \dot{\psi}_I[k] + \hat{\psi}_{BHA}[k] \quad (10.13c)$$

Where the change in the vertical displacement, given by the change in hoisting position is \dot{d} , and the change in the azimuth rotation orientation is $\dot{\psi}_I$. These angular velocities can be expressed in vector form [12].

$$\omega_{BHA} = \begin{bmatrix} \hat{\phi}_{BHA}[k+1] \\ \hat{\theta}_{BHA}[k+1] \\ \hat{\psi}_{BHA}[k+1] \end{bmatrix} \quad (10.14)$$

The rate of change given in the BHA body frame must be translated into the inertial frame, so it can be compared with previous measurements and a fixed reference. This transformation can be done with Equation 10.15. The rotation matrix rate of change is estimated to be close to zero [12]:

$$\hat{\Theta}_I[k+1] = \frac{1}{\cos(\hat{\theta}[k])} \begin{bmatrix} \cos(\hat{\theta}[k]) & \sin(\hat{\phi}[k]) \cdot \sin(\hat{\theta}[k]) & \cos(\hat{\phi}[k]) \cdot \sin(\hat{\theta}[k]) \\ 0 & \cos(\hat{\phi}[k]) \cdot \cos(\hat{\theta}[k]) & -\sin(\hat{\phi}[k]) \cdot \cos(\hat{\theta}[k]) \\ 0 & \sin(\hat{\phi}[k]) & \cos(\hat{\phi}[k]) \end{bmatrix} \hat{\Theta}_{BHA}[k+1] + \hat{\Theta}_I[k] \quad (10.15)$$

Since the estimates of orientation are done within the inertial frame, the current orientation can be calculated with the integration of the orientation change [12].

$$p[k+1] = \Delta t \cdot \hat{R}_{BHA}^I[k] \cdot \begin{bmatrix} 0 \\ 0 \\ \dot{d}[k] \end{bmatrix} + p[k] \quad (10.16)$$

10.6.2 Orientation Estimate

The methodology stated previously dictates that at each time step, a vertical displacement and a orientation change may have occurred. Then, it is assumed that the vertical displacement on the hoisting system can be translated into deviated movement downhole, following the BHA orientation. Since this estimation heavily relies on integrating orientation changes that are not accurate enough, then the process may result in unreliable estimations.

As a solution, downhole sensor readings are used to estimate the BHA orientation, which will be described in further detail in Section 11.5.1. In the aforementioned section, the methodology on how to use the data from the downhole sensor to estimate roll, pitch and yaw is discussed. In the upcoming sections, the complementary discussion about orientation estimate will be explained.

10.6.2.1 Gravity Field Model

When the sensor is stationary and not exposed to any external forces, the norm of the acceleration values from the accelerometer after calibration is equal to 1G. Since the gravity vector is constant and points along the inertial z-axis, the gravity field in the sensor body frame can be calculated as the inverse rotation matrix with the current inertial orientation estimate. This is further multiplied with the z-axis unit vector [12].

$$\hat{a}[k] = (\hat{R}_{BHA}^I[k])^T \cdot \begin{bmatrix} 0 \\ 0 \\ 1 \end{bmatrix} \quad (10.17)$$

Within this model, a low pass and noise rejection effect are applied to the accelerometer measurements used for the final orientation estimates.

10.6.2.2 Azimuth and Inclination Calculation

Given that the reference for orientation in the drilling industry are azimuth and inclination, then the Euler Angles must be converted into this convention. Yaw and azimuth can be used interchangeably, since both give a change in orientation in the horizontal plane.

The inclination is the angle measured between the BHA body frame and gravitational vector. The roll and pitch angles are used to calculate the inclination of the BHA. This is done by multiplying the rotational matrices for roll and pitch with the z-axis unit vector. This computation will result in a vector in the 2D-plane with an angular difference to the z-axis. Finally, the inverse cosine of the dot product of the two matrices is taken to estimate the inclination [12].

$$\psi_{inclination} = \arccos(\cos(\phi_I) \cdot \cos(\theta_I)) \quad (10.18)$$

10.7 Model Predictive Control

Model Predictive Control (MPC) is an advanced control technique commonly used in multivariable control situations. A complex process often involves multivariable inputs and outputs to be optimized. MPC is used to control the input and output relationship that are restricted by a set of initial constraints [7]. A dynamic model of the controlled process is often used to predict future output values that are further used and fed into the input variables.

A MPC controller forecasts and predicts a prediction horizon of a given system over a specific time interval. A dedicated algorithm ensures to search for input variables that together minimizes the sum of a belonging cost function. Weights are introduced to avoid large difference between the current variable value and the predicted value. To ensure this, an optimization algorithm and cost function is frequently used with quadratic penalty structure as follows [7]:

$$\min_{x,u} J = \min_{x,u} \sum_{k=0}^{N-1} (x_k^T Q x_k + u_k^T R u_k) \quad (10.19)$$

In the above equation N is the total length of the given prediction horizon, and k is the current time step. x_k is the predicted state with a corresponding matrix Q as the weight. Similarly, u_k is the reference input to the system where R is the weight on matrix form.

10.7.1 Model Predictive Control Implementation

The MPC controller implemented in the control system is used for trajectory control and steering while drilling with the autonomous system. After research performed by last year's team, results showed that there was no linear relationship of the movement of the BHA downhole. For that reason, Nonlinear Model Predictive Control (NMPC) was implemented instead of the regular MPC [12]. The NMPC controller is using a continuous time model in the implementation in Simulink. As the only option to steer the BHA in the desired direction is by adjusting the azimuth system, the rotational velocity is the only input parameter to the NMPC. Both the inertial frame coordinates for the BHA and cartesian coordinates have to be taken into account. For that reason, six states must be utilized by the NMPC controller. The Euler angles that express the BHA orientation in

the inertial frame are given by [12]:

$$\dot{\phi} = \frac{\cos \phi \cdot \sin \theta \cdot \dot{\psi}_I + DLS_{nom} \cdot \exp\left(-\frac{\dot{\psi}_I^2}{q}\right) \cdot \sin \phi \cdot v_{nom}}{\cos \theta} \quad (10.20a)$$

$$\dot{\theta} = DLS_{nom} \cdot \exp\left(-\frac{\dot{\psi}_I^2}{q}\right) \cdot \cos \phi \cdot v_{nom} - \sin \phi \cdot \dot{\psi}_I \quad (10.20b)$$

$$\dot{\psi} = \frac{\cos \phi \cdot \dot{\psi}_I + DLS_{nom} \cdot \exp\left(-\frac{\dot{\psi}_I^2}{q}\right) \cdot \sin \phi \cdot v_{nom}}{\cos \theta} \quad (10.20c)$$

Where $u = \dot{\psi}_I$ [rad/s] is the input to the MPC controller. DLS_{nom} is based on the expected build rate for the fixed bent sub in the BHA, and v_{nom} is based on experience of an average ROP while drilling [12].

Furthermore, the Cartesian coordinates of the BHA expressed in the inertial frame are given by the following equations [12]:

$$\dot{x} = v_{nom} \cdot (\sin \phi \cdot \sin \psi + \cos \phi \cdot \cos \psi \cdot \sin \theta) \quad (10.21a)$$

$$\dot{y} = -v_{nom} \cdot (\cos \psi \cdot \sin \phi - \cos \phi \cdot \sin \psi \cdot \sin \theta) \quad (10.21b)$$

$$\dot{z} = v_{nom} \cdot \cos \phi \cdot \cos \theta \quad (10.21c)$$

Where v_{nom} is the same as for the Euler angle equations above. All the above equations together with the cost function in Equation 10.19, are implemented in the control system in Simulink with a MPC block that supports NMPC by using the Model Predictive Controller Toolbox [71].

10.8 Well Trajectory Reference

The control system generates a well trajectory reference before the drilling operation starts. The generated well path is the reference that the NMPC controller continuously aims to steer the drill bit against. The curves used for the trajectory planning is called 3D Dubins Curves that minimize the total length of the trajectory. The work with these curves have been carried out by the petroleum engineers in this project, and more information about these curves is therefore found in Chapter 12.

Downhole Sensor Orientation

The position estimation of the drill bit downhole is highly important for safe and efficient drilling operations. Miscalculations can lead to catastrophic consequences such as not hitting the targets, entering a faulted zone or intercepting a nearby well. Even using the best tools and technologies available, the estimations will be subdued to error and uncertainty. This is caused by several parameters related to the equipment and to the environment they operate in [53].

The Drillbotics team last year struggled with determining the true drill bit orientation downhole. The magnetometer was not used, which meant precise readings of the yaw could not be obtained to calculate the orientation. Instead, the yaw was assumed to equal the azimuth change provided by the azimuth motor. Finally, to estimate the orientation of the bit, the assumed yaw was used together with the roll and pitch measurements from the accelerometer.

For these reasons, one petroleum engineering student from the team conducted thorough research on sensor understanding and downhole orientation with the aim to obtain a reasonable estimate of the yaw using the magnetometer. This chapter covers basic theory for the understanding of the components and principles of the sensor card. Furthermore, it is investigated whether calibration of the magnetometer and accelerometer can lead to an improved estimate of yaw. Unfortunately, the conclusion was that yaw could not be obtained using the magnetometer due to noisy environments around the rig that caused uncertainties in the sensor readings.

11.1 Sensor Card

The Arduino Nano 33 BLE sensor card is used in this project. It consists of a board with a powerful microcontroller of reference nRF52840 from Nordic Semiconductors and a 32-bit ARM Cortex®-M4 CPU [28]. In addition, the board has an embedded 9 axis Inertial Measurement Unit (IMU), which is composed of a 3-axis accelerometer, 3-axis

magnetometer, and 3-axis gyroscope [28]. The IMU is the model LSM9DS1. An IMU can also be called as a 9 Degrees of Freedom (9DOF) sensor, since each axis is completely independent from the others. This type of sensor can also be called Microelectromechanical systems (MEMS), given their small dimensions and mechanical principle of working [81]. The board with a width of 18 mm and a length of 45mm is seen in Figure 11.1.

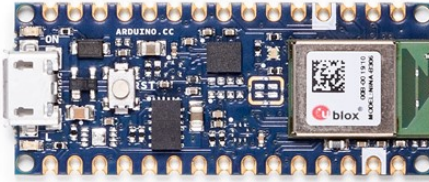


Figure 11.1: Arduino Nano 33 BLE [28].

11.2 Accelerometer

The accelerometer is a device designed to measure the acceleration force acting on an object. If the object is at rest, the only acceleration it will experience is the one caused by Earth's gravity [46]. There are several types of accelerometers in the market. The one integrated in the Arduino Nano 33 BLE is called capacitive accelerometer. The principle of this type of accelerometer is that it has a mass confined to move in one direction or axis between some plates with the use of springs. These plates measure the capacitance between themselves and the mass. When acceleration is applied to the system, the mass will move, changing the capacitance between the plates and the mass. This change in capacitance can be processed and interpreted as an acceleration value [81]. The mechanical principle is illustrated in Figure 11.2 [81].

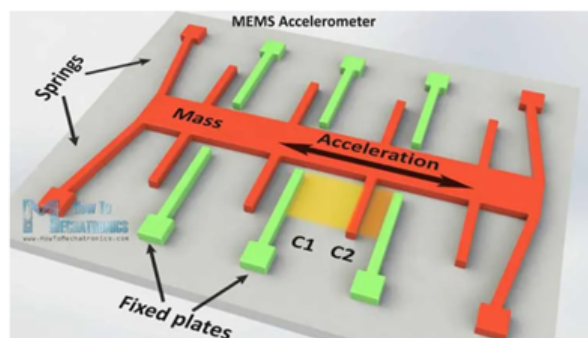


Figure 11.2: Accelerometer principle [81].

This principle is used for all three principal directions which are orthogonal to each other's plane.

11.3 Magnetometer

A magnetometer is a sensor that measures magnetism. Magnetism is "the direction, strength, or relative change of a magnetic field at a particular location" [29]. A general background of how the earth's magnetic field works will be presented before the principles behind the magnetometer.

11.3.1 Earth's Magnetic Field

The earth's magnetic field is produced by electrical currents that are flowing in the molten iron rich fluid in the outer core of the earth [103]. This can be illustrated by representing the earth as a gigantic dipole bar magnet in Figure 11.3 [23].

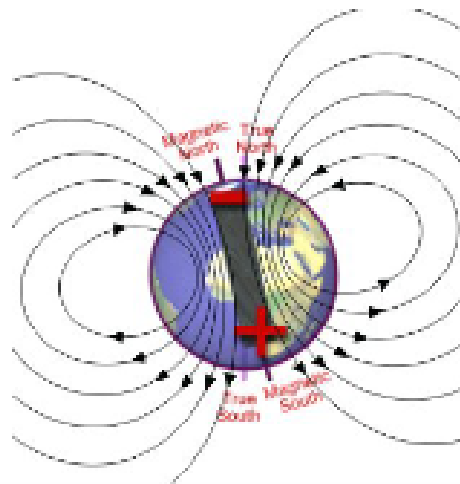


Figure 11.3: Earth's magnetic field [23].

Following this model, it is possible to observe how the field lines are originated at the Magnetic South Pole and are converging back in the Magnetic North pole. These lines continue in a close loop going through the earth from North to South. The field lines will vary in strength and inclination. Inclination is the angle between the direction of the field lines and the tangent plane of the earth's surface. Close to the poles, the lines will have an inclination of 90° . On the other hand, near the Equator, these lines are almost parallel to the ground, giving an inclination of 0° [49]. This can be evidenced in Figure 11.4.

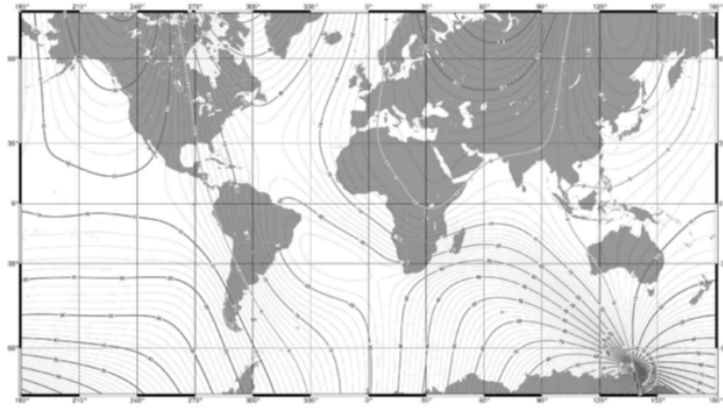


Figure 11.4: Magnetic field inclination according to the US/UK World Magnetic Model (WMM) [49].

True North is the direction towards the geographical north pole. Another key parameter for the magnetic field in terms of directional control is the difference between Magnetic North and True North, which is called declination. The reason for this difference is that the magnetic and geographical poles are not aligned.

The concepts reviewed are observed in Figure 11.5 [23].

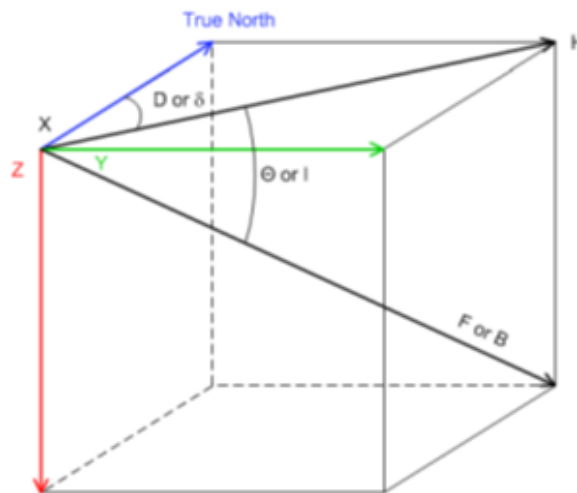


Figure 11.5: Earth's magnetic field (vector B or F) and its components [23].

Where [23]:

- the X - Y - Z frame is the reference frame called North-East-Down or NED.
- F or B is the magnetic field intensity vector.
- H is the projection of B in the horizontal plane X - Y .
- D or ϕ is the declination of B .
- I or θ is the inclination of B .

11.3.2 Magnetometer Sensor

The Arduino sensor card's magnetometer integrated in the IMU, is used to measure the magnetic field intensity in three axis with a reference to the sensor body, as seen in Figure 11.6 [29].

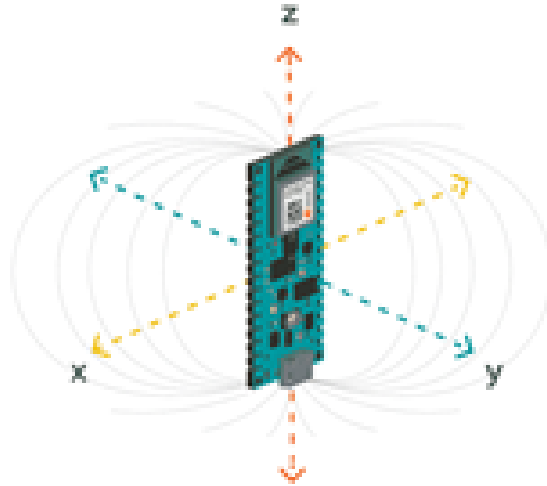


Figure 11.6: LSM9DS1 Magnetometer [29].

The magnetometer is based on the Hall Effect principle. It consists of a conductive plate where the electrons flow straight when undisturbed from one end to the other, as depicted in Figure 11.7 [81].

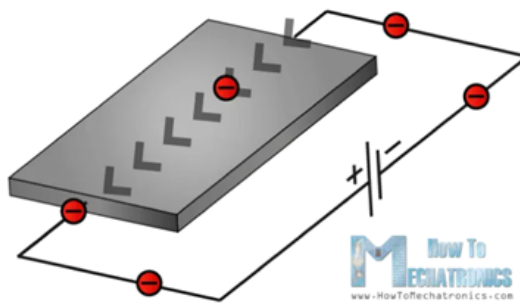


Figure 11.7: Undisturbed electrons flowing straight [81].

In the case of the presence of a magnetic field around the plate, the flow of electrons will be shifted to one side of the plate. This effect will create a voltage which depends on the magnetic field strength and direction. Figure 11.8 depicts this phenomenon [“cite –MEMS”].

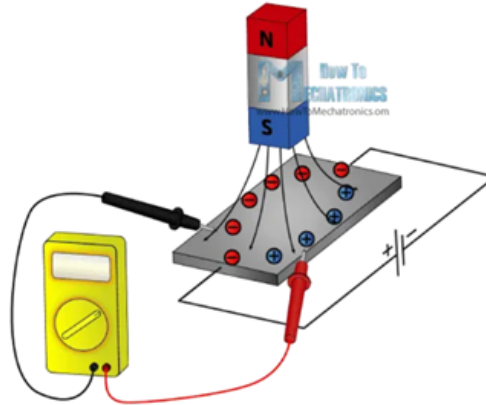


Figure 11.8: Voltage measurement in the plate in function of the magnetic field strength and direction [81].

11.4 Gyroscope

The gyroscope incorporated in the IMU is an inertial tool used to measure the angular velocity on each of the three axes of the body frame using the Coriolis effect. Following Figure 11.9, it is possible to observe what happens if a mass is moving in a direction with a determined velocity and then an angular rate is applied, depicted with the green arrow. This will cause a force, represented with the blue arrow, which will create a perpendicular displacement of the mass [81].

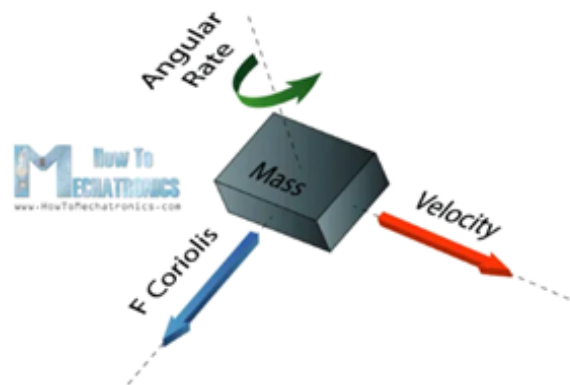


Figure 11.9: Coriolis Effect used for gyroscope [81].

The gyroscope uses a similar principle as the accelerometer. A mass is constantly moving within a fixed frame. When an angular rate is applied to the system, the springs on the mass move and there is a change in capacitance. This can then be interpreted as the angular velocity. The concept is illustrated in Figure 11.10 [81].

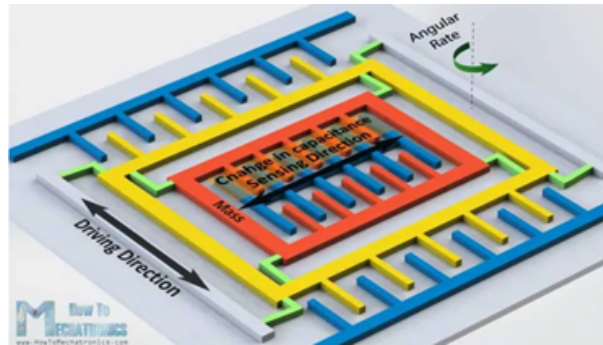


Figure 11.10: Gyroscope principle [81].

11.5 Orientation estimation

The downhole position is modelled in a coordinate system with a fixed reference point at the origin $(x,y,z) = (0,0,0)$. To calculate the position with the downhole sensor, the orientation of the tool needs to be estimated. The orientation estimation will use relative orientation of the body reference frame (BODY), with respect to the the fixed North-East-Down reference frame (NED). The principle directions in the NED coordinate system are defined as follows [49]:

- X_n -axis points towards the true North.
- Y_n -axis points towards the East.
- Z_n -axis points downwards, in a perpendicular direction to the Earth's surface.

In the same way, the reference frame BODY has three axis which are selected to coincide with the main axes of inertia of the body, which are normally given by [49]:

- x_b -axis is the longitudinal axis.
- y_b -axis is the transverse axis.
- z_b -axis is the normal axis.

The above definitions are shown in Figure 11.11 [49].

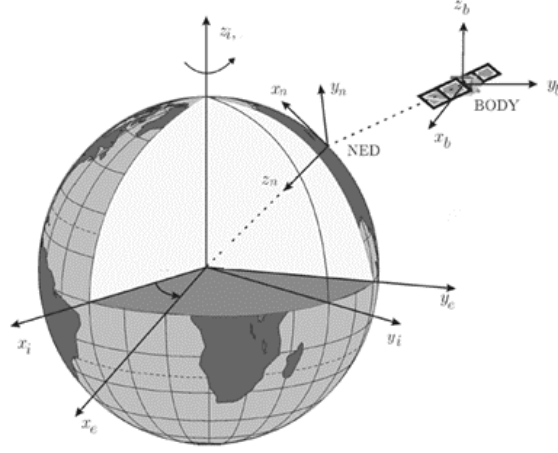


Figure 11.11: NED and BODY frames [49].

The BODY frame can rotate since it reflects the sensor itself which is located inside the BHA. On the hand, The reference frame NED will not be rotated since it is considered fixed. The description of the rotation of one of the axes in the BODY frame in function of the NED frame can be calculated using the Euler angles. These angles are [49]:

- *Roll: rotation of the x_b axis, denoted as ϕ .*
- *Pitch: rotation of the y_b axis, denoted as θ .*
- *Yaw: rotation of the z_b axis, denoted as ψ .*

Once the Euler Angles are calculated, they can be used to transform coordinates between BODY and NED frames with a rotation matrix. In this form, it is possible to compare different orientations from the BHA with a fixed reference frame of NED.

11.5.1 Roll, Pitch and Yaw Calculation

The methodology used to obtain the Euler angles by integrating the accelerometer and magnetometer data will be discussed. When the accelerometer is at static conditions, the readings on the 3 axes will be the 3-D decomposition of the gravity vector. The pitch and roll angles can be calculated from the accelerometer measurements using the following trigonometrical relations [21].

$$Pitch(\theta) = \arctan\left(\frac{A_x^b}{\sqrt{(A_x^b)^2 + (A_z^b)^2}}\right) \quad (11.1)$$

$$Roll(\phi) = \arctan\left(\frac{A_y^b}{A_z^b}\right) \quad (11.2)$$

These quantities are used in conjunction with the magnetometer readings to project the magnetic field strength vector into the horizontal X-Y plane. This can be achieved by [49]:

$$\begin{bmatrix} h_x \\ h_y \\ h_z \end{bmatrix} = R_{y,\theta} R_{x,\phi} \begin{bmatrix} m_x \\ m_y \\ m_z \end{bmatrix} \quad (11.3)$$

$$\begin{bmatrix} h_x \\ h_y \\ h_z \end{bmatrix} = \begin{bmatrix} \cos(\theta) & 0 & \sin(\theta) \\ 0 & 1 & 0 \\ -\sin(\theta) & 0 & \cos(\theta) \end{bmatrix} \begin{bmatrix} 1 & 0 & 0 \\ 0 & \cos(\phi) & -\sin(\phi) \\ 0 & \sin(\phi) & \cos(\phi) \end{bmatrix} \begin{bmatrix} m_x \\ m_y \\ m_z \end{bmatrix} \quad (11.4)$$

Finally, the horizontal components of this projection can be used to estimate the magnetic heading or yaw [49].

$$Yaw(\psi) = -\arctan^2\left(\frac{h_y}{h_x}\right) \quad (11.5)$$

11.6 Calibration

To use the sensor readings to estimate the attitude of the downhole tools, it is important to calibrate the sensors beforehand. Uncalibrated data can contain noise, be affected by bias and disturbances due to the working environment.

The gyroscope is an inertial tool and can not measure the angular velocity at static conditions. For this reason, it only becomes useful while rotating the downhole tool to determine its orientation. However, due to the noise created by downhole vibrations while drilling, these readings are inaccurate and can not be considered for attitude estimation. Therefore, sensor calibrations were only performed for the accelerometer and magnetometer.

11.6.1 Accelerometer Calibration

At static conditions, the accelerometer will only measure the force vector due to the gravity of the earth. Even though this value may have some fluctuations, it can be assumed constant. The average gravitational acceleration is $9.80665 \frac{m}{s^2}$. To simplify gravity related measurements, it is common to express acceleration in a normalized term known as “Gs”, where $1G = 9.80665 \frac{m}{s^2}$ [49].

The gravity vector is decomposed in the three axes of inertia of the sensor $x_{b,acc}$, $y_{b,acc}$, $z_{b,acc}$. The norm of these values should result in 1 G as shown in Equation 11.6. If this is not satisfied, the sensor needs to be calibrated [49].

$$\sqrt{x_{b,acc}^2 + y_{b,acc}^2 + z_{b,acc}^2} = 1G \quad (11.6)$$

The range of the sensor measurements on any axis G_i where $i = (x, y, z)$ is between -1 and 1 Gs. Therefore, a 3D plot of the measurements in the three axes would be represented by a sphere of radius $r = 1$ and center 0, 0, 0. Miscalibration of this sensor will result in the displacement of the origin of the sphere and can also induce a non-spherical shape. If this is observed, the uncalibrated data h is calibrated using the correction matrix A and bias correction vector b . The equation to obtain the calibrated data h_{cal} can be described by [49]:

$$h_{cal} = A^{-1}(h - b) \quad (11.7)$$

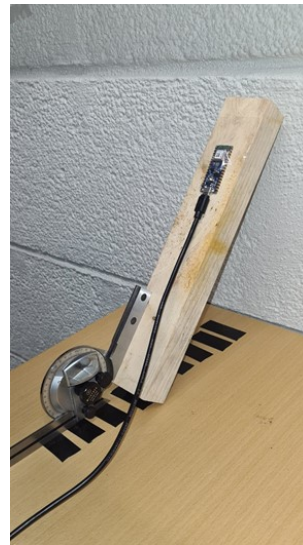
The tool used to calculate the correction matrix A and vector b was the free software Magneto® [98]. This software allows the user to introduce the uncalibrated data points and will calculate the correction factors.

Following is a summary of the methodology applied to the calibration of the accelerometer:

1. Collection of data points: For the accelerometer calibration, special care was taken since the accelerometer had to be completely still while taking the uncalibrated points, given that the norm of the measured acceleration vector $[x, y, z] \approx 1$. Any vibration or movement in the sensor during measurements will add unreal values to the calibration, thus biasing the results. For this reason, a simple set up was prepared to take multiple measurements in all the principal positions and orientations of the sensor as seen on Figure 11.12:



(a) Accelerometer in horizontal position for calibration.



(b) Accelerometer in inclined position for calibration.

Figure 11.12: Accelerometer set in different static positions for calibration measurements.

2. Generation of correction Matrix A and vector b: Once the data set of points have been obtained, the software Magneto was applied using the points and the normalized magnitude of 1. Then the software calculates the matrix A and vector b, as seen in Figure 11.13.

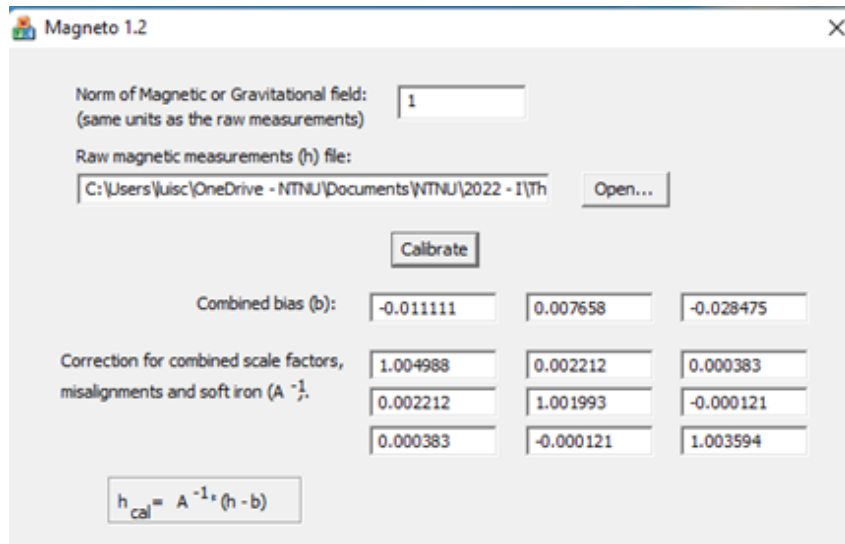


Figure 11.13: Magneto Software used for accelerometer calibration.

3. Once obtained, the correction factors were applied to the raw measurements. As a mean to evidence the difference between the calibrated and uncalibrated data, they are plotted as observed in Figure 11.14.

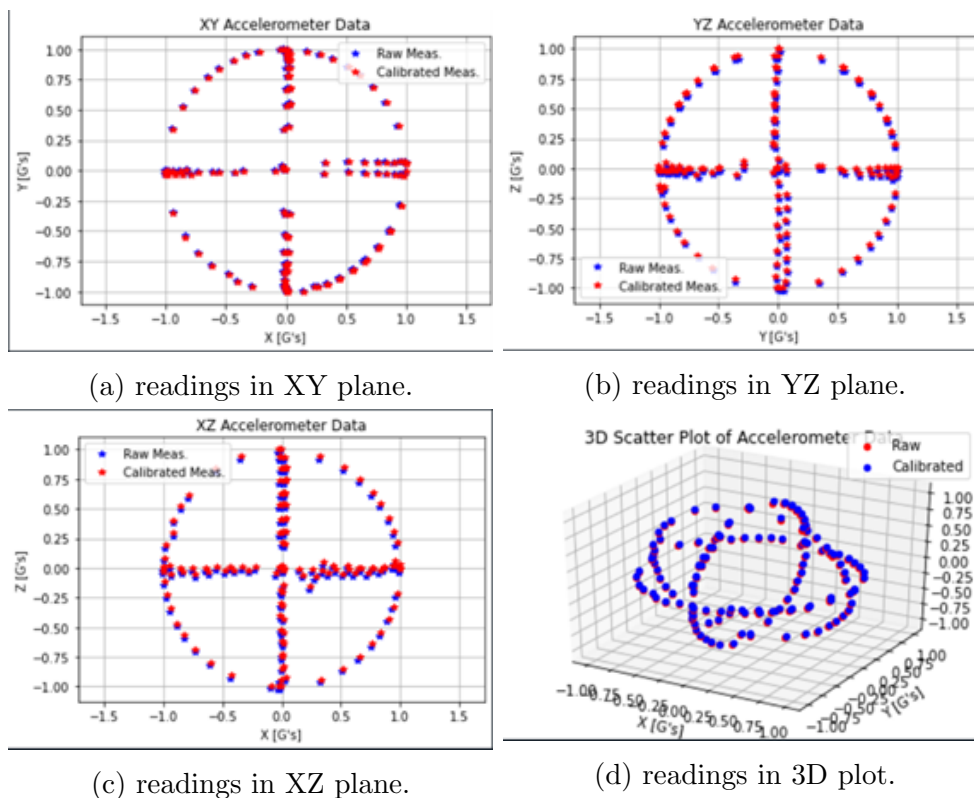
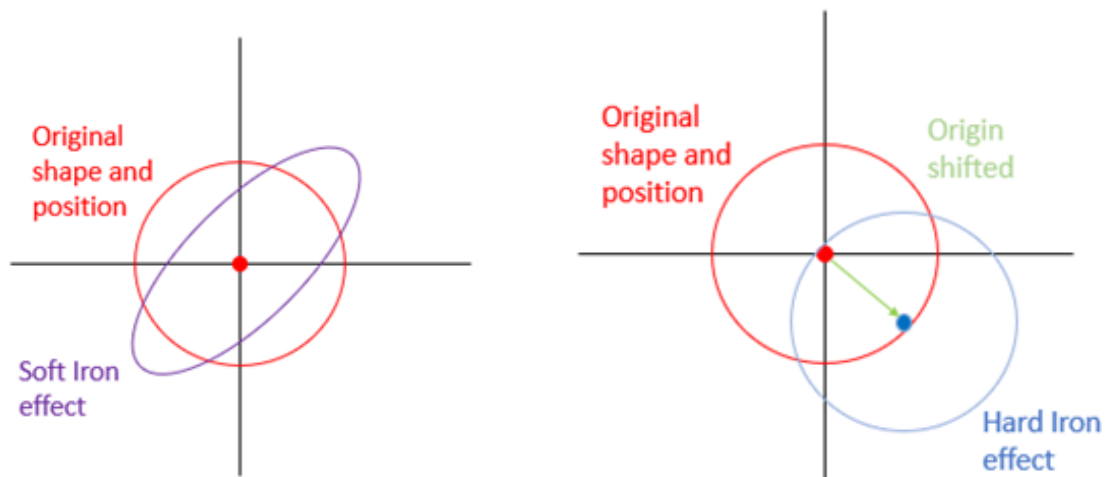


Figure 11.14: Calibrated vs uncalibrated accelerometer data.

To conclude, the original readings from the sensor prior to calibration gave decent results, but it is optimal to use the calibrated data for better accuracy. Since the gravity vector is fairly constant both in time and space in a certain area, the sensor calibration only has to be performed once.

11.6.2 Magnetometer Calibration

Unlike the accelerometer, the magnetometer readings are highly susceptible to magnetic disturbances in the surroundings of the sensor. These magnetic disturbances are caused by what is referred to as “hard iron” and “soft iron” effects. Data from a perfectly calibrated sensor should be represented by a spherical shape with origin coordinates of 0, 0, 0. If “soft iron” disturbances are present, the resulting shape will not be a sphere anymore, but more of a ellipsoid. In addition, if “hard iron” disturbs the readings of the sensor, the center of the readings will be shifted from the origin. The soft and hard iron effects can be observed in Figure 11.15. If these these circumstances are present, the sensor needs calibration to remove these effects [49].



(a) Soft Iron effect on magnetometer readings. (b) Hard Iron effect on magnetometer readings.

Figure 11.15: Soft and Hard iron effects on magnetometer readings.

The calibration procedure is very similar to the one performed for the accelerometer. The first step is to rotate the sensor in multiple directions and orientations, to obtain a cloud of points of raw data. Then, the raw data is analyzed with the software Magneto. To obtain the magnetic field strength magnitude needed for the program, data from a magnetic observatory station close to Trondheim was used. Once there is enough data for Magneto, the program is run and the correction matrix A and vector b are calculated as Figure 11.16.

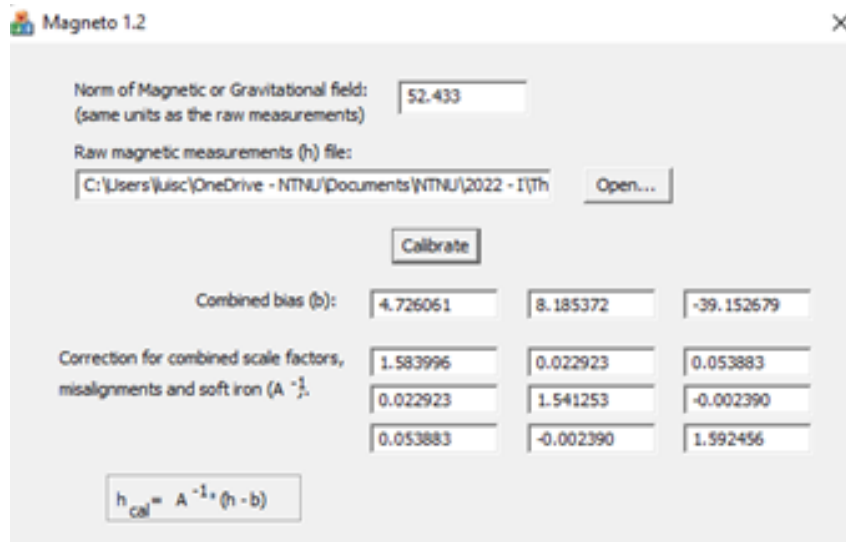


Figure 11.16: Calibration matrix A and vector B generation with Magneto.

Furthermore, the correction factors are applied to the raw data to obtain the calibrated values. A way to double check that the calibration was applied correctly is to run the Magneto software again but with the calibrated data. The resulting correction Matrix A should be a 1 diagonal matrix and the elements of vector b should be 0, as shown in Figure 11.17.

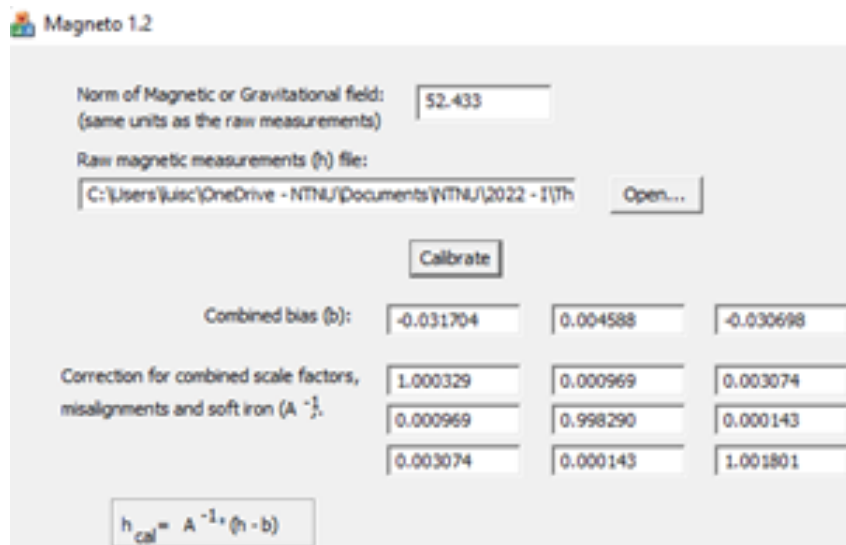


Figure 11.17: Magneto results for calibrated magnetometer data.

The data before and after calibration is plotted as seen in Figure 11.18. There is a large difference between the two clouds of points.

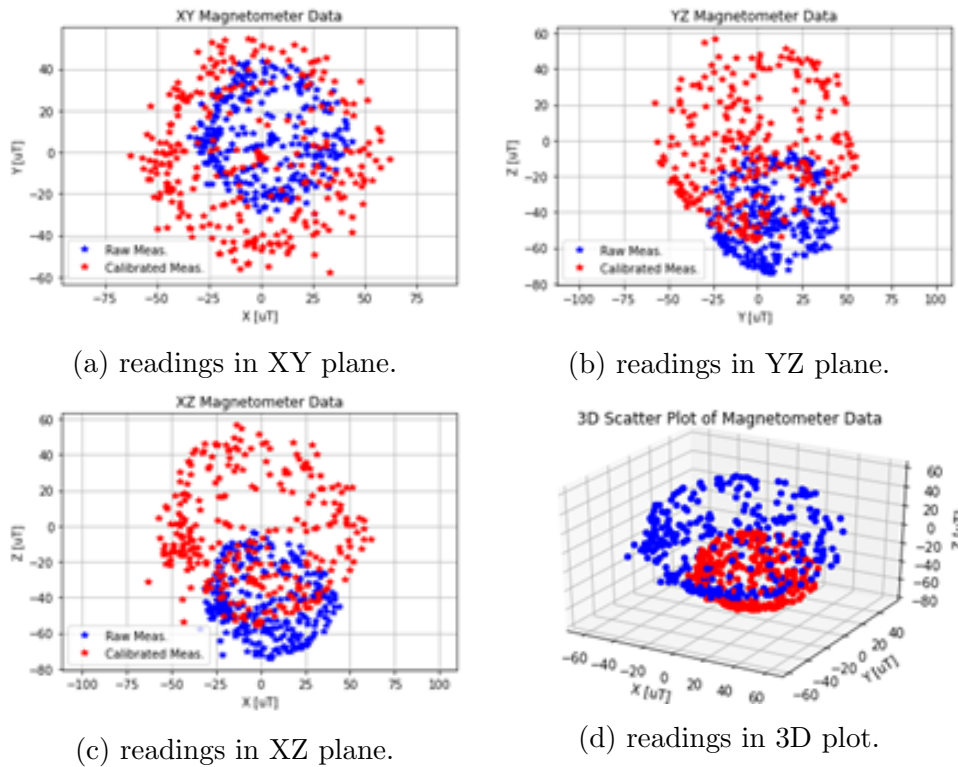


Figure 11.18: Calibrated vs uncalibrated magnetometer data.

This calibration needs to be done on a regular basis, given the high variability of the magnetic disturbances.

Additional tests were performed with the aim of better understanding the magnetometer. An experiment was recreated under the conditions which the sensor will be working while drilling. To achieve this, the sensor was set inside the sensor housing in the BHA. Then, the BHA was placed inside a pre-drilled vertical hole in one of the cement blocks.

This cement block was situated in the metal frame below the drilling rig. Once the set up was ready, the sensor was left to read static conditions throughout the night. As a control to compare the impacts of the metallic surroundings on the magnetometer, a second sensor was placed five meters away from the drilling rig, without any metal components surrounding it. Measurements from this sensor were also taken over night. The sensor with and without the housing is shown in Figure 11.19.



(a) Sensor inside housing.



(b) Sensor without housing.

Figure 11.19: Sensor with and without housing.

The sensor measurements were compared to the true magnetic field magnitude obtained from the magnetic observatory near Trondheim. It was evident that the sensor readings are extremely affected by magnetic disturbances from the housing and rig frame. Therefore, it is necessary to calibrate the magnetometer in the correct surroundings.

11.7 Azimuth or Yaw Calculation

Once the sensors were properly calibrated, it was attempted to calculate the yaw for orientation estimation of the BHA. This was done by integrating the roll and pitch obtained from the accelerometer with the magnetometer readings in Simulink. Although the roll and pitch readings were stable and reliable, it proved to be difficult as the data from the magnetometer fluctuated greatly. Experts from the university confirmed the working environment for the magnetometer was not ideal and consisted of too many magnetic disturbances. As a result, the calculated yaw fluctuated with more than 20° and could not provide an orientation estimate which was accurate enough for the Drillbotics competition.

Despite the work performed and time spent on understanding and calibrating the magnetometer, the team has concluded to not use the magnetometer as a tool to obtain the yaw. Instead, a decision was made to proceed with last year's assumption of estimating the yaw. This was done by setting the yaw equal to the bent sub orientation while drilling. This value is obtained from the azimuth motor in the control system. Together with roll and pitch values from the accelerometer, it is possible to estimate the orientation of the bit when drilling. The assumption of yaw leads to uncertainty in the position estimate, but this is the only remaining solution after concluding not to use the magnetometer.

Well Trajectory Planning

Drilling wells in the oil and gas industry is very costly. To maintain a profitable industry, it is crucial to minimize the overall expenditures by optimizing all possible design aspects. According to statistics, the cost of drilling a well is nearly linearly correlated with the trajectory length. Therefore, it is vital to optimize the well path by finding the shortest trajectory with curvature constraints. This can be done using Dubins curve, given that only forward motion is permitted between two directional points [68].

12.1 Dubins Curve

Dubins constructed the shortest 2D path by combining three circular arcs of maximum curvature or two circular arcs of maximum curvature with a single straight line. These curves are referred to be part of the curve-curve-curve CCC or curve-straight-curve CSC family, respectively. The circular arc is denoted by C and the straight line by S . Furthermore, the curves in each family are characterized by their turning motions. The letter R represents a right turn, and the letter L represents a left turn. Figure 12.1 shows the LRL and RLR curves belonging to the CCC family and the RSR, LSL, RSL and LSR curves belonging to the CSC family. One of these six designs will give the overall minimum trajectory with curvature constraints between two directional points [68].

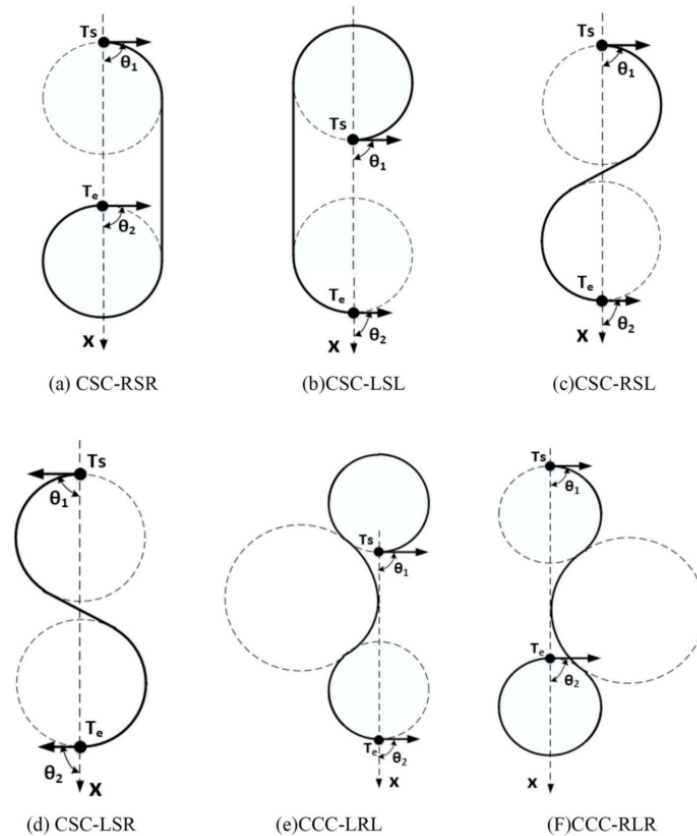


Figure 12.1: CCC and CSC families [68]

Dubins curve has been used in the autopilot industry for a long time to plan car and robot paths. However, the drilling industry has overlooked the possibilities and benefits of using these curves for designing the optimal well trajectory. Recently a PhD student at NTNU published a paper regarding the implementation of the 3D CSC Dubins curve in the drilling industry [68]. The characteristics of Dubins curve proves to be beneficial for drilling since it not only provides the shortest well path, but it also reduces the inclination of the straight section by minimizing the length of the curved sections. The CCC family is not considered because it requires many turning angles in the trajectory which is not suitable for drilling. The PhD student's framework for optimizing the well path using Dubins curve will be used as a basis in this chapter [68].

12.2 3D Dubins Curve

To successfully design a well trajectory using the 3D Dubins curve, several assumptions must be made . These are [68]:

- The formation can be drilled in any direction.
- The well's surface is found on a horizontal plane.

- The target is reasonable and can be easily reached.

The 3D CSC Dubins curve consists of a curved section followed by a straight section and another curved section. Each section will be constructed in their own plane. The two circular arcs are constrained by the maximum allowed dogleg severity denoted as $\frac{\kappa^\circ}{30m}$, which corresponds to a permitted minimum radius of curvature of $r_{min} = \frac{5400}{\pi\kappa}$. This radius will be used for both circular arcs in the well path design to minimize the length of the curved sections and optimize the overall well path [68].

Dubins curve only requires four input parameters when the curvature constraint is given. These are the highest allowed kickoff point $P_1 = (Px_1, Py_1, Pz_1)$ along with its drilling direction vector $V_1 = (Vx_1, Vy_1, Vz_1)$, and the target point $P_2 = (Px_2, Py_2, Pz_2)$ along with its drilling direction vector $V_2 = (Vx_2, Vy_2, Vz_2)$. Since the well is drilled vertically down towards the kickoff point, the direction vector at P_1 is always given as $V_1 = (0, 0, -1)$ [68].

Two separated 3D Dubins curves along with some of their properties are shown in Figure 12.2. O_1 and O_2 denote the centers of the corresponding circles of maximum curvature. C_1 represents the end of the first circular arc which is always a build-up section. C_2 on the other hand signifies the start of the second circular arc which can either be a build-up or drop-down section. In some cases, Dubins curves may not consist of two curved sections as C_1 can coincide with P_1 or C_2 can coincide with P_2 [68].

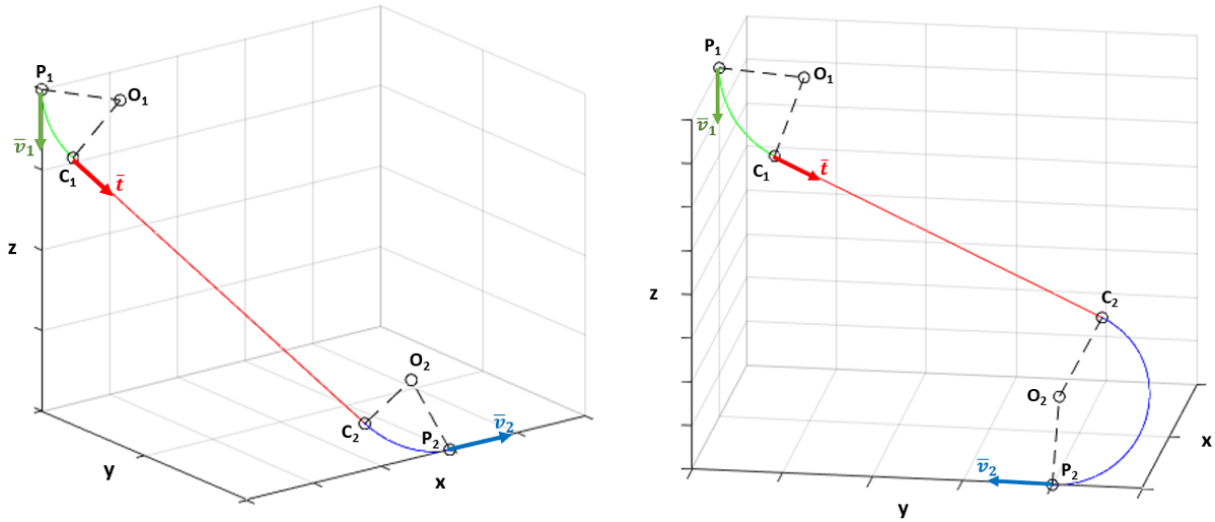


Figure 12.2: Dubins curve properties.

The general 3D Dubins curve is derived below [68].

The minimum radius of the curvature for both curves is denoted as:

$$r = r_{min} \tag{12.1}$$

The unknown vector belonging to the straight section of the path between C_1 and C_2 is given by:

$$T = (Tx, Ty, Tz) \quad (12.2)$$

Converting T into its unit vector yields:

$$t = \frac{T}{\|T\|} \quad (12.3)$$

The following cross products provide the vectors that are perpendicular to the circular planes.

$$U_1 = T \times V_1 \quad , \quad U_2 = T \times V_2 \quad (12.4)$$

Furthermore, the radius vectors pointing from P_1 to O_1 and P_2 to O_2 are:

$$\Omega_1 = V_1 \times U_1 \quad , \quad \Omega_2 = -V_2 \times U_2 \quad (12.5)$$

The unit vectors of these are:

$$\omega_1 = \frac{\Omega_1}{\|\Omega_1\|} \quad , \quad \omega_2 = \frac{\Omega_2}{\|\Omega_2\|} \quad (12.6)$$

The centres of the two circles are then defined as:

$$O_1 = P_1 + r \cdot \omega_1 \quad , \quad O_2 = P_2 + r \cdot \omega_2 \quad (12.7)$$

The vectors pointing from C_1 to O_1 and C_2 to O_2 are:

$$\Phi_1 = T \times U_1 \quad , \quad \Phi_2 = -T \times U_2 \quad (12.8)$$

The unit vector of the above vectors are:

$$\phi_1 = \frac{\Phi_1}{\|\Phi_1\|} \quad , \quad \phi_2 = \frac{\Phi_2}{\|\Phi_2\|} \quad (12.9)$$

Hence, C_1 and C_2 are obtained by:

$$C_1 = O_1 - r \cdot \phi_1 \quad , \quad C_2 = O_2 - r \cdot \phi_2 \quad (12.10)$$

Finally, the definition of T in Equation 12.2 gives an expression that can be used to compute Dubins curve.

$$T = C_2 - C_1 \quad (12.11)$$

C_1 and C_2 in the above expression are both functions of T . This set of three equations can be used to solve the three unknown variables Tx , Ty and Tz . It is difficult to obtain an analytical solution for these variables. For this reason, a numerical method must be utilized instead. By moving all the terms in Equation 12.11 to the left side, the minimum of the function can be solved using the gradient descent method. The built-in function *Fsolve* in Matlab can be used to solve the three equations and obtain the vector T [68].

When $T = (Tx, Ty, Tz)$ is obtained, several characteristics of the Dubins curve can be determined [68].

The turning angle on each circular plane is given by:

$$\gamma_1 = \angle P_1 O_1 C_1 = \arccos\left(\frac{V_1 \cdot T}{\|V_1\| \cdot \|T\|}\right) \quad (12.12)$$

$$\gamma_2 = \angle P_1 O_1 C_1 = \arccos\left(\frac{V_2 \cdot T}{\|V_2\| \cdot \|T\|}\right) \quad (12.13)$$

These are used to find the length of the two curved sections.

$$L_{c1} = \gamma_1 \cdot r \quad , \quad L_{c2} = \gamma_2 \cdot r \quad (12.14)$$

The length of the straight section is simply the length of vector T .

$$L_s = \|T\| \quad (12.15)$$

Finally, the total length of the Dubins curve well trajectory is calculated by:

$$L_t = L_{c1} + L_s + L_{c2} \quad (12.16)$$

12.3 Competition Well Trajectory

This thesis will adopt the 3D Dubins curve for well trajectory planning. However, to utilize this curve for the competition, several adjustments to the earlier derived 3D Dubins curve must be made.

On the day of the competition, Drillbotics will provide the team with multiple target points. This means several Dubins curves must be combined in series to generate the complete well trajectory. The first Dubins curves end coordinate and direction vector must therefore be the same as the second Dubins curve's start coordinate and direction vector. This concept is also applicable at the transition of the remaining curves. Table 12.2 shows the input parameters required for each Dubins curve and is used to better understand the fusion of Dubins curves to create a well path.

Table 12.1: Input parameters for Dubins curve.

	Start of Dubins Curve		End of Dubins Curve		Curvature Constraint
	Target Coordinate	Direction Vector	Target Coordinate	Direction Vector	Radius
Dubins Curve 1	P1	V1	P2	V2	r
Dubins Curve 2	P2	V2	P3	V3	r
Dubins Curve 3	P3	V3	P4	V4	r

Since Drillbotics only provides the target coordinates, the team will not know the corresponding direction vectors that are required as input parameters for the Dubins curves. However, as mentioned previously, the direction vector V_1 at the kickoff point P_1 always points straight down. Therefore, the only remaining unknown parameters are the direction vectors at the affiliated end coordinates. This concept is shown in Table 12.2 where the unknown parameters are indicated in red.

Table 12.2: Unknown direction vectors of Dubins curve.

	Start of Dubins Curve		End of Dubins Curve		Curvature Constraint
	Target Coordinate	Direction Vector	Target Coordinate	Direction Vector	Radius
Dubins Curve 1	P1 = KOP	V1 = (0, 0, -1)	P2	V2	r
Dubins Curve 2	P2	V2	P3	V3	r
Dubins Curve 3	P3	V3	P4	V4	r

The system can now be solved as there are an equal number of equations and unknowns. However, to optimize the well path, the system must be solved with a cost function that minimizes the total trajectory length. This cost function is written as follows:

$$COST = \sum_{i=1}^N (L_{c1,i} + L_{s,i} + L_{c2,i}) \tag{12.17}$$

Where N is the number of Dubins curves combined to generate the well trajectory.

The simplest way to solve this nonlinear optimization is by using the built-in function *Fmincon* in Matlab, which is based on the gradient descent algorithm. This will not only determine the optimum direction vectors at the end coordinates, but also produce the shortest well trajectory with a constrained curvature.

Finally, the straight section between the origin P_0 and kickoff point P_1 is added to the top of the optimized well path to give a complete representation of the well trajectory that will be drilled on the competition day. An example of such a well path with arbitrary targets is shown in Figure 12.3.

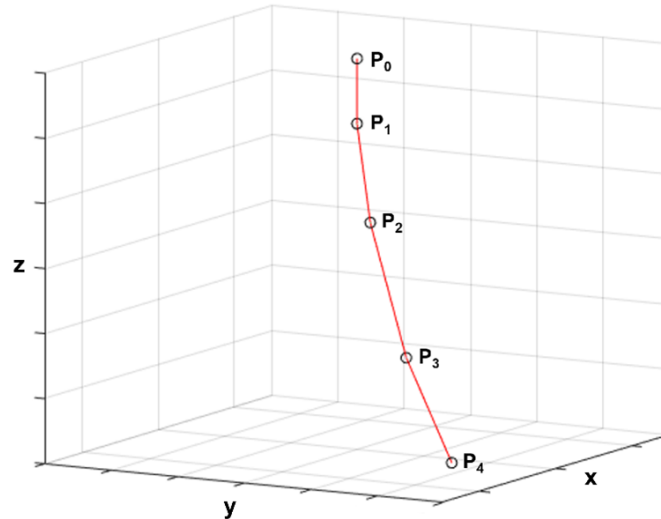


Figure 12.3: Well trajectory with arbitrary targets.

12.4 Well Trajectory Properties

The control system cannot handle well trajectories using analytical equations to describe the path. For this reason, the miniature drilling rig requires the planned well trajectory to be discretized. The discretized well path is then fed into the control system and will be the reference path for the BHA to follow while drilling.

The 3D Dubins curve is discretized by considering the curved and straight sections separately. To ensure that the step length of the discretization is the same for both the curved sections and the straight section, a mutual step length dL must be defined. The discretizing turning angle $d\gamma$ on each circular plane is then found using the following relationship:

$$d\gamma = \frac{dL}{r} \quad (12.18)$$

The two curved sections are discretized based on Figure 12.4.

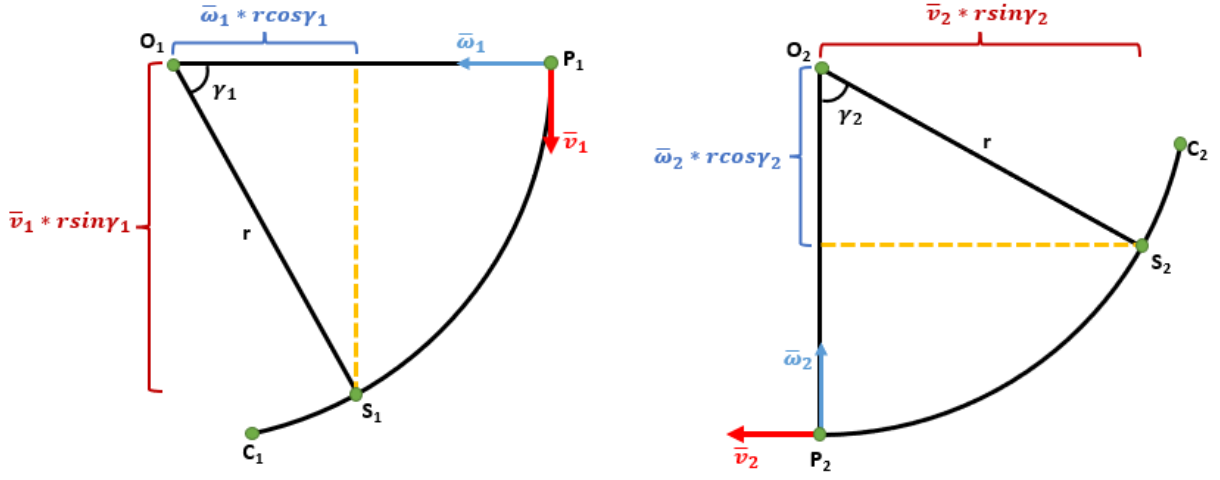


Figure 12.4: Characteristics of the curved sections.

First, an expression representing every point S on the curve must be found. With the help of the known vectors and geometry, point S_1 and S_2 as a function of their corresponding turning angles are determined as follows:

$$S_1 = O_1 + r \cdot (-\omega_1 \cdot \cos a + v_1 \cdot \sin a) \quad (12.19)$$

$$S_2 = O_2 + r \cdot (-\omega_2 \cdot \cos b + v_1 \cdot \sin b) \quad (12.20)$$

Where a and b are the turning angles between 0 and γ_1 , and $-\gamma_2$ and 0 , respectively. By using the discretizing turning angle $d\gamma_1$, the curves are discretized with the common well trajectory step length dL .

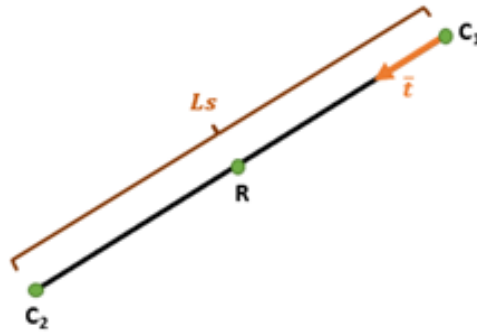


Figure 12.5: Characteristics of the straight section.

The principle for discretizing the straight section of the Dubins curve is similar to the curved section. With the calculated unit vector t starting from C_1 as shown in Figure 12.5, any point R on the straight section is represented by the following expression:

$$R = C_1 + c \cdot t \quad (12.21)$$

Where c is a quantity between 0 and the length of the straight section L_s with a step length of dL .

Finally, the discretized sections are combined and tabulated in the correct order to create the complete discretized well trajectory. This also includes the discretized straight section from the origin to the kickoff point. A table with x , y and z coordinates given at every step length dL until the final target is input to the miniature rig's control system. To visualize the well trajectory, the control system uses a symbolic variable and the 3D plotting function $fplot3$ in Matlab.

Several characteristics such as the inclination and azimuth can be extracted from the discretized well trajectory. The inclination and azimuth of a point on the well path is calculated using its corresponding tangent vector V_T .

For a straight section, the tangent vector is simply $V_T = T$. However, for a curved section, the tangent vector $V_T = V_{TC}$ must first be determined. V_{TC} is calculated similarly for both curved sections and the expression for the first curve is as follows:

$$V_N = (O_1 - S_1) \times (C_1 - P_1) \quad (12.22)$$

$$V_{TC} = V_N \times (O_1 - S_1) \quad (12.23)$$

Where V_N is the normal vector of the circular arc.

A point's inclination on the well trajectory is then numerically found by:

$$\theta = \cos^{-1} \left(\frac{V_1 \cdot V_T}{\|V_1\| \cdot \|V_T\|} \right) \quad (12.24)$$

This expression is graphically presented in Figure 12.6 for both the curved and straight section, respectively.

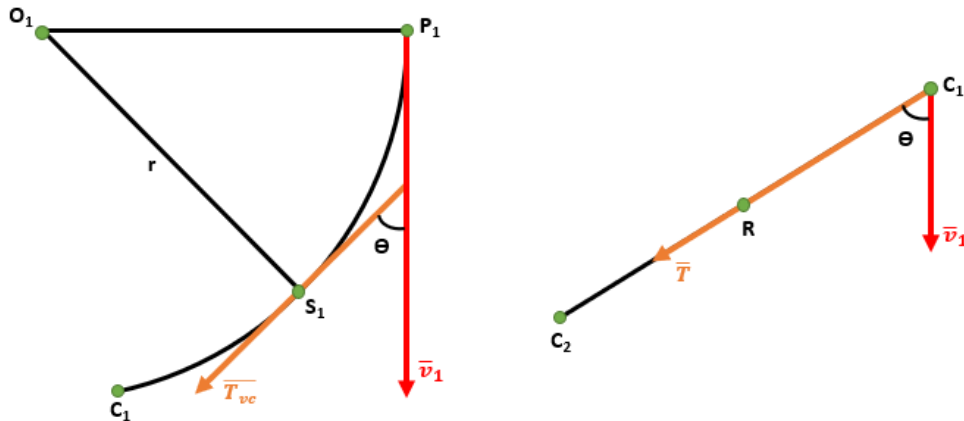


Figure 12.6: Inclination for the curved and straight section, respectively.

Finally, the azimuth of a point is calculated by:

$$\phi = \tan^{-1} \left(\frac{V_{Tx}}{V_{Ty}} \right) \quad (12.25)$$

This angle can be graphically seen in the xy plane in Figure 12.7, where the x axis is parallel to the North direction.

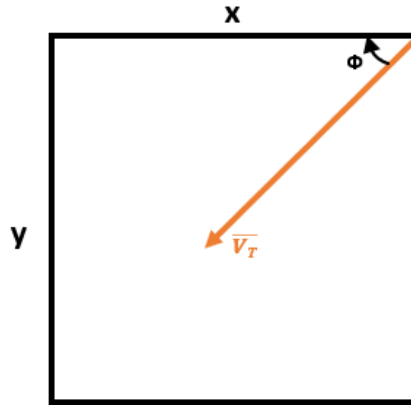


Figure 12.7: Azimuth calculated from a point's tangent vector in the xy plane.

Testing and Qualification

In order to prepare the miniature rig for the Drillbotics competition in June 2022, extensive testing of the rig and associated components have been performed. Functional tests were applied to important components on the rig such as load cell, top drive motor and hoisting motor. Furthermore, material tests of pipes and rods have been conducted to compare whether the practical values correspond to the theoretical values calculated in the Design Limits and Constraints chapter. Drill bit analysis of 4 new drill bits have been performed to determine the most efficient bit. In addition, emphasis has been placed on finding optimal drilling parameters for both the vertical section and deviated section. Another important aspect of the testing was to verify that the rig can drill in different directions with the required inclination and azimuth changes. The sensor card has also been tested to verify that the position it reports corresponds to the actual drilled well trajectory in the rock.

13.1 Functional Test

As the miniature rig has been further developed and improved from year to year by different NTNU teams, it is important to ensure that all components are still working as intended. The importance of having equipment that is calibrated and works optimally is also present in the oil and gas industry. The NORSOK standards is one example of procedures that have developed by the industry to ensure safe and efficient operations, also including equipment integrity and functionality [85].

The 2022 NTNU Drillbotics team have taken inspiration from the standards used in the industry and designed a functionality test. The functional test should contain quantitative measurements and visual inspection of all the critical components on the rig, for example to count the output RPMs of a motor. By testing that all components function properly, the integrity of the rig is ensured by eliminating potential uncertainties.

13.1.1 Top Drive Motor and Hoisting motor

The top drive motor and hoisting motor are important to verify that they work properly. The top drive was new last year and is therefore expected to work properly. The procedure to test the motors were to set a fixed RPM value in the control system, and then count the number of revolutions with a slow-motion camera. A mark on the motors as shown in Figure 13.1 made it easier to count these revolutions.

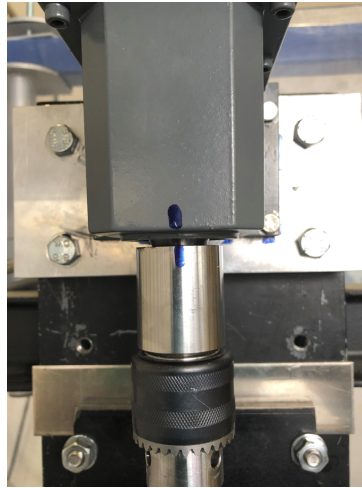


Figure 13.1: Set up top drive and hoisting motor functional test.

Table 13.1: Top drive and hoisting motor functional testing results

	Test number	RPM	Rounds counted	Measurement error [%]
Top Drive	1	5	4.90	2.00
	2	100	99.50	0.50
	3	300	300.25	-0.08
Hoisting motor	1	5	4.80	3
	2	100	99.75	0.25
	3	300	300.30	-0.10

The results in Table 13.1 show that there is a small deviation that is below 3% for both motors. There are also several sources of error present, such as human error when counting the revolutions. Nevertheless, the accuracy obtained for the motors in this test is sufficient for the scope of the drilling.

13.1.2 Load Cell

The load cell has been used for several years, and was therefore tested to verify that the outputs it provides to the control system are accurate. The procedure was to disconnect the drill pipe from the rig, and then place objects of known weight on. The items were

chosen in a range of what can be expected during drilling operations with the miniature rig. The applied weights could then be compared with the actual values that the load cell provides. The results from the functional test of the load cell are presented in Table 13.2.

Table 13.2: Load cell functional test

Test number	Applied weight [kg]	Load cell output [kg]	Measurement error [%]
1	5	4.73	5.40
2	10	9.77	2.30
3	15	14.84	1.07
4	20	19.33	3.35
5	25	24.53	1.88
6	30	30.12	-0.40

As the results in Table 13.2 show, it is evident that the load cell does not provide the exact values of weight that is applied. There are multiple error sources present, such as uncertainty in the reference weight. However, the measurement error is below 6% for all the test, which is acceptable in this project.

13.1.3 Azimuth System

The azimuth system was implemented last year and was also tested this year to ensure that it still works properly. A paper with a mark was used to easier count the revolutions of the rotary table as seen in Figure 13.2. As the system takes time to accelerate up to a certain value, some extra time was taken before the test to ensure that the correct RPM was reached.

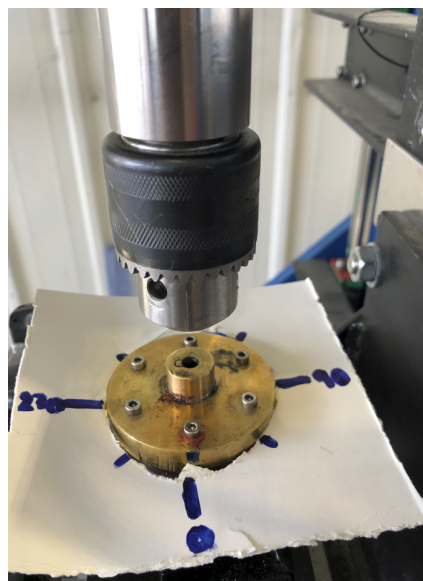


Figure 13.2: Experimental set up azimuth control system functional test.

Table 13.3: Azimuth system functional test

Test	Input [°/min]	Degrees counted [°]	Error deviation [%]
1	180	180	0
2	360	358	-0.55
3	540	540	0

The results in Table 13.3 state that the azimuth system is very accurate and that it only has small deviations. Since this system has control of the azimuth during drilling, this implies that the azimuth can be controlled very accurately.

13.2 Drill Pipe and Rod Tests

13.2.1 Combined Bending Test

The reason for performing the bending test is to ascertain that both the aluminum 7075-T6 drill pipe and the titanium grade 5 rod will withstand the forces that occur during drilling operations. The worst case scenario will be tested and occurs when the maximum inclination of the well is 30° with a corresponding horizontal displacement of 13.59 cm. The NTNU team in 2021 performed a similar test, but they did it on the rod and the drill pipe separately without being connected to the rig. For that reason, a combined bending test will be conducted this year while the rod and drill pipe are connected on the rig.

Experimental Set Up and Execution

The experiment is carried out in such a way that it will recreate a deviated drilling situation as much as possible. To simulate what is happening with the drill pipe and rod while drilling, the experimental set up will be using the rig itself without a rock sample inserted. By using the rig, the drill pipe and rod will get the same support from the upper stabilizer and the riser as they would when drilling.

A thin rope was used around the BHA to force it to a horizontal displacement of 15 cm as seen in Figure 13.3. This displacement should be sufficient enough as the displacement will never exceed 13.59 cm during drilling.



Figure 13.3: Experimental set up. 15 cm of displacement is marked on the floor.

After the test, the rod and the drill pipe were inspected separately for irregularities and signs of deformation. Further investigations were conducted by rolling the pipe and rod on a flat surface as shown in Figure 13.4. The goal of this exercise was to see if there was any air gap between the surface and the pipes. If this is the case, it can be stated that the materials have been permanently deformed because of bending.



(a) Drill pipe.



(b) Rod.

Figure 13.4: Roll test conducted after combined bending test.

Results

The experiment was performed on the titanium rod and the 7075-T6 aluminum drill pipe. The visual inspection showed that there were no signs of deformation to the pipe and rod. For that reason, both passed the test and are sufficient to withstand the bending stresses that occur during drilling operations.

Sources of Error and Interpretation

Prior to the experiment, it was expected that both materials would pass the test based on calculations performed in the design limits chapter. The experiment was organized in such a way that it should represent a normal drilling situation as much as possible. However, there are potential sources of error that may have affected the outcome.

The test does not reflect a real drilling situation as the BHA will get some support and stabilization from the rock. In addition, axial forces that will act on the drill pipe were not considered in the bending experiment. The bending forces increase gradually while drilling, compared to the rapid force that was applied in this test. All these aspects may have influenced the results, but the conclusion is that both the drill pipe and rod are not prone to permanent deformations because of bending during drilling.

13.2.2 Drill Pipe Twist Off

A twist off test was conducted in the workshop on the aluminum 7075-T6 drill pipe. The main purpose of the test was to determine the twist off strength of the material. The result will provide the maximum torque that can be applied to the drill pipe during drilling. However, since only slow and small azimuth changes are required, it is expected that the pipe not experience a torque near the twist off value.

Experimental Set Up and Execution

The experiment was performed by attaching the drill pipe in a lathe in one end, and using a digital torque wrench in the other end. To ensure a good grip for the wrench, the original drill pipe connector and spring were used in combination with an adaptor. The final set up is shown in Figure 13.5



Figure 13.5: Twist off experimental set up.

The test was performed by holding the wrench and by applying an increasing torque to the pipe. The digital torque wrench displayed the value where the pipe failed and represents the twist off strength in this experiment.

Results

The twist off test was performed on the aluminum 7075-T6 drill pipe. To ensure that the results are consistent, three different pipes were tested until failure. Table 13.4 summarizes the results and shows that the twist off occurs at around 50 Nm for all pipes.

Table 13.4: Drill pipe twist off test results

Pipe number	Failure (Y/N)	Twist off value (Nm)
1	Yes	49.8
2	Yes	50.1
3	Yes	49.9

Figure 13.6 shows one of the pipes after failure. All the failures happened close to where the pipe was attached to the lathe, which indicates that this is the weakest point along the drill pipe.

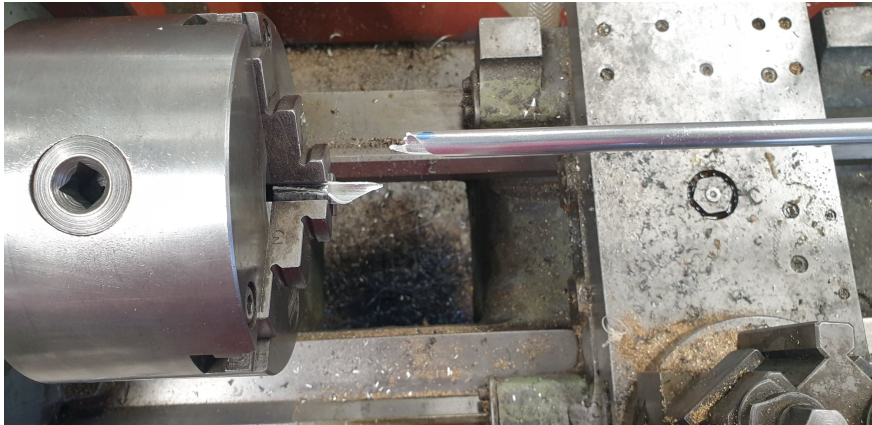


Figure 13.6: Drill pipe twist off.

Sources of Error and Interpretation

The test was performed without using the drilling rig which leads to sources of error and uncertainty in the results. When drilling using the rig, the drill pipe gets support from the stabilizer located on the drill floor. In the test conducted in the workshop there was no support at all. In addition, the person that used the wrench was not able to maintain the drill pipe 100% aligned throughout the experiment. This may have influenced the twist off value. Furthermore, the test did not include either rod nor any drilling fluid that may have affected the results. However, the test showed that the drill pipe can withstand an applied torque of almost 50 Nm, which is a lot higher than what will occur during drilling operations with the rig. The drill pipe will not experience more than 10 Nm during drilling, which yields a safety factor of almost 5 against twist off.

13.2.3 Rod Twist Off

A similar test as for the drill pipe was performed on the titanium rod. The main purpose of the test was to determine how much torque can be applied before the rod fails.

Experimental Set Up and Execution

The test was executed in the workshop by attaching the rod in a vice in one end and having the digital torque wrench in the other end. To connect the wrench, a drill chuck was used similar to the one on the physical rig. In addition, multiple adaptors were connected between the drill chuck and wrench. Once everything was set up as shown in Figure 13.7, more and more torque was manually applied to the rod.



Figure 13.7: Rod twist off test set up.

Results

The test was conducted on three different rods. Since the rod slipped in the vice it was not possible to run the test until the rod failed. Table 13.5 shows that only around 6 Nm was applied to all the rods before they started to slip.

Table 13.5: Rod twist off test results

Rod number	Failure (Y/N)	Applied torque (Nm)
1	No	5.8
2	No	6.1
3	No	6.3

Sources of Error and Interpretation

It was not possible to get any specific twist off value from the experiment. It was not optimal to use so many adaptors in the wrench connection as this may have lead to some momentum disappearing. This may have caused uncertainties in the digital wrench measurements. Although no twist off value was determined for the rod, it gave an upper limit of 6 Nm that can be applied by the top drive motor in drilling operations. This value is sufficient as the rig normally operates with 0.5-1 Nm applied to the rod.

13.2.4 Buckling

Buckling occurs when the pipe deforms due to external forces. A static buckling test was performed for the Aluminum 7075-T6 drill pipe with the aim to determine the amount of WOB that can be applied by the system.

Experimental Set Up and Execution

The upper end of the drill pipe was secured to the hydraulic swivel to represents a fixed point, while the lower end was pinned in the upper stabilizer. This corresponds to an unsupported drill pipe length of 0.67 and represents the circumstances where the drill pipe is most prone to buckling.

To provide stability, the bottom of the drill pipe was placed in a previous drilled pilot hole. Next, the hoisting system was lowered at 0.2 cm/min to systematically increase the WOB. Simultaneously, one team member monitored the WOB on the GUI, while another kept an eye on the behaviour of the drill pipe. The experiment was concluded when the drill pipe deforms and a sudden change in WOB is observed.

The large forces exerted under these test conditions could potentially damage the mechanical components and connections in the system. Therefore, only one buckling test was performed.

Results

A rapid decrease in WOB was observed after the system applied 146 kg. This quantity is therefore considered to be the maximum axial force that can be applied to the drill pipe. The deformation of the drill pipe from this test can be seen in Figure 13.8.



Figure 13.8: Buckled drill pipe.

Sources of Error and Interpretation

The buckling test is highly sensitive to drill pipe alignment. The maximum buckling limit is only obtained for a straight pipe that has no deflection along its axis. Any deviations would lead to a reduction in force that can be applied by the system for buckling to occur.

The buckling test was performed under static conditions. This does not represent a true drilling scenario since vibrations and a deviated well path are not considered. A drill pipe performing under realistic conditions would have a lower buckling limit compared to if it were static. A dynamic buckling test could have provided more realistic results for the operational limits, however, it was not performed as it poses a bigger risk to the components on the rig.

Nonetheless, a general indication of how much WOB the drill pipe can tolerate was obtained. The team only plans to operate the drilling rig with a WOB of 5-30 kg and buckling of drill pipe will therefore not be an issue.

13.3 Rock Sample Testing

The Drillbotics committee will provide a rock sample on the day of competition in June. The exact properties of the rock are unknown beforehand, but it is given that it will be a homogeneous sandstone. The Uniaxial Compressive Strength (UCS) of the rock can be within the range of 15.8 – 36.6 MPa. The extensive testing and qualification of the miniature drilling rig will require several rock samples. For that reason, the team will produce concrete rock samples with an UCS that can be expected in the competition.

To simplify the process by saving thickening time and cement sacks, smaller rock samples will be prepared and then sent for testing of the UCS. The same cement/water ratio can then be used and scaled up when making the real samples that should have dimensions of 30cm x 61cm x 61cm. 2-3 liters of water will be mixed with each 25 kg B20 cement sack. The theory states that the less water that is added, the stronger the sample becomes. This only applies to a lower limit, because at some point the hardening process does not occur properly. For that reason, samples are tested with different water/cement ratios to find the combination that provides the highest UCS with consistent results. The results showed that 3 litres per sack was the most optimum ratio and will therefore be used in the following derivations.

13.3.1 Full Scale Rock Sample Calculations

The bulk volume of the full scale rock sample is given as:

$$V_{block} = Width \cdot Length \cdot Height = 30.48cm \cdot 60.96cm \cdot 60.96cm \approx 0.1133m^3 \quad (13.1)$$

A sack with B20 cement has a mass of 25 kg and a corresponding density of 1750 kg/m³

in the hardened state. Using 3 liters of water, the slurry volume of one sack is found by:

$$V_{mixed\ sack} = M_c + V_w = \frac{25kg}{1750\frac{kg}{m^3}} + 3 \cdot 10^{-3}m^3 \approx 0.017m^3 \quad (13.2)$$

Furthermore, the number of sacks required to fill one rock sample is calculated by:

$$N_{bag} = \frac{V_{block}}{V_{mixed\ sack}} = \frac{0.1133m^3}{0.017m^3} \approx 6.65sacks \quad (13.3)$$

In total, the required amount of dry cement required is:

$$M_{c\ tot} = N_{bag} \cdot M_c = 6.65 \cdot 25kg = 166.25kg \quad (13.4)$$

..

The total water volume required is determined as:

$$V_{w\ tot} = N_{bag} \cdot V_w = 6.65 \cdot 3L = 19.95L \quad (13.5)$$

13.3.2 Test Sample Calculations and Procedure

Nine cylinders were used to prepare concrete samples for UCS testing. The cylinder has a height of 15 cm and radius of 2.25 cm as shown in Figure 13.9.



Figure 13.9: Test cylinder.

The volume of the test cylinder is calculated as follows:

$$V_{cylinder} = \pi \cdot r^2 \cdot h = \pi \cdot 2.25cm^2 \cdot 15cm = 2.39 \cdot 10^{-4}m^3 \quad (13.6)$$

Furthermore, the volume ratio that determines the relationship between the rock sample and the test cylinder is:

$$\frac{V_{cylinder}}{V_{block}} = \frac{2.39 \cdot 10^{-4}m^3}{0.1133m^3} = 2.11 \cdot 10^{-3} \quad (13.7)$$

Taking this ratio into account, the quantities of cement and water that are required to produce a full scale rock sample with the desired properties are calculated by:

$$M_{c \text{ cylinder}} = M_{c \text{ tot}} \cdot 2.11 \cdot 10^{-3} = 166.25 \text{ kg} \cdot 2.11 \cdot 10^{-3} = 351.63 \text{ g} \quad (13.8)$$

$$V_{W \text{ cylinder}} = V_{w \text{ tot}} \cdot 2.11 \cdot 10^{-3} = 19.95 \text{ L} \cdot 2.11 \cdot 10^{-3} = 42.09 \text{ mL} \quad (13.9)$$

As mentioned, the test samples were produced for three different water ratios; 2 L/25kg, 2.5 L/25kg and 3 L/25kg. The above calculations are based on 3 L/25kg and the results of the remaining water ratios will therefore vary.

Before the cylinders were filled with cement, they were lubricated with oil to prevent them from sticking. The slurry for the test samples were prepared using a mixer in the lab as shown in Figure 13.10. The mixing time was set to 10 minutes for each sample to ensure that all particles were mixed properly. The samples hardened for about two days before they could easily be removed.



Figure 13.10: Mixing of cement.

Lab facilities at the institute made it possible to determine the UCS of the various samples. The model of the machine that was used was RTR-4000, where RTR is short for Rapid Triaxial Testing. Before the actual test, a rubber sleeve was heated to seal around the rock sample to protect against any potential flying rock particles. When the rock was inserted properly in the machine, the actual test was performed by applying more and more weight on the sample until it failed. Figure 13.11 shows the machine and the set up used in this experiment.



Figure 13.11: RTR-4000 UCS Experimental set up.

13.3.3 Results

The samples after the UCS experiment are shown in Figure 13.12



Figure 13.12: Test samples after UCS experiment.

The results from the experiment are presented in Table 13.6 and shows that the UCS increases with decreasing water content. However, the results are inconsistent for the rock samples manufactured with a cement/water ratio of 2 L/25 kg. This may be due to the fact that there is not enough water in these samples to successfully consolidated. On the other hand, the results of the remaining 6 samples are more consistent and therefore considered more reliable. As the average UCS that can be expected in the competition is 36.9 MPa, the water/cement ratio that will be used for preparing the rock samples will be 3 L/25 kg.

Table 13.6: Results from UCS test

Number	D [mm]	L [mm]	M [g]	ρ [kg/m ³]	UCS [MPa]	W/C ratio [L/25 kg]
1	44.28	90.66	323.7	2.32	41.2	2
2	44.26	90.66	316.52	2.27	29.9	2
3	44.33	90.65	301.1	2.15	16.5	2
4	44.18	92.16	330.5	2.34	46.7	2.5
5	44.21	92.16	331.01	2.34	43.8	2.5
6	44.19	92.17	329.06	2.33	44.6	2.5
7	44.27	91.91	320.47	2.27	36.9	3
8	44.32	91.67	318.21	2.25	36.5	3
9	44.32	91.63	315.38	2.23	37.2	3

13.4 Diverter Test

The diverter was tested to ensure proper functionality of the semi-closed system. First, it was successfully connected to the lower end of the riser. However, the rock sample could not be inserted before drilling, as the diverter was too tall. As a result, the diverter had to be slightly modified by removing 2 cm from the original height. Afterwards, it was possible to insert the rock without problems. The diverter was lowered down with the manual hoisting system to ensure a proper sealing effect between the rubber seal and rock. A hose which led to the drain was connected to the bell nipple. The system was tested and the water proved to flow in the desired direction without any leakage. The installed diverter and hose is shown in Figure 13.13.



Figure 13.13: Installed diverter.

13.5 Drill Bit Analysis

The team aims to drill as smoothly and efficiently as possible on the competition day. For this to happen, the best available drill bit must be used. The team therefore prepared a series of tests to obtain objective parameters that can be used to rank the drill bits from best to worst. Six drill bits were tested in total. Bit 1 and 2 were manufactured last year, while Bit 3, 4, 5 and 6 were produced this year. In the following sections, the testing procedures and results in regard to drill bit wear, vibrations, hole quality and ROP will be presented. Finally, a concluding discussion to determine the ranking is held.

13.5.1 Testing Description

Five tests were designed to closely replicate the drilling requirements and conditions that the drill bit will be subjected to on the competition day. It was important for the team to drill in both vertical and deviated sections as the competition well trajectory will be composed of these segments. In order to objectively differentiate the performance of the drill bits, the drilling conditions for each test were controlled. This was done by establishing constant parameters such as distance drilled, WOB, top drive velocity and azimuth rotation velocity for each test. Table 13.7 gives an overview of the designed tests along with their respective controlled parameters. The five tests were performed for each available drill bit.

Table 13.7: Five tests for drill bit analysis.

Test	Section	Type of sub	Distance [cm]	WOB [kg]	Top drive velocity [RPM]	Azimuth Velocity [deg/min]
1	Vertical	Straight	30	25	900	0
2	Vertical	Bent	10	11	850	540
3	Deviated	Bent	17	14	850	0
4	Vertical	Bent	10	11	900	540
5	Deviated	Bent	50	14	900	0

13.5.2 Drill Bit Wear

Qualitative Assessment

Drill bit wear is the removal of material from the drill bit's working surface due to its mechanical contact with the rock surface. A drill bit with little wear and a high integrity is desired. To assess the wear, the team first performed a qualitative check on the final state of the drill bits once the testing was completed. Significant wear and damage to the drill bits were not anticipated, since the operations were short and the drill bits were tested under regular drilling conditions that were not viewed as excessively demanding. However, the team recognized that it is normal for some wear to occur due to the mechanical

loads endured while drilling. The initial and final states of the drill bits are shown in Figure 13.14 and 13.15, respectively.



Figure 13.14: State of drill bits before testing.



Figure 13.15: State of drill bits after testing.

From the before and after photos, it is possible to observe that much more wear and damage was experienced by the drill bits than expected. The number of worn cutters and missing inserts after testing are summarized in Table 13.8.

Table 13.8: Qualitative results of drill bit wear.

Drill Bit	1	2	3	4	5	6
Worn Cutters	0	2	0	0	2	4
Missing Inserts	0	0	0	3	2	5

Drill bits 1 and 3 were the only drill bits that did not suffer any unusual wear that could be evidenced visually. Drill bit 2 had two worn cutters, while drill bit 4 lost three inserts during testing. However, drill bits 5 and 6 clearly suffered the most wear, with several cutters worn down and inserts missing. A closer look at the damages of drill bit 5 and 6 are shown in Figure 13.16.

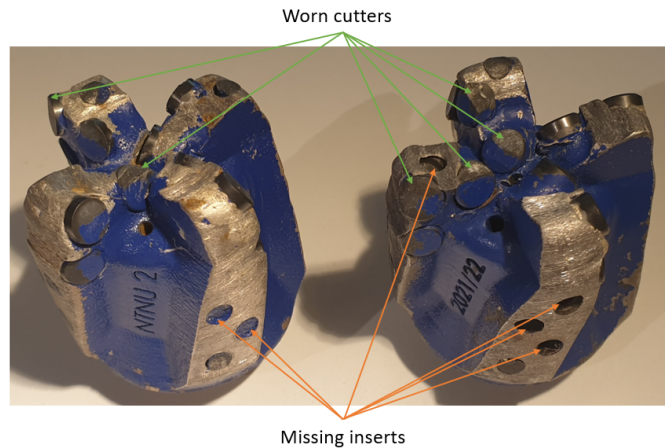


Figure 13.16: Wear and damage of drill bit 5 and 6, respectively.

The findings of drill bits 5 and 6 were extremely surprising to the team for two reasons. Firstly, the solidity of the drill bits were not expected to be compromised to such an extent, due to the short operation time and the moderate drilling conditions. Secondly, these drill bits were specifically redesigned to optimize their integrity and performance. The increased cutter density on the bit shoulders were intended to balance the distribution of forces applied to the individual cutters, and thereby expected to reduce the wear and impact damage.

The team believes that the damage resulting missing inserts is not caused by excessive loads applied outside of the operative range or a poor design of distributing drilling forces, but rather due to poor bit manufacturing. This deduction is supported by the visual inspection of the drill bits before and after testing. Some inserts were already cracked upon arrival, and after testing it was observed that some of the grooves in which the inserts were placed in were not very deep. It is therefore suspected that there may not have been enough space for good bonding between the inserts and drill bits.

Based on the qualitative assessment of the final state of the drill bits, the team arrived to the conclusion that drill bits 1, 3 and 4 have the most wear resistant cutter design. This is a relevant observation, since these three bits have the exact same design, except the cutters shape, which indicates that the sharp and beveled cutters have no direct impact on wear resistance.

Quantitative Assessment

In addition to the qualitative assessment of the drill bits, the team also performed quantitative measurements to evaluate the wear of the drill bits. Drill bit wear corresponds to the material mass lost during operations. For this reason, wear can be quantified by the difference in mass before and after testing. It is however important to note that wear does not present a linear behaviour with respect to operational time but tends to increase with a lower rate until it reaches an asymptotic behaviour. Therefore, the team expected to see more wear among the drill bits manufactured this year. Moreover, a gauge ring was 3D printed as shown in Figure 13.17 and used to determine whether the wear compromised

the drill bits external diameters.

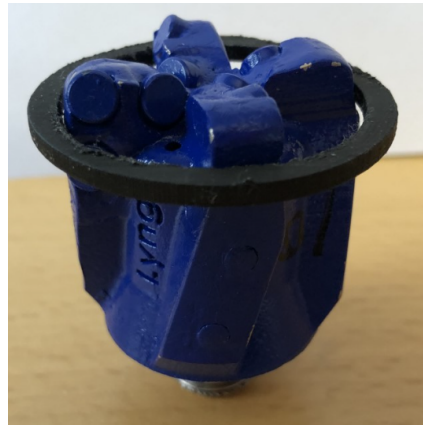


Figure 13.17: Gauge ring.

The results of these assessments are shown in Table 13.9.

Table 13.9: Quantitative results of drill bit wear.

Drill Bit		1	2	3	4	5	6
Initial mass	[g]	216.07	198.33	219.35	196.24	226.07	208.22
Final mass	[g]	213.72	197.48	214.38	191.71	222.25	203.93
Change in mass	[g]	2.35	0.84	4.97	4.53	3.82	4.29
Change in mass	[%]	1.09	0.43	2.27	2.31	1.69	2.06
In gauge	[Yes/No]	Yes	Yes	Yes	Yes	Yes	Yes

The results show that all drill bits have experienced some wear during testing and that their gauge has not been compromised. As anticipated, drill bits 3, 4, 5 and 6, which were new before testing, suffered a larger percentage of wear than drill bits 1 and 2, which have been in operation over the last year. However, the findings of drill bits 3 and 4 experiencing the most wear contradict the qualitative assessment, where drill bits 5 and 6 visibly suffered the most damage. Drill bit 1 has consistent results with being wear resistant and is therefore considered to be the best drill bit in this aspect.

13.5.3 Vibrations

A good drill bit is stable and minimizes the vibrations of the system. When drilling, the vibrations down hole causes the system to shake and create sound that can be measured at surface. Therefore, the team opted to assess noise levels as an indirect measurement of the stability of the available drill bits. This was done using the noise meter app “Decibel X”, which recorded the noise level in decibels at the miniature rig’s drill floor. The results for each test run are summarized in Table 13.10.

Table 13.10: Sound levels of various drill bits.

Test	Unit	Drill Bit						Average
		1	2	3	4	5	6	
1	[dB]	65.5	75.1	67.5	72.5	68.5	73.9	70.5
2	[dB]	73.0	71.1	65.5	67.8	68.4	63.8	68.3
3	[dB]	66.3	64.0	63.3	61.4	61.1	61.8	63.0
4	[dB]	63.2	69.7	70.9	66.1	70.5	66.9	67.9
5	[dB]	60.4	66.7	59.2	62.5	58.5	63.2	61.8
Average	[dB]	65.7	69.3	65.3	66.1	65.4	65.9	

First of all, the results show the average noise level for the various test runs are in the range of 58.5 and 75.1 dB. They are all below 85 dB, which is considered to be the minimum level harmful to the human ear [102]. Drill bit 3 produced the least amount of sound with 65.3 dB and is therefore considered to be the best in regard to bit stability and vibrations. However, drill bits 1, 4, 5 and 6 generated very similar noise levels and are therefore thought to have similar bit stability. This is reasonable considering they are all based off the same drill bit design. Drill bit 2, on the other hand, produced an average noise level of 69.3 dB, which is a sound with double the intensity compared to the other drill bits. Therefore, it is considered to be the worst drill bit in this aspect.

Another interesting finding from these results are the average sound levels for the individual test runs. Drill test 1, which was drilled with the highest WOB, produced the most amount of noise. This was anticipated as more vibrations are expected with higher drilling loads. Drill tests 1 and 2 and drill tests 3 and 4 were drilled with a top drive velocity of 850 and 900 RPM, respectively. Once again, harsher drilling conditions prove to create more vibrations and a higher sound level. The reason for drill tests 2 and 4 producing more noise than drill tests 3 and 5 is because they were used to drill the top hole section to the kick off point, while the latter were drilled further down in the rock sample. Drilling deeper in the rock sample means the decibel sound meter is further from the drill bit and more sound is absorbed by the rock.

13.5.4 Borehole Quality

The team desires a drill bit that produces a stable borehole and maintains its shape and gauge size. Therefore, the borehole quality of each test run is considered for ranking the various drill bits. The team will perform a visual inspection of the borehole after the each run and determine whether it is smooth, moderate or tortuous. A smooth borehole entails a hole that has a flat and even surface. A moderate borehole may have some jerks and indentations while a tortuous borehole has a rough wall and a clear indication of twists and turns. Examples of a smooth and tortuous boreholes are shown in Figure 13.18.



Figure 13.18: Smooth and tortuous borehole quality.

The results of the borehole qualities observed in the various tests are presented in Table 13.11.

Table 13.11: Borehole qualities of various drill bits.

Test	Drill Bit					
	1	2	3	4	5	6
1	Smooth	Smooth	Smooth	Smooth	Smooth	Smooth
2	Moderate	Moderate	Moderate	Moderate	Moderate	Moderate
3	Smooth	Smooth	Smooth	Smooth	Smooth	Smooth
4	Moderate	Moderate	Moderate	Moderate	Smooth	Moderate
5	Smooth	Smooth	Smooth	Smooth	Smooth	Smooth

The results show the borehole qualities for the various drill bits are almost identical. Test runs 1, 3 and 5 all produced great borehole qualities with smooth and even surfaces. Test runs 2 and 4 were on the other hand slightly compromised as faint spirals were observed on the walls of the borehole. These findings were coherent with the team's expectations, as test runs 2 and 4 were drilled using the azimuth system which entailed drilling in an eccentric manner to create a straight but larger borehole diameter. Overall, this assessment was not particularly useful in distinguishing between the performance of the various drill bits, and the team has concluded that this characteristic will not be used for the final ranking of the drill bits.

13.5.5 Rate of Penetration

The drill rate is a measure of how fast the drill bit can cut through the formation and is an indication of the drill bit's efficiency. A drill bit with a high ROP is therefore desired. The team evaluated this parameter by measuring the distance drilled and timing the length of each test run. The ROP is then calculated by dividing the distance by time. The result of each test run is shown in Table 13.12.

Table 13.12: Rate of penetration of various drill bits.

Test	Unit	Drill Bit						Average
		1	2	3	4	5	6	
1	[cm/min]	3.28	3.58	3.74	3.81	3.90	3.67	3.66
2	[cm/min]	2.65	2.22	0.59	1.08	2.54	1.75	1.81
3	[cm/min]	0.84	0.81	1.85	1.53	2.21	1.60	1.47
4	[cm/min]	1.95	1.73	3.85	3.49	4.17	2.65	2.97
5	[cm/min]	3.04	0.86	2.69	2.93	2.86	2.33	2.45
Average	[cm/min]	2.35	1.84	2.54	2.57	3.14	2.40	

Based on the results, it is clear that the design for drill bit 2 presents the poorest performance in rate of penetration, while design for bit 5 shows the best performance of all. It is apparent that the cutter geometry does not affect the drilling performance to a great extent. This can be stated since drill bit 1, 3 and 4 have the same design except for the cutter shape, but the three bits performed similarly in terms of ROP. At last, it is interesting to observe that, even though drill bit 5 and 6 have the same design, they showed a 24% difference in ROP between them. The only real difference between these two bits is that drill bit 6 has beveled cutters, while drill bit 5 has a mix of sharp and beveled cutters. Nevertheless, since these two bits endured more damage than the others, further research and testing are necessary to draw a conclusive statement regarding their performance.

Another relevant aspect is the average ROP for each test run. Test 1 had the highest ROP, given that during this test a straight hole was drilled with the highest WOB. Test 2 and 4 which were used to drill straight sections showed a higher ROP than the deviated sections drilled in test runs 3 and 5. This is caused by the fact that in deviated sections, the drill string has a bigger surface contact with the walls of the well. This causes that some of the WOB applied from surface to be dissipated in friction around the borehole. It is also evident that the top drive RPM affects the ROP. Tests 4 and 5 were drilled with 900 RPM and resulted in a larger ROP than tests 2 and 3, which only used 850 RPM.

13.5.6 Overall Performance and Ranking

The team performed several tests and looked at a number of factors to differentiate and rank the various drill bits. Since the hole quality assessment provided almost identical results for the different drill bits, it will not give valuable input into determining the best drill bit and is therefore not considered. Similarly, the results for the analysis of vibrations were fairly similar for all the bits, except for drill bit 2, which presented clear signs of higher vibrations, proving it to be the worst option regarding this parameter.

The qualitative and quantitative results of drill bit wear were not very consistent. Only drill bit 1 gave consistent results of having little wear and is therefore considered to be the best in this aspect. It was also concluded that the damage suffered by the bits during

the experiment were not caused by an incorrect design or low bit resistance, but due to a poor manufacturing. For this reason, this parameter will not be the main factor to differ between the bits, but will be used to remove drill bits 5 and 6 as possible options, since they presented the greatest damage.

Finally, the key parameter relevant and consistent enough to rank the drill bits and select the best one is the ROP. Following these results, it is once again evident that the only bit that does not have a suitable performance is drill bit 2. This is therefore considered as the worst drill bit. Although, drill bit 5 and 6 have a high ROP, they endured a lot of damage and are not reliable. Drill bits number 1, 3 and 4 have similar ROPs and perform in such consistent way, that any of them can be used to drill efficiently on the competition day.

13.6 Drill Bit Vibration Observation

On the day of the competition, the first inch of the hole is required to be drilled with a pilot hole of 2". Based on this, the first part of all the wells in this project has been drilled with a pilot hole bit from Alibaba as seen in Figure 13.19.



Figure 13.19: Alibaba pilot hole bit.

During the test phase, it was observed that this bit led to much greater vibrations compared to the self-designed bits from Lyng Drilling. Measurements were therefore performed to illustrate the difference in vibrations between the different bits. By measuring the gravitational acceleration using the accelerometer in the sensor card, this can be used to determine the order of magnitude of the vibrations present during drilling. Figure 13.20 and 13.21 show measurements of the gravitational acceleration for the Alibaba bit and Lyng bit, respectively. The results show that there is a greater amplitude and span in the measurements for the Alibaba bit, compared to the Lyng bit. These results reinforce the physical observation that the Alibaba causes higher vibrations. These vibrations lead to a poor hole quality and wear on mechanical components on the rig. The positive side of

these findings is that the pilot hole bite from Alibaba is only used for a very small part of the well. The bit from Lyng, on the other hand, has much less vibrations which is good as most of the well is drilled with this type of drill bit.

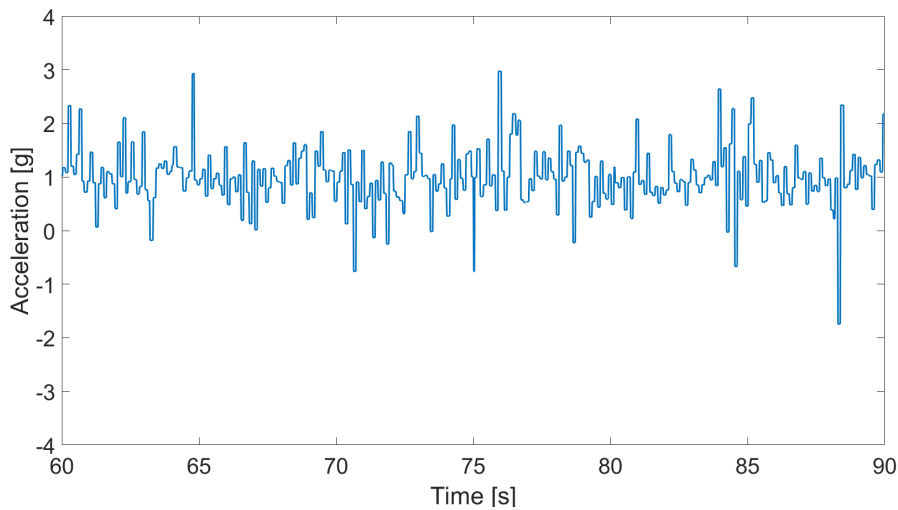


Figure 13.20: Accelerometer noise with Alibaba pilot hole bit.

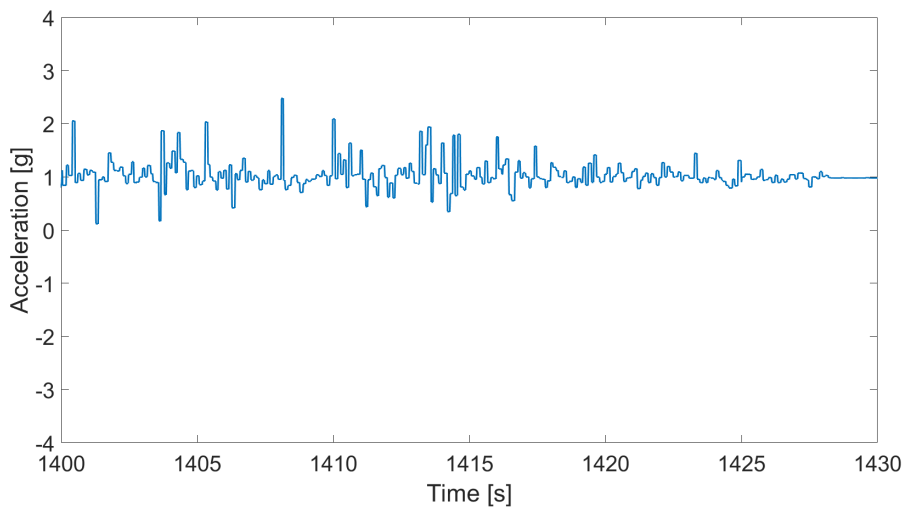


Figure 13.21: Accelerometer noise with Lyng bit.

13.7 Drilling Optimization Tests

Optimal drilling parameters need to be established for the miniature rig to carry out efficient autonomous operations. Therefore, the team has prepared several tests to determine the ideal WOB, top drive velocity and azimuth rotational velocity to be used during drilling. The findings will be based on an evaluation of the torque, ROP and MSE for each run. The torque experienced by the rod should be minimized to avoid fatigue and twist off failure. The ROP must be sufficient to complete the well within the 3 hour time constraint, and the MSE should be kept at a minimum to reduce the overall energy

consumption of the rig. In the following sections, the optimization tests will be described in further detail and the optimal drilling parameters for both the vertical and deviated section of the well trajectory will be presented.

13.7.1 Testing Description

The team has in total designed 18 different tests with the aim to determine the optimal drilling parameters. The tests are planned with the competition requirements and conditions in mind in order to replicate the competition run as closely as possible. The ideal WOB, top drive velocity and azimuth rotation velocity for both the vertical and deviated section have to be determined as these are the operational input parameters controlled by the team in the autonomous system. Only one parameter can be altered for each test run while the other two have to remain constant, in order to analyse the parameters individually. The chosen set points for the different tests are selected based on drilling experiences from previous years.

The 12 tests designed for the vertical section are presented in Table 13.13. The parameters shown will be used to drill a 10 cm hole from the origin to the kick off point using a bent sub with continuous azimuth rotation.

Table 13.13: Drilling optimization tests for the vertical section.

Test	WOB kg	Top Drive Speed RPM	Azimuth Rotation deg/min
1	8	900	540
2	8	900	720
3	8	1100	540
4	8	1100	720
5	11	900	540
6	11	900	720
7	11	1100	540
8	11	1100	720
9	14	900	540
10	14	900	720
11	14	1100	540
12	14	1100	720

Table 13.14 shows the 6 tests planned for the deviated section. This segment consists of a 50 cm controlled well trajectory from the kick off point to the bottom of the rock sample. Unfortunately, the control system's NMPC was not functioning at the time the tests were performed and the optimal azimuth rotational velocity for this section could not be analysed.

Table 13.14: Drilling optimization tests for the deviated section.

Test	WOB	Top Drive Speed
	kg	RPM
1	15	900
2	15	1100
3	20	900
4	20	1100
5	25	900
6	25	1100

13.7.2 Optimal Parameters for Vertical Drilling

The results of the vertical drilling tests are presented in Table 13.15.

Table 13.15: Results of the drilling optimization tests for the vertical section.

Test	WOB kg	Top Drive Speed RPM	Torque Nm	ROP cm/min	MSE MPa	Excess Energy Used %
1	8	900	0.23	2.05	55.46	49.89
3	8	1100	0.24	2.33	62.86	69.89
5	11	900	0.24	1.87	64.95	75.54
7	11	1100	0.25	2.33	64.71	74.90
9	14	900	0.26	2.35	55.08	48.86
11	14	1100	0.27	3.17	52.28	41.31

As displayed, only 6 out of the 12 tests were completed. The reason being that the miniature drilling rig did not function well with an azimuth rotation velocity of 720 deg/min. It produced a lot of vibrations and concerning noise which the team was not confident proceeding with. Since, drilling vertically with an azimuth rotation velocity of 540 deg/min has been satisfactory both in terms of vibrations and hole quality, the team chose to regard this as the ideal quantity for this parameter and only continue testing under these conditions. Hence, the only optimal parameters left to determine for the vertical section are the WOB and top drive velocity.

The average torque experienced by the rod was obtained from the recorded data of each test. The results show a clear trend of the torque increasing marginally with an increasing WOB and top drive velocity. However, the findings are insignificant in determining the ideal operational parameters as the changes are so small. Nevertheless, a torque of 0.23-0.27 Nm is well below the 9.55 Nm twist off torque, which deems all the tested parameters to be suitable for the operation.

The ROP for each test was attained by taking the average of the instantaneous ROP measurements recorded by the control system. The results for the different tests varied

between 1.87 and 3.17 cm/min, which are all above the minimum ROP of 0.51 cm/min that is required to complete the well trajectory within the given competition time constraint. Similar to the torque findings, this means that all the assessed parameters are satisfactory for the operation. Furthermore, Table 13.15 shows a clear trend of an increasing ROP with an increasing top drive velocity but no clear relationship between the ROP and WOB. The highest ROP is typically desired for most efficient drilling and this was obtained while drilling with a 1100 RPM top drive velocity and a 14 kg WOB. However, since the miniature rig experienced substantial vibrations while drilling with a 14 kg WOB, the team chose to sacrifice some drilling efficiency towards rig stability. Therefore, the optimal parameters were based on tests 1, 3, 5 and 7. The largest ROP among these results was 2.33 cm/min and was obtained while drilling with both 8 kg and 1100 RPM, and 11 kg and 1100 RPM.

The MSE is used to assess the drilling efficiency and was calculated using Equation 6.48 for each test. As stated in Section 6.6, the optimal quantity of the MSE should coincide with the UCS of the rock drilled. Since the team prepared rock samples with a UCS of 37 MPa, the optimal parameters are those which utilize a MSE close to this value during drilling. To better understand the results obtained in Table 13.15, the excess energy used in each test was calculated as follows.

$$\text{Excess Energy Used} = \frac{MSE - 37MPa}{37MPa} \cdot 100 \quad (13.10)$$

The excess energy used varies between 41 and 76%. It was difficult to determine the ideal operational parameters based on these results as there is no apparent relationship between the excess energy used and the top drive velocity or WOB for these tests. However, drilling with a 11 kg WOB clearly required the most energy and will not be considered for efficient drilling. The optimal parameters will therefore be selected in regard to tests 1, 3, 9 and 11.

Based on the analysis performed above, tests 1 and 3 both gave great results in regard to ROP and MSE for efficient drilling. Since the ROP for these tests is well above the minimum required value, the team has chosen to prioritize MSE in determining the ideal drilling parameters. Therefore, drilling the vertical section of the well trajectory with a 8 kg WOB and 900 RPM top drive velocity are considered to give the optimal results.

13.7.3 Optimal Parameters for Deviated Drilling

The results of the deviated drilling tests are presented in Table 13.16. The torque, ROP, MSE and excess energy used are calculated using the same methods as described in the previous subsection.

Table 13.16: Results of the drilling optimization tests for the deviated section.

Test	WOB kg	Top drive speed RPM	Torque Nm	ROP cm/min	MSE MPa	Excess Energy Used %
1	15	900	0.15	1.74	43.39	17.28
2	15	1100	0.15	2.06	43.46	17.45
3	20	900	0.17	2.21	38.92	5.18
4	20	1100	0.17	2.52	39.98	8.04
5	25	900	0.20	2.55	38.58	4.28
6	25	1100	0.19	2.77	42.07	13.70

According to the discoveries, the average torque experienced by the rod is barely affected by the top drive velocity. There is, on the other hand, a clear trend of the torque increasing slightly with an increasing WOB. Typically, the torque should be minimized to avoid rod failure and a lower WOB should be selected. However, since the findings are substantially lower than the twist off limit, the changes caused by the WOB are considered insignificant.

The ROP for the deviated drilling tests are all above the minimum requirement to complete the competition well trajectory. The results also show a clear trend of the ROP increasing with both an increasing top drive velocity and WOB. Since the ROP is to be maximized for most efficient drilling, the optimal parameters will be selected based on tests 4, 5 and 6 which give the highest values.

The MSE for the tests varies between 39 and 43 MPa which corresponds to 4 - 17% excess energy used by the miniature rig. Although there is no clear relationship between the MSE and operational input parameters, the team is satisfied with the results as it shows the rig is drilling very efficiently in the deviated section of the well trajectory without a high dependence on the operational inputs. Tests 3, 4 and 5 performed the best and the ideal drilling parameters will therefore be determined from these.

Based on the analysis performed in this section, tests 4 and 5 both produced great results in regard to ROP and MSE. The optimal parameters for the deviated section are selected as 25 kg WOB and 900 RPM top drive velocity, because test 5 indicated a superior drilling efficiency compared to test 4 based on both ROP and MSE.

13.8 Sensor Card Test and Well Path Verification

Several tests were performed with the aim to compare the planned well trajectory with the sensor output data and the actual drilled well path. To check for consistency, four tests were performed along different axes. Due to similar results, only the data performed along the positive y-axis is presented in this section.

The sensor card is used to estimate the position of the drill bit while drilling. To test the sensor output data, the well had to be drilled with the autonomous system. This is to

avoid noise while allowing the system to take surveys. To easily interpret and compare the results, a well path with a constant build up rate and no azimuth change was chosen. Since the system uses a bent sub with a fixed angle, the well path's final inclination is 30° , which corresponds to a horizontal displacement of 13.59 cm.

The sensor card estimated the final displacement of the well trajectory to be 9.92 cm, as shown in Figure 13.22.

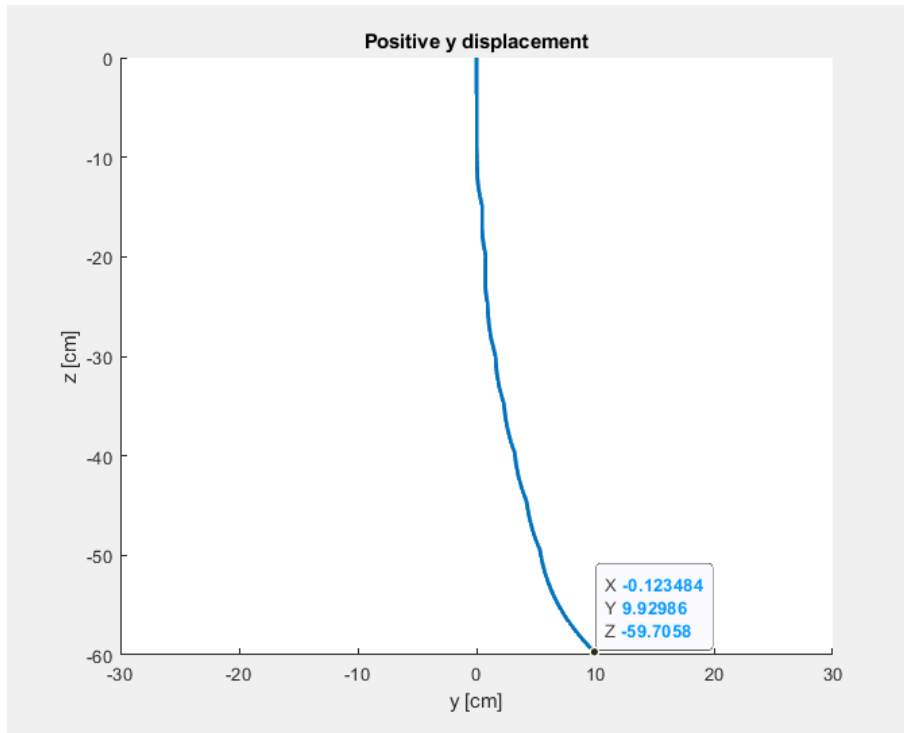


Figure 13.22: Results of sensor card test along positive y-axis.

As the results in Figure 13.22 shows, there is an offset of 3.67 cm between the estimated displacement and the theoretical value of 13.59 cm. To investigate whether this is due to uncertainties in the sensor measurements or mechanical incapacities, a measurement of the actual displacement in the rock was performed.

By tilting the rock sample on the side, the length from the well centre to the edge of the rock was measured both on top and bottom of the well with a measuring tape. By subtracting these lengths, the actual horizontal displacement was found equal to 12.5 cm as shown in Figure 13.23. The result has an offset of 1.09 cm compared to what was calculated theoretically. This means that the system was able to build 28° , which is not considered a significant deviation.



Figure 13.23: Measured horizontal displacement of 12.5 cm when rock sample is tilted on the side.

To conclude, there is a discrepancy between the theoretical calculated displacement, the estimated displacement from the sensor card, and the actual measured displacement in the rock. It is relatively difficult to determine what the reasons for these differences are. Possible causes are sensor card inaccuracy, Kalman filtering leading to accumulation of error that affects the estimation of position, or human error in the measurement process of the horizontal displacement in the rock sample. Overall, the sensor card is considered to provide a good indication of the position of the drill bit. In addition, the actual well trajectory's horizontal displacement was sufficiently close to the theoretical value, and is considered accurate enough for this project.

13.9 Bru21 Conference Demo

NTNU Drillbotics team presented its work at the Bru21 Conference, performing a demonstrative drill test via live-stream. The experience allowed the team to prepare for the Drillbotics competition and ensure the miniature rig functioned as desired. This section will focus on the autonomous test run and discuss the behaviour of the system.

13.9.1 Well Trajectory

The planned well trajectory displayed by the green line in Figure 13.24, was oriented along the positive y -axis and had a final target coordinate of $[x, y, z] = [0, 12.9, 60]$. The red

line exhibits the well drilled by the autonomous system. The sensor estimated the end of the well path to be at $[-0.1, 9.9, 60]$. Overall, the miniature rig followed the planned well trajectory quite well. Small deviations, as seen towards the lower end, were expected due to the uncertainty of the sensor card readings and the inability of the bent sub to drill tangents.

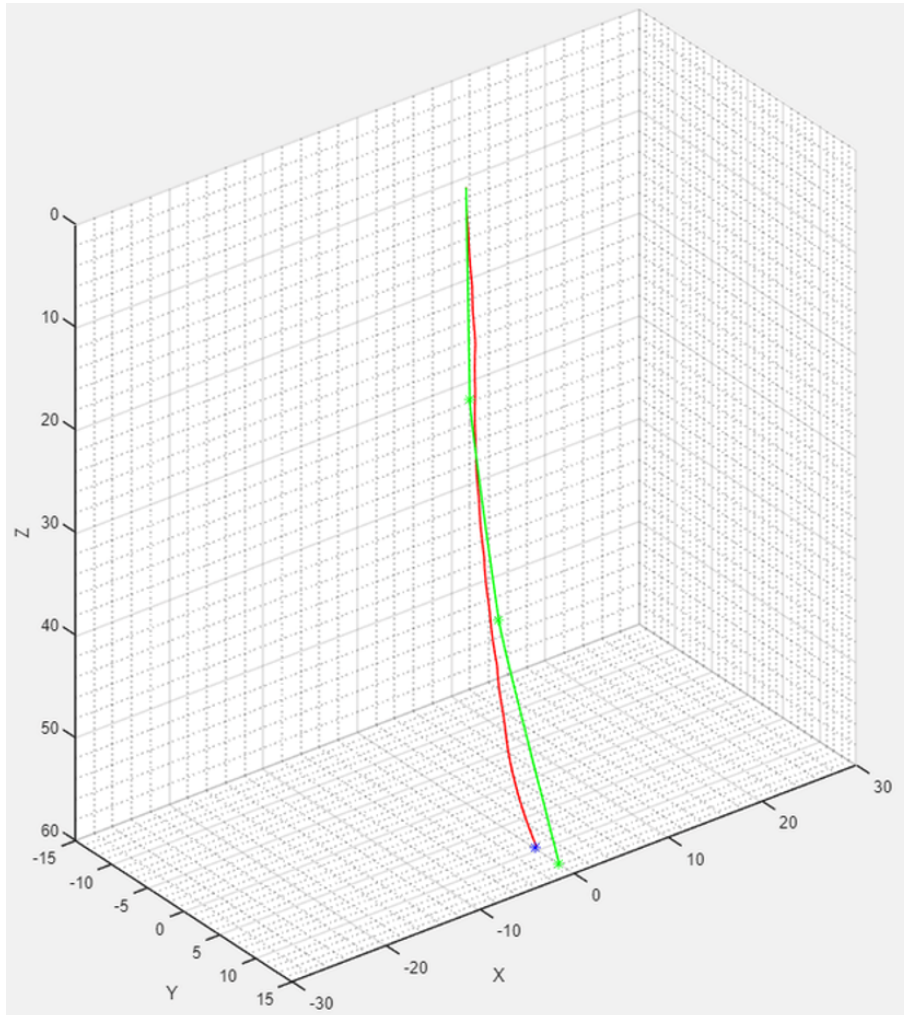


Figure 13.24: Planned and drilled well trajectory.

13.9.2 Autonomous States

The autonomous system consists of 7 states: init, drill vertically, target intersection, drill towards exit, rock exit detection, completed and unexpected termination. Since the last target point is so close to the bottom of the rock sample, the system skipped the drill towards exit state and transitioned directly from target intersection to rock exit detection. The unexpected termination stage was also never reached as there were no problems encountered throughout the run.

The existing states can be observed by examining the trends in parameters such as WOB and ROP. The init, drill vertically and target intersection states are initiated at 0, 140 and

400 seconds, respectively. The rock exit detection state is then reached at 2000 seconds, before the well trajectory is completed at 2085 seconds. The states are differentiated by vertical black lines in Figure 13.25, and will be described in further detail below.

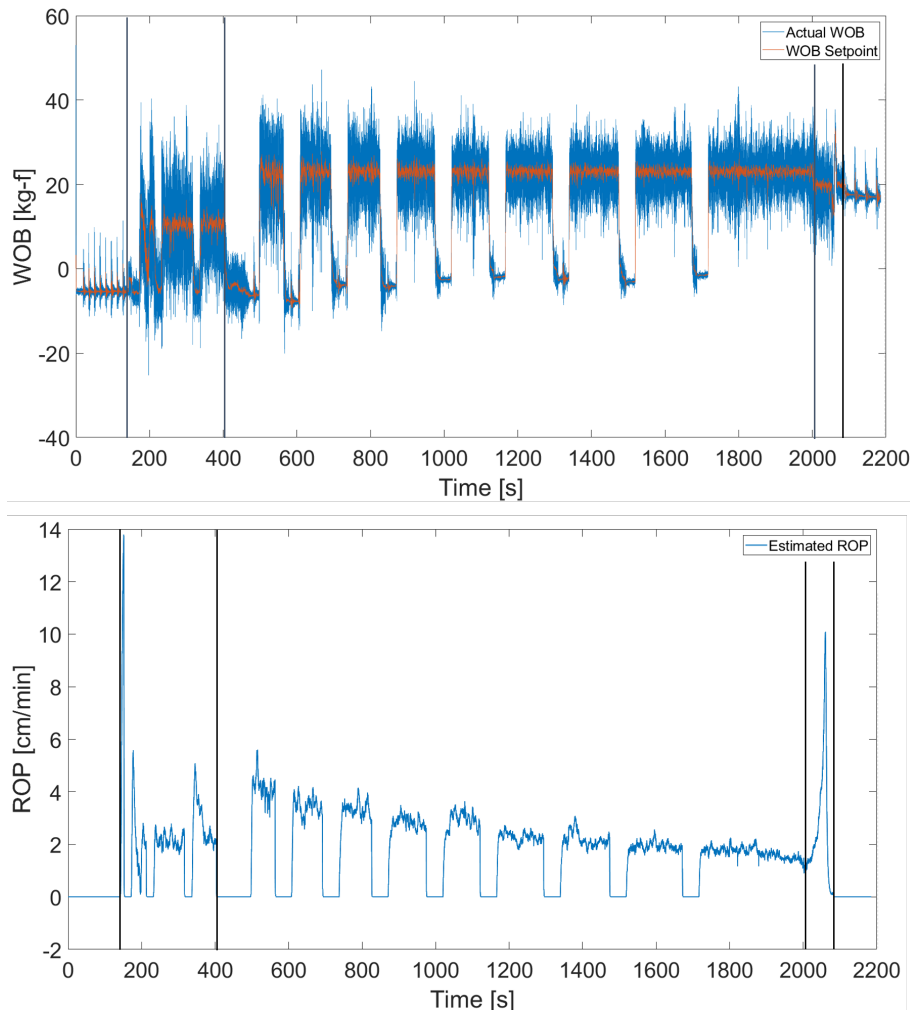


Figure 13.25: Autonomous states differentiated by trends in WOB and ROP.

Init

The autonomous system is in its init state between 0-150 seconds. This implies that all motors are disabled, and the system is ready to be initiated by the user. This state is distinguished by a constant WOB and a ROP equal to zero. The small WOB variations are due to the continuous adjustment performed by the hoisting motor to keep the system still.

Drill Vertically

The vertical drilling state commenced when the driller initiated the autonomous system at 140 seconds. Figures 13.26 - 13.29 show the azimuth rotational velocity, WOB, ROP and rod torque as a function of time for this section, respectively.

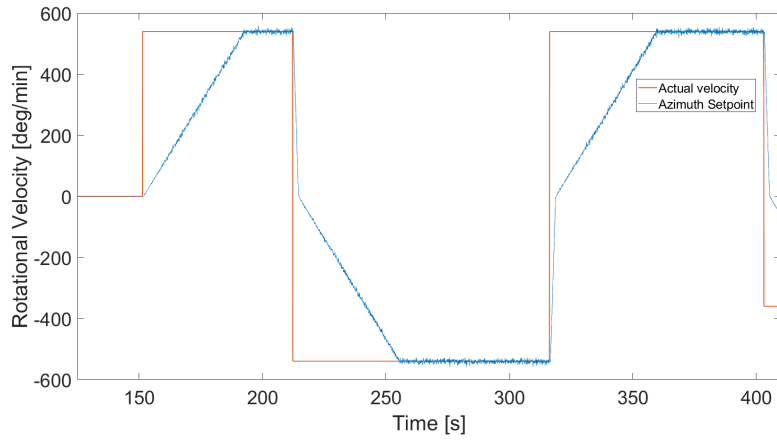


Figure 13.26: Rotational velocity for drill vertical state.

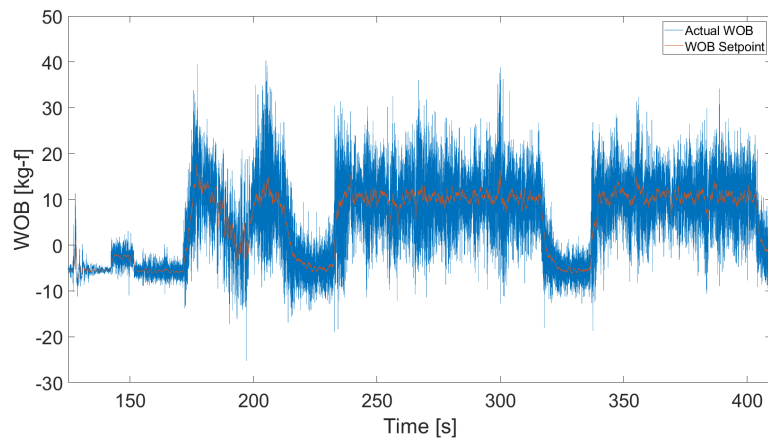


Figure 13.27: WOB for drill vertical state.

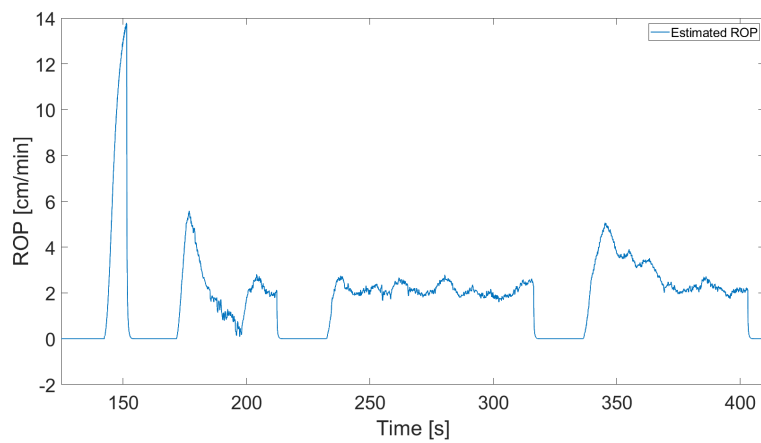


Figure 13.28: ROP for drill vertical state.

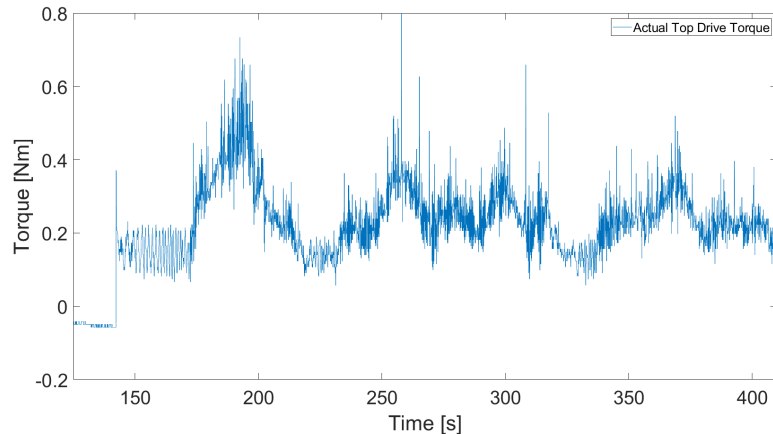


Figure 13.29: Torque for drill vertical state.

The ROP initially increases to 14 cm/min as the drill bit is lowered into the pilot hole. At 150 seconds, the system is exposed to a load, and it recognizes that the bottom of the pilot hole is reached. At this moment, the hoisting motor is disabled, the ROP drops to zero and the azimuth motor begins to accelerate to 540 deg/min. The hoisting motor is only re-enabled once the rotational velocity has reached half its set point. This takes about 20 seconds, and as a result the drilling efficiency is reduced. The team however deems this loss necessary in order to obtain the desired hole quality. Since the top drive motor remains powered as the azimuth system is accelerated, the friction between the drill bit and borehole results in a torque of 0.17 Nm.

After the acceleration, the miniature rig continues drilling the vertical section with an alternating rotational velocity as seen in Figure 13.26. This is crucial to prevent the USB cable from winding around the drill string. When the kick off point is reached at around 400 seconds, the hoisting motor is turned off. The average torque and ROP for the vertical section is around 2.5 Nm and 2.0 cm/min, respectively.

Target Intersection

The autonomous system enters the target intersection state as soon as the kick off point is reached. As seen in Figure 13.30, the system spends the first 50 seconds orienting the BHA towards the first target point. The system overshoot slightly and therefore reversed the rotational velocity at 440 seconds. Before drilling the deviated section, the hoisting and azimuth motor are disabled to take the first survey point at 452 seconds. The motors are stopped to minimize the vibrations and produce precise sensor readings.

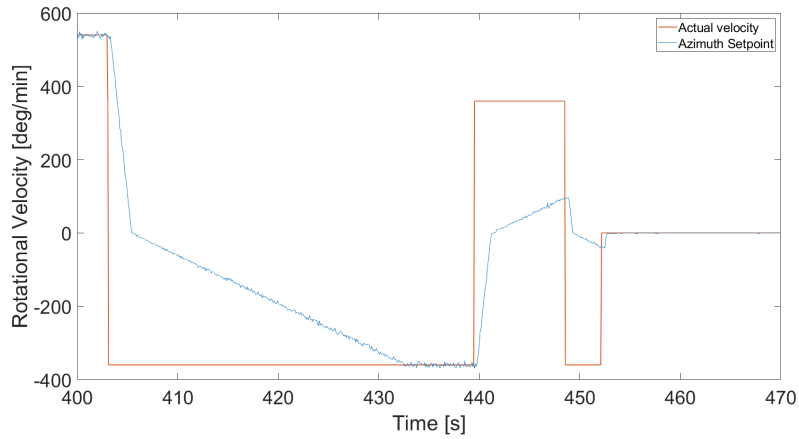


Figure 13.30: Orientation of BHA for target intersection state.

Next, the system attempts to follow the planned well trajectory. The azimuth rotational velocity, WOB, ROP and rod torque for the deviated section are presented in Figures 13.31 - 13.34, respectively.

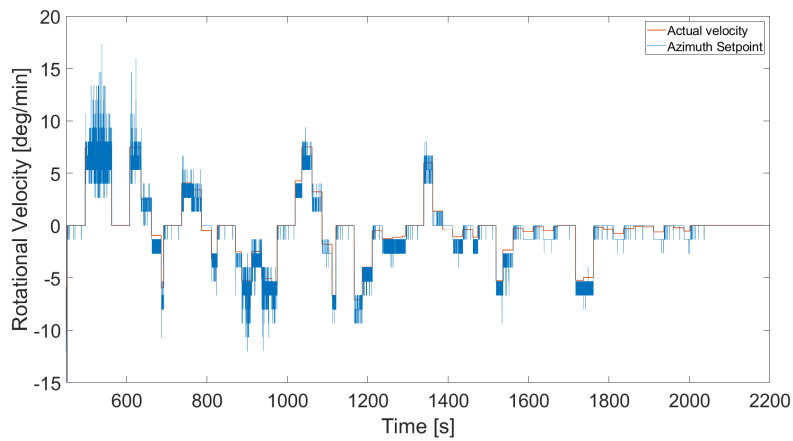


Figure 13.31: Rotational velocity for target intersection state.

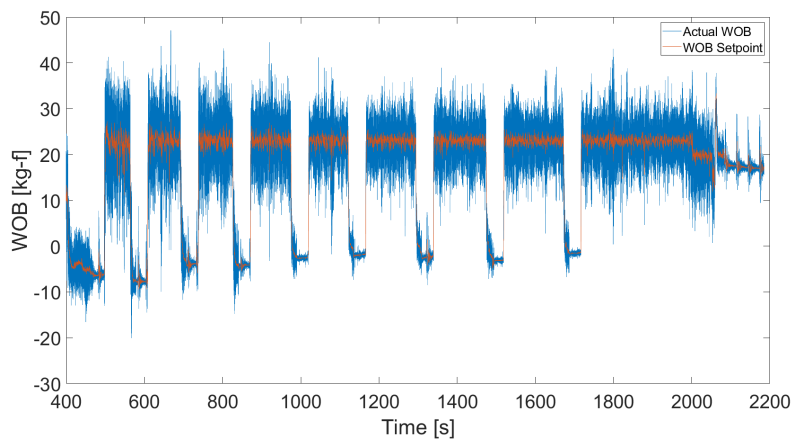


Figure 13.32: WOB for target intersection state.

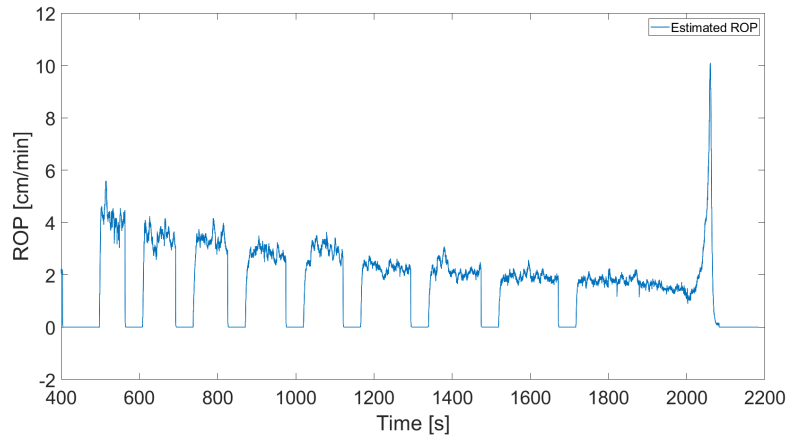


Figure 13.33: ROP for target intersection state.

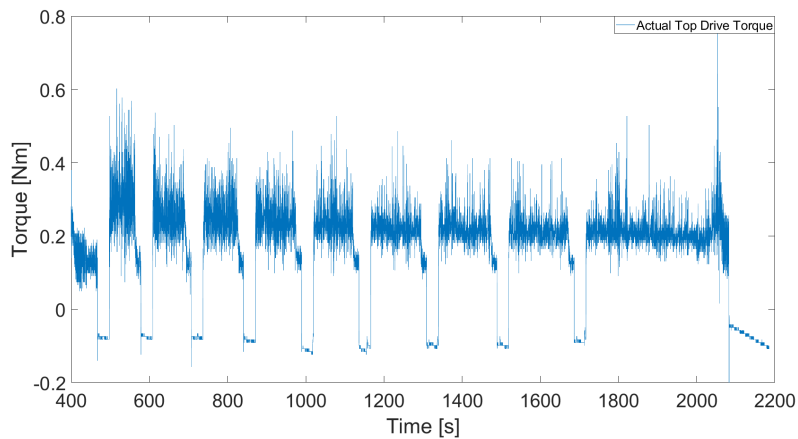


Figure 13.34: Torque for target intersection state.

The graphs show that the system stops drilling for around 45 seconds at 5 cm intervals to perform surveys. The surveys and continuous sensor card readings provide the control system with an estimated position and orientation of the BHA. In return, the NMPC controller gives the azimuth system inputs to follow the reference path and hit the targets. The continuous adjustments made while drilling are shown in Figure 13.31.

The rotational velocity required in the deviated section is considerably lower than the vertical section. It is therefore possible to double the WOB and ROP, and still produce a high quality borehole. However, Figure 13.33 reveals a decreasing trend in ROP. This occurs because the friction forces increase as the drill string descends further into the rock sample. Another reason could be that the rock sample is denser towards the bottom due to some segregation of the cement during the sedimentation process.

Figure 13.34 reveals that the torque remains fairly constant at 0.25 Nm throughout the drilling process.

Rock Exit Detection

As mentioned, the autonomous system transitions directly to the rock exit detection state as the BHA approaches the last target which is situated close to the outer margin of the rock sample. Figure 13.32 shows the initiation of this state at 2000 seconds with a drop in WOB. The WOB is decreased to reduce the ROP and prevent potentially damaging the system by drilling out of the rock sample with a high load.

Figure 13.33 shows an increasing trend of the ROP after 2020 seconds. This indicates that the drill bit has gone from drilling concrete to the rock container made of wood. The system recognizes the increase in ROP and turns off all motors at 2080 seconds.

Completed

Finally, the autonomous system reached the completed state which indicates the well trajectory was drilled successfully. It took the system a total of 34 minutes to transition between all the autonomous states which is well within the time constraint given for the Drillbotics competition.

In conclusion, the drilling demonstration for the BRU21 conference went well and the team is satisfied with the results. The rig proved to be well tuned and is ready for the Drillbitics competition.

Chapter 14

Project Accounting

Project accounting is important due to the complexity of the Drillbotics project and the number of persons involved. A proper overview of the budget is required to keep track of all the necessary costs and to have room unforeseen expenses.

The total expenses associated with the Drillbotics project is limited to US\$ 10 000 by DSATS [90]. However, the competition guidelines state that “in-kind” contributions such as laboratory equipment and supplies do not need to be accounted for in the project costs. Salaries of employees and students must be reported but do not count towards the expenses. This chapter will present the funding distribution, unlisted expenses, wage estimates and incurred costs of the project.

14.1 Funding Distribution

The budget of US\$ 10 000 will be covered by a corporate agreement between NTNU and Equinor. NTNU BRU21 covers US\$ 7500 of the budget, while Equinor covers the remaining part.

14.2 Unlisted Expenses

In-Kind Contributions

In-kind contributions are not incorporated in the final accounts. This comprises all recycled rig components from previous years. In addition, all tools and equipment that are available in the workshop are also considered to be at the team’s free disposal. One example is the production of the diverter, where all the supplies and equipment required were already present in the workshop.

The team also received in-kind contributions from Lyng Drilling. The company produced

and supplied the team with 4 new customized drill bits. Lyng Drilling was also available and in charge of maintenance and intervention of the drill bits throughout the project.

Wage Estimate

The salary costs of the employees and students involved in the project should not be included in the budget. Nevertheless, an estimate of the number of hours spent for those involved was determined. This is to emphasize how much salary expenses contributes to the total cost picture. It is also relevant for the sake of learning outcome and experience.

In total, there are four students who each have their own supervisor. In addition, there are four lab engineers that support the project. The student's workload has been estimated to be around 45 hours a week on average. The supervisors are mainly involved one hour every two weeks to assist the project. The four lab engineers have varying time spent on the project, but are estimated to have spent five hours on average every week per person. To conclude, the total salary estimates for all persons involved in the project is presented in Table 14.1.

Table 14.1: Wage Estimate for students and employees.

	Hours	Weeks	Hourly wage [NOK]	Employees	Total Cost [NOK]
Students	45	18	170	4	550 800
Supervisors	0.5	18	520	4	18 720
Lab Engineers	5	18	370	4	133 200
Total					702 720 NOK US\$ 74 161

14.3 Incurred Costs

All costs that incurred over the duration of the project are presented in Table 14.2. The expenses are given in US\$ as Drillbotics is managed from the US.

Table 14.2: Summary of all expenses related to the Drillbotics project. Exchange rate where 1 USD = 9.71 NOK.

Item	Price per item [\$]	Quantity	Total cost [\$]
Computer	1544.8	1	1544.8
Titanium rod	7.0	50	350.2
3D printer plastic	30.9	2	61.8
Sensor card	26.4	10	263.5
Epoxy sealing	47.9	5	239.5
Polyurethane potting	53.5	1	53.5
Drill chuck	106.4	1	106.4
USB cable	9.2	5	46.0
Cement sacks	6.1	50	303.8
Computer cabinet	126.2	1	126.2
Valves for cabinet	56.6	1	56.6
USB socket for cabinet	136.3	1	136.3
Camera	411.9	1	411.9
Total			US\$ 3 700 35 932 NOK

As Table 14.2 shows, the largest costs in this project are associated with the new computer, rods and camera. The total costs are well below the US\$ 10 000 budget that can be used for competition preparations. This is partly due to many components being recycled from previous and the team receiving “in-kind” contributions. For this reason, it has not become necessary to spend the full budget.

Chapter 15

Challenges and Lessons Learned

Drillbotics is a project that involves challenges in terms of delivery of critical parts, manufacturing of components, and a general risk that equipment can get damaged or not work properly. This means that the team members must be solution-oriented when the challenges arise to be able to have progression in the project. In this chapter, the challenges and lessons learned experienced throughout the project will be presented.

15.1 Project Management

Project management has been a critical issue throughout the semester. Among the factors that majorly impacted the project are the Covid-19 situation, conflicting schedules, critical components and allocation of fixed roles while drilling for optimized situational awareness. These factors will be discussed in further detail.

15.1.1 Covid-19 Impacts

The Covid-19 pandemic has been ongoing since 2020. It has affected the work related to NTNU Drillbotics this year. Some students and personnel fell ill with this virus, which prevented both physical attendance in the meetings and laboratory. This influenced the progress of the project as tasks were delayed. A temporary solution for this issue was to host virtual meetings which allowed for planning and discussions.

Additionally, the Covid-19 situation created large uncertainties in regard to the competition. The competition date, location and acquirement of rock sample were late determined. This created confusion and extra administrative work. The various options were to either have the competition virtually or physically at a location, which demanded different requirements to be fulfilled in an efficient way. The final decision became that the competition will be held virtually at NTNU in Trondheim with judges both present in

the lab and online. Due to DSATS and external suppliers not being able to provide a rock sample, the team had to look for alternative solutions. In the end, a rock sample was manufactured in house.

15.1.2 Lab and Workshop Schedule

As the competition day was approaching, testing and implementation at the lab became top priority. For this reason, the team spent a lot of time in the lab and also worked after office hours and during the weekends. The workshop is closed after normal working hours, which posed some problems when mechanical components were broken and had to be fixed. As a consequence, the project was delayed as drilling operations had to be suspended for several days during weekends or holidays. In order to minimize the impact, the team maximized the time spent in the lab during office hours and acquired back ups for the most critical components so that they could be replaced immediately.

15.1.3 Allocation of Fixed Roles While Drilling

The team identified a major concern related situational awareness in the early phases of rig testing. This finding came after all four members team members were present during a test run. One member acted as the rig operator, while the other three assisted. This situation generated a loss of situational awareness, since there were too many people around the rig with different points of views. As a consequence, unclear messages and orders were given to the operator, which resulted in misunderstandings and poor decisions. All this led to a buckled drill pipe which could have resulted in major consequences to both the operators and the environment.

In the aftermath, the team understood that in order to have an optimal control over the drilling rig, it was necessary to only have one rig operator and one assistant. The assistant helps determine when and how the rig should be operated. Any additional persons present must be completely silent and must not be a direct part of the operation of the rig.

15.2 Rig Alignment

The misalignment of any of the components on the rig can have negative effects on the operation. If the drilling system is not aligned with the upper stabilizer, the weight can induce a buckling event, since the buckling limits are reduced under these circumstances. In addition, the misalignment can severely increase the friction or create a local stuck problem when running the BHA in and out of the riser. For these reasons, rig alignment plays a vital role in guaranteeing efficient and safe drilling operations.

Figure 15.1a demonstrates how the drill pipe is run through the upper stabilizer from

below. It is clear that the alignment is not sufficient since the drill pipe can not be properly connected to the hydraulic swivel without risking damage to the threads. After several adjustments, the drill pipe is aligned and connects perfectly as shown in Figure 15.1b.



(a) Rig not aligned.



(b) Correct rig alignment

Figure 15.1: Rig alignment.

Thin metal plates were used to adjust drilling components to ensure complete rig alignment as shown in Figure 15.2.



Figure 15.2: Alignment plates

This method proved to be simple and effective, as the plates could be quickly rearranged without major interventions to the rig. This was beneficial as the rig had to be realigned on multiple occasions throughout the project, due to vibrations experienced during drilling operations.

15.3 Connection Between Drill Pipe and BHA

The connection between the drill pipe and the BHA is exposed to large forces during drilling. It was experienced that this connection became loose during drilling. This was not discovered until after the actual operation was completed, and it could in worst case have led to damage to the downhole equipment. The biggest consequence during this incident was that the orientation of the bent sub came completely out of control, and it was impossible to know anything about which direction the BHA was moving. Afterwards, the connection was examined more thoroughly, and it was observed that it had worn over time, and that it had to be replaced with a new one. To avoid similar incidents in the future, preventive measures were introduced which involved checking this connection in advance of each drilling session.

15.4 Universal Joint

Several challenges have been related to the universal joint throughout the project. In the following the different problems encountered will be presented.

Bit Sub Connection

From time to time the drilling equipment has to undergo planned maintenance in the workshop. When one of the lab engineers was dismantling the universal joint from the bit sub, the whole connection broke because he had to put so much force to get it loose. The conclusion was that too many wells had been drilled without dismantling the coupling. This happened in the early phase of the project and was not something that the team had thought about before. Producing a new universal joint is a very time consuming process that requires welding. In addition, two operational days can be lost while the engineers work on producing the new part. For these reasons, this incident must be avoided as far as possible. As a risk mitigation measure, it has become a part of the procedure to loosen the universal joint connection to the bit sub prior to each drilling run.

Slipping Rod

A repeating problem while drilling was that the universal joint lost the grip of the rod. The consequence was that neither torque or RPM were transferred from the top drive to the bit. As a solution, the rod was milled down on both sides where the sets screws are connected as shown in Figure 15.3. This will increase the friction and in aftermath it turned out to solve the problem.



Figure 15.3: One of two flat sides marked in red.

Damaged threads

Throughout the project repeated problems were experienced with the two threaded parts in the universal joint. A set screw is screwed into these holes, one on both sides to fasten the rod. The rod has to be changed sometimes due to twist-off incidents. At one point it was impossible to release one of the set screws. As a result of heat and rotation, it turned out that the set screw had been welded completely together with the universal joint so that it was impossible to get out. To avoid this from reoccurring, one of the lab engineers suggested to put copper paste to avoid the welding process to occur. The copper paste that was used is shown in Figure 15.4.



Figure 15.4: Copper paste and set screw.

Furthermore, during the replacement process of the rod, it was discovered that many of the threads have been worn away. As a consequence, it was not possible to insert and tighten the set screw when installing the new rod. To recover the threads, a new steel material was welded on top of the old threads. Then it was possible to create new threads using a special threading tool in the workshop. The result of the universal joint with the new threads is shown in Figure 15.5.



Figure 15.5: New welded threads in the universal joint.

15.5 Wear Plate Improvement

The primary function of the wear plate is to avoid friction between the bit sub and the lower stabilizer during drilling. At one point while drilling in March, more unusual wear was observed compared to earlier experience. Figure 15.6a clearly shows that the wear plate made of peek has been subjected to friction forces as a result of significant rotation against the bit sub. On the other hand, Figure 15.6b shows that a big part of the bit sub is worn away, which is due to the two screws that were used to fasten the wear plate have scratched against and completely destroyed it.



(a) Damaged wear plate after drilling.

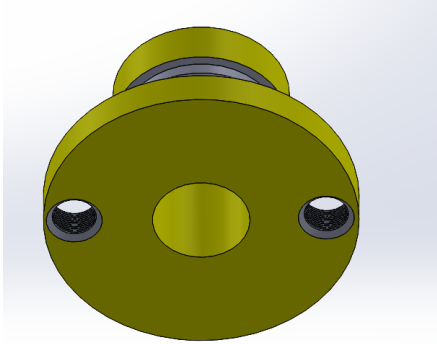


(b) Worn bit sub.

Figure 15.6: Wear on different components.

Several possible solutions to this problem were investigated in the hope of avoiding the same situation in the future. After consulting with the lab engineers, an improved design was created which allowed the two screws to be lowered so that they do not have direct

contact with the bit sub as shown in Figure 15.7. This solution proved to work well and no similar problem have been experienced since the new wear plate was installed.



(a) New wear plate design in Solidworks.



(b) New wear plate installed.

Figure 15.7: Improved wear plate design.

15.6 Leakage in Swivel and Drill Pipe Connection

Through the work with the rig, it has been shown that it can be difficult to connect the drill pipe in the hydraulic swivel and get a full sealing effect. Leakage in the connection point has been observed multiple times. Experience shows that tightening the screw properly has been the solution to the problem. Figure 15.8a shows how the connection point should look like after installation. However, if the connection looks like Figure 15.8b, the installation is wrong and it has to be taken off and reinstalled again. The process has proven to be easier to achieve if the drill pipe is 100% aligned inside the center of the hydraulic swivel.



(a) Correct installed drill pipe.



(b) Drill pipe connection leading to leakage.

Figure 15.8: Drill pipe connected to hydraulic swivel.

15.7 Leakage in T-shaft

The T-shaft was designed to include a safety outlet in case of water migrating up in the T-shaft. While drilling, it was observed that there was water flowing out the outlet as shown in Figure 15.9. After a small period of time, it also started to flow out of the top of the T-shaft. Water should not come out this way because it can damage components of the azimuth system and in worst case lead to short circuit. The reason that this occurred is because the o-ring that sits in the transition between the swivel shaft and the T-shaft had become worn and damaged over time due to the water pressure in the hydraulic swivel.

Fortunately, replacing the o-ring is an easy procedure. The replacement is done by loosening the T-shaft on the top and then unscrewing the nut where the o-ring is located. The old one can then be removed, and a new one can be inserted before the parts are screwed back together. As a preventive measure of this experience, it has become a procedure to change the o-ring every 3 weeks to prevent the leakage from occurring.



Figure 15.9: Water flowing through safety outlet.

15.8 Drill Chuck

The drill chuck from last year proved to be too weak to be used in this year's design. The tool used to tighten the chuck was completely worn down which made it difficult to tighten with proper torque around the rod. Figure 15.10 clearly shows that the tool has a lot of wear and therefore reduced functionality.



Figure 15.10: Worn drill chuck tool.

An attempt was made to procure a new tool, but it was difficult to find the exact size and dimension. Nevertheless, the old chuck still had a certain functionality, and an attempt was made to clean it for grease as shown in Figure 15.11. Furthermore, three sides of the rod were milled down to achieve flat sides. The purpose of trying these measures was to increase the friction around the rod, but it turned out to give only an effect to a certain degree. For that reason, a new drill chuck was acquired as explained in Section 7.5.2.



Figure 15.11: Old drill chuck disassembled for cleaning.

15.9 Rod Twist Off

During testing, the rod twisted off several times. This resulted in the test being interrupted and the intended objectives of the run were not achieved. A twist off incident is shown in Figure 15.12.



Figure 15.12: Rod twist off during drilling.

The team noticed twisting and deformation of the rod occurred after around 7-8 runs. A constant rotation velocity of 900 RPM gives a total of 27000 revolutions in a 30 minute test run. Multiplying this by 8 runs means the rod has endured a total of 217 000 revolutions. This continuous use may have resulted in wear and fatigue which could have decreased the natural twist off resistance substantially. Therefore, as a preventive measure against twist off, the team decided to replace the rod every fifth run.

15.10 Intervention of Drill Bits

As mentioned in Section 13.5, the team was surprised by the amount of wear and damage the newly manufactured drill bits endured during the first drill tests. These issues were discussed with Lyng Drilling and it was concluded that they were challenging to avoid due to the small dimensions. Nevertheless, Lyng Drilling agreed to perform an intervention and restore the drill bits. New inserts were implemented, and the cutters were turned and reattached to provide a new sharp cutter area as shown in Figure 15.13. Overall, the intervention was successful and drill bits kept their integrity for the remaining for project.



Figure 15.13: Drill bit intervention.

15.11 Integration of the Sensor Card in the BHA

Communication with the downhole sensor is crucial when drilling along a well trajectory as it provides the control system with the drill bit's position and orientation. The sensor card is positioned in an open compartment in the BHA sensor housing and is powered by a USB cable which runs through the upper stabilizer as shown in Figure 15.14.

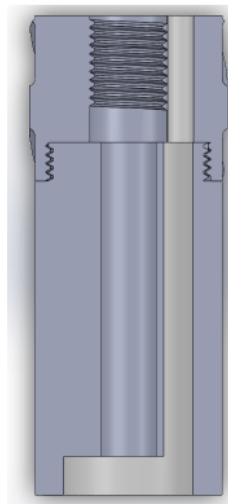


Figure 15.14: Position of the sensor card and cable in the BHA.

To ensure reliable communication with the sensor card, it must be shielded against exposure to mechanical stress, as well as contact with dust, water and the surrounding metal. This proved to be much more difficult than anticipated, and numerous attempts were made without long-lasting success. The sensor card became the bottleneck of the project due to the continuous setbacks and time consuming sealing process that halted further testing of the miniature rig. However, after multiple learnings, the team finally succeeded. This section will present the first integration process, as well as the challenges faced, and

the adjustments made to tackle the issues encountered. Lastly, a back up solution will be presented.

15.11.1 Integration Process

The integration of the sensor card in the BHA is a complicated and demanding process. Following is a description of the steps taken in the first attempt to protect and seal the sensor card.

1. The dimensions of the original sensor card are slightly larger than the compartment of the sensor housing. Therefore, to make it fit, a guillotine cutter was used to reduce the width. This procedure had to be performed carefully to avoid damaging any electrical components on the circuit board. The original and cut sensor card are shown in Figure 15.15.



Figure 15.15: Original and guillotine cut sensor card.

2. The micro USB connector is originally bulky to protect the power and communication wires from breaking during connection and disconnection. However, to attach it to the sensor card and place it inside the BHA, the rubber shielding had to be removed using a carpet knife. This was done with high precision and accuracy to avoid cutting the wires inside the cable. The micro USB connector before and after this procedure is shown in Figure 15.16

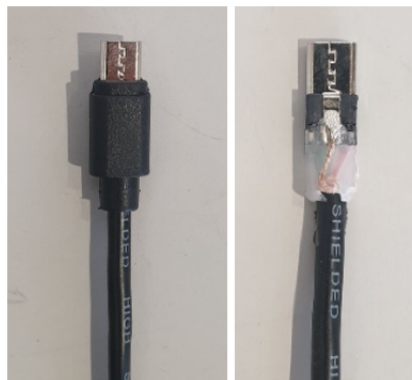


Figure 15.16: Original and carpet knife trimmed cable.

3. Once the sensor card and connector were guaranteed to fit inside the sensor housing, the next challenge became to prevent a short circuit caused by water, dust and the surrounding metal. This was done by coating the coupled components with multiple layers of Plasti Dip. Plasti Dip is a thin rubber coating that can withstand a large temperature range and has flexible, waterproof and electrically insulating attributes. A total of 6 layers were applied with an hour wait between each application.
4. A thin layer of Epoxy was then applied as a second protective barrier as shown in Figure 15.17. The 3M Scotch-Weld DP100 Epoxy is a two-part structural adhesive that attains similar properties as the Plasti Dip. In addition, Epoxy has the benefit of providing a strong and permanent bond to plastics and metals and should be able to maintain its integrity when exposed to vibrations and impact. Since the space in the sensor housing is limited, it was important to keep this layer as thin as possible while still ensuring a proper seal. The epoxy covered sensor card was then left overnight as it required at least 24 hours to cure.



Figure 15.17: Sensor card and cable covered in thin layer of epoxy.

5. Next, the sensor housing and upper stabilizer were screwed together and secured using a set screw. The cable near the USB-A port had to be cut in order to thread the cable through the upper stabilizer. However, before pulling it all the way through, the sensor compartment was filled with some epoxy. This was done to ensure an airtight seal between the cable and upper stabilizer. The sensor card was pushed into the sensor compartment using a flat head screwdriver. It was important to avoid forcing the sensor card too far in as this could potentially damage the micro USB connector.
6. Once the cable and sensor card were inserted, the complete sensor compartment was filled with epoxy using the dispensing gun shown in Figure 15.18. This was done to secure the sensor card in place, create a final waterproof seal and protect it against the mechanical stresses it would be exposed to during drilling operations. Due to the epoxy's high viscosity, it was difficult to determine whether it effectively filled all the void spaces in the compartment. To increase the chances, the epoxy

was made to flow more freely by simultaneously heating the sensor housing with a heating gun.



Figure 15.18: Epoxy dispensing gun.

As an additional precaution against water leakage, an epoxy layer was applied to the upper section of the cable as shown to right in Figure 15.19. Finally, the BHA was left to cure for at least a day.



Figure 15.19: Epoxy sealing the sensor card and USB cable.

7. To restore the power and communication of the sensor card through the USB cable, the cable had to be soldered back together with lead. This is shown in Figure 15.20. Small shrinking tubes were then used to cover all exposed wires and prevent a short circuit. Lastly, a larger sized shrinking tube was applied to hide the soldering and protect the cable.

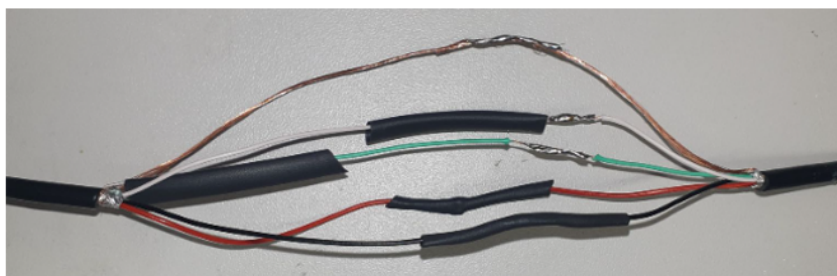


Figure 15.20: Soldered cable with protective shrinking tubes.

8. The waterproof seal was tested by submerging the BHA containing the sensor card and cable connection into a bucket of water as shown in Figure 15.21. After 10

minutes, the USB-A port was plugged into the computer. Power and communication were both established, and the integration process proved to be successful.



Figure 15.21: Water test.

9. Finally, the excess epoxy was drilled out from the centre of the BHA and removed from the threads using a rotating steel brush.
10. The integration process was completed and drilling commenced.

15.11.2 Challenges and Modifications

Due to the challenges faced with the sealing of the sensor card throughout the project, the team had to modify the initial integration procedure many times. A total of 7 attempts were made before the team was successful in producing a strong and long-lasting seal. The problems encountered, the possible causes and the adjustments made are summarized below.

URC coating instead of Plasti Dip

The first challenge the team was faced with was that the sensor card did not fit inside the sensor compartment after applying multiple layers of Plasti Dip. The protective coat became too thick as shown to the left in Figure 15.22. This most likely occurred due to heavy application and spraying the Plasti Dip within a close proximity. Nevertheless, the team was not satisfied with the results and decided to experiment with a new material. URC200D is a sprayable and quick drying urethane coating which attains identical properties to the Plasti Dip. The team was able to produce a much thinner seal on the sensor card as shown to the right in Figure 15.22, which allowed it to fit inside the sensor housing. Therefore, the urethane coating aerosol was favoured over Plasti Dip.



Figure 15.22: Plasti Dip and URC200D coating on sensor card.

PVC electrical tape over the micro USB connection

While performing a drill test, the team observed the USB cable had become pressurized with water and was leaking from the shrinking tube. The sensor card was still able to send and receive data, but all power and transmission stopped the following day. The team believed the communication ceased due to rust in the cable. The water was suspected to have seeped in through a small tear in the micro USB connection, which was caused by incautious trimming of the cable. The main learning from this experience was to be more precise when removing the rubber shield from the connection port. In addition, the connection between the sensor card and cable was secured with PVC electrical tape as shown in Figure 15.23. This was done to create an extra seal from the drilling fluid and ensure a stable connection between the cable and sensor card.

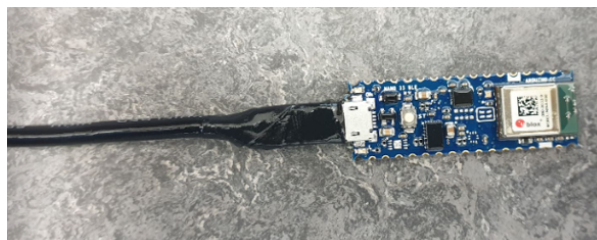


Figure 15.23: Micro USB connection secured with electrical tape.

Tec7 instead of Epoxy

On several occasions, the sensor card suddenly stopped working while drilling. The sensor card was still detectable by the computer, however, it could not receive or send any data. Although the cause is unknown, the team believed that either the data transfer wires in the USB cable were damaged or the sensor card had been exposed to water. After a discussion with the workshop, it was concluded that the epoxy may have developed cracks in the seal due to the loads endured while drilling. Therefore, the team looked for a new sealing alternative.

Tec7 is a strong waterproof adhesive. It is considered to be extremely flexible and should therefore endure the drilling loads better than the Epoxy. In addition, it is less viscous which makes the application process easier and allows the agent to produce a tighter seal. Thus, it was attempted to coat the sensor card and fill the sensor compartment with Tec7. This was done using the dispensing gun shown in Figure 15.24. The BHA was then left overnight to cure.

Unfortunately, the attempt was unsuccessful. Since Tec7 is a one component agent and the layer in the sensor compartment is thick, it was not able to cure and form a strong waterproof seal. The use of Tec7 was therefore discontinued.



Figure 15.24: Sensor card coated with Tec7 using the dispensing gun.

PUR coating instead of Epoxy

After several more unsuccessful attempts using Epoxy, the team was able to recover the seal from the sensor housing as a whole. Several cracks and holes were revealed as shown in Figure 15.25, which allowed direct exposure of water to the sensor card. This confirmed the belief of the epoxy being too viscous to completely fill the void spaces in the compartment.



Figure 15.25: Improperly sealed sensor card with Epoxy.

The team found the less viscous two-part polyurethane (PUR) potting compound shown in Figure 15.26. The agent provides excellent physical protection due to its flexibility

and creates minimum stress on the circuit board. The 2:1 mix ratio was applied to the sensor housing using a syringe and needle, which allowed for more precise application. In addition, the PUR's free flowing properties permitted it to penetrate all the potential paths in the sensor housing and create a strong seal. The potting was then left for 24 hours to cure.



Figure 15.26: Potting Compounds.

Once dry, a layer of epoxy was applied to the bottom of the sensor housing and top of the upper stabilizer as an extra precaution.

The change to PUR coating proved to be successful as the power and communication to the sensor card has functioned since.

15.11.3 Potential Improvement

If the polyurethane coating should fail, the team has already contemplated a further adjustment. Damage as a result of water leakage most likely occurs from inside the BHA due to the water pressure pressing on the seal between the upper stabilizer and sensor housing. To eliminate large pressures, the team has produced a shaft shown in Figure 15.27 which will redirect the water past the sensor housing. This will result in the sensor card only being exposed to hydrostatic pressure which should reduce the risk of water damage.



Figure 15.27: Back up solution.

15.12 Computer and Control System Related Challenges

As there is only one student from Cybernetics involved in this project, one of the petroleum engineers helped the responsible student with issues related to the computers and the control system. These challenges and lessons learned will be documented in the following sections.

15.12.1 Load cell and Hoisting Motor

Problems with the load cell occurred when the drilling tests started in March. The readings from the load cell sensor started to drift and did not converge to a fixed value as it should. This happened especially at static conditions when there was no WOB applied at all. After a time period, the readings drifted towards -10 kg as shown in Figure 15.28. This was of high priority to get fixed because the whole control system and inputs are dependent on the WOB readings from the load cell.

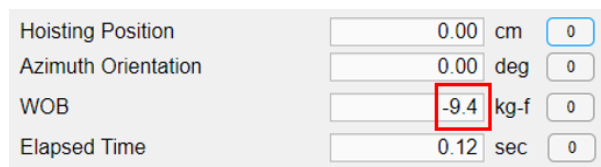


Figure 15.28: Wrong load cell reading when no WOB is applied at static conditions.

The team spent time and effort on trying to fix this problem together with the lab engineers. The load cell was disconnected from the hoisting motor and tested separately from the other systems by applying a known weight to it. After substantial troubleshooting, it was concluded that there was nothing wrong with the load cell itself. For that reason, it was only the hoisting motor that the problem could be caused by. Eventually it was found out that when the hoisting motor was set to be at rest at static conditions, it exerted a force to the system that was captured and detected by the load cell. After consulting with the lab engineers at NTNU, they suggested to contact the supplier of the motor in order to fix the problem. Together with support from Nordic Automation, it was determined that implementation of a hysteresis in the motor software could fix the problem. Fortunately, the implementation led to the load cell providing correct values for the WOB.

15.12.2 Implementation of New Computer

The control system is run on two separate computers. For that reason, User Datagram Protocol (UDP) is used to share data between the two systems [12]. During the implementation of a new computer, it was not possible to receive or process any data from the

other computer. This had major impact on the overall drilling performance of the rig, as the NMPC controller that steers the BHA in the correct direction was not functioning. Large resources were therefore invested in finding the cause of this. After looking through the network settings on the computer, it was discovered that the Windows Firewall was blocking Matlab to receive any data from unknown computers. After whitelisting Matlab in the Windows Firewall settings as shown in Figure 15.29, the communication problem was solved and the computers could transfer data between each other.

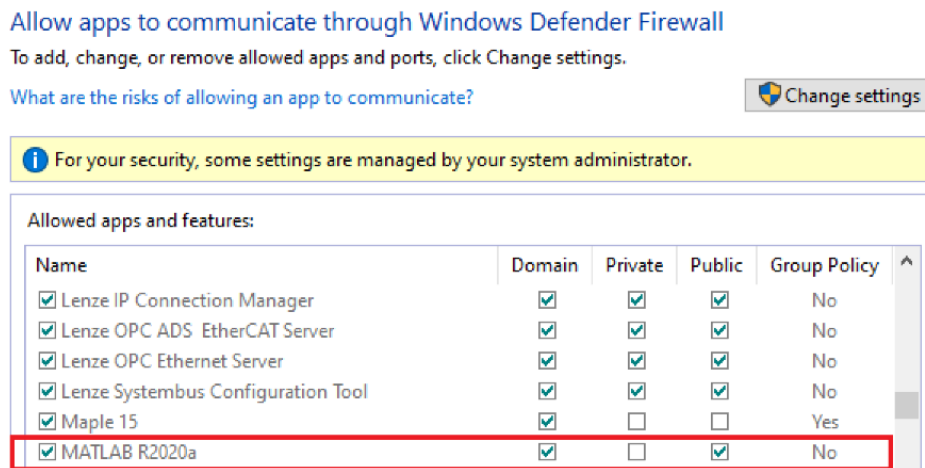


Figure 15.29: How to enable that Matlab can receive data from other devices.

15.12.3 Simulink Data Acquisition Problem

Repeated incidents have occurred where Simulink does not receive data from the downhole sensor. Figure 15.30 shows what the incoming data port looks like when no data is retrieved from the sensor.

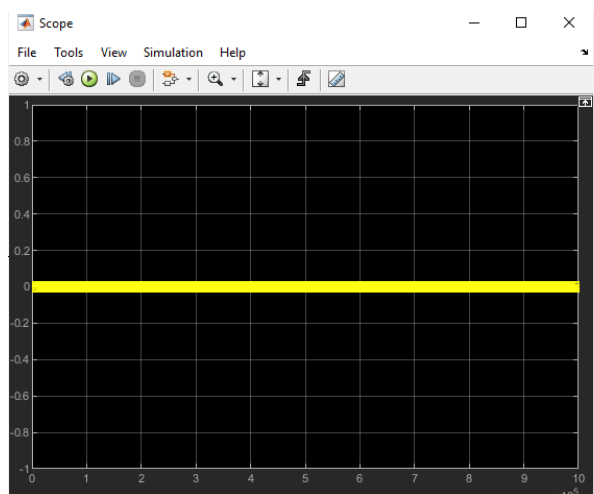


Figure 15.30: No data received by Simulink.

It was difficult to find the reason why this happened randomly. Troubleshooting was

initiated and several possibilities were tested with the aim of correcting the error. After shutting down the power to all electrical components on the rig and resetting the sensor card configurations, Simulink could receive data again. In retrospect, it is difficult to determine whether the error was resolved because of this, or whether it was due to coincidences or a bug in the system. To illustrate, Figure 15.31 shows what the port should look like when Simulink is capable of receiving data.

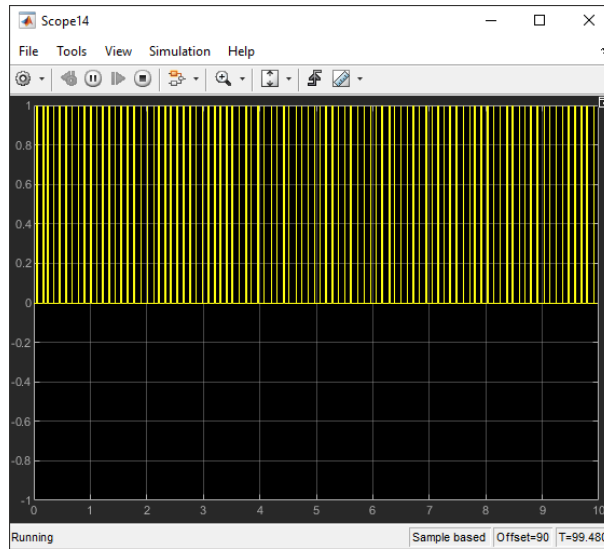


Figure 15.31: Simulink receives data.

Conclusion

This master thesis presents the work performed by three petroleum students in preparations of the Drillbotics 2022 competition. The team completed the objective to successfully drill a deviated well using the autonomous miniature rig. To ensure peak performance, both the mechanical and control system were enhanced and optimized through research, testing and analysis. The central conclusions and outcomes of this project are presented below.

- Working in a multidisciplinary team proved to be beneficial to the project. The team's close collaboration with the supervisors, lab engineers and industry experts contributed to new innovative solutions and perspectives. Experiences with leadership, problem-solving and time management have prepared the team members for further challenges in their upcoming professional careers.
- The focus on human factors and safety was early requested by the Drillbotics jury and has been an important part of the practical lab work with the miniature drilling rig. Through a comprehensive literature study, a greater understanding of the importance of these topics was attained. A safe and secure work environment was achieved by identifying and mitigating potential hazards. Furthermore, the situational awareness of the operators was raised through education, assigning roles and performing bow tie analysis to identify and protect against hazardous events.
- The drilling concept consists of a freely rotating rod inside the drill pipe that transmits rotation to the drill bit. An independently motorized rotary table used in combination with a fixed bent sub is used to steer the bit. The drilling concept has proven to be robust and reliable to comply with the drilling requirements of the competition.
- A new drill chuck was implemented to ensure proper transmission of torque to the drill bit. This solved challenges related to the rod slipping and prevented drilling activities from being interrupted. As a result the NPT was significantly reduced.

- A hydraulic semi-closed system was also implemented to the rig by designing a new diverter, which allowed for controlled disposal of the returns from the well through a hose. This solution improved the overall safety of the rig, by eliminating the risks related to slippery floors in the lab and respiratory problems due to cement particles in the air.
- The control system is in charge of the autonomous operation and steers the bit towards the well path reference using NMPC control. After debugging and further developing the system in Matlab and Simulink, enhanced directional control was achieved. A GUI allows the operator to use the rig in manual mode or in autonomous mode.
- After multiple failed attempts to seal the downhole sensor inside the BHA, proper sensor isolation was achieved. This allowed the team to perform real-time measurements at survey stations during drilling operations and send information to the computer at surface. The data was sent through a USB cable to the control system for further processing and estimation of drill bit position and orientation.
- A new innovative method for well trajectory planning called Dubins Curves was investigated and implemented in the control system. By using this method, an optimized well path with curvature constraints was achieved in function of the fixed bent sub geometry.
- With the goal of achieving a sufficient ROP and steerability, thorough work was put into analysing different drill bit designs. After an evaluation of previous NTNU bit designs, four new proposals were sent for production. An extensive testing regime was carried out, and the most optimal design was determined based on ROP and drill bit wear.
- A total of 62 directional wells were drilled in the testing phase of the project that met the Drillbotics competition objectives. These tests were performed to enhance the control system and optimize the drilling parameters for the competition.

The work performed in this thesis has prepared the team for the Drillbotics 2022 competition in Trondheim on the 16th of June. NTNU will compete against other universities to determine which team has the best autonomous miniature drilling rig.

Future Work

During the preparation stage of the Drillbotics competition, the team conducted both theoretical research and testing of the mechanical rig system. These were performed with the aim of enhancing the drilling system. Regardless of the successful results obtained in this project, there is still room for improvement. For example, some of the ideas tested or reviewed could not be implemented due to different factors, such as time limitations or technological constraints. Therefore, recommendations for future work will be presented in the following section.

17.1 Rock Sample Positioning

When the rock sample is to be placed in the cabinet before drilling, it has at times been difficult to position the block properly. When testing was performed, it is common to drill many wells in the same sample. In order to make the most of the stone, accurate precision is required to obtain optimal positioning. A jack trolley was used for this purpose. It was difficult to position the sample accurately, especially after pilot holes were drilled and the sample had to be taken in and out and placed in the exact same location. In addition, when the wells had to be drilled at the outer edges of the rock, it often conflicts with the manual guide mechanism of the riser. Furthermore, block tends to shift slightly when relieved of the jack trolley due to the uneven surface on the laboratory floor.

A suggested change is that instead of using a jack trolley, a furniture board with brakes can be customized as shown in Figure 17.1. The block can then be placed on top of this, and guided directly into the desired position. To prevent the board from moving due to vibrations endured while drilling, the rock sample and board can be fixed to the floor with straps or similar mechanisms.



Figure 17.1: Furniture board for rock positioning [50].

17.2 Protective Glass

The rig has a sliding protective glass that encloses the drilling system containing rotating components. This used to protect the personnel from possible projectiles. The cover must be lifted for maintenance and intervention of the drilling components.

The main problem with this protective glass is that it is very heavy and needs to be lifted approximately 2 meters above the floor by one person while another locks it in place with two prisoner screws. This is a demanding and tedious process which can lead to injuries if not performed correctly.

As a solution, the team proposes to introduce a counter weight and implement a self locking mechanism. This would prevent ergonomic injuries related to lifting and potential dangers a falling cabinet if the prisoner screws are not inserted properly.

17.3 BHA Back Up

As discussed in Section 15.11, the principal bottle neck that caused several drawbacks and loss of time to the team was the sealing of the sensor card in the BHA. This did not only restrict the sensor in providing downhole measurements, but it also prevented manual testing of the mechanical system since the upper stabilizer and sensor housing are needed for a functional BHA.

The team recommends to manufacture a dummy for the upper stabilizer and sensor housing with the same dimensions as the original ones. This will make it possible to perform mechanical tests of the system that are not dependent on sensor card measurements. In this way, progress can be ensured on the drilling front while waiting for the sensor card to be sealed.

The ideal solution would be to produce a back up which would allow for testing of the autonomous system with sensor card readings.

17.4 Length of BHA

The team believes there is an opportunity to improve the steerability of the system by reducing the current length of the BHA. A shorter BHA would reduce the friction while drilling and allow the system to take sharper turns. This would provide better directional control. In addition, an improved hole quality could be expected.

A solution to reduce the length of the BHA is to eliminate one coupling point by re-designing the upper stabilizer and sensor housing into one single piece. In addition, a smaller sensor card can be obtained, to potentially further reduce the length of the sensor housing.

17.5 Stabilizer Gauge

The upper and lower stabilizers mechanically stabilize the BHA. They are used to prevent large drill string vibrations, avoid unexpected sidetracking and create a smooth borehole. For the best results, the stabilizers should have a diameter equal to the drill bit. However, both the upper and lower stabilizers have been exposed to wear throughout the project, and they are no longer in gauge. It is therefore recommended to produce new stabilizers with the appropriate diameter to ensure the maximum stability while drilling.

17.6 Sensor Card Size

As mentioned in Section 15.11, the downhole sensor card integration process proved to be very challenging. It was difficult to fit and successfully seal the large sensor card in the sensor house compartment without losing communication and power transmission. Therefore, it is encouraged to find and use a smaller sensor card, which will allow a simpler application and more effective sealing.

17.7 Pilot Hole Bit

Consideration should be given to acquiring a new pilot hole bit to drill the first inch of each well. The drill bit from Alibaba causes a lot of unwanted vibrations that over time can have impact on mechanical parts of the system as explained in Section 13.6. A future team is therefore encouraged to design and produce a new 2" drill bit that can be used for this purpose. It is recommended to contact Lyng Drilling for advice regarding a potential new design of a pilot hole bit. By doing this, the pilot hole quality will most likely be improved significantly, and excessive vibrations are avoided.

17.8 Wireless Communication with Downhole Sensor

The current design uses a USB cable to transfer data from the downhole sensor to the computer at surface. As discussed in Section 7.9, several wireless alternatives were explored, but did not prove to be feasible due to the density of the rock and sensor card dimensions. The team suggest future teams to conduct further research on this aspect as wireless communication would be a beneficial contribution to the system. It would enhance the drilling capabilities as straight sections can be drilled without being restricted by a cable downhole.

17.9 Magnetometer Development

As stated in Chapter 11, it was not possible to obtain reliable measurements from the magnetometer in the sensor card. This implied that azimuth could not be estimated with the magnetometer, which led to uncertainty in the position estimate of the drill bit. Future teams are therefore advised to look into the possibilities of using other types of magnetometers and technologies to determine the azimuth. This will most likely increase the estimation of the position of the bit considerably. Several opportunities are suggested in the following sections.

17.9.1 Fluxgate Magnetometer

The current magnetometer used in the current sensor card is based on the Hall effect. However, there are different types of magnetometers on the market that can be used as an alternative.

For example, Fluxgate is one type of magnetometer that was suggested by the experts consulted in this project, and is worth investigating. It is one of the oldest magnetometers available. In simple terms it is based the principle of magnetically saturating a permeable core in alternating directions. This can be achieved by exciting a coil or a ring in square or sine waveform. Since the ambient magnetic field is present before the excitation of the core, a flux with a constant direction will be present. This will collapse under the excitation stages and recover once the excitation is removed. These fluctuations can be detected by the induced voltage in the Fluxgate magnetometer [101].

If a Fluxgate magnetometer is introduced, it is expected to gain accurate sensor readings.

17.9.2 Artificial Magnetic Pulses

Given the high influence that the surroundings of the magnetometer can have on its readings, it is almost impossible to shield them from magnetic disturbances while operating in

the current drilling conditions. The metal rig frame, drilling components and rock itself can be magnetized or have residual magnetism. This creates uneven disturbances in the measurements that are difficult to filter out, even after calibration of the sensor card.

A solution proposal for this is to introduce an electrical coil to one side of the rock. The current going through will create a magnetic field. If the intensity of electrical current is known and the current is set at fixed intervals, then the magnetic field magnitude will be controlled and emitted in fixed pulses.

Since the frequency and magnitude of the magnetic field is known, a sensor inside the rock can detect the magnitude of the pulses while drilling inside the rock.

The magnitude read by the sensor coming from the coil is proportional to the distance between the sensor and the coil. For example, a larger sensor reading corresponds to the bit drilling towards the direction of the coil. With this relationship it is possible to determine the change in position of the drill bit along one axis.

This is a unidirectional solution. If additional coils are implemented on the orthogonal faces of the rock with different magnitudes and pulse frequencies, a 3-D space positioning estimate can be obtained.

17.9.3 Material Selection

A final recommendation is to improve the accuracy of the magnetometer readings by using of brass as the material of the sensor housing. The optimum solution would be to manufacture the entire BHA in this material. This is suggested because brass is less conductive compared to iron. Since the magnetic field magnitude is proportional to distance, the closer the source of disturbance is from the sensor, the higher the impact on the the readings. A BHA in brass would significantly reduce the magnetic disturbances reflected in the magnetometer readings.

Bibliography

- [1] Human Factors 101. *The Ironies of Automation*. URL: <https://humanfactors101.com/2020/05/24/the-ironies-of-automation/0>. Accessed: 04.11.2021.
- [2] Airswift. *Stop Work Authority (SWA)*. URL: <https://www.airswift.com/about/safety/stop-work-authority>. Accessed: 24.03.2022.
- [3] A. Sikal et al. *Drill Pipe Stress and Cumulative Fatigue Analysis in Complex Wells Drilling: New Approach in Fatigue Optimization*. URL: <https://onepetro.org/SPEATCE/proceedings/08ATCE/All-08ATCE/SPE-116029-MS/145025>. Accessed: 10.08.2021.
- [4] A. Sneddon et al. 'Stress, fatigue, situation awareness and safety in offshore drilling crews'. In: *Safety Science* (2013). URL: <https://doi.org/10.1016/j.ssci.2012.05.027>.
- [5] A. Thuve et al. *Design Considerations for a Miniature Autonomous Drilling Rig*. Master's thesis, NTNU, 2017.
- [6] B. Brechan et al. 'Digital Well Planning - New Cost Saving Well Construction and Life Cycle Well Integrity Model'. In: *Offshore Technology Conference* (2018). URL: <https://doi.org/10.4043/28772-MS>.
- [7] B. Foss et al. *Merging Optimization and Control*. Institutt for teknisk kybernetikk, 2013.
- [8] F. Iversen et al. 'Drilling Automation: Potential for Human Error'. In: *IADC/SPE* (2012). URL: <https://doi.org/10.2118/151474-MS>.
- [9] G. Hånsnar et al. *Design and Implementation of a Miniature Rig for Autonomous and Directional Drilling*. Master's thesis in Petroleum Geoscience and Engineering, 2021.
- [10] Gjersdal et al. *Design Report NTNU - Drillbotics™ 2021 Phase I*. Department of Geoscience and Petroleum, 2020.
- [11] J. Winter et al. 'Reflections on the 1951 Fitts List: Do Humans Believe Now that Machines Surpass them?' In: *Procedia Manufacturing* (2015). URL: https://www.researchgate.net/publication/281587449_Reflections_on_the_1951_Fitts_List_Do_Humans_Believe_Now_that_Machines_Surpass_them.

-
- [12] M. Steinstrøm et al. *Implementation of a Miniature Autonomous Directional Drilling Rig With Nonlinear Model Predictive Trajectory Control*. Master's thesis in Industrial Cybernetics, 2021.
- [13] N. Eliaz et al. 'Comparative Quality Control of Titanium Alloy Ti-6Al-4V, 17-4 PH Stainless Steel, and Aluminum Alloy 4047 Either Manufactured or Repaired by Laser Engineered Net Shaping (LENS)'. In: *Additive Manufacturing Materials and Their Applications* (2000). URL: <https://doi.org/10.3390/ma13184171>.
- [14] Natalia Krygier et al. *A Drilling Company's Perspective on Non-Productive Time NPT Due to Well Stability Issues*. URL: <https://onepetro.org/SPEBERG/proceedings/20BERG/1-20BERG/D011S004R002/448663>. Accessed: 21.05.2022.
- [15] R. Parasuraman et al. 'A model for types and levels of human interaction with automation'. In: *IEEE Transactions on Systems Man and Cybernetics - Part A Systems and Humans* (2000). URL: <https://doi.org/10.2118/151474-MS>.
- [16] R. Roberts et al. "“Everything was fine”: An analysis of the drill crew's situation awareness on Deepwater Horizon". In: *Journal of Loss Prevention in the Process Industries* (2015). URL: https://www.researchgate.net/publication/282448445_Everything_was_fine_An_analysis_of_the_drill_crew's_situation_awareness_on_Deepwater_Horizon.
- [17] R. Wylie et al. 'Automating Directional Drilling: Technology Adoption Staircase Mapping Levels of Human Interaction'. In: *SPE* (2018). URL: <https://doi.org/10.2118/191408-MS>.
- [18] S. Chen et al. *A new theory on cutter layout for improving PDC-bit performance in hard-and transit- formation drilling*. URL: <https://onepetro.org/DC/article/28/04/338/204975/A-New-Theory-on-Cutter-Layout-for-Improving-PDC>. Accessed: 05.10.2021.
- [19] S. Hovda et al. *Introduction to Drilling Engineering*. Department of Geoscience and Petroleum, 2019.
- [20] Y. Dong et al. 'Improving safety of DP operations: learning from accidents and incidents during offshore loading operations'. In: *EURO Journal on Decision Processes* (2017). URL: https://www.researchgate.net/publication/320259497_Improving_safety_of_DP_operations_learning_from_accidents_and_incidents_during_offshore_loading_operations.
- [21] Z. Chu et al. 'Magnetic orientation system based on magnetometer, accelerometer and gyroscope'. In: *CAAI Transactions on Intelligence Technology* (2017). URL: <https://ietresearch.onlinelibrary.wiley.com/doi/epdf/10.1049/trit.2017.0024>.
- [22] A.T. Bourgoyne Jr et al. *Applied Drilling Engineering*. 2nd ed. Society of Petroleum Engineers, 1991.
- [23] B. Brechan et al. *Drilling, Completion, Intervention and P&A - design and operations*. Department of Geoscience and Petroleum, 2017.
- [24] H. Helgeland et al. *Design Report NTNU – Drillbotics 2022 Phase I*. Department of Geoscience and Petroleum - NTNU, 2021.
-

-
- [25] J. Mannsverk et al. *Design Report NTNU - Drillbotics™ 2020 Phase I*. Department of Geoscience and Petroleum, 2019.
- [26] S. Johnsen et al. *Automation and autonomous systems: Human-centred design in drilling and well*. Sintef Digital, 2020.
- [27] AmesWeb. *Modulus of Rigidity*. URL: <https://amesweb.info/Materials/Modulus-of-Rigidity-Formula.aspx>. Accessed: 19.11.2021.
- [28] Arduino. *Arduino Nano 33 BLE*. URL: <http://store.arduino.cc/products/arduino-nano-33-ble>. Accessed: 12.02.2022.
- [29] Nefeli Alushi - Arduino. *Accessing Magnetometer Data on Nano 33 BLE Sense*. URL: https://docs.arduino.cc/tutorials/nano-33-ble-sense/imu_magnetometer. Accessed: 14.02.2022.
- [30] Australian Government Comcare. *Ergonomic Hazards*. URL: <https://www.comcare.gov.au/safe-healthy-work/prevent-harm/ergonomic-hazards>. Accessed: 27.09.2021.
- [31] Hardware Corner. *Dell OptiPlex 7060 SFF*. URL: <https://www.hardware-corner.net/desktop-models/Dell-OptiPlex-7060-SFF>. Accessed: 17.12.2021.
- [32] Dell. *Dell UltraSharp 34 Curved Ultrawide Monitor: U3415W*. URL: https://www.dell.com/en-hr/work/shop/cty/pdp/spd/dell-u3415w-monitor#features_section. Accessed: 17.12.2021.
- [33] International Association of Drilling Contractors. *Real-time data offers critical tool to redefine well control, safety*. URL: <https://www.drillingcontractor.org/real-time-data-offers-critical-tool-to-redefine-well-control-safety-19320>. Accessed: 03.11.2021.
- [34] E. Dupriest. ‘Maximizing Drill Rates with Real-Time Surveillance of Mechanical Specific Energy’. In: *SPE/IADC Drilling Conference (2005)*. URL: <https://onepetro.org/SPEDC/proceedings-abstract/05DC/All-05DC/SPE-92194-MS/72603>.
- [35] Enggcyclopedia ed. *Absolute Pipe Roughness*. URL: <https://www.enggcyclopedia.com/2011/09/absolute-roughness/>. Accessed: 12.11.2021.
- [36] MechaniCalc ed. *Column Buckling*. URL: <https://mechanicalc.com/reference/column-buckling>. Accessed: 21.10.2021.
- [37] MechaniCalc ed. *Cross Sections*. URL: <https://mechanicalc.com/reference/cross-sections#radius-of-gyration>. Accessed: 21.10.2021.
- [38] Micon Downhole Tools ed. *Positive Displacement Motors (PDM)*. URL: https://micon-drilling.de/Download/Catalog_PDM_EN.pdf. Accessed: 30.09.2021.
- [39] NIOSH ed. *Hierarchy of Controls*. URL: <https://www.cdc.gov/niosh/topics/hierarchy/default.html>. Accessed: 27.09.2021.
- [40] Petrowiki ed. *Cuttings Transport*. URL: https://petrowiki.spe.org/Cuttings_transport. Accessed: 15.10.2021.
- [41] Petrowiki ed. *Directional Deviation Tools*. URL: https://petrowiki.spe.org/Directional_deviation_tools. Accessed: 05.10.2021.
-

-
- [42] Petrowiki ed. *PDC bit design*. URL: https://petrowiki.spe.org/PDC_bit_design. Accessed: 05.10.2021.
- [43] Schlumberger ed. ‘Drill bit cutting structure - Basic information’. 2021.
- [44] Wiki ed. *Angular velocity*. URL: https://en.wikipedia.org/wiki/Angular_velocity. Accessed: 05.10.2021.
- [45] Ubong Edet. *Mechanical hazards and common mechanical injuries*. URL: <https://www.hsewatch.com/mechanical-hazards>. Accessed: 27.09.2021.
- [46] Danny Jost - Fierce Electronics. *What is an accelerometer?* URL: <https://www.fierceelectronics.com/sensors/what-accelerometer>. Accessed: 10.02.2022.
- [47] R. Endsley. ‘From here to autonomy: Lessons learned from human–automation research’. In: *Human Factors The Journal of the Human Factors and Ergonomics Society* (2016). URL: https://www.researchgate.net/publication/312548354_From_Here_to_Autonomy_Lessons_Learned_From_Human-Automation_Research.
- [48] Folkehelseinstituttet. *Smittevernrad for befolkningen*. URL: <https://www.fhi.no/nettpub/coronavirus/befolkningen/smittevernrad-for-befolkningen/?term=&h=1>. Accessed: 14.03.2022.
- [49] T.I. Fossen. *Handbook of Marine Craft Hydrodynamics and Motion Control*. Wiley-Blackwell, 2021.
- [50] Gerdmans. *Tralle Bele*. URL: <https://www.gerdmans.no/lager-og-industri/transport/traller/tralle-bele-580x580-mm-kapasitet-300-kg-gummihjul>. Accessed: 22.05.2022.
- [51] Gigager. *GSH Hypoid Gear Rotary Table*. URL: <https://5.imimg.com/data5/VT/DC/CF/SELLER-2308089/hypoid-gear-rotary-table.pdf>. Accessed: 27.03.2022.
- [52] Gigager’. *Right Angle Gearboxes*. URL: <https://www.gigager.net/right-angle-gearbox/right-angle-gearboxes.html>. Accessed: 27.03.2022.
- [53] Halliburton. *Compass Software Release 5000.1.7 Training Manual*. Halliburton, 2011.
- [54] Todd Robert Hamrick. *Optimization of Operating Parameters for Minimum Mechanical Specific Energy in Drilling*. Department of Mechanical and Aerospace Engineering, 2011.
- [55] A. Handeland. *Design and optimization of a miniature autonomous drilling rig contribution to the drillbotics competition 2018*. Master’s thesis, NTNU, 2018.
- [56] Health and Safety Executive. *Construction hazardous substances: Cement*. URL: <https://www.hse.gov.uk/construction/healthrisks/hazardous-substances/cement.htm>. Accessed: 27.09.2021.
- [57] H. Helle. *Design and Implementation of an Autonomous Miniature Drilling Rig for Directional Drilling*. Master’s thesis, NTNU, 2019.
- [58] A. Hiwa. *Trajectory control, kick-detection and friction test: Transitioning to an automated drilling system*. Master’s thesis, NTNU, 2020.
-

-
- [59] Arduino project hub. *NRF24L01 Interfacing with Arduino — Wireless Communication*. URL: <https://create.arduino.cc/projecthub/muhammad-aqib/nrf24l01-interfacing-with-arduino-wireless-communication-0c13d4>. Accessed: 23.11.2021.
- [60] Arduino project hub. *Wireless Magnetic Data Transfer*. URL: https://create.arduino.cc/projecthub/tctree333/wireless-magnetic-data-transfer-e19171?ref=similar&ref_id=157798&offset=4#similar-proj. Accessed: 23.11.2021.
- [61] RS Hydro. *Sound Speeds in Water, Liquid and Materials*. URL: <https://www.rshydro.co.uk/sound-speeds/>. Accessed: 03.05.2022.
- [62] Insight. *Dell OptiPlex 7090*. URL: https://www.insight.com/en_US/shop/product/NWWNW/DELL/NWWNW/Dell-OptiPlex-7090---MT---Core-i7-10700-2-9-GHz---vPro---16-GB---SSD-256-GB/. Accessed: 30.04.2022.
- [63] National Instruments. *USB-6212*. URL: <https://www.ni.com/en-no/support/model-usb-6212.html>. Accessed: 30.04.2022.
- [64] Fridtjov Irgens. *Fasthetslære*. 7th ed. Tapir Akademisk Forlag, 2006.
- [65] Henning Johansen. *Aksler*. URL: <https://materialteknologi.files.wordpress.com/2018/01/sb-aksler-kompendium.pdf>. Accessed: 10.10.2021.
- [66] B. Larsen. *Måle- og reguleringssteknikk*. Instrutek A/S, 1994.
- [67] Lenze. *Catalog GST GFL gearboxes with MD MH AC motors*. URL: https://download.lenze.com/TD/E84AVTCx_8400%5C%20TopLine%20C_v11-1_EN.pdf. Accessed: 25.10.2021.
- [68] Haoge Liu. *Subsea field layout optimization (Part I) – directional well trajectory planning based on 3D Dubins Curve*. URL: <https://www.sciencedirect.com/science/article/pii/S0920410521010937>. Accessed: 02.02.2022.
- [69] MathWorks. *Anti-Windup Control Using a PID Controller*. URL: <https://se.mathworks.com/help/simulink/slref/anti-windup-control-using-a-pid-controller.html>. Accessed: 11.05.2022.
- [70] MathWorks. *Closed-Loop PID Autotuner*. URL: <https://se.mathworks.com/help/slcontrol/ug/closedlooppidautotuner.html>. Accessed: 10.05.2022.
- [71] MathWorks. *Design MPC Controller in Simulink*. URL: <https://se.mathworks.com/help/mpc/gs/designing-a-model-predictive-controller-for-a-simulink-plant.html>. Accessed: 11.05.2022.
- [72] MathWorks. *Extended Kalman Filter*. URL: https://se.mathworks.com/help/control/ref/ekf_block.html. Accessed: 11.05.2022.
- [73] MathWorks. *Math. Graphics. Programming*. URL: <https://se.mathworks.com/products/matlab.html>. Accessed: 08.05.2022.
- [74] MathWorks. *Simulink*. URL: <https://se.mathworks.com/products/simulink.html>. Accessed: 08.05.2022.
- [75] MathWorks. *Simulink Environment Fundamentals*. URL: <https://se.mathworks.com/help/simulink/simulink-environment.html>. Accessed: 08.05.2022.
-

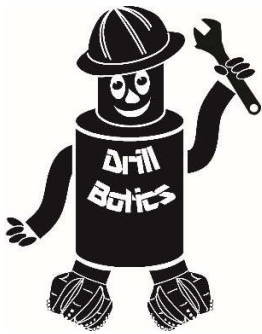
-
- [76] MathWorks. *Understanding Kalman Filters, Part 3: An Optimal State Estimator*. URL: <https://se.mathworks.com/videos/understanding-kalman-filters-part-3-optimal-state-estimator--1490710645421.html>. Accessed: 10.05.2022.
- [77] MathWorks. *What Is MATLAB?*. URL: <https://se.mathworks.com/discovery/what-is-matlab.html>. Accessed: 08.05.2022.
- [78] MatWeb. *AISI Type 316L Stainless Steel, annealed sheet*. URL: <http://www.matweb.com/search/DataSheet.aspx?MatGUID=1336be6d0c594b55afb5ca8bf1f3e042>. Accessed: 19.11.2021.
- [79] MatWeb. *Aluminum 6061-T6; 6061-T651*. URL: <http://www.matweb.com/search/DataSheet.aspx?MatGUID=b8d536e0b9b54bd7b69e4124d8f1d20a>. Accessed: 19.11.2021.
- [80] MatWeb. *Aluminum 7075-T6; 7075-T651*. URL: <http://www.matweb.com/search/DataSheet.aspx?MatGUID=4f19a42be94546b686bbf43f79c51b7d&ckck=1>. Accessed: 19.11.2021.
- [81] Dejan - How to mechatronics. *What is MEMS? Accelerometer, Gyroscope & Magnetometer with Arduino*. URL: <https://howtomechatronics.com/how-it-works/electrical-engineering/mems-accelerometer-gyroscope-magnetometer-arduino/>. Accessed: 11.02.2022.
- [82] Moons'. *M2DV-1D82IP*. URL: <https://www.moonsindustries.com/p/m2dv-series-servo-drives/m2dv-1d82ip-000004696351001660>. Accessed: 27.03.2022.
- [83] M.B. Nãmdal. *Design and Implementation of an Autonomous Miniature Drilling Rig for Directional Drilling*. Thesis. Department of Engineering Cybernetics, 2019.
- [84] Jarle Ness. *Implementation of a Miniature Autonomous Directional Drilling Rig*. Department of Cybernetics, 2022.
- [85] Standards Norway. *NORSOK standards*. URL: <https://www.standard.no/en/sectors/energi-og-klima/petroleum/norsok-standards/#.YqN-BnZByUk>. Accessed: 30.04.2022.
- [86] NOV. *Iron Roughnecks*. URL: <https://www.nov.com/products/iron-roughnecks>. Accessed: 21.05.2022.
- [87] OG21. *A continued high attention to cost is required to stay competitive*. URL: <https://www.og21.no/strategi-og-analyser/og21-strategien-2021/the-need-for-new-technology-to-improve-competitiveness/a-continued-high-attention-to-cost-is-required-to-stay-competitive/>. Accessed: 21.05.2022.
- [88] Omega. *What is a PID Controller?* URL: <https://www.omega.co.uk/prodinfo/pid-controllers.html>. Accessed: 03.05.2022.
- [89] PartsBadger. *Properties of Titanium Ti-6Al-4V (Grade 5)*. URL: <https://partsbadger.com/properties-of-grade-5-titanium/>. Accessed: 19.11.2021.
- [90] Society of Petroleum Engineers (SPE) and Drilling Systems Automation Technical Section (DSATS) ed. *Drillbotics™ Guidelines*. URL: <https://drillbotics.com/wp-content/uploads/simple-file-list/Guidelines/Guidelines-2022/2022-Drillbotics-Guidelines-Rev-1-Group-B.pdf>. Accessed: 22.10.2021.
-

-
- [91] Petroleumstilsynet. *Om regelverket*. URL: <https://www.ptil.no/regelverk/lover/om-regelverket/>. Accessed: 14.03.2022.
- [92] Petroleumstilsynet. *Risikonivå i norsk petroleumsvirksomhet*. URL: <https://www.ptil.no/contentassets/c4222734927b44f2bf2281446ab3ca1c/rnnp-2020-sammendragsrapport-rev-1.pdf>. Accessed: 14.03.2022.
- [93] Doza pro. *Right circular cylinder*. URL: <https://doza.pro/art/math/geometry/en/cylinder>. Accessed: 14.11.2021.
- [94] Material Properties. *What is Fatigue Life – S-N Curve – Woehler Curve - Definition*. URL: <https://material-properties.org/what-is-fatigue-life-s-n-curve-woehler-curve-definition/>. Accessed: 10.08.2021.
- [95] M. S. Ramsey. *Practical Wellbore Hydraulics and Hole Cleaning: Unlock Faster, more efficient, and trouble-free drilling operations*. Gulf Professional Publishing, 2019.
- [96] Singiresu S. Rao. *Vibration of Continuous Systems*. URL: <https://wp.kntu.ac.ir/hrahmani/Adv-Vibrations-Books/Continuous-Vibrations-Rao.pdf>. Accessed: 03.05.2022.
- [97] Stephen Rassenfoss. *Drilling Automation: Are We There Yet?* URL: <https://jpt.spe.org/drilling-automation-are-we-there-yet>. Accessed: 21.05.2022.
- [98] S. James Remington. *Mahony AHRS and Tilt Compensated Compass for Arduino and the LSM9DS1 sensor*. URL: <https://github.com/jremington/LSM9DS1-AHRS>. Accessed: 30.03.2022.
- [99] CGE Risk. *Bowtie risk assessment for inspection authorities*. URL: https://www.cgerisk.com/knowledgebase/The_bowtie_method. Accessed: 27.11.2021.
- [100] Schlumberger. *Drillstring Vibrations and Vibration Modelling*. URL: <https://www.slb.com/-/media/files/drilling/brochure/drillstring-vib-br>. Accessed: 03.05.2022.
- [101] sensorland.com. *What is a Fluxgate ?* URL: <https://www.sensorland.com/HowPage071.html>. Accessed: 14.03.2022.
- [102] SoundEar. *Decibel Scale*. URL: <https://soundear.com/decibel-scale/>. Accessed: 03.04.2022.
- [103] British Geological Survey. *The Earth's Magnetic Field: An Overview*. URL: <http://www.geomag.bgs.ac.uk/education/earthmag.html>. Accessed: 14.02.2022.
- [104] R. Teale. 'THE CONCEPT OF SPECIFIC ENERGY IN ROCK DRILLING'. In: *International Journal of Rock Mechanics and Mining Sciences & Geomechanics Abstracts* (1965). URL: <https://www.sciencedirect.com/science/article/abs/pii/0148906265900227>.
- [105] TotalEnergies. *Shaping up to be a leader in safer, more effective drilling*. URL: <https://ep.totalenergies.com/en/expertise/drilling-wells/shaping-be-leader-safer-more-effective-drilling>. Accessed: 03.11.2021.
- [106] AEP Transducers. *TC4-AMP AEP Transducer*. URL: <https://www.aep.it/prodotto/trasduttori-di-forza/tc4-amp/>. Accessed: 25.10.2021.
-

- [107] Electrical Safety UK. *What Are Electrical Hazards?* URL: <https://elecsafety.co.uk/what-are-electrical-hazards/>. Accessed: 27.09.2021.
- [108] Wikipedia. *Natural frequency*. URL: https://en.wikipedia.org/wiki/Natural_frequency. Accessed: 03.05.2022.
- [109] WPI. *Introduction to PID*. URL: <https://docs.wpilib.org/pt/latest/docs/software/advanced-controls/introduction/introduction-to-pid.html>. Accessed: 10.05.2022.

Appendix **A**

Drillbotics 2022 Guidelines



Society of Petroleum Engineers
Drilling Systems Automation
Technical Section (DSATS)
International University Competition
2021-2022



Drillbotics® Guidelines Group B

Revised 11 October 2021

1. Introduction

This year marks the eighth competition for the title of Drillbotics® champion and a chance for students to learn about the drilling process from industry experts and for winning team(s) to travel and present a paper at the next SPE/IADC Drilling Conference and at an event organized by DSATS. The past years involved undergraduates, masters and doctoral students from a variety of disciplines who built innovative drilling machines and downhole tools while developing a deeper understanding of automating the drilling process. Recently, this was extended to include teams who created models of the rig, the drilling process, and various downhole interactions. Teams freely shared lessons learned, which more rapidly advances the science of drilling automation. Everyone involved claims to have had a lot of fun while learning things that are not in the textbooks or published papers. Students also participated in related events at conferences, workshop meetings and networking with industry leaders in drilling automation. This year's contest promises to be just as challenging and hopefully as much fun.

This year's competition will be to create a virtual rig, including drill string/BHA and wellbore interaction, and to demonstrate the model using a control model developed by each team in Group A. Due to the COVID-19 pandemic, the Drillbotics challenge committee decided to focus this year's competition on a virtual rig in an effort to facilitate competition success while teams work together remotely. If school policies allow a team to design and build a physical rig and there are a sufficient number of teams capable of building a physical rig, the Committee will allow these teams to compete as a second group as mentioned below and referred to as Group B.

New for 2022

- Continue with two groups
 - A – Virtual
 - B – Physical
 - Directional drilling with two targets, but the second target may require a turn
- Separate guidelines for each group to reduce confusion
- Okay for two schools to join together for their entry
- Added a new section to include Human Factors in your process
- Plan for a hybrid in-person/virtual test next year due to COVID

Version	Date	Section	Description
2022.01	3 October 2021	All	initial release
2022.02	11 October 2021	Footer	Corrected typo from Group A to Group B

Last year, teams reviewing the contest rules had to jump between the main body of the guidelines to various appendices depending on which group they chose. This year we have created separate guidelines for Groups A and B. The general information items that are common to both groups are identical. Rules specific to each group are listed in an appendix. Teams must also monitor the website (www.Drillbotics.com) to check any Frequently Asked Questions (FAQs) since they become part of these guidelines.

How did the competition first come about? The origins began in 2008 when several SPE members established the Drilling Systems Automation Technical Section (DSATS) to help accelerate the uptake of automation in the drilling industry. DSATS' goal was to link the surface machines with downhole machines, tools, and measurements in drilling systems automation (DSA), thereby improving drilling safety and efficiency. Later, at an SPE Forum in Paris, the idea of a student competition began to take shape; a DSATS sub-committee was formed to develop the competition format and guidelines further. Several universities were polled to find out the ability of academic institutions to create and manage multi-disciplinary teams. The Drillbotics committee began small in 2014-2015 to see if the format could succeed. With fine tuning, we continue along those lines as we start the 2022 process.

Competition Overview:

Group A

- The challenge requires teams to develop a full-scale drilling system model, including its corresponding control scheme, to virtually drill a directional well following a given trajectory.
- The teams will design a control system that will virtually control the full-scale drilling system model to test and demonstrate the automated system. The teams should incorporate virtual downhole and surface sensors in their automation and controls scheme.

Group B

- The challenge requires teams to develop a small-scale drilling rig and control system to autonomously drill a directional well following a given trajectory.
- Downhole sensors are mandatory, and their data must be included in the control algorithms.

Phase I

- Both groups must submit a Phase I Design Report not later than 31 December.
- A Phase I Design Video is optional, due not later than 15 January.
- Judges will review the reports and select finalists to be announced in early February.

Phase II

- Teams will submit a pre-recorded team presentation approximately one week before the Phase II test.
- Group A and B Phase II tests will be held on separate dates, to be advised in April.

The DSATS technical section believes that this challenge benefits students in several ways. Petroleum, mechanical, electrical, and control engineers gain hands-on experience in each person's area of expertise that forms a solid foundation for post-graduate careers. Those involved with system modeling gain insight into how models can gain sufficient fidelity to be applied to industry specific problems. Students also develop experience working in multi-disciplinary teams, which is essential in today's technology-driven industries. Winning teams must possess a variety of skills. The mechanical and electrical engineers need to build a stable, reliable, and functional drilling rig. Control engineers need to architect a system for real-time control, including a selection of sensors, data handling, and fast-acting control algorithms. The petroleum engineers need an understanding of drilling dysfunctions and mitigation techniques. Modeling engineers must understand all of these basics and how to organize numerous modules into a complex model. Everyone must work collectively to establish functional system requirements, often fully understood by each team member to accurately portray the drilling issues and create an integrated package working seamlessly together.

The oil and gas industry today seeks lower costs through efficiency and innovation. Many student competitors may discover innovative tools and control processes that will assist drillers in speeding the time to drill and complete a well. This includes more than a faster ROP, such as problem avoidance for dysfunctions like excessive vibrations, stuck pipe, and wellbore stability issues. Student teams built new downhole tools using 3D printing techniques of designs that would be difficult, if not impossible to machine. They used creative hoisting and lowering systems. Teams modeled drilling performance in particular formations and adjusted the drilling parameters accordingly for changing downhole conditions. While they have a lot to learn yet about our business, we have a lot to learn about their fresh approach to today's problems. Good Luck!

Drillbotics® Committee

Drillbotics Challenge Team

Aleksandra Khramtseva
Bader Al-Otaibi
Enrique Z Losoya
Eric Cayeux
Fred Florence
Marcin Nazaruk
Mike Attrell
Peter Gibson
Salem H. Al-Gharbi
Shashi Talya

Judges and their primary affiliation¹

DSATS

Shashi Talya (Chair)	Eric Cayeux	Oliver Hoehn
Fred Florence (Co-Chair)	Jana Hochard	Ritthy Son
Alex Ngan	Mathew Keller	Scott Petrie
Dimitrios Pirovolou	Mike Attrell	Tony Pink
Dmitriy Dashevskiy	Mohamed Ali Ibrahim	Victor Soriano
Duane Cuku	Hassan	Vimlesh Bavadiya
Enrique Z Losoya	Nii Ahele Nunoo	

Digital Energy

DUPTS

Salem H. Al-Gharbi (Chair)
Bader Al-Otaibi

HFTS

Marcin Nazaruk (Chair)
Aleksandra Khramtseva
Peter Gibson

WPTS

Mike Attrell
Bader Al-Otaibi

¹ DSATS, the sponsoring technical committee, could not hold this competition without the expertise and energy contributed by members of the other technical sections within SPE.

Contents

1. Introduction	1
2. Objectives for the 2021 Competition.....	6
3. Background	6
4. General Competition Guidelines.....	7
5. Team Members	8
6. Safety.....	9
7. Expenditures.....	9
8. Other Considerations.....	10
9. Project Timeline	10
10. Project reports	10
11. Group A Prizes	12
12. Group B Prizes	13
13. Terms and Conditions.....	13
14. Marketing.....	14
Appendix A: Group B Project Definition	15
A. Overview.....	15
B. Directional Objective Requirements.....	15
C. Safety.....	17
D. Phase I – Design Competition.....	17
E. Design Criteria	19
F. Phase I Design Report.....	30
G. Phase II – Drilling Competition	31
H. Final Report and Paper.....	34
Appendix B: Automation & Interface Design from a Human Factors Perspective	36
Appendix C: Additional References.....	39

2. Objectives for the 2021 Competition

- 2.1. During the school year, beginning in the fall of 2021, a team of students will organize themselves to solve a drilling-related problem outlined in Appendix A below. The team should preferably be a multi-disciplinary team that will bring unique skills to the group to allow them to design and construct hardware, software and models to demonstrate that they understand the underlying physics, the drilling issues and the usual means to mitigate the issues. We cannot stress enough the need to involve students with different technical training and backgrounds. They will need to develop skills to understand drilling dysfunctions and mitigation strategies, but they must also have the mechanical engineering and controls capabilities to model, design the rig/drilling package and develop the controls system. Even when the project involves only software, an understanding of the physical limits of a rig's machinery and tubulars is critical. In past years, some entrants have not adequately considered the control network and algorithms needed for autonomous drilling. They have often misunderstood the need for calibrated sensors and fast, accurate data handling. Some teams did not consider measurement errors. Teams from both Group A and B ignored uncertainty principles. All of this and more is needed to build and operate a complete automated drilling system. We encourage all teams to start out with a simple concept done well, and then build on it from year to year adding complexity when warranted. Planning for this evolution will make it easier on future team members.
- 2.2. The students should produce novel ideas leading to new drilling models, improved drilling machines and sensors, and the ability to integrate the data, models and machines that will hopefully create new, more efficient ways to drill wells in the future. Any such innovation will belong to the students and their university in accordance with the university's written policies. DSATS and SPE waive any claims to students' intellectual property.
- 2.3. The students, working as a multi-disciplinary team, will gain hands-on experience that will be directly applicable to a career in the upstream drilling industry.

3. Background

3.1. What is DSATS?

DSATS is a technical section of the Society of Petroleum Engineers (SPE) organized to promote the adoption of automation techniques using surface and downhole machines and instrumentation to improve the safety and efficiency of the drilling process. More information is available about DSATS at the DSATS homepage (<http://connect.spe.org/DSATS/Home/>).

3.2. Why an international competition?

DSATS and the other technical sections, as part of the SPE, are a group of volunteers from many nations, connected by their belief that drilling automation will have a long-term, positive influence on the drilling industry. This diversity helped to shape the direction of the organization. The group feels that the industry needs to attract young professionals from all cultures and disciplines to advance drilling practices in all areas of the world. The winners of the Group A competition will receive a grant for economy class transportation and accommodations to attend the next SPE Drilling Conference and

will present an SPE paper that will be added to the SPE archives of One Petro². Winners of Group B will publicly receive recognition of their achievement and have the opportunity³ to publish an SPE paper that will be added to the SPE archives of One Petro. DSATS believes recognition at one of the industry's leading technical conferences will help encourage student participation. Also, the practical experience with drilling automation systems increases the students' visibility to the companies that are leading automation activities.

3.3. Why include Human Factors?

Any complex, engineered system that is wholly reliant upon human operators to achieve its goal is likely to experience issues. Humans are inconsistent when performing monitoring tasks, they tend to not make wholly rational decisions, are impacted by external factors and are prone to error. As technology advances and complexity increases (such as the control regimes proposed in remote drilling operations for example) such issues become more prevalent. However, many of the issues associated with such complexity can be countered by reallocating certain tasks to automation. Maintaining appropriate levels of automation and ensuring that your 'projected' drilling operator remains 'in the loop' through good interface design will be one of the key challenges you will face in the Drillbotics competition.

Students working with automated systems should learn about the risks and proper strategies to allow humans and machines to work together safely and efficiently. Reference documents are listed in Appendix B. Requirements for human factors provisions are shown in Appendix A.

3.4. Items posted on the website are part of these Guidelines

The Drillbotics website at www.Drillbotics.com includes official updates to the competition guidelines and schedule, as well as FAQs, photos, and previous entrants' submittals and reports and numerous reference documents. **Any updates to the guidelines posted on the Drillbotics website via FAQs or blog entries from the Committee are considered to be an official revision to these Guidelines.**

3.5. Questions should be directed to the competition email at 2022@Drillbotics.com. Please provide the reference number of the section of the guideless when you ask questions. Questions and answers will be incorporated into the FAQs periodically.

4. *General Competition Guidelines*

4.1. The Group A challenge requires teams to develop a drilling system model that represents a full-scale system and corresponding control scheme to virtually drill a directional well to a given trajectory as efficiently as possible within constraints of safety and economics. The Group A challenge does not involve building a rig or drilling system. The teams will design automation and

² Publication is subject to the SPE program committee's acceptance of the abstract/paper. If the abstract is not accepted, DSATS will solicit other SPE events try to get the paper into OnePetro. Travel authorization will depend on any international or local travel restrictions in place at the time of certain events.

³ DSATS will submit an abstract to SPE, and if need be, to other organizations, in an effort to help teams publish the results of their work.

control modules to develop a virtual drilling system (i.e., computer models) to test and demonstrate the controls.

- 4.2. The Group B challenge requires the design, construction, and operation of a physical mini-rig to physically drill a directional well to a given trajectory as efficiently as possible within constraints of safety and economics. The guidelines for Group B are published separately.
- 4.3. The contest covers only the drilling of one hole section. There is no need to run casing. There is no need for automated pipe handling at the surface. There is no logging or cementing. This is just a drilling problem.
- 4.4. Judges want to see evidence that teams know about drilling and modeling aspects of well construction. Because teams will either build or model a physical rig and downhole conditions, they must specify the assumptions made about their project. Allowing judges to understand “why” you made certain choices affects their evaluation of your project.
- 4.5. While the teams will have to meet minimum competition requirements, any exceptional contributions “above and beyond” the main theme will be rewarded with additional points to encourage creativity and innovation.
- 4.6. Teams are free to choose the hardware and software most suited to their design except where explicitly specified. Teams are free to choose any software language. Judges would like to see an explanation of the reason certain hardware or software was selected.

5. *Team Members*

- 5.1. DSATS envisions that the students would be at least at the senior undergraduate or Masters level, well versed in the disciplines needed for such a project. The core team shall consist of at least three (3) team members and no more than five (5). Contributions from other team members is allowed, and all contributors should be recognized in the Phase I Design Report. The travel grant for the winning team will be limited to five (5) team members and one (1) supervisor due to budget constraints.
- 5.2. Any team that loses team members during the project can recruit a replacement. Note any changes to the team membership in the monthly reports. At least one member of the core team must be a Petroleum Engineering candidate with sufficient coursework completed to understand the physics relating to the drilling problems and the normal industry practices used to mitigate the problem.
- 5.3. Students with a background in mining, applied mathematics, mechanical and electrical engineering, as well as controls, mechatronics and automation or software development, are the most likely candidates, but students with any applicable background is encouraged.
- 5.4. A multi-disciplinary team simulates the working environment in the drilling industry today, as most products and services are produced with the cooperation of technical personnel from differing backgrounds and cultures.
- 5.5. A university may enter more than one team in a group and may enter teams in one or both groups.
- 5.6. A collaboration between not more than two universities is allowed, especially where one school may not offer a curriculum in a specific technical area needed to successfully conduct the project. The resulting team may only submit one Phase I design report. Also, the travel grant will still be limited to

five (5) students and one (1) supervisor. Note: Any differences with intellectual property ownership between the two schools must be settled by the teams and shall not involve DSATS.

5.7. Students shall register their team not later than 15 October using the registration form on the Drillbotics website <https://drillbotics.com/guidelines/>. Any changes to the team members or university supervisor over the course of the competition should be reported in the monthly reports.

6. *Safety*

6.1. The team's safety plan should consider all foreseeable hazards and methods to mitigate them. Personal protective equipment is part of a safety plan but is far from sufficient. Teams must consider risks due to handling the rock, rotating machinery, electrical shock and others. What health considerations are in place? How the team communicates with each other before and during operations is also important. Judges will grade each team on its comprehensive safety plan.

6.2. Because most of the Group B rigs have equipment spinning at high RPMs, some form of protective cover must be included in the team's rig design. A broken coupling, a loose screw or similar item becomes a projectile that can lead to serious injury to the team members, judges or visitors. Judges may decide to deny a team from competing if their design is unsafe.

6.3. The following links are a good starting point, but is by no means a comprehensive list of links:

6.3.1. OSHA Pocket Guide, Worker Safety Series:

<https://www.osha.gov/Publications/OSHA3252/3252.html>

6.3.2. OSHA Checklist for General Industry: <http://www.scosha.llronline.com/pdfs/genind.pdf>

7. *Expenditures*

7.1. Teams selected to advance to the second phase must limit the cost of the physical or virtual rig and materials to US\$ 10,000 or its equivalent in other currencies. The students shall find a source of funding and report the source in the Phase I proposal. All funding and procurement should comply with university policy. These funds are intended to cover the majority of expenses for hardware, software and labor to construct and operate the team's equipment. DSATS shall not be liable for any expenditure other than DSATS provided material and specified travel expenses.

7.2. DSATS will assist, when possible, to obtain free PLCs or similar control devices from suppliers affiliated with the DSATS organization. Such "in-kind" donations shall not be included in the team's project costs.

7.3. Students and universities may use other "in-kind" contributions which will not be included in the team's project costs. Such contributions may include modeling software, laboratory equipment and supplies, and similar paraphernalia usually associated with university laboratory projects.

7.4. Any team spending more than US\$ 10,000, or its equivalent in other currencies, may be penalized for running over budget.

7.5. DSATS reserves the right to audit the team's and university's expenditures on this project.

7.6. Any devices built for the project will become the property of the university and can be used in future research and competitions. Any maintenance or operating costs incurred after the competition will not be paid by DSATS.

8. *Other Considerations*

- 8.1. University coursework and credit: Each university will decide whether or not this project qualifies as a credit(s) towards any degree program.
- 8.2. The design concepts shall be developed by the student team under the supervision of the faculty. Faculty and lab assistants should review the designs to ensure student safety.
- 8.3. Construction of any equipment shall be supervised by the student team, but may use skilled labor such as welders and lab technicians. The use of outside assistance shall be discussed in the reports and the final paper. DSATS encourages the students to gain hands-on experience with the construction of the rig since this experience will be helpful to the career of individuals in the drilling industry.

9. *Project Timeline*

Phase I - Design:	Fall 2021
Submit monthly reports	On or before the final day of each month starting in October
Submit final design to DSATS	31 Dec 2021, midnight UTC
Submit an abstract to DSATS*	31 Dec 2021, midnight UTC
Finalists to advance to Phase II	Announced in mid-February 2022

*DSATS will submit an abstract to the SPE that will include excerpts from the student abstracts by the conference paper-submittal deadline, typically in mid-summer, for consideration of a paper by the conference program committee.

Phase II

Group A: Model enhancement/testing and controls development	Spring 2022
Group B: Model & controls development/Construction	Spring 2022
Group A and B Phase II Test	May/June 2022

10. *Project reports*

10.1. *Report File Names*

To avoid extra work by the committee to rename all files, teams must use this convention for all reports:

Monthly Reports

Year-Month# University Name (abbreviated)

(Note this is the competition year (spring term))

Example: for the 2021- 2022 entry from the University of Drillbotics Competition

Use: 2022-10 UDC

Design reports

Year University Name (abbreviated)

(Note this is the competition year (spring term))

Example: for the 2021- 2022 entry from the University of Drillbotics Competition

Use: 2022 UDC Phase I Design Report

10.2. Monthly Report Contents

Starting in October for the fall term, the student team shall submit to DSATS a short monthly project report that is no more than one page in length (additional pages will be ignored) due on or before the last day of each month. Send all reports via email to 2022@Drillbotics.com. The monthly report should include:

Phase I Monthly Report Contents

- Key project activities over the past month.
- Literature survey, rig modeling considerations, trade-offs, critical decision points etc.
- Cost updates
- Significant new learning, if any

Phase II Monthly Report Contents

- Key project activities over the past month.
- Model enhancements, controls development updates.
- Preliminary results of exercising the drilling model and controls
- Cost updates
- Significant new learning, if any

10.3. Other items of interest

To teach students that their work involves economic trade-offs, the monthly report should include at a minimum a summary estimate of team member labor hours for each step in the project: modeling, controls, testing etc. and a cost summary for hardware and software related expenditures. Also include labor for non-students that affect the cost of the project. Labor rates are not considered, as to eliminate international currency effects. Labor is not considered in the cost limits of section 7.1 but should be discussed in the reports.

10.4. Phase I Design Report

Detailed requirements for each group are listed in their respective Appendix A.

10.5. Final report, presentation and paper

- 10.5.1. The finalists shall prepare a project report that addresses items specific to each Group. We suggest you use the format of most SPE papers. For reference, please see <http://spe.org/authors/resources/>

- 10.5.2. [Finalists shall prepare a pre-recorded presentation one week prior to the Phase II test.](#)
- 10.5.3. The reports, presentations, paper and all communications with DSATS shall be in the English language. The presentation must be made by at least one member of the student team, not the team supervisor.

11. Group A Prizes

- 11.1. The winning team of Group A will be sponsored by DSATS to attend the next SPE/IADC Drilling Conference to present a paper that explains their project in detail.
- 11.2. The program committee of the Drilling Conference awarded the Drillbotics subcommittee a permanent slot⁴ in one of the drilling sessions at the conference. As per SPE's customary procedures, the paper will be archived in OnePetro. In addition, SPE has agreed to furnish a booth⁵ in the exhibition area during the conference where the team can erect their rig and describe its operation to the conference attendees. This is an excellent opportunity for students to network with the industry.
- 11.3. The winning team will receive a travel grant⁶ to attend the Drilling Conference. Note that this is for a limited number of team members, not to exceed five (5) plus one (1) supervisor. Pre-approval of expenses is required.
- 11.3.1. Upon submittal to DSATS of a valid expense statement of covered expenses (typically a spreadsheet supported by written receipts) individuals will be reimbursed by the treasurer of DSATS for the following:
- 11.3.2. Round trip economy airfare for the team and one university sponsor/supervisor to the gateway city of the next SPE/IADC Drilling Conference. Entrants should use the SPE approved carrier where possible to minimize cost. Airfares that exceed the SPE rate must be pre-approved by the committee, or the reimbursement will be limited to the SPE rate. Information of reduced fare flights is available on the conference website. Please note that reservations must be made before the SPE published deadline. The departure point will be a city near the university, the student's home, or current place of work, subject to review by the Committee. Alternately, a mileage reimbursement will be made in lieu of airfare should the entrants decide to drive rather than fly to the conference. The reimbursement is based on current allowable mileage rates authorized by the US Internal Revenue Service.
- 11.3.3. One rental car/van at the gateway city for those teams that fly to the conference.
- 11.3.4. Lodging related to one hotel room per team member will be reimbursed at a rate not to exceed the SPE rate. Note that the room reservations are limited, so entrants must book their rooms early. Room and taxes for the night before the DSATS symposium, the night of the symposium and for the nights of the conference are covered. Charges for the room on the last day of the conference need to be pre-approved by the Committee as most

⁴ Subject to continued approval by the conference program committee.

⁵ Subject to continued approval by the SPE conference staff.

⁶ Travel authorization will depend on any international or local travel restrictions in place at the time of certain events.

conference attendees depart on the last day of the conference unless there are unusual circumstances.

- 11.3.5. A per diem will be pre-approved by the Committee each year, which will vary with the cost of living in the gateway city. The per diem is intended to cover average meals (breakfast, lunch and dinner) and incidentals.
- 11.3.6. Conference registration will be reimbursed. Students should register for the conference at the student rate. Early registration is appreciated.
- 11.4. Individual award certificates will be presented to all participants upon request, with special certificates given to all finalists.
- 11.5. DSATS may provide additional awards, at its sole discretion.
- 11.6. The evaluation and all decisions on any matter in the competition by the Drillbotics judges and DSATS board are final.

12. Group B Prizes

- 12.1. The winning team of Group B may submit an abstract for a SPE whitepaper that explains their project in detail. If the quality of the abstract is approved by the SPE Conference program committee, as per SPE's customary procedures, the paper will be archived in OnePetro. If the abstract is not accepted, the Drillbotics committee will endeavor to secure a position in a different SPE conference.
- 12.2. Unfortunately, a travel grant for Group B is not budgeted, but could later be authorized solely at the discretion of the DSATS and the Drillbotics Committee.
- 12.3. *Other prize information*
 - 12.3.1. Individual award certificates will be presented to all participants upon request, with special certificates given to all finalists.
 - 12.3.2. DSATS may provide additional awards, at its sole discretion.
 - 12.3.3. The evaluation and all decisions on any matter in the competition by the Drillbotics judges and DSATS board of directors are final.

13. Terms and Conditions

- 13.1. In no event will SPE, including its directors, officers, employees and agents, as well as DSATS members and officers, and sponsors of the competition, be liable for any damages whatsoever, including without limitation, direct, indirect, special, incidental, consequential, lost profits, or punitive, whether based on contract, tort or any other legal theory, even if SPE or DSATS has been advised of the possibility of such damages.
- 13.2. By entering this competition,
 - 13.2.1. Participants and Universities agree to indemnify and hold harmless SPE, its directors, officers, employees and agents, as well as DSATS members and officers, and sponsors of the competition, from all liability, injuries, loss damages, costs or expenses (including attorneys'

fees) which are sustained, incurred or required arising out of participation by any parties involved in the competition.

13.2.2. Participants and Universities agree and acknowledge that participation in the competition is an agreement to all of the rules, regulations, terms and conditions in this document, including revisions and FAQs posted to the DSATS and Drillbotics websites (see section 3.1).

13.2.3. Winning teams and finalists must agree to the publication of their names, photographs and final paper on the DSATS web site.

13.3. All entries will be distributed to the Drillbotics Committee for the purpose of judging the competition. Design features will not be published until after all teams have been judged and a winner is announced. Previous years' submittals, reports, photos and similar documentation will be publicly available to foster an open exchange of information that will hopefully lead to faster learning for all participants, both new and experienced.

13.4. DSATS and the SPE cannot provide funding to sanctioned individuals and organization per current US law.

13.5. Participants must comply with all local laws applicable to this contest.

14. Marketing

14.1. Upon request, DSATS will provide a link on its website to all participating universities.

14.2. If university policy allows, various industry journals may send a reporter to witness the tests and interview students to publicize the project.

14.3. Drillbotics is now a registered trademark. According to international law, the proper reference is to use Drillbotics® instead of Drillbotics™. The trademark reference is only needed the first time Drillbotics is referenced.

14.4. Any team that wishes to use the trademark on signs, tee shirts, technical papers or for other purposes may receive a no-cost license upon request. Send the request by email to the committee at 2022@Drillbotics.com. Upon completion of the license agreement, access to the files with the logo will be made available.

Appendix A: Group B Project Definition

A. Overview

The following attached pages describe the directional objectives as well as the data/deliverables requirements. Scoring for the directional competition objective will be primarily based on how accurately the directional targets are intersected by the calculated well trajectory.

B. Directional Objective Requirements

- a. Objectives
 - i. Hit one or more targets at one or more vertical depth(s) and X/Y coordinates
 - ii. For the Group B competition, the starting directional plan to hit the targets will not require wellbore inclinations in excess of 30° from vertical, 15° change in azimuth, or 10" displacement (departure from the vertical axis at well center) The max displacement/inclination/azimuth are total/accumulated from the start to the end of the well path.
 - iii. Please note: Teams should be prepared to drill any given trajectory within the specified parameters, so the coordinates will not be provided in advance of the test.
- b. Automation Requirements
 - i. Drilling mode/survey mode switching must be automated (i.e. built-in survey interval and drill string movement for on/off-bottom, slide/rotation mode switching)
 - ii. Steering requirements (e.g. toolface direction, slide length) must be calculated autonomously
 - iii. NOTE: Steering mechanism can still require human intervention for placement and/or retrieval (e.g. whipstock) but orientation of steering mechanism must be calculated by the system and shown on the rig floor display.
 - iv. Directional surveying process must be entirely autonomous
 - v. Survey qualification must be done autonomously, however secondary qualification/verification/override can be made by a human
 - vi. Dogleg severity required to hit target(s), distance/direction to plan must be autonomously calculated at each survey station and shown on the rig floor display
- c. Deliverables Requirements (Magnetic surveying)
 - vii. All teams are required to provide a definitive directional survey (TXT, LAS, or CSV format) meeting the following minimum requirements:
 - viii. Header info to include:
 1. Team/school name
 2. Directional Survey Date
 3. Well Center Coordinates (WGS84 Latitude & Longitude)
 4. True Vertical Depth Reference (in depth units above block level)
 5. Grid Convergence
 6. Geomagnetic model used (if applicable)

7. Magnetic declination applied (Geomagnetic model or in-field referenced)
8. Total Azimuth Correction
9. Magnetic field dip reference (Geomagnetic model or in-field referenced)
10. Total magnetic field strength reference (Geomagnetic model or in-field referenced)
11. Error model associated with well trajectory (ISCWSA/OWSG error model or otherwise)
12. If non-standard error model is being used (i.e. formulas being modified and/or coefficients being changed), error model description (using standard variable/coefficient naming conventions) and justification must be included in project design
13. Minimum Curvature calculated trajectory (using appropriate survey station interval to accurately represent the drilled wellbore position)
14. Each survey station is to include the following data:
 - a. Measured Depth
 - b. Inclination
 - c. Azimuth (referenced to "block north")
 - d. True Vertical Depth
 - e. Northing (from well center)
 - f. Easting (from well center)
 - g. Dogleg Severity
15. Final survey station is to be an extrapolation to total depth at the bit
16. All teams are required to provide plan vs. actual plots containing the following minimum requirements:
17. As-drilled trajectory and original planned trajectory shown on same TVD vs. Vertical Section plot
 - a. Vertical section direction to be determined by well center-to-target bearing
18. As-drilled trajectory and original planned trajectory shown on same X/Y plot
 - a. Grid north reference to "block north"
 - b. [0,0] at well center
19. All teams are required to provide directional survey raw data logs containing the following minimum requirements:
 - a. Each log entry is to include the following data:
 - i. Time stamp (containing year, month, date, hour, minute, second)
 - ii. Sensor measured depth
 - iii. Downhole sensor value(s) recorded
 1. Sensor axes values
 2. Calculated survey qualifier values
 - iv. Accepted survey indicator (if log entry is an intended survey station)

- v. If secondary (i.e. human) qualification is also used, both acceptance indicators must be shown

C. Safety

The team's safety plan should consider all foreseeable hazards and methods to mitigate them. Personal protective equipment is part of a safety plan but is far from sufficient. Teams must consider risks due to handling the rock, rotating machinery, electrical shock and others. How the team communicates with each other before and during rig operations is also important. Judges will grade each team on its comprehensive safety case.

Because most of the rigs have equipment spinning at high RPMs, some form of protective cover must be included in the team's rig design. A broken coupling, a loose screw or similar item becomes a projectile that can lead to serious injury to the team members, judges or visitors. Judges may decide to deny a team from competing if their design is unsafe.

The following links are a good starting point, but is by no means a comprehensive list of links:

- OSHA Pocket Guide, Worker Safety Series: <https://www.osha.gov/Publications/OSHA3252/3252.html>
- OSHA Checklist for General Industry: <http://www.scohsa.llronline.com/pdfs/genind.pdf>

D. Phase I – Design Competition

- a. Prepare a safety plan at the beginning of the project and update it continually as needed.
- b. Consider how you will use Human Factors within your project to improve your team processes and interactions with your model. You should include such items as:
 - i. Who are the operators of your drilling rig and how do their characteristics impact the design?
 - ii. Which functions of your drilling rig will be automated, and which will be manual (refer to Ref. 2)?
 - iii. How are you going to ensure that the operator remains 'in the loop' at all times?
 - iv. The workflow that your drilling rig will follow (very important as this will guide your interface design).
 - v. The control and feedback needs for your defined operators.
 - vi. The 'concept' of your interface design. This can be as simple as a 'wireframe' drawing with pen and paper, but it should show an appreciation of Human Factors Relevant Good Practice (refer to the resources provided below).
- c. The first phase of the project starts in the fall, requiring teams to organize to design an automatic drilling machine to solve the project problem. It is not necessary to build any equipment in this phase, but it is okay to do so. Design considerations should include current industry practices and the team should evaluate the advantages and shortcomings of today's devices. The design effort may be assisted by university faculty, but the students are encouraged to introduce novel designs for consideration. The design should also include a downhole sensor and a control

system to automatically control the drilling process. The level of student, faculty and technical staff involvement shall be reported when submitting the design. For returning teams, the Phase I Design Report should include an analysis of data and learnings from previous (“offset”) wells drilled.

- d. During the second phase, in the spring, the finalist selected by DSATS to proceed to the construction and drilling operation will use the previous semester’s design to build an automated drilling machine. As per industry practices, it is common during construction and initial operations to run into problems that require a re-design.
 - i. The team may change the design as needed in order to solve any problems they encounter.
 - ii. Changes should be reported to the Committee via students’ monthly reports. A summary of all significant changes, including the reason modifications were necessary, must be included in the students’ final report.
 - iii. Teams may use all or part of a previous year’s rig.
- e. Phase I Design Report
The design submittal by the students shall include:
 - i. Student Biographies
 - Name
 - Previous degree attained – major
 - Current degree and expected graduation date (month/year)
 - Main area of contribution to the project
 - Other information as deemed appropriate by the team
 - ii. A description of your safety plan that is appropriate for the project
 - iii. Engineering sketches or drawings of the rig concept, mechanical and electrical and auxiliary systems, if any, that explain your design assumptions
 - iv. Include any design notes and calculations regarding rig, drillstring and other limitations for the particular modules used in your models.
 - v. A block diagram/flowchart of the modeled control system architecture. Describe the key features. The response time of measurements, data aggregation and control algorithms should be estimated. Explain how individual measurements are used are in the control code. Are they all given equal weight, and if not, what criteria is used to assign importance?
 - vi. Since this is a directional drilling problem, be sure to include how downhole data is used for steering and other drilling aspects? Judges are looking for a description of the principles being applied to directionally steer the wellbore and hit the required targets with the intent to score the maximum number of points.
 - vii. Proposed user interface/data display that shows the drilling progress in real time.
 - viii. Cost estimate and funding plan
 - ix. Key features for any models/modules and control software. What drilling dysfunctions are addressed?

- x. Proposed data handling, i.e., inherent time delays and uncertainty.
- xi. The Phase I design report should include a discussion regarding the major design concept as modeled (mechanical and otherwise) with respect to the feasibility for use on today's working rigs? If not, what would be needed to allow implementation?

Additional optional items:

- xii. A design summary video used to outline the design submittal not to exceed five (5) minutes in length. Videos shall be the property of the university, but DSATS shall have the rights to use the videos on its websites and in its meetings or events.

f. Phase I Evaluation

- i. The judges will review the design reports and rank teams using the same criteria as the Phase II evaluation information below.
- ii. The results will be announced in mid-February with comments that teams may want to incorporate into their Phase II efforts.
- iii. The committee will advance as many teams as is economically possible as finalists for Phase II.

E. Design Criteria

a. Overview

Teams will design, create and operate a small-scale rig drill a directional well safely and efficiently. The Drillbotics committee will provide certain information in advance but will not provide the actual well targets until the day of the Phase II test. The following attached pages describe the directional objectives as well as the data/deliverables requirements. Scoring for the directional competition objective will be primarily based on how accurately the directional targets are intersected by the calculated well trajectory. An example of the criteria for scoring is included below.

The end goal is for teams to develop a mini-rig with automated controls to drill autonomously prepare a planned well path once the target points are established. The well directional well should be drilled as close to the targets as is practical, keeping in mind build rates, wellbore tortuosity, and overcoming drilling dysfunctions while operating within the limits imposed by the drilling equipment and drillstring.

b. Objectives

- i. Hit one or more targets at one or more vertical depth(s) and X/Y coordinates
- ii. For the Group B competition, the starting directional plan to hit the targets will not require wellbore inclinations in excess of 30° from vertical, 15° change in azimuth, or 10" displacement (departure from the vertical axis at well center) The max displacement/inclination/azimuth are total/accumulated from the start to the end of the well path.

- iii. Please note: Teams should be prepared to drill any given trajectory within the specified parameters, so the coordinates will not be provided in advance of the test.
- iv. Teams must deal with multiple constraints like those faced by practicing drilling engineers designing difficult wells. Each team should design their own well trajectory plan after receiving competition targets. Their systems should autonomously determine the trajectory, taking into consideration the physical limitations that they have defined for their specific system. If a team feels that their system will not be able to hit the targets, the plan should be designed to get as close to the targets as possible. Judges will assess your assumptions and calculations to see how well you understand the issues. Be sure to explain what testing was done to confirm your assumptions.

c. Rig Design

- i. DSATS envisions a small (perhaps 2 meters high) drilling machine that can physically imitate the functionality of full-scale rig machinery. Since the winning machines will be presented at the SPE conference, there may be height restrictions imposed by the conference facility, so machines that are too tall may not be allowed on the exhibit floor.
- ii. The winning team may need to ship their rig by airfreight to display it at an industry conference. Please give considerable thought to the physical design to reduce the overall dimensions. Designs with a folding and/or telescopic derrick and nested bases can reduce the shipping costs considerably. For this reason, Drillbotics asks students to calculate the “chargeable weight” per section d.vi.1 below, and judges use this figure when comparing team performance.
- iii. The machine will be the property of the university and can be used in future research and competitions. New and novel approaches that improve on existing industry designs are preferred. While innovative designs are welcome, they should have a practical application to drilling for oil and gas.
- iv. The drilling machine will use electrical power from the local grid not to exceed 25 horsepower. Lower power consumption resulting from energy efficient designs will receive additional consideration.
- v. The design must provide an accurate and continuous measurement of Weight-On-Bit (WOB), inclination, azimuth, and depth; as well as other drilling parameters (see Appendix “A” for directional surveying-specific data requirements), that should be presented as a digital record across the period of the test. All depth related measurements shall use the rig floor as the datum, not the top of the rock (the offset between the rock surface and the rig floor must be adequately processed within the control algorithms). Appropriate statistical measurements should be made at frequencies and with an accuracy and appropriate frequency content for the dynamics of the drilling system both at surface and downhole. Discussion of such choices should be included in the design report.

1. Distinguish in all data and documentation the difference between Weight-On-Bit and Hook Load; be specific when referring to these parameters
- vi. A closed-loop fluid circulation system is not required, but could be of advantage for directional drilling, the bit and machinery should be cooled with air or fluid/water if needed. The design of the fluid system, if any, should be included in the Phase I design.
 1. The rock sample will be homogeneous and will be capable of aiding in closed-loop fluid circulation.
 2. Note that the rock samples will leak once the drillbit punctures a rock face, so a rig design that includes a containment system is required.

d. Design Calculations

- i. Design submittal by the students shall include:
 1. Engineering drawings of the rig concept, mechanical and electrical and auxiliary systems, if any
- ii. Design notes and calculations
 1. All engineering calculations shall be included in the Phase I report, even if the rig is built using previous years' designs. This ensures that the 2022 team reviewed and understood the previous design assumptions and calculations.
 2. Calculations should include each formula considered in the design, a reference that shows the origins of the formula, why it was chosen, what engineering assumptions were made, a definition of all variables and the values used in the calculation.

Example:

Buckling limit Euler's Equation (1) cite a reference here or in the reference section of your design report

The critical buckling load, P_{bcr} , is calculated:

$$P_{bcr} = \pi^2 * E * I / (K * L)^2$$

P_{bcr} : Critical buckling load

E : Modulus elasticity of the aluminum drill pipe

I : Area moment of inertia

L : Length of the column

K : Column effective length factor (explain how you chose the appropriate k or n factor)

- iii. The report should include a table that summarizes ALL calculations.

Example

Parameter	Symbol	Calculated Results		Safety Factor	Max Allowable		Reference	(Other as needed)
		Field Units	Metric Units		Field Units	Metric Units		
Critical buckling load								
Burst limit								
Torque limit								
... Other								

- iv. Because the winning team’s rig could be shipped to a different country for display in the SPE booth at the Drilling Conference, the Drillbotics team needs to prepare in advance to provide adequate electrical power for the rig. Please provide a table showing the expected power consumption. Rename devices as appropriate:

Device	Voltage	Current	Estimated		Single or Three ϕ	(Other as needed)
			HP	Watts		
Rotation						
Hoist						
Pump						
... Other						
Controls						
Displays						
...						
Total						

- v. Also provide a diagram showing maximum dimensions of rig when operational (Include all auxiliaries) [Needed to determine size of display area as the Drilling Conference and confirm the height is within the limits imposed by the conference organizers]
- vi. Please calculate and include in your report the “Chargeable Weight” of the rig, including shipping crates/boxes for the rig and auxiliaries
1. The Chargeable Weight of Freight shipments are calculated as the Actual Weight (Gross Weight) or the Volumetric (also called Volume or Dimensional) Weight of the shipment, whichever is the greater. This uses an estimated weight that is calculated based on the dimensions (length,

width and height) of a package (shipments are always shown in the order of L x W x H). Typically, large items with a light overall weight take up more space on an aircraft than a small, heavy item. That's why the shippers charge according to Chargeable Weight.

2. Multiply the length by the width by the height (L x W x H) in inches to obtain the cubic inches, then:
 3. To obtain the dimensional weight in pounds using inches, divide the cubic inch result by 166
 4. To obtain the dimensional weight in kilograms using inches, divide the cubic inch result by 366
 5. Using Dimensions in Centimeters: To obtain the dimensional weight in kilograms using centimeters, multiply the length by the width by the height (L x W x H) in centimeters and divide the result by 6000
- vii. Control system architecture. (The response time of measurements, data aggregation and control algorithms should be estimated.)
 - viii. Key features for any models and control software.
 - ix. Proposed data handling and display.
 - x. Specification for sensors, signal processing and instrumentation, (verifying their accuracy, precision, frequency response and environmental stability), including the methods planned for calibration before and after the Phase II testing.
 - xi. Plan for instrumentation of sensors in the BHA, as well as a method to synchronize all measurements and utilize both the surface and downhole sensors for real-time control of the drilling process.
 - xii. An explanation of the implementation of the output of the BHA sensors to improve the trajectory of the wellbore, drilling efficiency and other drilling concerns.
 - xiii. An explanation of the algorithm used to autonomously control the drilling rig based on the output of the BHA sensors
 - xiv. An explanation of the principles being applied to directionally steer the wellbore and hit the required targets with the intent to score the maximum amount of points
 - xv. Cost estimate and funding plan
 - xvi. A design summary video used to outline the design submittal not to exceed five (5) minutes in length. Videos shall be the property of the university, but DSATS shall have the rights to use the videos on its websites and in its meetings or events.
 - xvii. All design, construction and operation of the project are subject to the terms and conditions of section 13 above.
 - xviii. The Committee) will review the Phase I designs and select the top-ranking teams who will progress to Phase II of the competition.

e. *Automation Requirements*

Drilling mode/survey mode switching must be automated (i.e. built-in survey interval and drill string movement for on/off-bottom, slide/rotation mode switching)

f. Steering

- a. Directional steering is a critical part of the competition for 2022. The wellbore must be started vertically and then kicked off below a specified depth to hit multiple directional targets (at varying X/Y coordinates and vertical depths). Teams score more points based on how accurately each directional target is hit.
- b. The targets for the final test will be provided only on the day of the test.
- c. Steering requirements (e.g., toolface direction, slide length) must be calculated autonomously.
- d. Orientation of the steering mechanism must be calculated by the system with results shown on the rig floor display.
- e. Downhole sensors are mandatory, and it is also mandatory to implement their data into the control algorithm of the rig. A severe penalty will be applied to teams who do not use downhole sensors. Closed loop control of the rig based on downhole data is mandatory in this year's competition and not integrating this data set into the control algorithm is considered a "F- Failing grade" in this year's competition.

g. Surveys

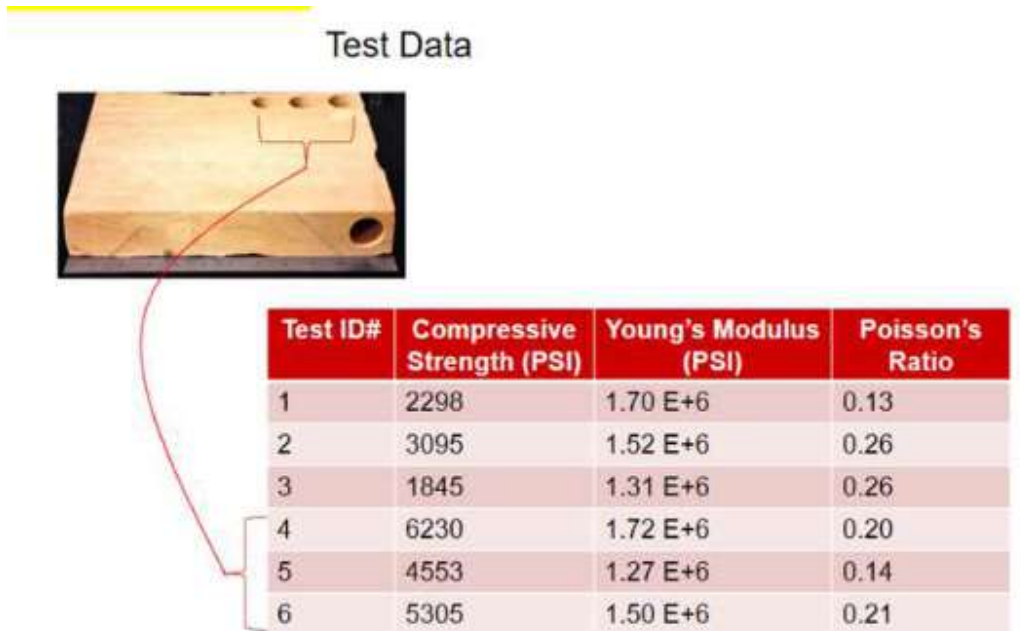
- a. Directional surveying process must be entirely autonomous
- b. Survey qualification must be done autonomously, however secondary qualification/verification/override can be made by a human
- c. Dogleg severity required to hit target(s), distance/direction to plan must be autonomously calculated at each survey station and shown on the rig floor display

h. Deliverables Requirements (Magnetic surveying)

- a. All teams are required to provide a definitive directional survey (TXT, LAS, or CSV format) meeting the following minimum requirements:
- b. Header info to include:
 - i. Team/school name
 - ii. Directional Survey Date
 - iii. Well Center Coordinates (WGS84 Latitude & Longitude)
 - iv. True Vertical Depth Reference (in depth units above block level)
 - v. Grid Convergence
 - vi. Geomagnetic model used (if applicable)
 - vii. Magnetic declination applied (Geomagnetic model or in-field referenced)
 - viii. Total Azimuth Correction
 - ix. Magnetic field dip reference (Geomagnetic model or in-field referenced)
 - x. Total magnetic field strength reference (Geomagnetic model or in-field referenced)
 - xi. Error model associated with well trajectory (ISCWSA/OWSG error model or otherwise)
 1. If non-standard error model is being used (i.e., formulas being modified and/or coefficients being changed), error model description (using standard variable/coefficient naming conventions) and justification must be included in project design

- c. Minimum Curvature calculated trajectory (using appropriate survey station interval to accurately represent the drilled wellbore position)
 - i. Each survey station is to include the following data:
 - 2. Measured Depth
 - 3. Inclination
 - 4. Azimuth (referenced to “block north”)
 - 5. True Vertical Depth
 - 6. Northing (from well center)
 - 7. Easting (from well center)
 - 8. Dogleg Severity
 - ii. Final survey station is to be an extrapolation to total depth at the bit
- i. *Plots*
 - a. All teams are required to provide plan vs. actual plots containing the following minimum requirements:
 - b. As-drilled trajectory and original planned trajectory shown on same TVD vs.
 - c. Vertical Section plot
 - i. Vertical section direction to be determined by well center-to-target bearing
 - ii. As-drilled trajectory and original planned trajectory shown on same X/Y plot
 - iii. Grid north reference to “block north”
 - iv. [0,0] at well center
- j. *Data Logs*
 - a. All teams are required to provide directional survey raw data logs containing the following minimum requirements:
 - b. Each log entry is to include the following data:
 - i. Time stamp (containing year, month, date, hour, minute, second)
 - ii. Sensor measured depth
 - iii. Downhole sensor value(s) recorded
 - Sensor axes values
 - Calculated survey qualifier values
 - iv. Accepted survey indicator (if log entry is an intended survey station)
 - If secondary (i.e., human) qualification is also used, both acceptance indicators must be shown
- k. *Formation/Rock*
 - i. The university and/or students must acquire or produce at their own cost rock samples as needed to verify the design and allow students to practice using their machine prior to the test. Drilling of any samples provided by DSATS prior to Phase II testing is not allowed and could lead to disqualification, except for the pilot hole to be drilled at the test location.

- ii. For the final test, if teams are using rock provided by Drillbotics, the rock properties will depend on the actual sample taken from a quarry in the USA or Europe. A typical sample has the following properties:



- iii. Whether the rock sample is provided by Drillbotics or procured by the team, the sample should be prepared per the following:
 - 1. A homogeneous sandstone samples appx. 12" W x 24" L x 24" H (30 x 60 x 60 cm) for the final demonstration
- iv. Please contact Drillbotics at 2022@Drillbotics.com if you have difficulty obtaining your sample.

l. Targets

The targets will not be available until immediately prior to the Phase II test. However, the starting directional plan to hit the targets will not require wellbore inclinations in excess of 30° from vertical, 15° change in azimuth. Note: This is a maximum. Be prepared for much smaller build rates.

m. Trajectory

Teams shall choose their own trajectory to optimize the drilling, the well path and closeness to the given targets. This should be computed autonomously after the targets are manually entered. Limit the scope to 2-D for both the steering model as well as the formation model for BHA/bit deflection behavior. Optionally, you may add 3-D steering if you need to make course corrections along the nominally 2-D well path.

n. Bits

- i. Upon request, DSATS will send a bit to the finalist teams for use in Phase II. It is expected that the BHA and pipe will cause some difficulty, both for initiating drilling dysfunction and for sensor integration and data telemetry. The judges will look for creative concepts supported by sound reasoning showing an understanding of how the BHA, bit and drillstring function together, and how the downhole system measures, samples and transmits the drilling data.
- ii. Upon request, the bit shall be returned to the Committee following Phase II testing for reconditioning for use in future competitions.
- iii. One (1) PDC bit will be provided by DSATS to be used during the Phase II tests. For 2020-2021 the bit will be:
 1. A micro-bit 1.5" in (38.1 mm) diameter and 2.0" in total length.
 2. Low axial aggressiveness and high side aggressiveness (i.e. high bit anisotropy).
 3. Bits will not be available before mid-April at the earliest.
- iv. Students are encouraged to consider bit wear prior to the final test and its impact on drilling performance during the onsite testing. Based on prior competitions, bit wear should be minimal, but some cutter damage is always possible. **Teams will only receive at most one bit.**
- v. Student teams may build or buy similar drill bits to test their design with the rock samples they sourced. The students must not engage any third parties or receive professional assistance in designing their own bit, however manufacturing can be performed by a third party.
- vi. For the final competition, the students may use the directional drill bit provided by DSATS or use their own bit design. However, the dimensions of their bits must not exceed 1.5 inches in diameter and 2 inches long. This provision is made to enable students to fully optimize the bit design for their specific directional system.

o. Drillstring

i. Drillpipe

1. Preliminary typical tubing specifications for aluminum tubing are listed below to assist with the mechanical and electrical design of the rig. Stainless steel tubing or aluminum tubing is permitted for the competition but must use the same dimensions as below, or the nearest metric equivalent. Teams may choose durability over flexibility and shall explain their choice in the design report.
2. The drill pipe specifications for the 2020-2021 competition are subject to change, but should be:
 - a. Round Aluminum Tube 3/8 inch diameter x 36 inches long; 0.049 inch wall or equivalent
 - b. The material from KS Precision Metals is a typical low alloy material: "Our Aluminum tubing with wall thickness of .035 or .049 is 6061 T6"

3. DSATS will not be providing tubing to the competition teams.
4. The use of a metric equivalent of the tubing is permitted.
5. Tubing is usually available from various hobby shops such as K-S Hobby and Craft Metal Tubing and via Amazon and other suppliers.
<http://www.hobbylinc.com/htm/k+s/k+s9409.htm>

ii. Tool joints

1. Students may design their own tool joints as long as the design concept is included in the Phase I proposal.
2. Alternately, students may use commercially available connectors/fittings attached to the drillpipe using threads, epoxy cement or other material, and/or may use retaining screws if desired, as long as the design concept is included in the Phase I proposal.
3. A fitting used somewhat successfully in 2017 is available from Swagelock. In 2018, the winning team used a fitting from Vertex.
4. A fitting used successfully in 2016, but which did not work well in 2017, is available from Lenz (<http://lenzinc.com/products/o-ring-seal-hydraulic-tube-fitting/hydraulic-straight-connectors>) that uses a split-ring to allow a torque transfer across the fitting.
5. Students must state WHY they choose a tooljoint design in the Phase I proposal.



iii. Bit sub/drill collar/stabilizers

1. It is expected that each team will design and build their own bit sub. Instrumentation of the bit sub is ideal for directional sensors.
2. Additional weight may be added to the bit sub, or surface weight/force (above the rock sample) may be applied to provide weight on bit and drill pipe tension
3. Stabilizers are permitted but will be limited in length at the discretion of the Challenge Committee. Advise the committee of your choice and why and include this in the Phase I design for committee consideration.
4. Students must add sensors to the drillstring but are not permitted to instrument the rock samples. They must have a smaller diameter than the stabilizers and bit by at least 10%. Please include design concepts in the Phase I design.
5. The addition of along-string sensors to measure vibrations, verticality and/or tortuosity or other parameters will receive extra consideration. They must have a smaller diameter than the stabilizers and bit by at least 10%.

p. Automated Drilling

- i. Drilling automation should be considered a combination of data, control AND dynamic modeling so that the control algorithm can determine how to respond to differences between the expected and actual performance. Process state detection can often enhance automation performance. Refer to documents posted on the DSATS website for more information.
- ii. Once drilling of the sample commences, the machine should operate autonomously. Remote operation and/or intervention is not allowed.
- iii. All directional control operations should be autonomously controlled by the drilling rig
 1. Manual intervention to add and/or remove a steering mechanism (e.g., whipstock) is permitted, however the determination/calculation of the orientation setting of the mechanism is required to be autonomous and must be shown on the rig floor display during each steering mechanism manipulation activity
 2. Length and timing of drilling modes (e.g., switching from slide drilling to rotational drilling, initiating the directional surveying procedure at the appropriate survey interval), must be autonomously determined/calculated and controlled
 3. Directional surveys acquired by the system need to be used as feedback for the steering control (and/or calculation of the steering requirements) logic.
- iv. Set-point commands for drilling parameters (WOB, RPM, ROP, etc.) should be optimized such that drilling dysfunctions are avoided, and drilling can be completed within the given time frame. Real-time optimization should be done automatically. The controllers need to ensure that the drilling parameters respond once the set points are altered.

q. Sensors

- i. The team may elect to use existing oilfield sensors or may look to other industries for alternate sensors.
- ii. The team may develop its own sensors if so desired.
- iii. Sensor quality differs from data quality. Both are important considerations in this competition.
- iv. The final report shall address which sensors were selected and why. The sensor calibration process shall also be explained.

r. Data collection and handling

- i. The team may elect to use standard data collection and recording techniques or may develop their own. Data handling techniques and why they were chosen should be described in the Phase I submittal.
- ii. The final report shall address which data systems were selected and why.
- iii. The observed response time of measurements, data aggregation and control algorithms should be compared to the Phase I estimates and published in the final report.

- iv. Describe how data is measured, aggregated, stored and retrieved. Describe calibration and data validation techniques used.
- s. *Data visualization*
 - i. *Novel ways of presenting the data and progress of drilling in real time while drilling will receive particular attention from the judges.*
 - ii. *Visualization of the processes (automation, optimization, drilling state, etc.) should be intuitive and easily understood by the judges, who will view this from the perspective of the driller operating a rig equipped with automated controls.*
 - iii. *Data must be presented in a format that allows the judges to easily determine bit depth, elapsed drilling time, ROP, MSE, verticality/inclination, vibration, and any other calculated or measured variable used to outline the drilling rigs performance to the judges. Lack of an appealing and usable Graphic User Interface (GUI) will be noted to the detriment of the team.*
 - iv. *All depths shall use the industry-standard datum of rotary/kelly bushing interface (RKB), which should be the top of the rig's "drill floor."*
 - v. *An End of Well (EOW) report should be provided to the judges at the conclusion of drilling.*
- t. *Measure and analyze the performance*
 - i. *The drilling machine should react to changing "downhole" conditions to select the optimal drilling parameters for improved performance, as measured by the rate of penetration (ROP), mechanical specific energy (MSE), verticality, cost per foot or meter, and other standard drilling measures or key performance indicators. Adding parameters such as MSE, or similar features, to the control algorithms will receive special attention from the judges.*
 - ii. *Design limits of the drilling machine shall be determined and shall be incorporated in the programming of the controls during the construction phase.*
 - iii. *Downhole measurements from directional sensors are to be used for adjusting drilling parameters and control of drilling machines used to aid in directional drilling*
- u. *Not included in the 2021-2022 competition*
 - i. *The drilling will not include automating the making or breaking of connections. If connections are necessary due to the rig and drillstring design, connections should be made manually, and the time involved with the connections will be included with respect to its effect on drilling performance (rate of penetration reduction).*
 - ii. *A rig move, walking or skidding is not required, but the mobility of the rig will be considered in the design phase.*

F. Phase I Design Report

- a. Teams will submit a detailed report containing detailed literature review, model assumptions, overall plan of the virtual system, including the system architecture, different layers (such as data layer, control layer etc.), mathematical framework for modeling and control schemes, a

plan for implementation, and relevant details. It is preferable to include special section for the API, if other system need to interact with your system. Preliminary results from the virtual drilling rig model should be included, along with a discussion on the results.

- b. There are numerous examples of previous reports on the Drillbotics website. Feel free to use this as a resource. Should a team choose to use the concepts in previous reports in their design, be sure to cite the source of the information to avoid plagiarism concerns.
- c. A safety case shall be part of the Phase I design (see Appendix “B”). Include a review of potential hazards during the planned construction and operation of the rig, and for the unloading and handling of any rock samples or other heavy items. An example of a safety case will be posted on the Drillbotics.com website.
- d. The Phase I design report should include a discussion regarding the major design features proposed (mechanical and otherwise) - are they scalable to today’s working rigs? If not, what would be needed to allow implementation?
- e. The Phase I design report should include a discussion regarding the control scheme and algorithm - How is each individual measurement used in the control code? Are they all given equal weight, and if not, what criteria is used to assign importance? What is the expected response time of the control system’s key components? How will this affect equipment selection? The teams are encouraged to perform control simulations to verify the control scheme.

G. Phase II – Drilling Competition

- a. Phase II Activities
 1. Monthly progress reports are due at the end of each month.
 2. Teams will deliver a pre-recorded presentation for the Phase II test two weeks prior to the test:
 3. The students will present a BRIEF summary of their final design, highlighting changes from their Phase I design, if any. Include an explanation of why any changes were necessary, as this indicates to the judges how much students learned during the design and construction process. Explain what key features have been deployed. Describe novel developments or things learned that were worthwhile. Also include how actual expenses compared with the initial estimate. At some time during your talk, let us know who the team members are and what background they have that pertains to the project. Try to include all your team members as presenters, not just one spokesperson. The committee wants to see if all team members have a good understanding of key issues.
 4. Previous teams used a short PowerPoint presentation of about ten slides or so. Use any format you like.
- b. Phase II Testing
 1. In the spring term of 2022, qualifying teams will build the rig and use it to drill rock samples provided by DSATS. Drilling a deviated well to hit the required targets (see

Appendix “A”), efficiently through the sample while controlling drilling dysfunctions is the primary technical objective of the competition. Scoring of the directional drilling component will be primarily based on the horizontal distance from the target coordinate at which each target vertical depth was intersected. The use of both surface and downhole measurements to control the drilling process in real-time is mandatory, failure to do so will result in a failing grade. To avoid disqualification due to a downhole sensor failure, redundant or immediately replaceable items should be part of the design and implementation. Time to replace a sensor will be added to the drilling time for calculation of ROP.

2. Prior to the start of the test:
 - a. Teams are to use manual control to pre-drill a vertical pilot hole not more than 1” deep measured from the rock’s top face. This hole is to be drilled using the competition drilling rig. Location of this pilot hole will be marked on each sample by the committee at the intersection of two lines drawn from opposite corners of the rock sample. Drillbotics could modify the starting point a few weeks before the contest, so design your rig and rock handline equipment accordingly.
 - b. At their option, teams may use a straight housing for the pilot hole and then replace it with the bent housing for the drilling. Also, it is permitted to use a bit with larger size for the pilot hole.
 - c. Teams may use glue or use a mechanical fastener to attach a bell nipple or diverter housing to the top of the rock to allow connection of a flowline for return mud flow. The maximum allowable length of the bell nipple is 8 inches. If you use a fastener, be careful not to break the rock.
3. The drilling plan will be presented to the teams on the day of competition.
4. Presentations
 - a. The contest will begin with streaming of a pre-recorded presentation by each team. This will be followed by period of questions and answers (Q&A) via on-line or in-person or a hybrid of both. Teams will draw lots to determine the order of presentation. All teams may sit in for the presentations and Q&A of the other teams.
 - b. Depending on the time available, the actual test will start shortly after the last presentation of the day. It is possible that the presentations and tests could take two days to complete.
 - c. The presentations should include the details of the rig and downhole equipment and control schemes. If the team wishes to protect confidential proprietary concepts, please contact the Committee in advance so we can prepare accordingly to shield your ideas.
5. The Test
 - a. When the competition drilling begins, teams will be required to continue to drill the pilot hole vertically to the kickoff point. The kick off point may be at any depth greater than 4” below the surface of the rock. An RSS or AKO motor BHA will be

specified on the day of the competition. Thus, the model should be capable of simulating both steering systems.

- b. All rigs start the drilling competition at the same time.
- c. Navigation shall be done autonomously
- d. Manual intervention to add and/or remove a steering mechanism (e.g., whipstock) is permitted, however the determination/calculation of the orientation setting of the mechanism is required to be autonomous and must be shown on the rig floor display during each steering mechanism manipulation activity. The time to change orientation will affect the team’s ROP calculation.
- e. No lateral forces are allowed to be applied above the top face of the rock.
- f. No forces are allowed to be applied external to the rock that will force the drill bit in a particular direction
- g. External magnetic field effects from the drilling rigs will be present on the directional sensors used to drill the wellbore. The industry has accepted practice of magnetic ranging. This may be a technique worth investigating to improve the signal to noise of magnetic measurements
- h. Once drilling commences, the test will continue until the drill bit exits the rock sample, or three (3) hours, whichever comes first

6. Evaluation

- a. Drilling performance will be observed and measured by Drillbotics judges invited to attend and witness the test. This could be a virtual event depending on travel restrictions. The details will be announced in early April 2022.
- b. DSATS will judge the competitors primarily on their ability to hit the required targets as accurately (i.e. as close to target center at the given target vertical depth) as possible.
- c. With respect to well path tortuosity, judges may insert a “flexible casing” to drift the wellbore to obtain a relative measure of borehole quality.

Scoring of the directional drilling component will be primarily based on the following criteria, with the weighting of individual items as indicated:

Criteria	Parameter	Weighting
Phase I:		
a. Safety	Safety: construction and operation	10
b. Mobility of rig	Rig up, move, rig down	5
c. Design considerations and lessons learned		10
d. Mechanical design and functionality, versatility		25
e. Simulation/Model/Algorithm		25
f. Control scheme	Data, controls, response times	25
	Total	100%
Phase II:		

a. Creative Ability	Analysis, concepts, development	10
B .Engineering Skills	Problem/Goal, design criteria, feasibility	10
c. Construction Quality		10
d. Cost Control		10
e. Performance		30
Various parameters such as:	ROP, MSE, Landing Bit, Inclination, and other	
Are these used within the control algorithms		
Accuracy of drilled wellbore trajectory (see Appendix "A" for details)	Proximity of drilled wellbore to required target X/Y coordinates and vertical depths	
f. Quality of wellbore	Tested using the Go-No-Go flexible 'Casing'	10
	Verticality, tortuosity, caliper, other	
g. Data	Data handling, data visualization, data comparison to judges' wellbore logs, and other	20
h. Downhole Sensor Data Used in Control Algorithm	Pass/Fail	Pass/Fail
	Total	100%
Intangibles	Additional score may be added or subtracted by the judges at their discretion	

H. Final Report and Paper

The finalists shall prepare a project report that addresses the items below. We suggest you use the format of most SPE papers. For reference, please see <http://spe.org/authors/resources/>

- a. The final report is simply an update following the Phase II test to explain what worked and what did not and to discuss future plans that would improve your design. The final report should outline drilling performance and efficiency criteria and measured results.
- b. The winning team in Group B will need to start work on a abstract for their paper shortly after the Phase II test results are announced.
- c. If the abstract is accepted, in August or September, the team needs to start writing their SPE paper. The abstract must generate sufficient interest with the SPE review committees to warrant publication, although DSATS will help promote acceptance elsewhere if necessary.
- d. The timing for submittal of the abstract and paper will be the published deadlines per the call for papers and conference guidelines as posted on the SPE's website (www.spe.org).
- e. The paper should address at a minimum:
 - i. The technical and economic considerations for the control system, rig, and BHA design, including why certain features were chosen and why others were rejected.
 - ii. The setup of the experimental test, the results and shortcomings.
 - iii. Recommendations for improvements to the design and testing procedures.
 - iv. Recommendations for improvements by DSATS of the competition guidelines, scheduling and provided material.
 - v. Areas of learning gained through the competition not covered in the university course material.
 - vi. A brief bio or CV of the team members and their sponsoring faculty.

- vii. Note that the SPE audience already knows a lot of the background information that you presented the judges to demonstrate your capabilities, so adjust the paper content accordingly.

Appendix B: Automation & Interface Design from a Human Factors Perspective

Background on Automation

Any complex, engineered system that is wholly reliant upon human operators to achieve its goal is likely to experience issues. Humans are inconsistent when performing monitoring tasks, they tend to not make wholly rational decisions, are impacted by external factors and are prone to error. As technology advances and complexity increases (such as the control regimes proposed in remote drilling operations for example) such issues become more prevalent. However, many of the issues associated with such complexity can be countered by reallocating certain tasks to automation.

The concept that 'machines' (read automation) are better at some tasks than humans and vice versa has been prevalent for decades. The original incarnation of this notion was presented in 'Fitts List' [Ref. 1]. 'Fitts List' is 11 statements designed to provide guidance on 'what humans are best at' compared to 'what machines are best at' for example:

Humans surpass machines in respect to:

- 'Their ability to improvise and use flexible procedures'

Machines surpass humans in respect to:

- 'Their ability to handle highly complex operations i.e., to do many different things at once'.

Although Fitts List was originally published in 1951, the vast majority of the statements still ring true today (after all humans have changed very little in the last 70 years) but with advances in research and technology, automation is now viewed on a sliding scale (from wholly manual to wholly autonomous) This has recently been subject to consideration by the Drilling Systems Automation Roadmap who have chosen to adopt a 10-point level of automation taxonomy as follows [Ref. 2]:

1. The computer offers no assistance, and the human must do it all
2. The computer suggests alternative ways to do the task and the human selects from those suggestions and executes the task
3. The computer selects one way to do the task, which triggers five possible scenarios including:
 - the human executes that selection
 - the computer executes that suggestion if the human approves
 - the computer allows the human a restricted time to veto before automatic execution
 - the computer executes the suggestion automatically necessarily informs the human
 - the computer executes the suggestion automatically and informs the human only if asked
4. The computer selects the method, executes the task, and ignores the human.

Superficially, for highly complex systems, it may appear that there are very few downsides to providing very high levels of automation with little to no required user input. However, as is often stated, there is no such thing as a 'free lunch' and there are often overlooked downsides to providing high levels of

automation usually termed the 'Ironies of Automation' [Ref. 3] which must be suitably managed. Two examples of this are:

1. Any autonomous system is ultimately conceived and designed by humans – Attempts to design out the human merely shift the responsibility further up the chain. Operators involuntarily inherit the biases and Performance Shaping Factors that influenced the design team.
2. The autonomous system cannot account for unforeseeable scenarios – This is one of the predominant reasons humans remain part of complex systems, to address the 'unknown unknowns'. However, expecting human operators to flip between a passive 'monitoring' role and an active 'doing' role is difficult to achieve, they may be 'out of the loop' and their Situation Awareness may be compromised.

Maintaining appropriate levels of automation and ensuring that your 'projected' drilling operator remains 'in the loop' through good interface design will be one of the key challenges you will face in the Drillbotics competition.

Resources

The following resources have been selected to assist you in the design of your drilling interface and the levels of autonomy you decide upon. Where possible free resources have been chosen (either available through OnePetro or elsewhere on the Internet) but two textbooks have also been selected as they offer an excellent primer on usability heuristics and the importance of good design.

1. de Winter JCF, Hancock PA. Reflections on the 1951 Fitts List: Do Humans Believe Now that Machines Surpass them? *Procedia Manufacturing*. 2015;3:5334–41.
Useful for reference, refer to Table 1 in particular for the original Fitts list.
2. Parasuraman R, Sheridan TB, Wickens CD. A model for types and levels of human interaction with automation. *IEEE Trans Syst, Man, Cybern A*. 2000 May;30(3):286–97.
Automation taxonomy chosen by the DSA.
3. HUMANFACTORS101. The Ironies of Automation [Internet]. *Human Factors 101*. 2020 [cited 2021 Sep 9]. Available from: <https://humanfactors101.com/2020/05/24/the-ironies-of-automation/>
A condensed version of the so called 'ironies of automation' as originally written by Lianne Bainbridge.
4. Norman DA. *The design of everyday things*. Revised and expanded edition. New York, New York: Basic Books; 2013. 347 p.
A seminal text, a little dated in terms of examples but provides great insight into the impact of poor design.

5. Lidwell W, Holden K, Butler J. Universal principles of design: 125 ways to enhance usability, influence perception, increase appeal, make better design decisions, and teach through design ; [25 additional design principles]. rev. and updated. Beverly, Mass: Rockport Publ; 2010. 272 p.
An excellent 'style guide' to assist in designing your drilling interface.
6. Lauche K, Sawaryn SJ, Thorogood JL. Human-Factors Implications of Remote Drilling Operations: A Case Study From the North Sea. SPE Drilling & Completion. 2009 Mar 15;24(01):7–14.
Consideration of the implications of remote drilling operations from an impact on current work practices perspective.
7. Experience WL in R-BU. 10 Usability Heuristics for User Interface Design [Internet]. Nielsen Norman Group. [cited 2021 Sep 9]. Available from: <https://www.nngroup.com/articles/ten-usability-heuristics/>
A condensed take on a number of key usability heuristics.
8. Human factors/ergonomics – Alarm management [Internet]. [cited 2021 Sep 29]. Available from: <https://www.hse.gov.uk/humanfactors/topics/alarm-management.htm>
HSE background information on alarm management and prioritisation.
9. EEMUA Publication 191 Alarm systems - a guide to design, management and procurement. Available from: <https://www.eemua.org/Products/Publications/Digital/EEMUA-Publication-191.aspx>
This is a lengthy publication dedicated to alarm system design, will be useful for additional, wider reading. EEMUA membership is required otherwise the document requires payment.
10. Henderson J, Wright K, Brazier A, Great Britain, Health and Safety Executive. Human factors aspects of remote operation in process plants. Great Britain, Health and Safety Executive; 2002.
Useful background for wider reading.
11. Johnsen SO, Holen S, Aalberg AL, Bjørkevoll KS, Evjemo TE, Johansen G, et al. Automation and autonomous systems: Human-centred design in drilling and well. :150.
Report commissioned by the Petroleum Safety Authority Norway. Very comprehensive with some good case study examples included.

Appendix C: Additional References

- a. Florence, F., Losoya, E., Drillbotics with Fred Florence and Enrique Losoya (2020, August 18), SPE Podcast, [Link](#).
- b. Pessier, R. C., & Fear, M. J. (1992, January 1). Quantifying Common Drilling Problems With Mechanical Specific Energy and a Bit-Specific Coefficient of Sliding Friction. Society of Petroleum Engineers. doi:10.2118/24584-MS
- c. Menand, S., Simon, C., Gerbaud, L., Ben Hamida, M., Denoix, H. J., Cuillier, B., Sinardet, H. (2012, January 1). PDC Bit Steerability Modeling and Testing for Push-the-bit and Point-the-bit RSS. Society of Petroleum Engineers. doi:10.2118/151283-MS
- d. Pehlivan Türk, C., D'Angelo, J., Cao, D., Chen, D., Ashok, P., & Van Oort, E. (2019, March 4). Slide Drilling Guidance System for Directional Drilling Path Optimization. Society of Petroleum Engineers. doi:10.2118/194096-MS
- e. Marck, J., Detournay, E., Perturbation to Borehole Trajectory across an Interface, ARMA-2014-7479, 48th US Rock Mechanics/Geomechanics Symposium, Minneapolis, Minnesota, June 1-4, 2014.
- f. Zalluhoglu, U., Marck, J., Gharib, H., & Zhao Y. (2019) Borehole Propagation with Undergaged Stabilizers: Theory and Validation. ASME Journal of Dynamic Systems, Measurement and Control, vol. 141, no. 5: 051013. doi: 10.1115/1.4042380
- g. Perneder, L., Marck, J. and Detournay, E., 2017. A model of planar borehole propagation. SIAM Journal on Applied Mathematics, 77(4), pp.1089-1114. doi: 10.1137/16M1094518
- h. Zalluhoglu, U., Demirer, N., Marck, J., Gharib, H., & Darbe, R. (2019) Steering advisory system for rotary steerable systems. SPE/IADC Drilling Conference and Exhibition, 5-7 March, The Hague, The Netherlands. SPE-194090-MS, doi: 10.2118/194090-MS
- i. Zalluhoglu, U., Gharib, H., Marck, J., Demirer, N., & Darbe, R. (2019) Steering advisory system for mud motors. SPE/IADC Drilling Conference and Exhibition, 5-7 March, The Hague, The Netherlands. SPE-194077-MS. doi: 10.2118/194077-MS
- j. Franklin, G. F., Powell, J. D., Emami-Naeini, A., & Powell, J. D. (1994). Feedback control of dynamic systems, 3rd Edition, Reading, MA: Addison-Wesley.
- k. Ogata, K. (2003). System dynamics, 4th Edition, Upper Saddle River, NJ: Prentice Hall.
- l. Ogata, K. (2009). Modern control engineering, 5th Edition, Upper Saddle River, NJ: Prentice Hall.
- m. Li, Y., Ang, K. H., & Chong, G. C. (2006). PID control system analysis and design. IEEE Control Systems Magazine, 26(1), 32-41.
- n. Rawlings, J. B. (2000). Tutorial overview of model predictive control. IEEE control systems magazine, 20(3), 38-52.
- o. Webinar: Machine Learning and Physics-based Solutions for Drilling Automation by SPE Distinguished Lecturer Prof. John Hedengren, Brigham Young University, YouTube [Video](#).
- p. Webinar: Drilling Automation and Downhole Monitoring with Physics-based Models. [Link](#).
- q. Video and Webinar Series: Understanding Control Systems by Mathworks. [Link](#).

Bowtie Diagrams

In this appendix, the bowtie diagrams for the other three risks identified are displayed in Figure B.1 Figure B.2 Figure B.3 :

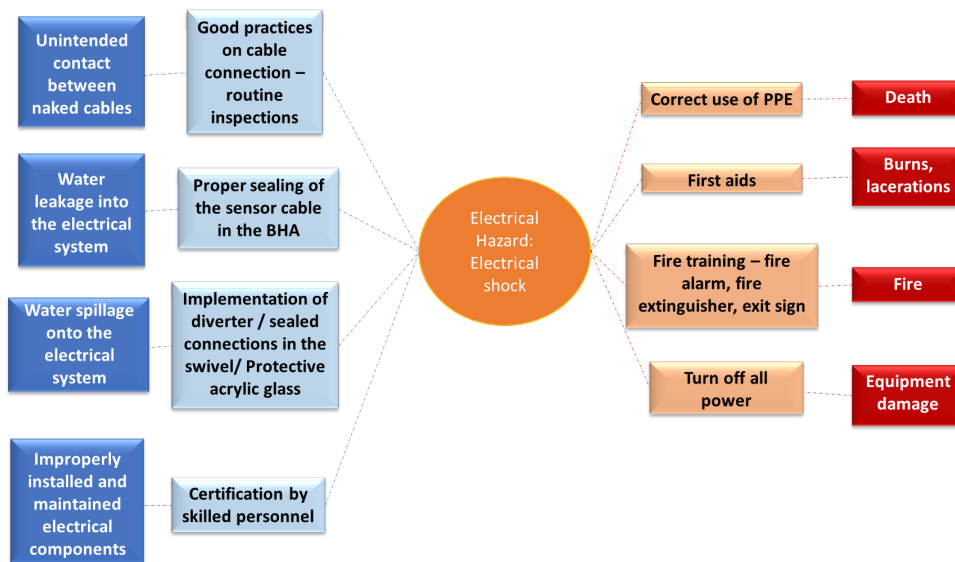


Figure B.1: Bow Tie Analysis for an electrical shock event.

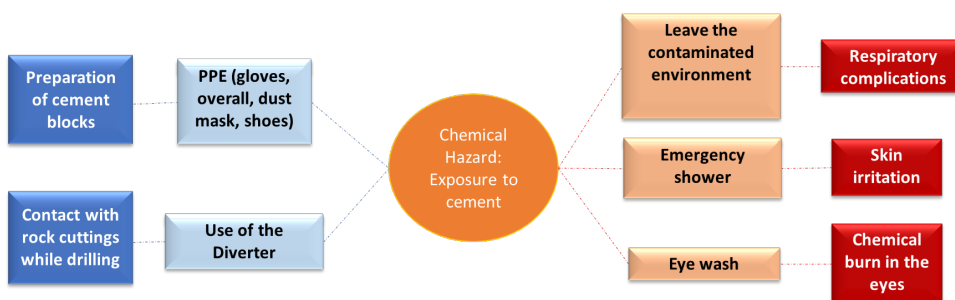


Figure B.2: Bow Tie Analysis for a cement related event.

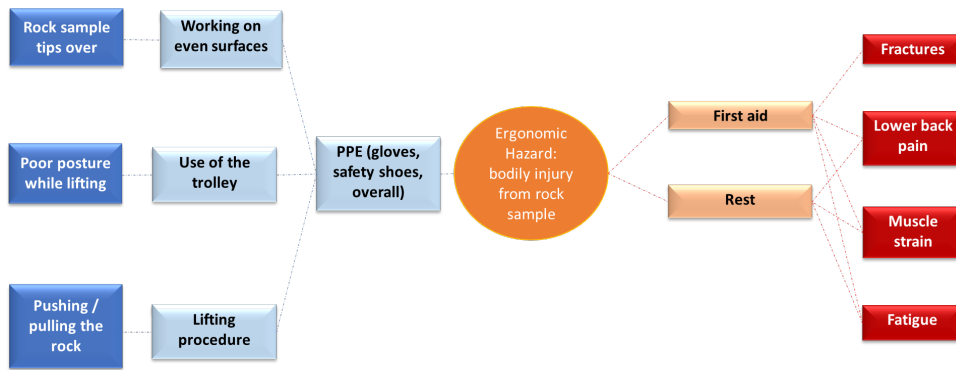


Figure B.3: Bow Tie Analysis for a rock handling event.

Cuttings Transportation Derivation

Searching to optimize hole cleaning, the drilling fluid must be efficient at removing the cuttings and cavings out of the wellbore. In order to achieve this, the design of the fluid must guarantee that the viscous drag forces and the buoyant forces are greater than the slip velocity and the gravitational forces. The aforementioned concepts will be discussed in the following equations [40].

The gravitational force is calculated as follows:

$$W = -\rho_s \frac{\pi}{6} d_s^3 g \quad (C.1)$$

where $W[N]$ is the gravitational force, $\rho_s[kg/m^3]$ is the density of the cuttings, $d_s[m]$ is the cutting diameter and $g[m/s^2]$ is the gravity.

then, Equation C.2 is used to calculate the buoyant force acting on the particle:

$$F_b = \rho_f \frac{\pi}{6} d_s^3 g \quad (C.2)$$

Where $F_b[N]$ is the buoyant force and $\rho_f[kg/m^3]$ is the density of the drilling fluid. Finally, the viscous drag force acting on the particle can be calculated with [40]:

$$F_d = 3\pi\mu_f d_s v_{sl} \quad (C.3)$$

where $\mu_f[Pa\cdot s]$ is the fluid viscosity and $v_{sl}[m/s]$ is the slip velocity.

Once the gravitational, buoyant and viscous forces have been obtained, the Newton's First Law of motion is used to calculate the slip velocity v_{sl} of the cuttings.

$$\sum F = W + F_b + F_d = 0 \quad (C.4)$$

$$v_{sl} = \frac{d_s^2 g (\rho_s - \rho_f)}{18 \mu_f} \quad (C.5)$$

Equation C.3 and Equation C.5 are only valid for Newtonian fluids in a laminar flow regime. For other flow regimes, the shear drag force is given by [23]:

$$F_d = f \frac{\pi}{8} d_s \rho_f v_{sl}^2 \quad (C.6)$$

where $f[-]$ is an empirical value known as friction factor, obtained with Figure C.1. The cutting particles are assumed to be completely spherical, thus $\Psi = 1$.

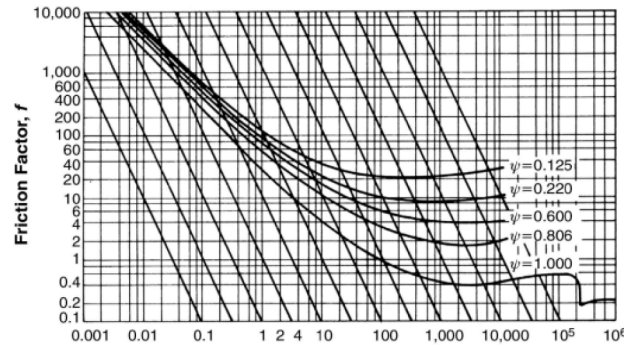


Figure C.1: Relationship between Re and f for settling particles in Newtonian fluids [22].

The Reynolds number $Re[-]$, is obtained using Equation C.7, once the slip velocity, $v_{sl}[m/s]$, has been obtained with Equation C.5.

$$Re = \frac{\rho_f v_{sl} d_h}{\mu_f} \quad (C.7)$$

Where d_h is the hydraulic diameter. For the space between the pipe and the borehole, or annular section, this is calculated with:

$$d_h = OD_{hole} - OD_{DP/BHA} \quad (C.8)$$

The hydraulic diameter for the flow inside the drill pipe or BHA is defined by:

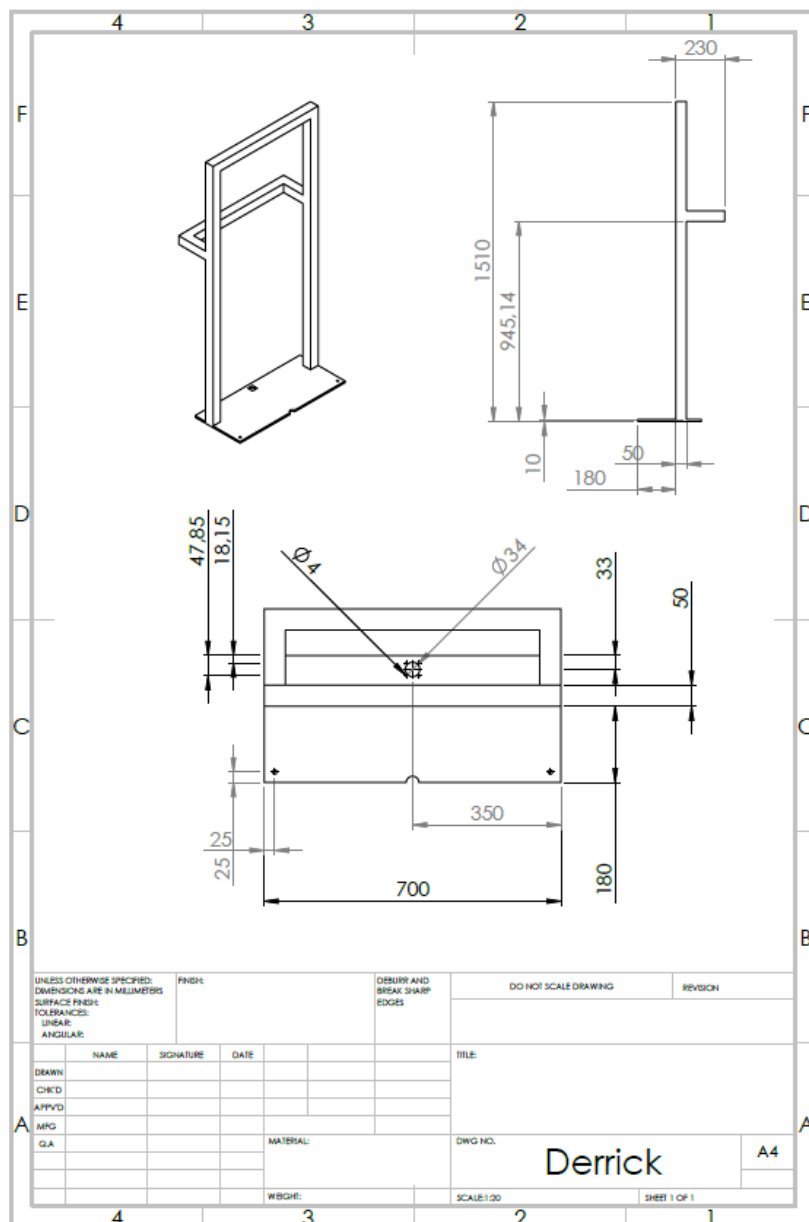
$$d_h = ID_{DP/BHA} \quad (C.9)$$

The slip velocity of a cutting particle in any flow regime is then obtained with the combination of Equation C.4 and Equation C.6 [40]:

$$v_{sl} = \sqrt{\frac{4(\rho_s - \rho_f) g d_s^2}{3f \rho_f}} \quad (C.10)$$

Appendix D

Rig Derrick



Appendix E

Hoisting Motor

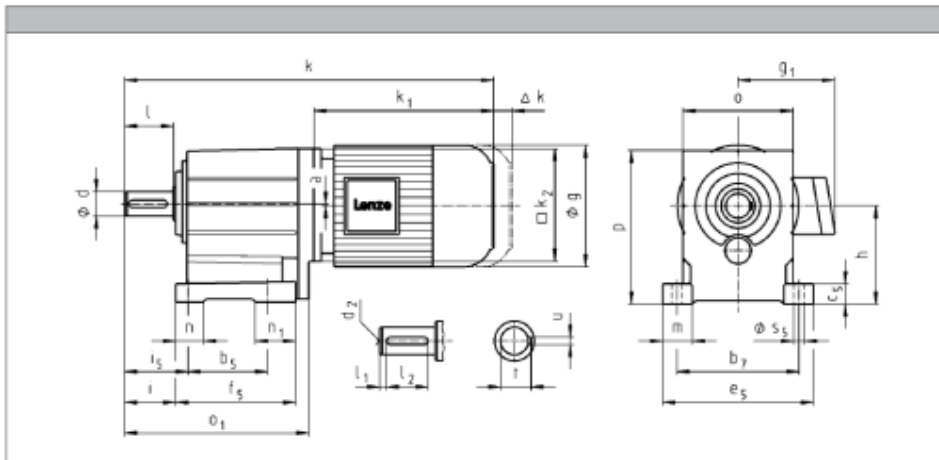
GST helical gearboxes

Technical data



Dimensions

GST□□-2M VBR



	063C42	071C11	071C13 071C31	071C32	071C33	071C42	080C13 080C33
g	123			139			156
B1	MDEMAYX MDSMAXX	100		109			150
	MDEMABR MDSMABR	107		118			132
k1	MDEMAYX MDSMAXX	187		207			224.5
				120			145
Δ k	MDEMABR MDSMABR	40		52			73
	MDFMAXX MDFMABR	170		128 165			183
k							
GST03	329			349		349	
GST04	371			391			413
GST05	401			421			443
GST06	427			447			469
GST07							525

Appendix **F**

Top Drive Motor

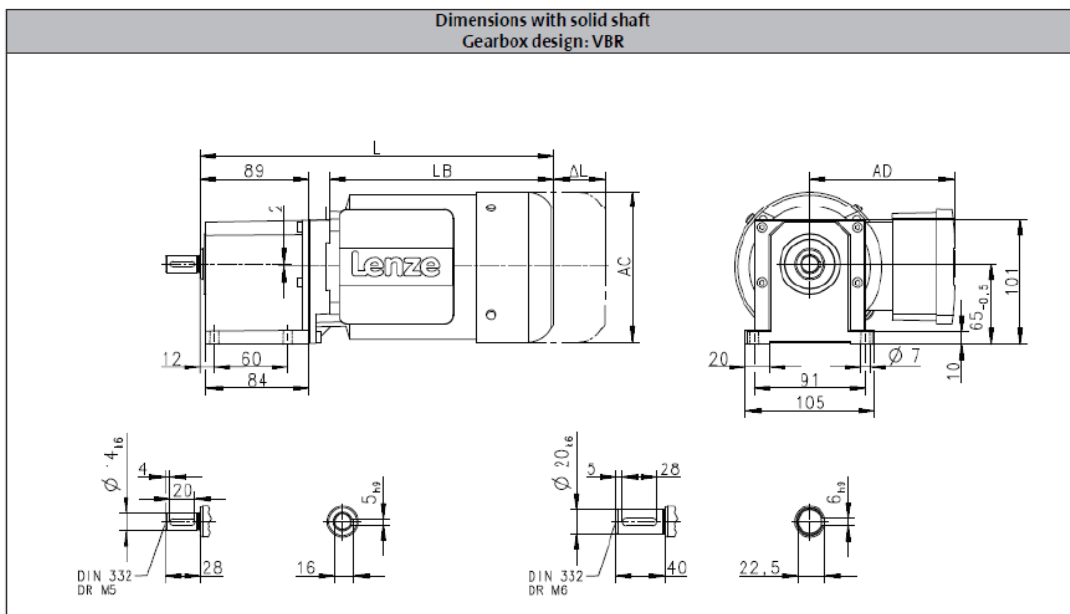
g500-H helical geared motors

Technical data



Dimensions, 4-pole motors

g500-H45



Motor data MF

Technical data



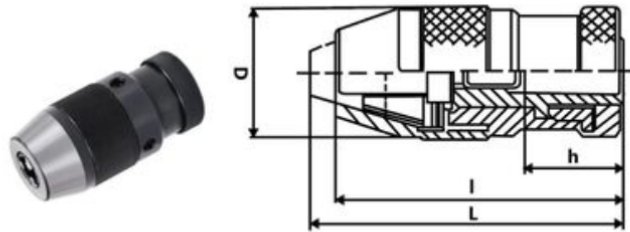
Rated data for 120 Hz

4-pole motors

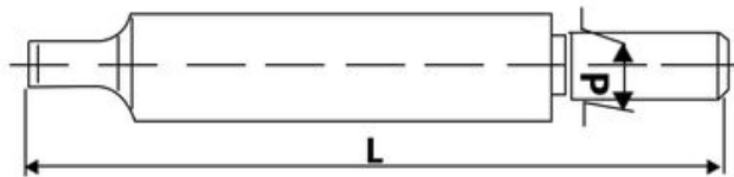
Product	P_N	n_N	M_N	M_{max}	$J^1)$	$m^1)$
	[kW]	[r/min]	[Nm]	[Nm]	[kgcm ²]	[kg]
MF□MA□□063-32	0.55	3440	1.53	6.00	3.70	4.40
MF□MA□□063-42	0.75	3400	2.11	8.00	3.70	4.40
MF□MA□□071-32	1.10	3490	3.01	12.0	12.8	6.40
MF□MA□□071-42	1.50	3450	4.15	16.0	12.8	6.40
MF□MA□□080-32	2.20	3500	6.00	24.0	28.0	11.0
MF□MA□□080-42	3.00	3480	8.20	32.0	28.0	11.0
MF□MA□□090-32	4.00	3480	10.9	44.0	32.0	18.0
MF□MA□□100-12	5.50	3525	14.9	60.0	61.0	26.5
MF□MA□□100-32	7.50	3515	20.3	80.0	61.0	26.5
MF□MA□□112-22	11.0	3530	29.7	120	107	38.0

Appendix G

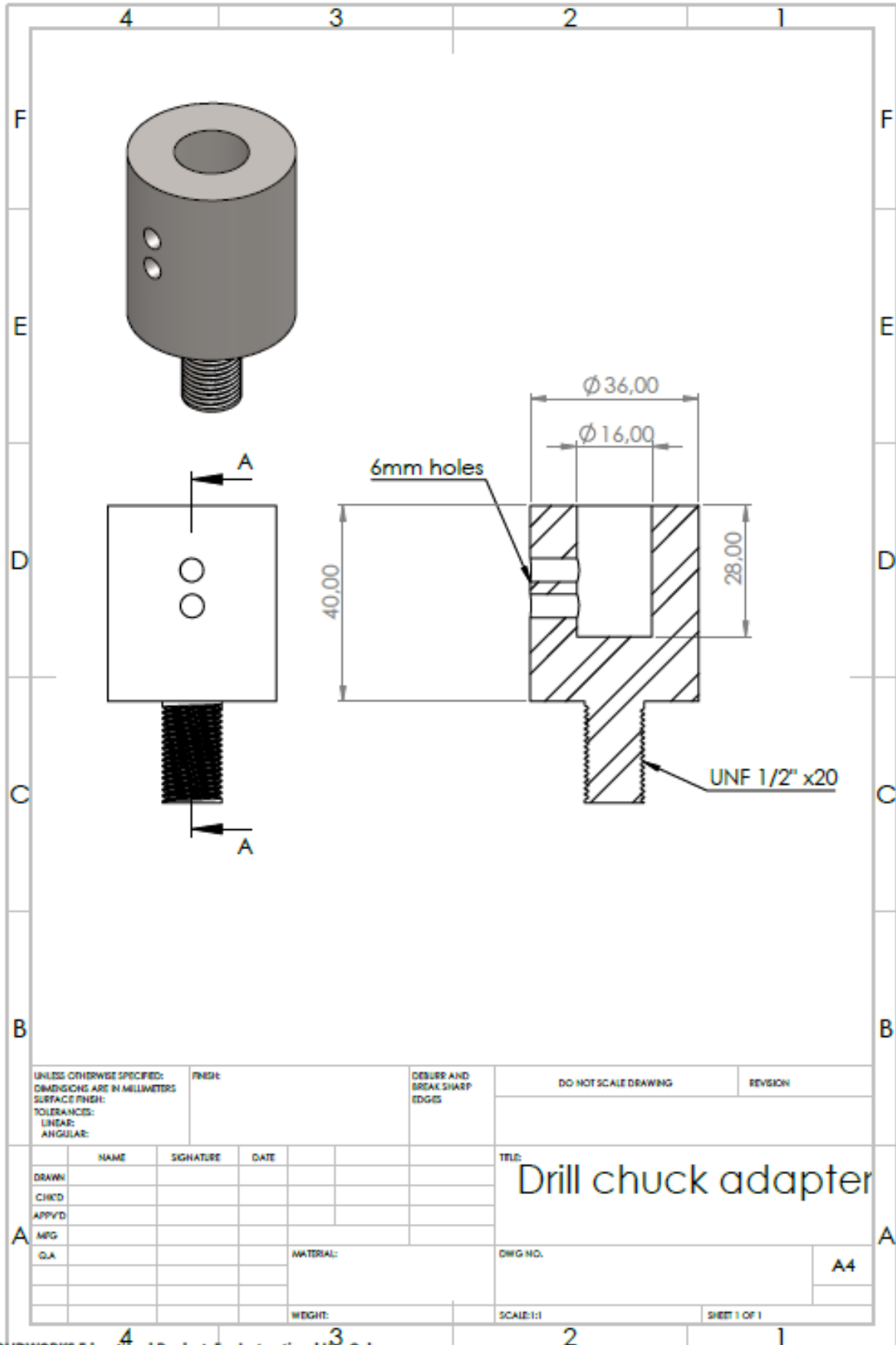
Drill Chuck



Capacity	Taper	h	D	L	l
1-13	B16	24	44	97	88



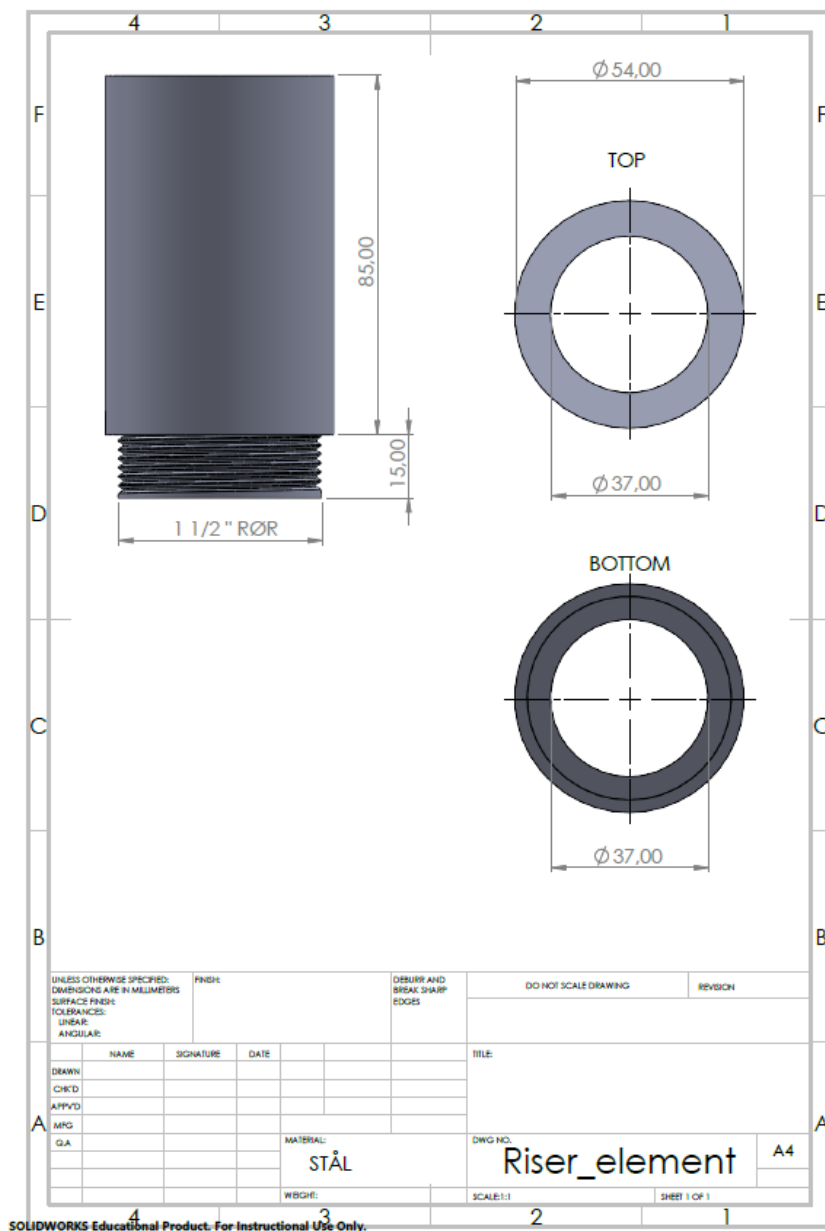
L	d
112	15.733



SOLIDWORKS Educational Product. For Instructional Use Only.

Appendix H

Riser

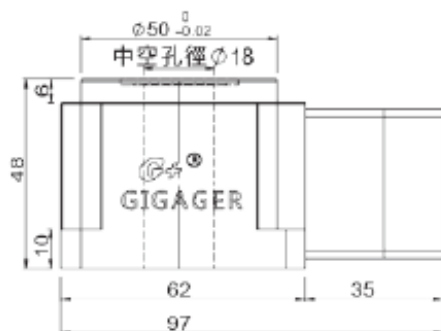
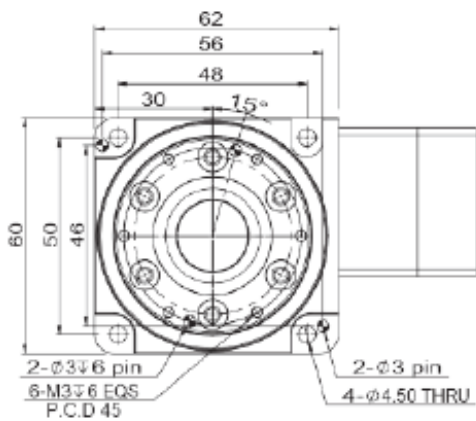


SOLIDWORKS Educational Product. For Instructional Use Only.

Appendix I

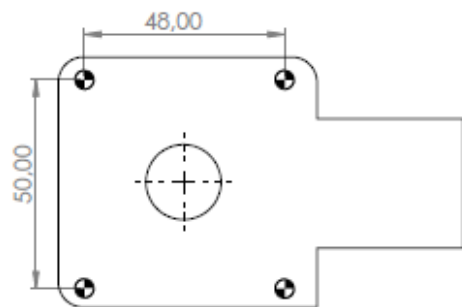
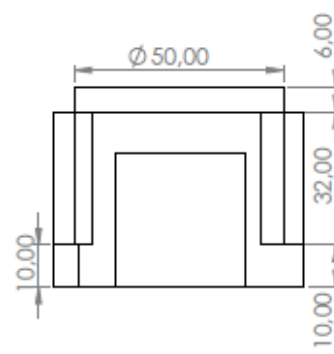
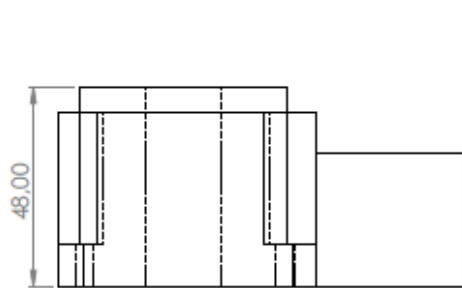
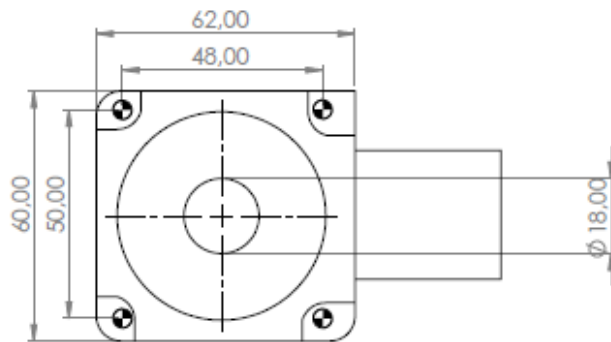
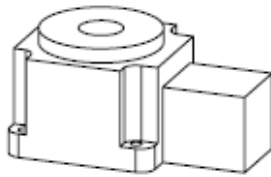
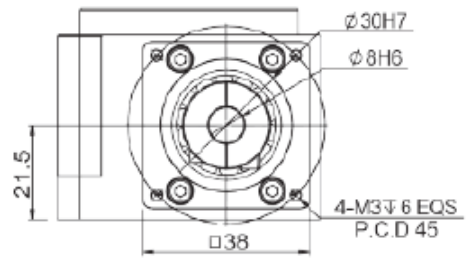
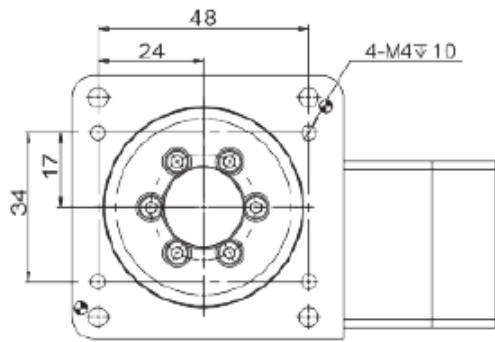
Hollow Shaft Gearbox

Series	Size	Ratio	Motor Model				
GSH	60	30K	SV1				
	<table border="1"> <tr><td>60</td></tr> <tr><td>100</td></tr> <tr><td>150</td></tr> <tr><td>200</td></tr> </table>	60	100	150	200		<p>SV1 : Servo Ø8 PCD45,M3 SV2 : Servo Ø8 PCD46,M4 suit for any brand 100W AC servo motor</p> <p>ST1 : Stepper Ø5 PCD43.8,M3 ST2 : Stepper Ø6 PCD43.8,M3 suit for any brand 42 stepper motor</p>
60							
100							
150							
200							



Parameter

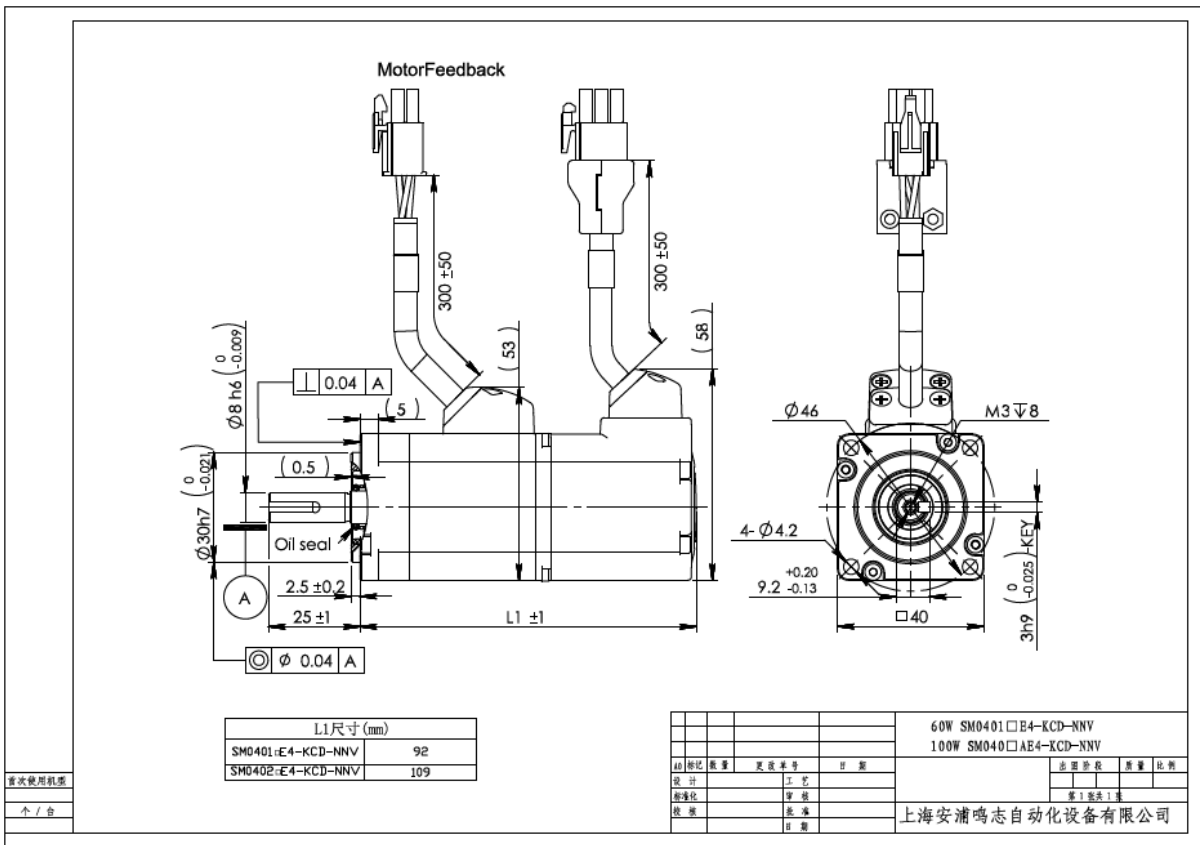
Bearing		Cross Roller Bearing
Permissible Torque	N m	30
Permissible Table Surface Speed	rpm	90
Gear Ratio	i	30
Repeatability	arc-sec	≤ 10
Positioning Accuracy	arc-sec	≤ 50
Permissible Axial Load	N m	300
Table Flatness	mm	≤ 0.01
Table Concentricity	mm	≤ 0.01
Precision Life hr (Intermittent)		30000
IP Grade	IP	40
Weight	kg	0.9



SOLIDWORKS Educational Product. For Instructional Use Only.

Appendix J

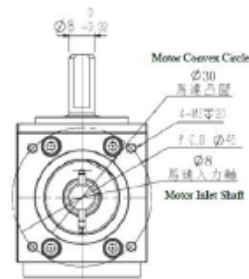
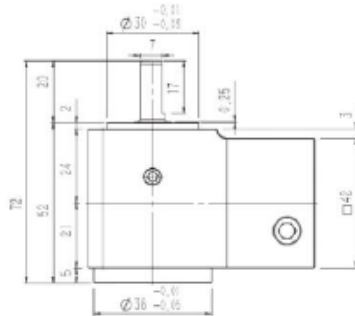
Azimuth Servo Motor



Appendix **K**

Azimuth Right Angle Gearbox

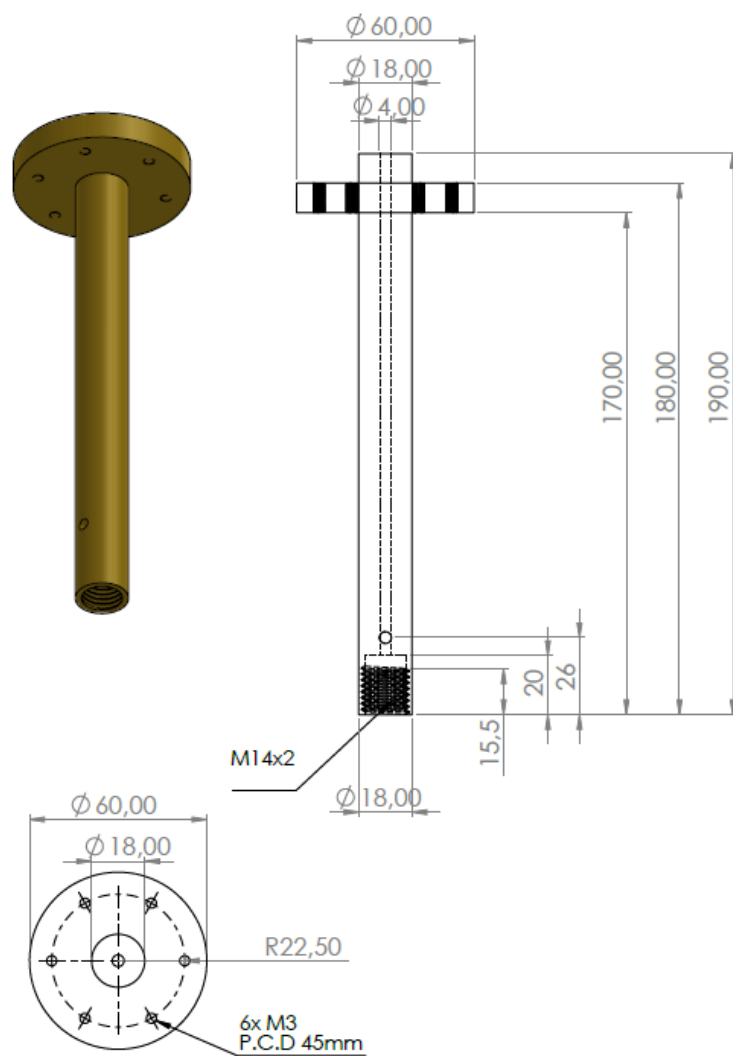
■ GSZ42-03K-SV



Parameter		
Gear Ratio	1:3	
Permissible Torque	N.m	12
Destructive torque	N.m	40
Permissible Input Speed	rpm	2500
Backlash	min	0.5
Weight	kg	0.45

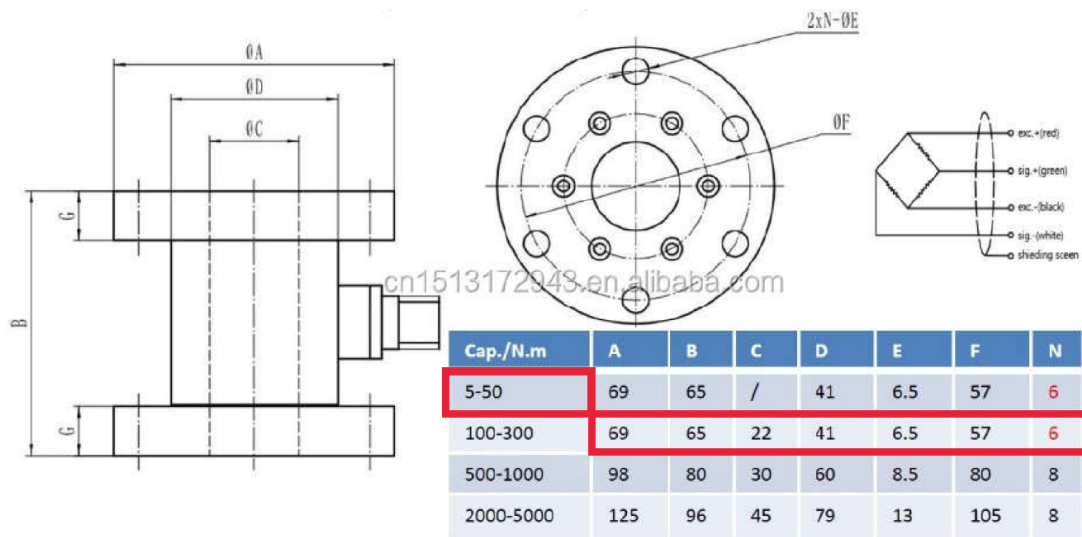
Appendix **L**

T-Shaft

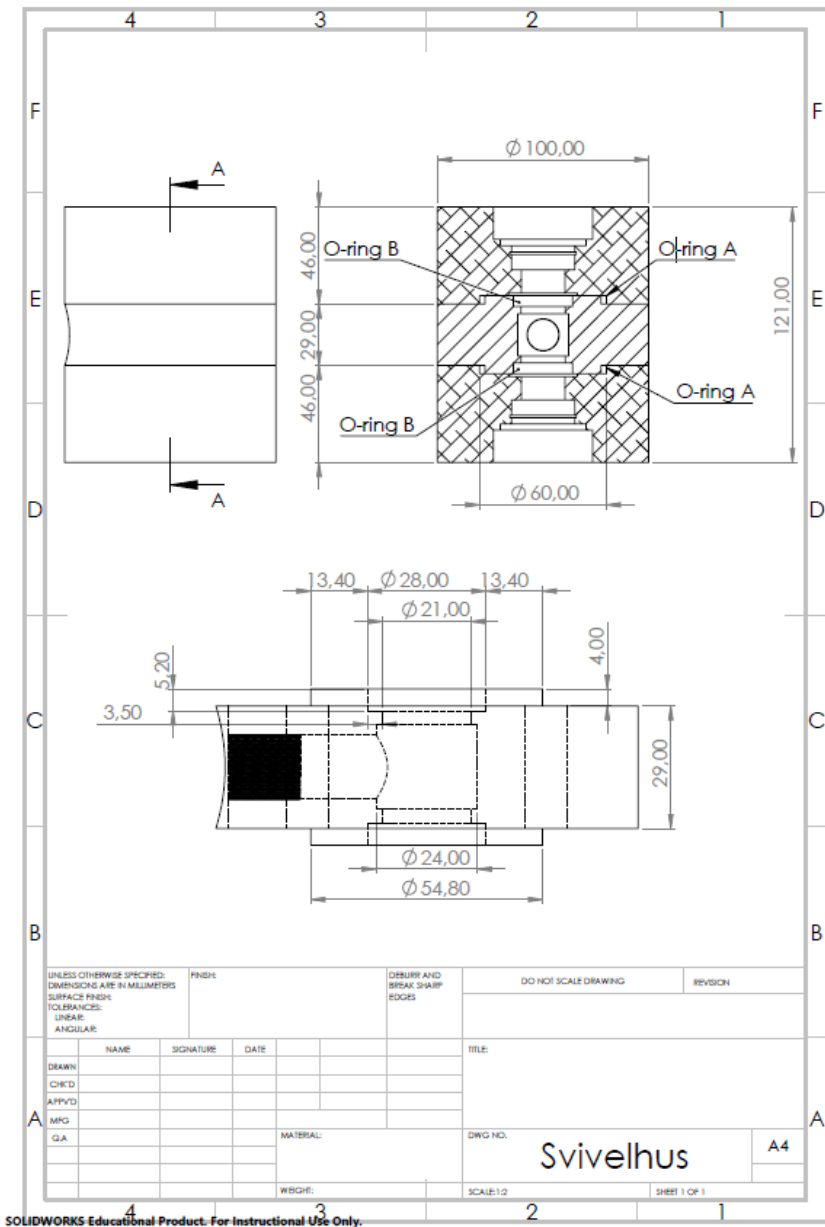


Appendix M

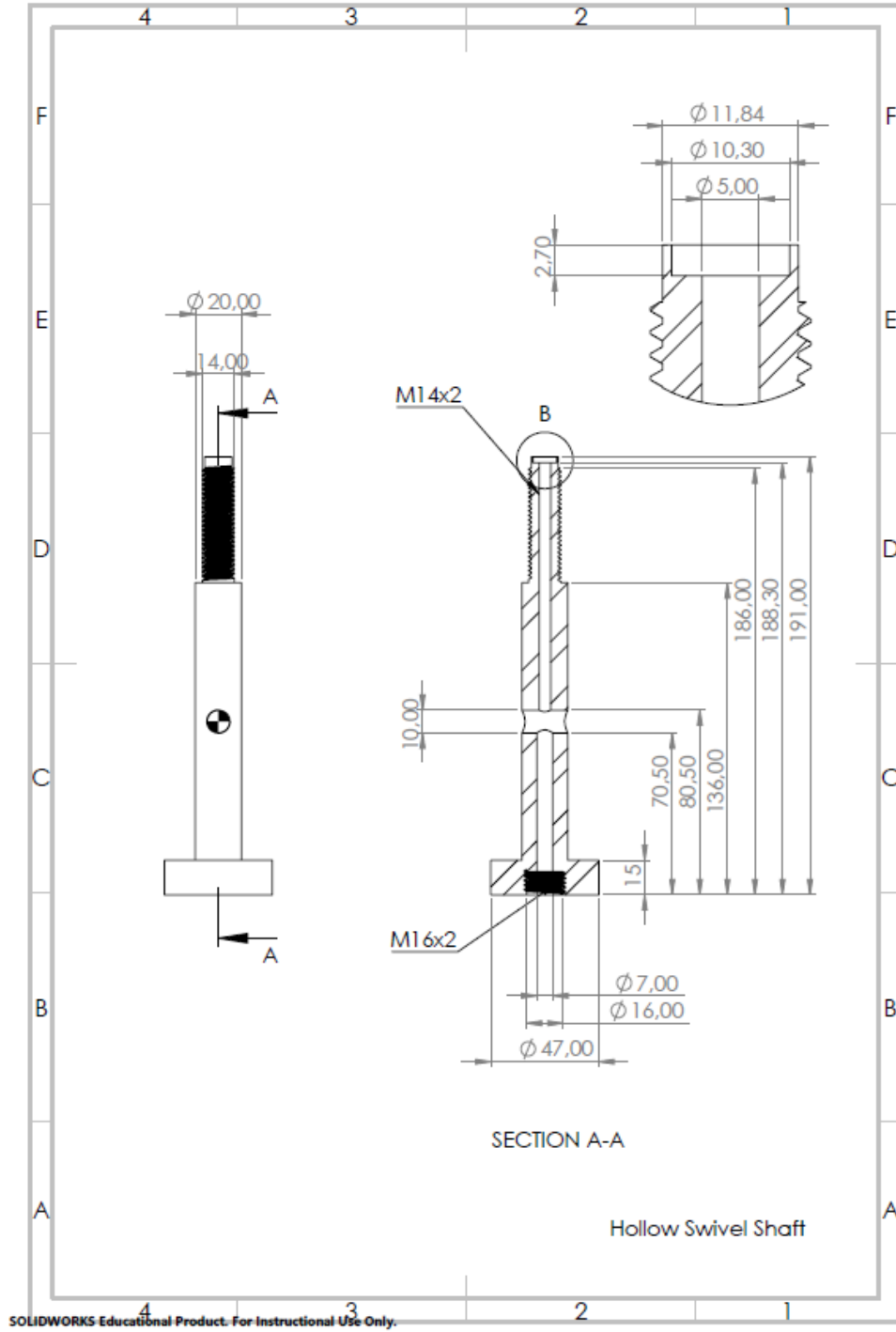
Torque Sensor



Hydraulic Swivel

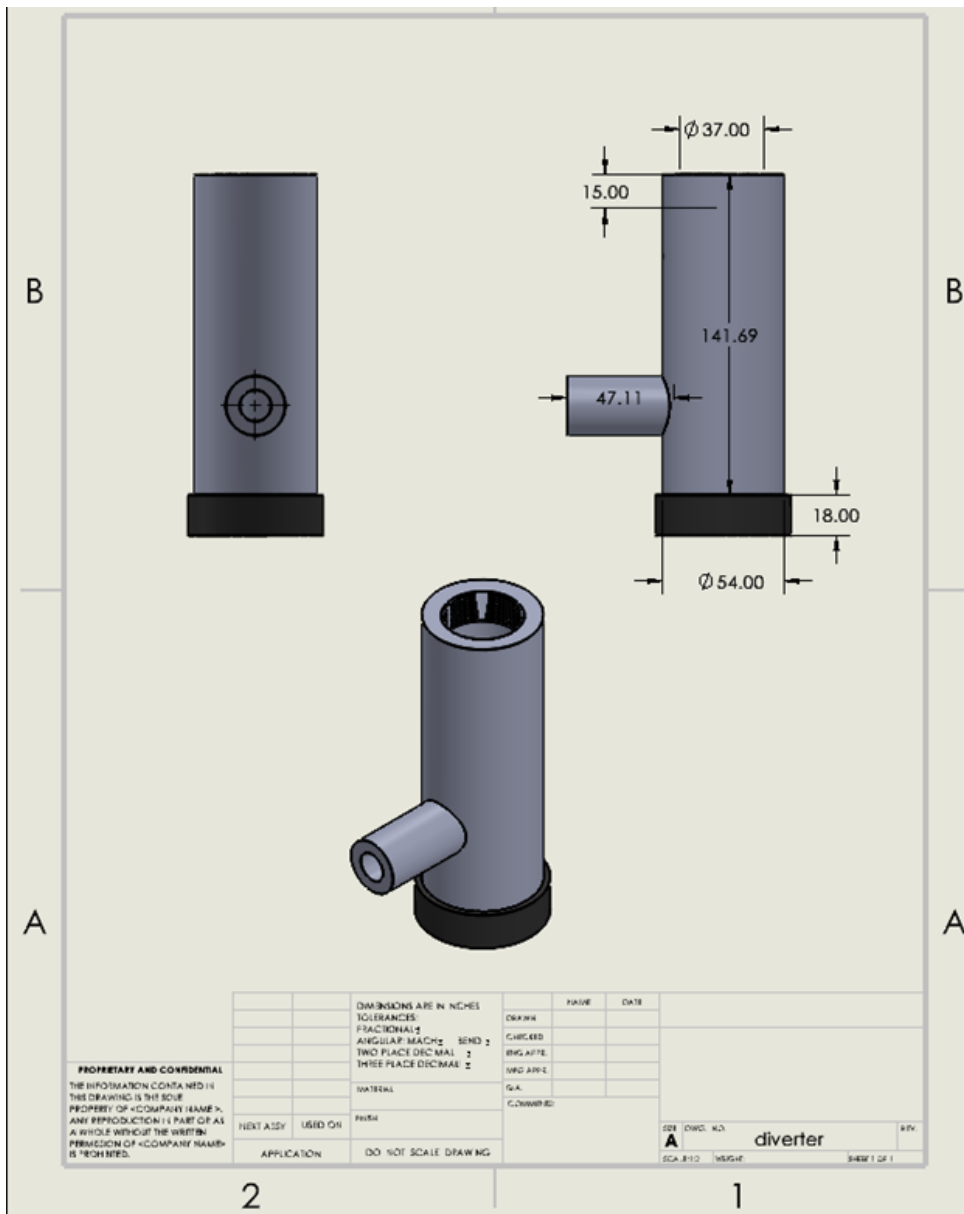


SOLIDWORKS Educational Product. For Instructional Use Only.



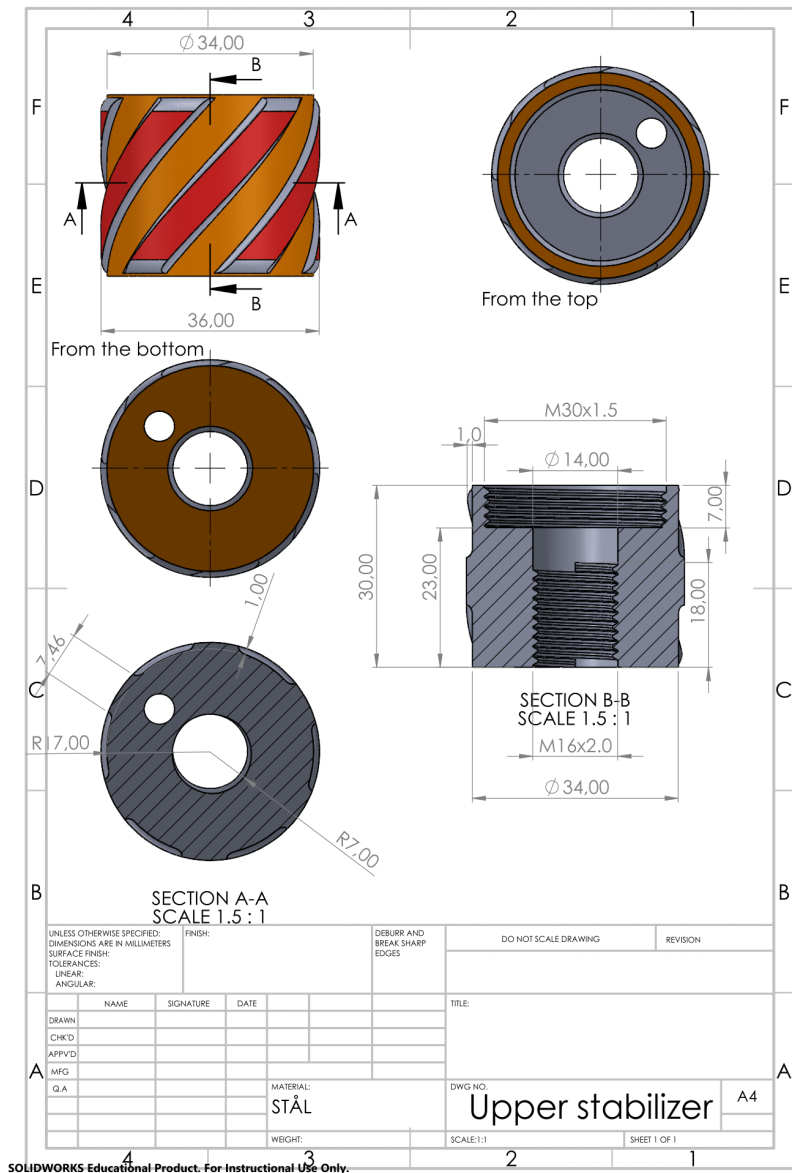
Appendix O

Diverter Design

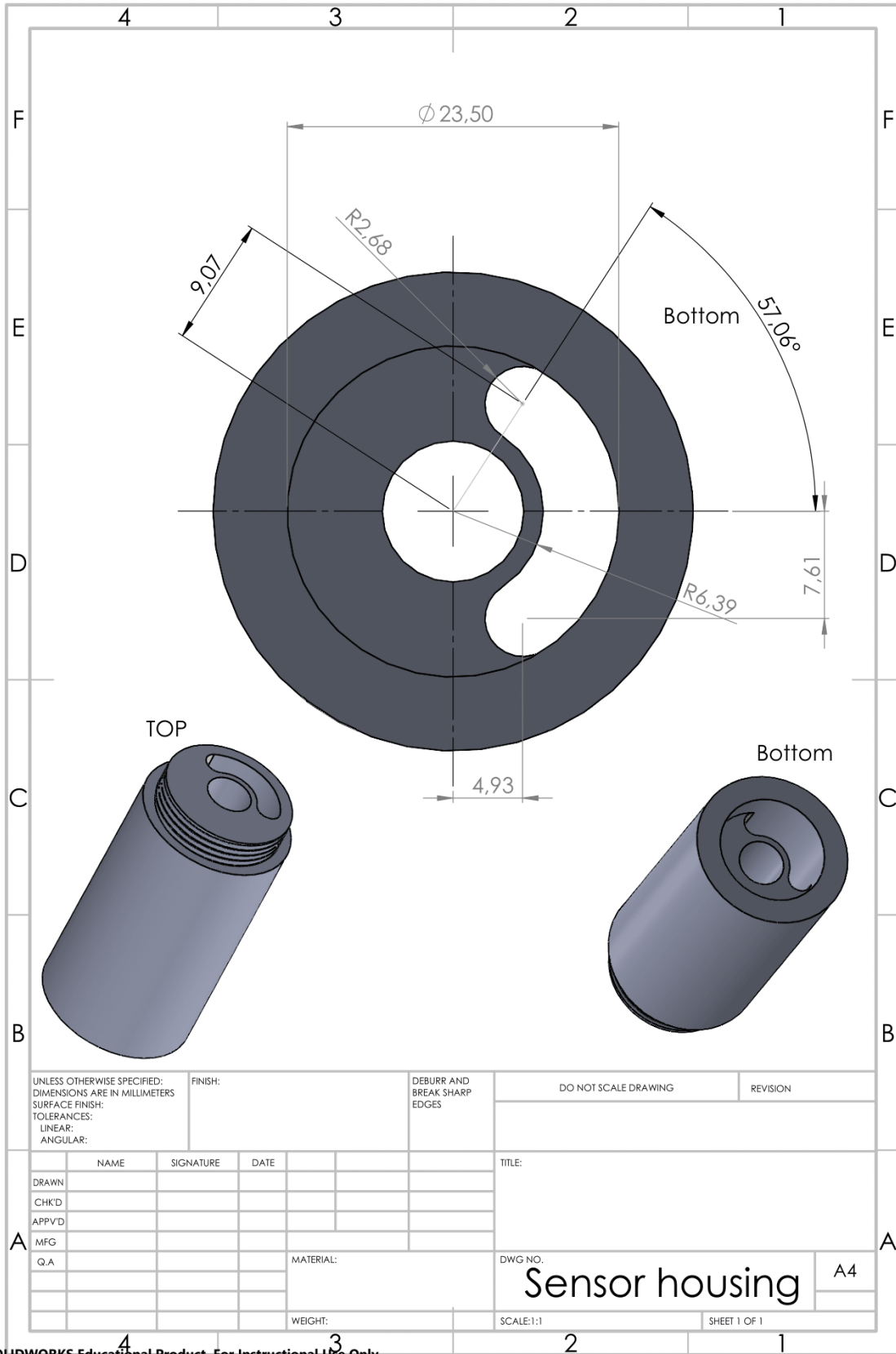


Appendix P

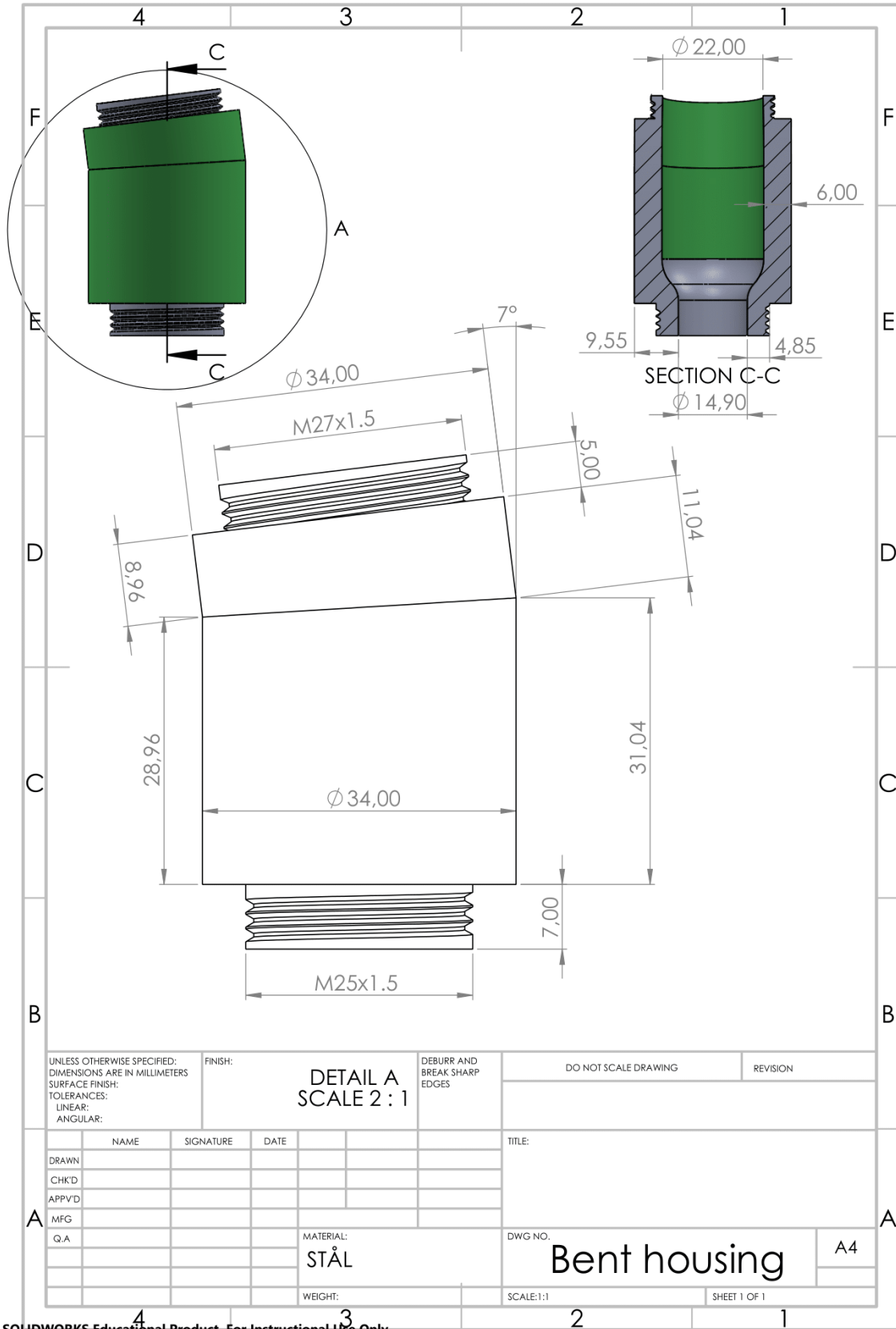
BHA Components



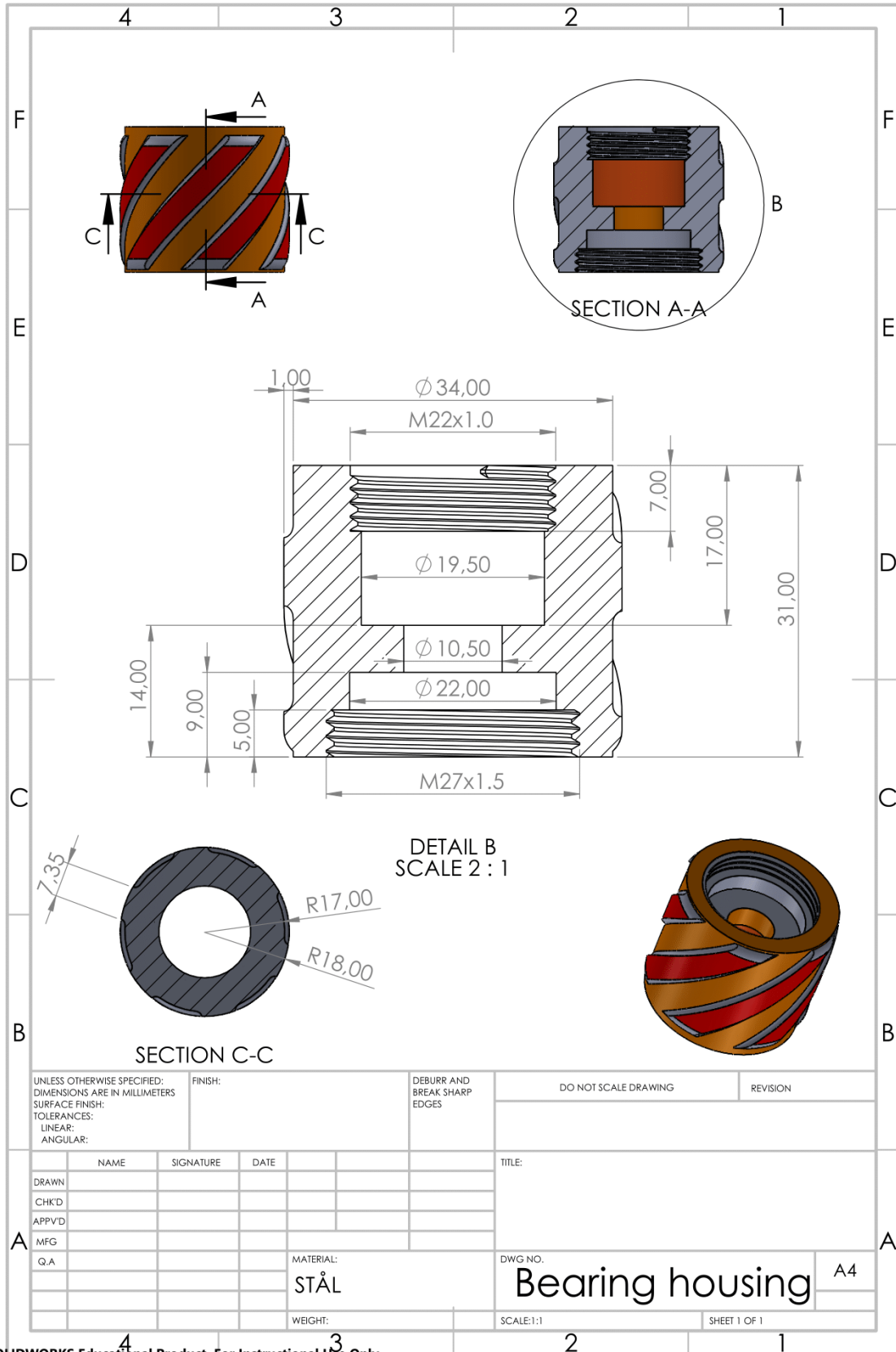
SOLIDWORKS Educational Product. For Instructional Use Only.



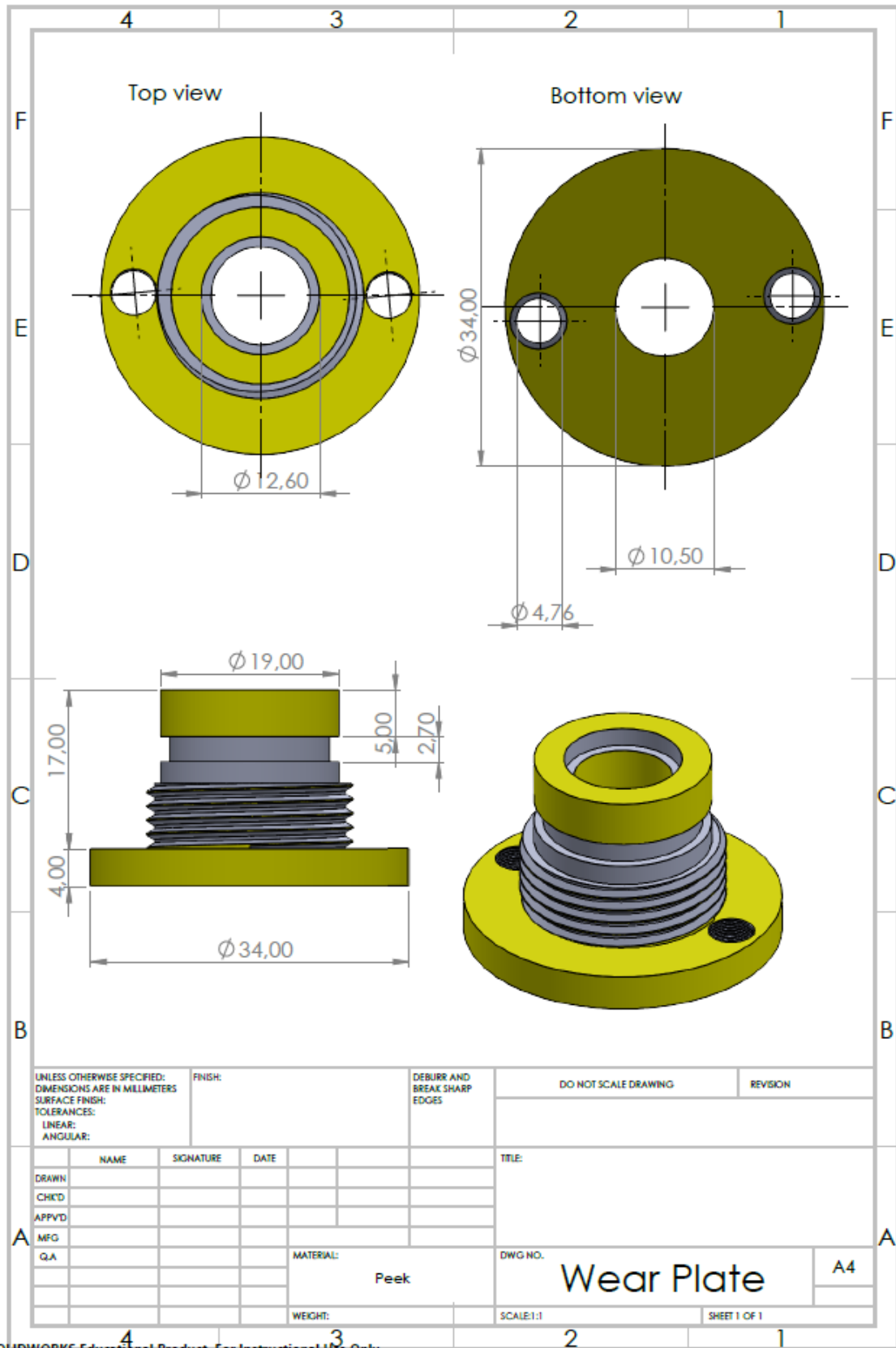
SOLIDWORKS Educational Product. For Instructional Use Only.



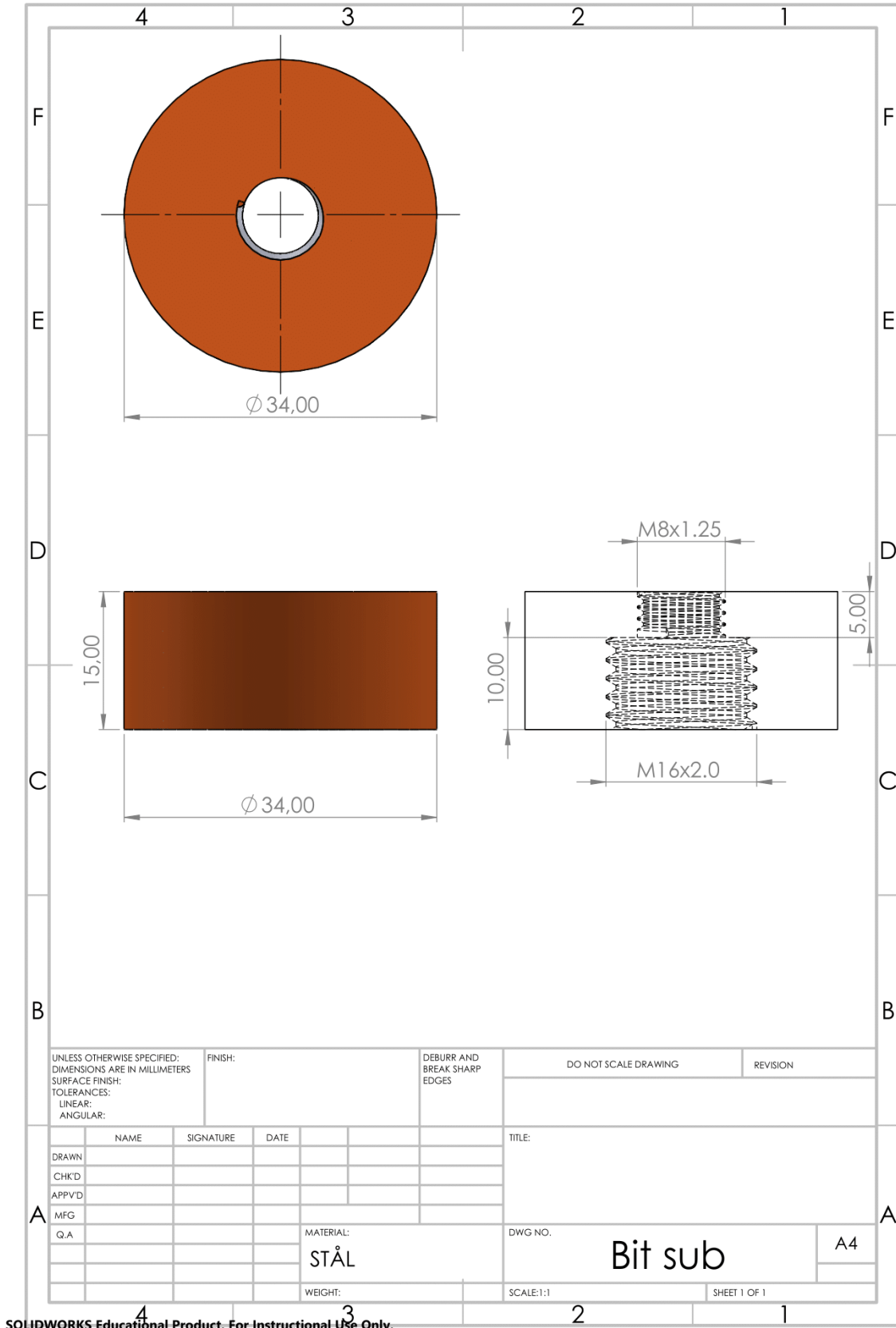
SOLIDWORKS Educational Product. For Instructional Use Only.

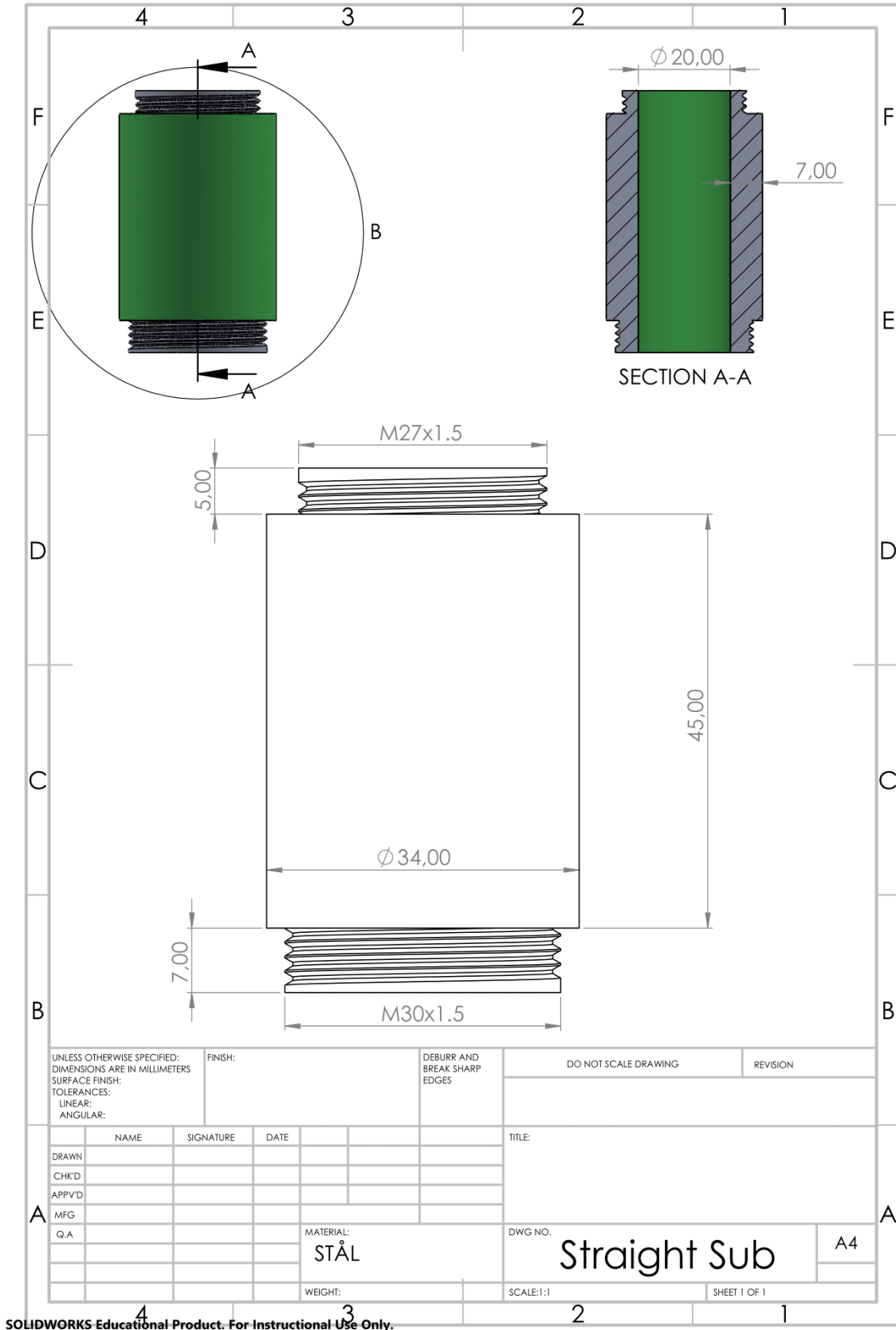


SOLIDWORKS Educational Product. For Instructional Use Only.



SOLIDWORKS Educational Product. For Instructional Use Only.

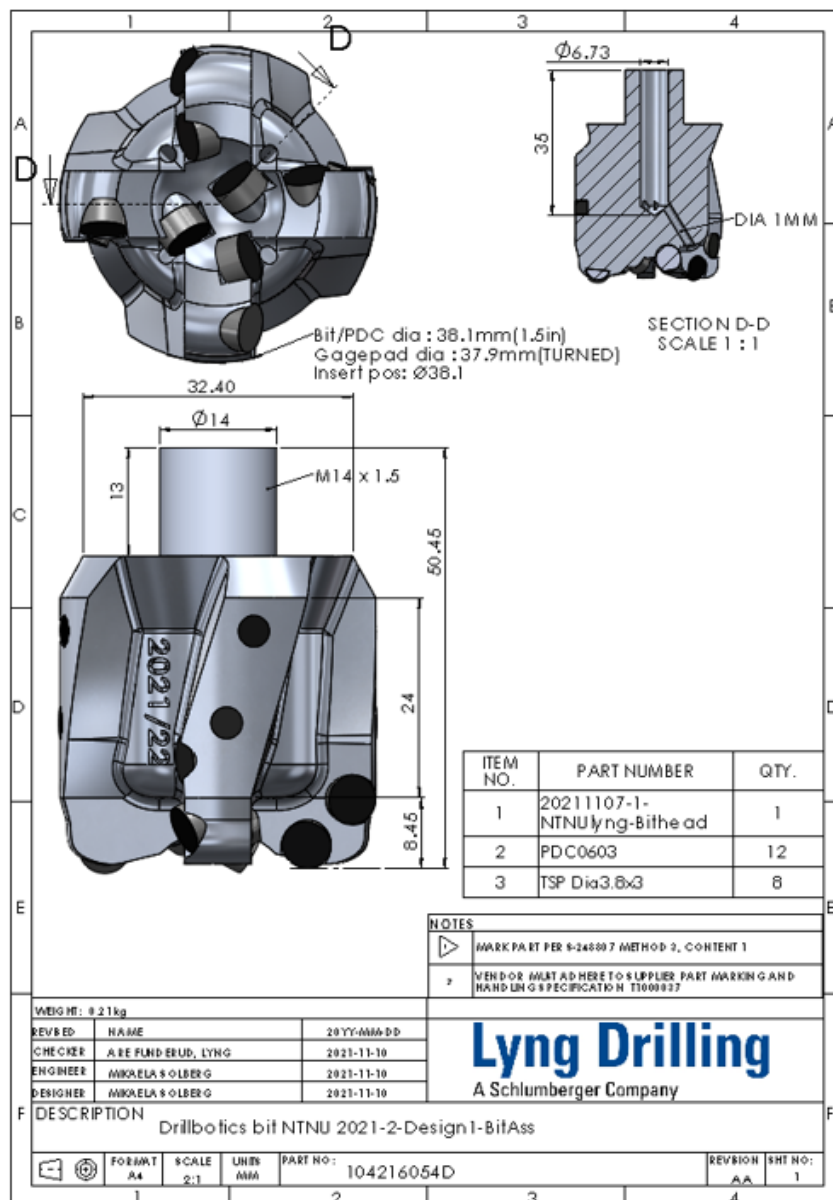


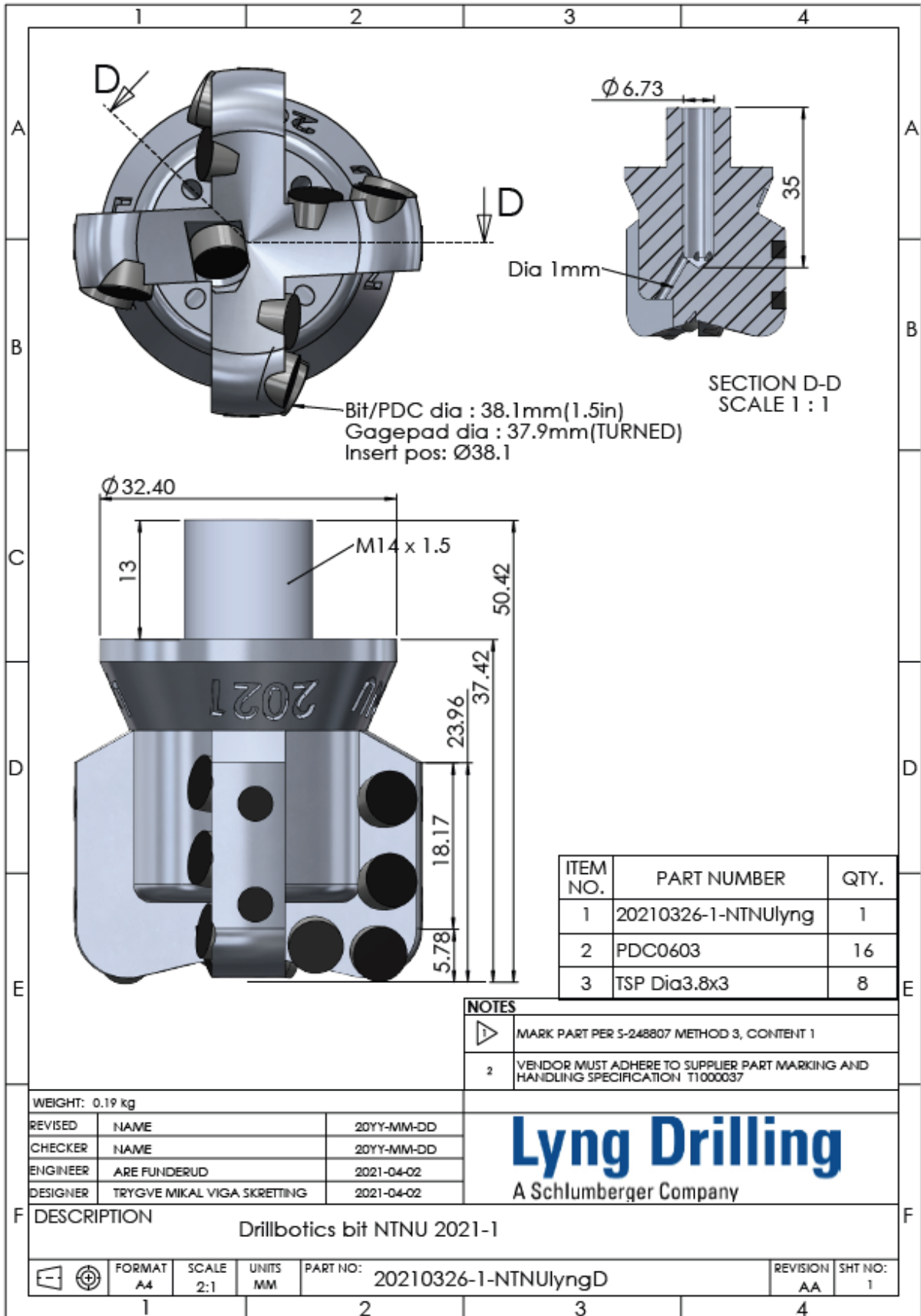


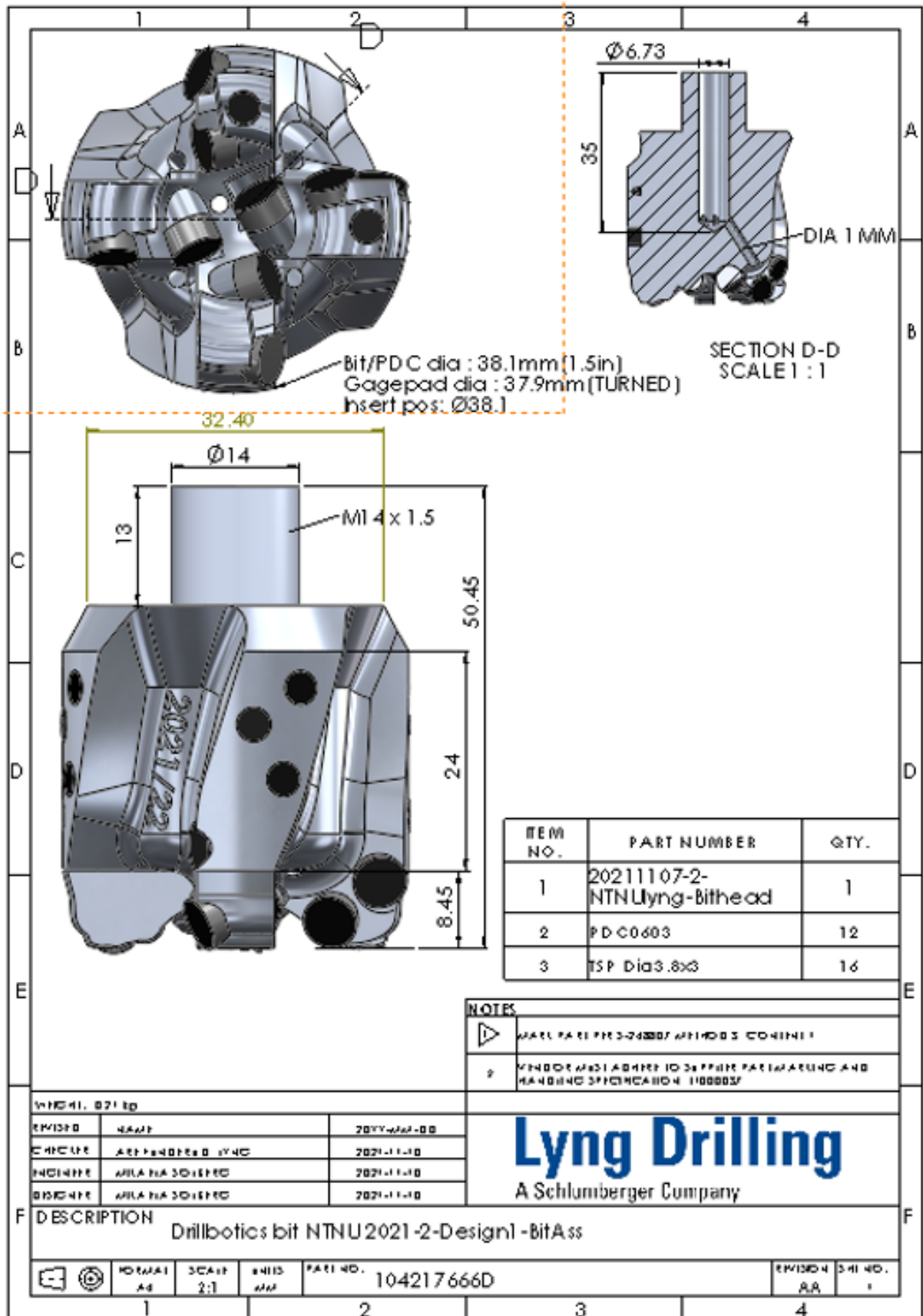
SOLIDWORKS Educational Product. For Instructional Use Only.

Appendix Q

Drill Bit







X1 Metal 420i™

60% 420 Steel Infiltrated with 40% Bronze



X1 Metal 420i™ is a matrix material composed of 60% 420 steel infiltrated with 40% bronze. This material offers good mechanical properties, is available in both an annealed and non-annealed condition, is able to be machined, welded and polished, and offers excellent wear resistance.

Applications

This material system is ideally suited for parts exposed to highly abrasive environments such as pump components, and parts for down-hole drilling and mining equipment. Additional applications include industrial components, molds, tooling, art objects and decorative hardware.



Printed part

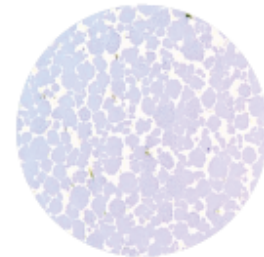
Composition

Stainless Steel: Alloy 420

Bronze: 90% Cu / 10% Sn

Printing

Using binder jetting technology, ExOne's state-of-the-art 3D printing machines produce parts directly from CAD models by precisely controlling the jetting of binder onto a powder bed, and then subsequently spreading new layers of powder. This process is repeated until the part is completed. This 3D printing process offers increased design flexibility, reduced manufacturing cost and shortened lead times.



X1 Metal 420i™

Post Processing

After printing is complete, the parts are cured in an oven, which enables the parts to be handled. After curing, the parts are sintered and infiltrated with bronze above 1100°C. Cool down can be varied to control the machinability and hardness of the material.

X1 Metal 420i™
60% 420 Steel Infiltrated with 40% Bronze



Typical Material Properties

Material Properties	Test Method	X1 Metal 420i™
Tensile Strength		
Ultimate Strength	ASTM E8	99 ksi (682 MPa)
Yield Strength (0.2% offset)		66 ksi (455 MPa)
Elastic Modulus		21.4 Mpsi (147 GPa)
Elongation		2.3%
Hardness	ASTM E18	97 HRb
Fractional Density	MPIF 42	95%+
Density		0.284 lbs./in ³ (7.86 g/cm ³)
Machinability		Refer to ExOne for recommendations
Weldability		Use silicone bronze rod & TIG weld
Thermal Conductivity	ASTM E1530	13 BTU/hr ft ² °F (22.6 W/m ² °K)
Specific Heat	ASTM E1263	0.114 BTU/lb °F (478 J/kg°K)
Thermal Expansion Coefficient	ASTM E228	7.4 x 10 ⁻⁶ /°F (13.4 x 10 ⁻⁶ /°K)

Surface Finish

- After sintering: ≈ 600 μin R_a (15 μm R_a)
- Bead blasting: ≈ 300 μin R_a (7.5 μm R_a)
- Barrel finishing: ≈ 50 μin R_a (1.25 μm R_a)



Printed part, raw finish



Printed part, polished

ExOne disclaims all warranties and liabilities for the content hereof and makes no representations as to its accuracy or fitness for use for any purpose. Any tradenames, trademarks, or service marks of others appearing herein are used strictly nominatively and are not to be construed as implying any affiliation, connection, association, sponsorship, or approval of the owners thereof for ExOne, its products, or the content hereof.

For information about ExOne systems, materials and applications, contact an ExOne Production Service Center or visit www.ExOne.com

Corporate Headquarters
The ExOne Company
Pennsylvania, USA
americas@exone.com
+1 877 773 9663

European Headquarters
ExOne GmbH
Gersthofen, Germany
europe@exone.com
+49 821 65063-0

Asian Headquarters
ExOne KK
Kanagawa, Japan
asia@exone.com
+81 465 44 1303

REV. 06/17/2021

17-4PH Stainless Steel



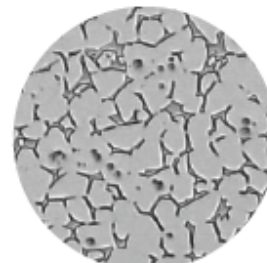
Typical Material Properties

Material Properties	Test Method	17-4PH H900
Tensile Strength		
Ultimate Strength	ASTM E8	X & Y: 1070 - 1310 MPa Z: 1070 - 1310 MPa
Yield Strength (0.2% offset)		X & Y: 970 - 1030 MPa Z: 970 - 1020 MPa
Elongation		X & Y: 4% - 12% Z: 4% - 11%
Elastic Modulus		X & Y: 180 - 190 GPa Z: 180 - 200 GPa
Hardness	ASTM E18	35 - 41 HRC
Impact	ASTM E23	55 - 75 J
Poisson's Ratio		0.28 - 0.30
Relative Density		96 - 99%
Density		7.5 - 7.7 g/cc
Surface Roughness		3 - 12 µm Ra



17-4PH Printed Part

Material Composition			
Iron	bal	Niobium + Tantalum	0.15-0.45%
Nickel	3-5%	Manganese	1.0% max
Chromium	15.5-17.5%	Silicon	1.0% max
Carbon	0.07% max		
Copper	3-5%		



Microstructure

ExOne disclaims all warranties and liabilities for the content hereof and makes no representations as to its accuracy or fitness for use for any purpose. Any tradenames, trademarks, or service marks of others appearing herein are used strictly nominatively and are not to be construed as implying any affiliation, connection, association, sponsorship, or approval of the owners thereof for ExOne, its products, or the content hereof.

